TARGETING LIPOGENESIS IN RETINOBLASTOMA: EVALUATION OF CHEMICAL INHIBITORS OF FATTY ACID SYNTHASE (FASN) AS ANTI-CANCER AGENTS

THESIS

Submitted in partial fulfillment

of the requirements for the degree of

DOCTOR OF PHILOSOPHY

by

S. VANDHANA

2007 PHXF426

Under the supervision of

Dr. S. KRISHNAKUMAR

Dr. P. R. DEEPA

BIRLA INSTITUTE OF TECHNOLOGY AND SCIENCE

PILANI (RAJASTHAN) INDIA

2012

BIRLA INSTITUTE OF TECHNOLOGY & SCIENCE

PILANI - RAJASTHAN

CERTIFICATE

This is to certify that the thesis entitled "Targeting Lipogenesis in Retinoblastoma: Evaluation of Chemical Inhibitors of Fatty Acid Synthase (FASN) as Anti-Cancer Agents" which is submitted by Ms. S.Vandhana, ID. No. 2007PHXF426 for award of Ph.D. Degree of the Institute, embodies original work done by her under our supervision.

Signature of the Supervisor **:**

Name in Block Capital letters : **Dr. S. KRISHNAKUMAR**

Designation : **Incharge Nanobiotechnology Department & Stem Cell Laboratory**
Head of the Department of Ocular Pathology
Vision Research Foundation
Sankara Nethralaya, Chennai 600 006
Tamil Nadu, India

Signature of the Co-supervisor **:**

Name in Block Capital letters : **Dr. P.R. DEEPA**

Designation : **Asst. Professor (Dept. of Biological Sciences),**
Practice School Division,
BITS Pilani (Rajasthan), BITS Pilani – Chennai Centre
No. 5, Montieth Lane (Opp. ICWA Institute),
Egmore, Chennai – 600 008

Date:

ACKNOWLEDGEMENTS

The most expected pleasant time has come now for me to express my gratitude to all of them who guided, supported and encouraged me throughout my PhD tenure. My first thanks to **GOD ALMIGHTY**.

Next my sincere thanks to my supervisor, **Dr. S. Krishnakumar**, Professor and Pathologist, Department of Ocular Pathology for his supervision, guidance, support and encouragement to complete my work.

I thank **Dr P. R. Deepa** for giving me an opportunity to work in this project and for giving me the fellowship. Madam has been constantly encouraging me and has given me complete guidance throughout the project for data analysis, paper preparation and thesis writing. I have learnt a lot from her about using Microsoft Excel, managing literature papers, preparation of manuscripts, and presentation of data. I feel very much blessed, and proud to be her student. I take this opportunity to convey my heartfelt gratitude to her.

I would like to thank **Prof. H.N. Madhavan,** President, Vision Research Foundation, Director of VIBS for his support and encouragement.

I would like to thank Padmabhushan **Dr. S.S. Badrinath**, Chairman Emeritus, and **Dr. S. Vasanthi Badrinath**, Director, Laboratory Services, and **Dr. S. Bhaskaran,** Chairman, Sankara Nethralaya, Chennai, India for providing me the opportunity to work in this esteemed institution and to pursue my doctoral programme.

I thank **Dr. Ronnie Jacob George,** Director of Research, Vision Research Foundation, **Dr. Tarun Sharma**, Honorary Secretary and Treasurer, Vision Research Foundation, **Dr. T.S Surendran**, Vice-Chairman, Medical Research Foundation for their support.

I sincerely thank the **Indian council of medical research (ICMR), New Delhi** for funding my project (Grant No. 58/15/2005-BMS) and granting me the fellowship for

research. My sincere thanks to the **Dept. of Biotechnology (DBT), Ministry of Science and Technology**, New Delhi, India for the granting funds for the oxidative stress work (Grant No: BT/PR13091/GBD/27/180/2009).

My sincere thanks to **Prof. L.K. Maheswari** former Vice Chancellor and Director, BITS, Pilani, and **Prof. B.N. Jain**, Vice Chancellor, **Prof. G. Raghurama**, Director, Pilani Campus, **Prof R.N. Saha,** Dean, Educational Development & Sponsored Research and Consulting, for giving me the opportunity to do my thesis under the esteemed university. I would also like to thank **Dr Ashish Kumar Das,** Former Dean, Research and Consultancy Division, **Prof. S. K. Verma**, Dean, Academic Research (Ph. D. Programme), **Prof G. Sundar,** Deputy Director, (Off-Campus Programmes), **Dr Sanjay D Pohekar, Dr Deshmukh, Dr Monica Sharma, Dr Hemant R Jadhav** and **Dr Dinesh Kumar** for their constant support and help during my Ph D program. I sincerely thank **Dr Rajesh Mehrothra** and **Dr Monalisa Mishra,** my Doctoral Advisory Committee (DAC) members for reviewing my draft thesis and for giving their valuable suggestions and comments.

I extend my sincere thanks to **Mr.S.Narayan**, Manager, Vision Research foundation and **Mr.N.Sivakumar**, Academic Officer for their support.

My sincere thanks to **Prof. J. Biswas**, Director, Ocular Pathology Department, **Dr. Niveditha Chatterjee** Ocular Pathology Department**, Prof. K.N.Sulochana**, Director, and **Dr. N. Angayarkanni,** Department of Biochemistry and Cell biology, **Prof. Lily Therese**, Head, L&T Microbiology Research Centre, **Dr. A.J.Pandian,** Head, ONGC Department of Genetics and Molecular Biology, **Dr.B.Mahalakshmi**, Lecturer, **Dr. J. Malathi,** Reader, L&T Microbiology Research Centre, Vision Research Foundation, **Dr. Doreen Gracious**, consultant, clinical lab for their kind words, support and encouragement during my research work.

I thank **Mr.Thiagarajan** HOD, Medical records Department and all his colleagues for their support in giving me Retinoblastoma patient's files. I wish to extend my thanks

to all the colleagues from the departments of Microbiology, Ocular Pathology, Genetics and Molecular Biology and Clinical Laboratory for their support.

I would like to express my sincere gratitude to **Dr.K.Coral** my first guide in the research life during my post graduation, for her moral support and for guiding me in the HPLC experiments standardization and in the analysis of the data. I would also like to thank **Ms M Bharath Selvi** for helping me during the HPLC experiments.

I thank **Dr Srujana** and **Ms Lakshmi,** core facility staff and the former incharge persons **Ms Uma,** and **Ms Krishnakumari** for their help in performing the flow cytometry experiments.

I thank **Dr. V. Uma Shankar,** Head, Bioinformatics Department **and Mr. S. Muthukumaran** for their technical help in performing the bioinformatics work.

I thank **Ms Kalaivani** and **Ms Aiyaz** (Genotypic Technology Pvt Ltd, Bangalore, India) for their technical support for the microarray analysis and **Mr Hitesh**, (Bionivid Technology, Bangalore, India) for pathway analysis in the oxidative stress work.

I thank **Ms U Jayanthi** who worked with me throughout the project and helped me constantly for all the experiments. A special mention is needed for her expertise in performing PCR and DNA extraction techniques. I had the pleasure to work with **Ms Aparna Ganesan** dissertation student who did her graduation work in our projects. It has been beneficial to the present work.

I also like to thank my dear friends**, Dr Bharathi devi, Ms Srilatha Jasty, Mr Job Sudhakar, Mr Gopinath, Ms Selvi, Ms Sai Jyothi, Ms Karthiyayini, Ms Vinitha, Ms Kamatchi, Dr Gayathri, Dr Mahalakshmi, Ms Sushma Kalmodia, Mr Samson Moses, Ms. Vidhya, Mrs. Parvathy Devi** for their timely help, moral support and encouragement throughout my Ph.D.

My colleagues **Ms Aparna, Ms Vidya, Ms Sangeetha, Mr Ravikanth, Mr Madhu, Ms Deepa, Ms Jaisy, Ms Nalini, Ms Nithya, Ms Kalaivani, Ms Meena, Ms Shyama, Ms Charanya** working in my department who had been a constant support for me

and have given me mental strength and encouragement. I also thank **Ms Vanitha** for her help in taking tissue sections for the work and for her support. I would also like to thank **Ms Uma and Ms Tamil mozhi** for their help in aligning and printing of the thesis. I thank **Mr.Annadurai and Mr Vinoth,** Lab attendant for his help during this period.

I am very grateful to **Mr P.L.Lakshmanan** my father in Law and **Mrs M Bavani** my mother in law who has been very kind to allow me to pursue my studies, and accept the kind burden of taking care of my son. My beloved husband **Mr.Prasanna Venkatesh,** needs a special mention, supported me throughout my Ph D and allowing me to continue this journey after marriage and for giving me moral support and timely advice.

My lovable kisses to my three year old son **Master P. Visweswaran**, who made a complete **'me'** and adjusting himself during my work time. His smile boosts my energy. Nothing in life is equivalent to the feel of **'mother'.** Thank GOD.

My special thanks to my sisters **Dr Rema Ramesh, Ms Vidya Gopal, Ms Mahalakshmi Sriram** for their constant moral support & encouragement from my child hood, and my brother in laws **Mr Ramesh, Mr Gopal Iyer, Mr Sriram and Mr. Vinoth** for their support and encouragement. Sweet kisses to **Divya Ramesh** and **Mahathi Gopal, Anirud Ramesh** for their love and affection.

I feel proud to express my deep sense of gratitude for my father **Mr.V.Suryanarayanan**, who is very perfect, well planned, and very affectionate to me, my mother **Mrs Janaki** who is calm and patient. Constant prayers of my parents must have helped me greatly in my achievements. They are also responsible for all the good things in my life. **I dedicate this thesis to my 'PARENTS'**.

Last but not the least, my dear friend **Mrs Seethalakshmi Sreenivasan,** needs to be given a special mention. We are together and working together for the past 12 years right from our graduation. I am very lucky to be her friend and work together with her during my Ph D. She is very helpful, self-confident, perfect in work and very

silent. Without seeing her in the lab, the day is not complete for me. We enjoyed being together and I pray GOD that we will be together forever.

S.VANDHANA

ABSTRACT

Retinoblastoma (RB) is a malignant intra-ocular neoplasm that affects children below the age of 5 years. Newer therapeutic approaches would reduce the morbidity of chemotherapy in children with RB. In addition to conventional chemotherapy, novel therapeutic strategies that target metabolic pathways such as glycolysis and lipid metabolism are emerging. One such metabolic target is fatty acid synthase (FASN), a lipogenic multi-enzyme complex that catalyses the synthesis of long chain fatty acids. FASN is minimally expressed in normal tissues, whereas it is over-expressed in many cancers, making it a promising clinical and pharmacological target.

The present study aimed at evaluating FASN as a target for retinoblastoma therapy. The research was initiated by firstly investigating the FASN protein expression in RB tumor tissues. Forty four RB tumour tissues analysed, were positive for FASN. The immunostaining for FASN showed markedly high expression of FASN protein in poorly differentiated and in retinoblastoma sections invading the choroid, optic nerve and/or orbit, which correlated strongly with tumour aggressiveness in retinoblastoma. Multi-fold over-expression of FASN mRNA and protein were observed in RB tissues, although at varying levels of expression.

Oxidative damage contributes to the development and pathology of several diseases. In cancers, reactive oxygen species (ROS) is implicated in the multi-stage carcinogenesis and tumor progression, and is also implicated in anti-cancer therapy. FASN functions to stabilize the redox balance in cancer cells, more favorably towards proliferation. Paradoxically, during FASN inhibition, increased ROS levels causing oxidative stress precede the apoptotic cell death. This association between fatty acid synthase and oxidative stress prompted us to analyze the status of oxidative stress in RB tumour tissues. Reactive oxygen species (ROS) levels and biochemical indicator of oxidative stress, malondialdehyde (MDA) was found in

higher levels in invasive RB tumours compared to non-invasive RB. Oxidant (H_2O_2) induced Y79 RB cells (retinoblastoma cell line) showed differentially expressed genes involved in cellular processes such as: oxidative stress, angiogenesis, lipid metabolism, cell proliferation, and cell signaling pathways suggesting the active involvement of redox signaling pathways in the pathogenesis of RB.

In this dissertation, the anti-cancer effects of three chemical inhibitors of FASN [cerulenin, triclosan and Xenical™ (orlistat)] were evaluated in cultured Y79 RB cells. Cerulenin targets the keto acyl synthase (KS) domain, triclosan inhibits enoyl reductase (ER) domain and orlistat targets thioesterase (TE) domain of the FASN multi-enzyme complex.

Optimal solubilization condition to dissolve the hydrophobic drug triclosan, for use in cell culture was identified using a systematic approach. Triclosan did not dissolve completely in DMSO, absolute ethanol and 1N NaOH when diluted with culture medium resulting in a turbid solution, whereas acetone and PEM (55% PEG-400 + 45% ethanol mixture) resulted in a clear solution. The pH of the final solutions (pH 8.0) with 1N NaOH and ethanol was unfavourable. Based on the pH and solubility criteria, acetone and PEM were tested further for their suitability as triclosan solubilisers in breast cancer (MCF-7) and retinoblastoma (Y79) cells. The results suggested that acetone lacked any cytotoxicity of its own, and conferred better drug sensitivity to triclosan in cancer cells, and was therefore more suitable than PEM for dissolving triclosan in cell culture conditions.

In vitro cytotoxicity assays with the three FASN inhibitors showed dose- and time-dependent cytotoxic effects in Y79 RB cells, and their respective IC_{50} (50% inhibitory concentration) was determined at 48, 72, and 96 h. The IC_{50} of cerulenin, triclosan, and Xenical™ (orlistat) at 48 h were 7 μg/ml, 20 μg/ml and 250 μg/ml respectively. The IC_{30}/ IC_{70} ratio was calculated for all the three FASN inhibitors, to indicate the fold increment in drug concentration needed to produce the drug-response

(inhibition of cell viability) in Y79 RB cancer cells. The higher the ratio, lesser the sensitivity of cancer cells to the drug's anti-proliferative effects. Neoplastic Y79 RB cells were more sensitive to cerulenin at 48 h, and to triclosan at 72 h, while at 96 h treatment, their sensitivity was comparable to both orlistat (Xenical™) and triclosan.

FASN inhibitors were tested for their safety profile in normal cells by using two non-neoplastic cells: muller glial (MIO-M1) and mouse embryonic fibroblast (3T3). In these cells, the FASN inhibitors were found to be non-toxic at their anti-neoplastic IC_{50} dosage. The relative efficacy was analyzed by computing the therapeutic index. The order of efficacy was cerulenin > triclosan > orlistat. Cell morphology analysis revealed cell shrinkage with the higher dosage of FASN inhibitors and no observable morphology changes at their respective IC_{50} dosage. FASN inhibitors were found to induce no major changes in the morphology of the non-neoplastic (MIO-M1 and 3T3) cells.

FASN protein expression in the cerulenin, triclosan and orlistat (Xenical™) treated Y79 RB cells and untreated cells were measured by FASN-specific ELISA. FASN mRNA was measured by real time quantitative RT-PCR (reverse transcriptase PCR). Differential modulation of FASN protein and mRNA expression was observed in FASN inhibitor treated Y79 RB cells.

Significant inhibition of FASN enzyme activity was observed in Y79 RB cells when treated with each of the FASN inhibitors – cerulenin, triclosan, and orlistat ($P<0.05$). The extent of enzyme-inhibition on cerulenin treatment at 48 h and 72 h exceeded that of triclosan, which in turn showed greater degree of inhibition than orlistat [Cerulenin (50% & 64%) > triclosan (37% & 45%) > orlistat (29% & 23%) at their IC_{50} dosages respectively]. At 96 h, orlistat induced a relatively greater inhibition of FASN activity by 59%, compared to cerulenin and triclosan. In all the experimentally treated groups, the decreased FASN activity was accompanied by a decrease in the

product levels (palmitate), and accumulation of substrate (malonyl CoA) that was quantified by high performance liquid chromatography (HPLC) technique.

Lipid profile was biochemically estimated in neoplastic and non-neoplastic cells with and without FASN inhibitor treatment. Untreated Y79 RB cancer cells and 3T3 fibroblast cells were compared for their distribution of lipids by computing the phospholipid to neutral lipids ratio. Phospholipid was represented by phosphatidyl choline in the present study. Triglycerides and total cholesterol represented the neutral lipids. The relative proportion of phosphatidyl choline to neutral lipids (triglyceride + total cholesterol) in Y79 RB cancer cells was higher than the non-neoplastic fibroblast (3T3) cells, indicative of altered lipid distribution and utilization in tumour cells. FASN inhibitor treated Y79 RB and fibroblast (3T3) cells showed decrease in the cellular lipids (triglyceride, cholesterol and phosphatidyl choline) levels.

Effects of FASN inhibitors on inducing apoptosis in Y79 RB cancer cells was evident by DNA smearing and laddering observed in agarose gel electrophoresis. This was confirmed by the presence of Annexin V positive Y79 RB cancer cells in the early and late apoptotic stages during the inhibitor treatment. This apoptotic DNA damage induced by FASN inhibitors was accompanied by lipid peroxidation (increased malondialdehyde, MDA levels). On one hand, increased oxidative stress is correlated with increased tumor aggressiveness; while on the other hand, therapeutic anti-cancer cytotoxicity also induces oxidative stress. Hence, the oxidative stress generation should be understood in the context of its biological role in the cancer cells, and clearly delineated. This would help in effective therapeutic approaches and clinical management of cancer patients. Microarray analysis of cerulenin treated Y79 RB cells revealed differential expression of genes involved in various cellular processes such as lipid metabolism, cell cycle/apoptosis, cell signaling/proliferation.

Molecular docking analysis with catalytic domains of FASN with the respective inhibitors was performed and the docking characteristics were studied. Human FASN KS and TE domain structures were optimized. The human ER domain was modelled and predicted based on porcine FASN I crystal structure and was optimised. *In silico* docking inhibition constant (Ki) correlated well with the biochemical IC_{50} and FASN enzyme activity in Y79 RB cells treated with FASN inhibitors.

The promising results obtained in the present study can pave the way for further investigations on fatty acid synthase. For example, FASN gene silencing strategies by siRNA technique could provide mechanistic insights into the molecular pathways involving lipid metabolism, oxidative stress and cell death/proliferation. Identification of novel small molecule inhibitors targeting FASN, and structural characterization of the catalytic domains that are not yet elucidated, could be helpful in developing anti-FASN therapeutics for treating cancers, and other disease conditions where FASN over-expression is being identified. FASN inhibitors are indicated to have immense potential as anti-cancer agents, and FASN could be explored as a therapeutic target for the effective treatment of retinoblastoma.

TABLE OF CONTENTS

LIST OF TABLES

LIST OF FIGURES

6.11	Sensitivity of FASN inhibitors with multi-fold increase in dosages of drug exposed for 48, 72 & 96 h on cultured retinoblastoma cells
6.12	Response of cancer cells to cytotoxic (IC_{70}) and cytostatic (IC_{30}) concentrations of the FASN inhibitors at different times of treatment
6.13	Cell Morphology analysis on FASN inhibitor treated Y79 RB cells
7.1	FASN regulation in normal and cancer cells mediated by SREBP1c
7.2	Assessment of safety of anti-FASN drugs in non-neoplastic cells
7.3	Determination of IC_{50} of FASN inhibitors in MIO-M1 cells.
7.4	Determination of IC_{50} of FASN inhibitors in 3T3 cells.
7.5	Comparison of Therapeutic Indices of FASN inhibitors
7.6	Morphology of non-neoplastic cells treated with FASN inhibitors for 48 h
8.1	Effect of FASN inhibitors on FASN protein content and mRNA expression in Y79 RB cells
8.2	Determination of free fatty acid levels in Y79 RB cells after 48 h treatment with FASN inhibitors
8.3	Inhibition of FASN enzyme activity by FASN inhibitors in Y79 RB cells
8.4	Analysis of malonyl CoA (substrate) accumulation on FASN inhibitor treatment in Y79 RB cells by HPLC
8.5	Calibration curves for cellular lipids
8.6.	Distribution of phosphatidyl choline, triglyceride and total cholesterol in Y79 RB and 3T3 cells
8.7	Decrease in cellular lipid levels in FASN inhibitor treated RB (Y79) and normal (3T3) cells
8.8	DNA fragmentation analysis of FASN inhibitor treated RB cells
8.9	Assessment of apoptosis in FASN inhibitor-treated RB cells by Annexin V assay
8.10.	Assessment of MDA levels in FASN inhibitor treated Y79 RB cell lysates and in supernatant
8.11	Cerulenin treatment in Y79 RB cells: Gene expression profile and validation of microarray analysis
9.1	Types of Fatty acid synthase (FASN)
9.2	The crystal structure of yeast FASN
9.3	Crystal structure of mammalian FASN from porcine model
9.4	Structure of orlistat and its binding regions
9.5	*In silico* docking studies of FASN KS domain with cerulenin
9.6	*In silico* docking studies of FASN ER domain with triclosan
9.7	*In silico* docking studies of FASN TE domain with orlistat
10.1	Lipid and oxidative metabolism in RB tumour pathogenesis – Summarizing our findings
10.2	Schematic representation of FASN regulation in normal and cancer cells
10.3	Anti-cancer effects of FASN inhibitors: Summarizing our experimental findings

LIST OF ABBREVIATIONS / SYMBOLS

Abbreviation	Expansion
ACACA	Acetyl CoA carboxylase alpha
ACACB	Acetyl CoA carboxylase beta
ACC	Acetyl CoA carboxylase
Acetyl CoA	Acetyl Coenzyme A
ACLY	ATP citrate lyase
ACP	Acyl carrier protein
AKT	Protein kinase B
AT	Acetyl transacylase
ATP	Adenosine triphosphate
bHLH/LZ	Basic helix-loop-helix/leucine zipper
bp	Base pairs
BNIP3	BCL2/adenovirus E1B 19 kDa protein-interacting protein 3
CAT	Catalase
CDC25A	Cell division cycle homolog 25A
CDK2AP1	Cyclin dependent kinase 2 associated protein 1
CEV	Carboplatin- etoposide-vincristine
ChREBP	Carbohydrate regulatory element binding protein
CPT1	Carnitine palmitoyl transferase 1
CREBBP	CREB binding protein
CRYAA	Crystallin alpha A
CYCS	Cytochrome C (somatic)
DAPK2	Death-associated protein kinase 2
DCF	2′, 7′ Dichlorodihydrofluorescein
DCFH-DA	2′, 7′-Dichlorodihydrofluorescin diacetate
DH	β-hydroxy acyl dehydratase
DMSO	Dimethyl sulfoxide
DNA	Deoxy ribonucleic acid
EC	Enzyme commission
EDTA	Ethylene diamine tetra acetate
EGCG	Epigallo catechin 3 gallate
EGFR	Epidermal growth factor receptor
ELISA	Enzyme Linked Immuno Sorbent Assay
eNOS	Endothelial Nitric oxide Synthase
EpCAM	Epithelial cell adhesion molecule
ER	Enoyl reductase
ERK	Extracellular-signal-regulated kinases
FA	Fatty acid
FACL3	Long chain fatty acyl CoA ligase 3
FACS	Fluorescence-activated cell sorter

FASN	Fatty acid synthase
FFA	Free fatty acid
FSC	Forward Scatter
GAPDH	Glyceraldehyde 3-phosphate dehydrogenase
GPx	Glutathione peroxidase
GRed	Glutathione reductase
GSH	Glutathione (reduced)
GSSG	Glutathione (oxidized)
h	hour (s)
H & E	Hematoxylin and eosin
H_2O_2	Hydrogen peroxide
HER-2/neu	Human Epidermal Growth Factor Receptor 2
HIF	Hypoxia inducible factor
HMG CoA	Hydroxy methyl guanyl Coenzyme A
HMGCR	Hydroxy methyl guanyl Coenzyme A reductase
HPLC	High Performance Liquid Chromatography
IC_{50}	50% inhibitory concentration
ICRB	International classification of retinoblastoma
ICMR	Indian council of medical research
iNOS	Inducible nitric oxide synthase
IU	International units
IRE	Insulin responsive element
JNK	c-Jun N-terminal kinases
JUN	Proto oncogene
kDa	Kilo dalton
Ki	Docking inhibition constant
KR	β-ketoacyl reductase
KS	β-ketoacyl synthase
LDH	Lactate dehydrogenase
LXR	Liver X receptor
M	Molar
Malonyl CoA	Malonyl Coenzyme A
MAPK	Mitogen-activated protein kinase
MDA	Malondialdehyde
min	minute(s)
Ml	milli liter
MMP	Matrix metalloproteinase
MMP-2 & 9	Matrix metallo proteinases – 2 & -9
MPT	Malonyl palmitoyl transferase
MRP1	Multi drug resistant protein -1
MT	Malonyl transacylase
mTOR	Mammalian target of rapamycin
MTT	[3-(4,5-dimethylthiazol-2-yl)-2,5-diphenyltetrazolium bromide
MW	Molecular weight
NADPH	Nicotinamide adenine dinucleotide phosphate (reduced)
NO	Nitric oxide
NOS	Nitric oxide synthase
NT	Nitro tyrosine

OA	Oleic acid
OA-519	Oncogenic antigen -519
PC	Phosphatidyl choline
PDB	Protein data bank
PEG	Poly ethylene glycol
PEM	55% Polethylene glycol 400 + 45% Ethanol mixture
P-gp	P-glycoprotein
PI	Propidium iodide
PI3K	Phosphoinositide 3-kinase
PK	Pyruvate kinase
PLK1	Polo-like kinase 1
PPARA	Peroxisome proliferator activated receptor alpha
PPT	Phosphopantetheinyl transferase
PRDX6	Peroxiredoxin 6
PTEN	Phosphatase and tensin homolog
PUFA	Poly unsaturated fatty acids
RB	Retinoblastoma
RIPA buffer	Radio immunoprecipitation buffer
RMSD	Root mean square deviation
RNA	Ribonucleic acid
RO	Reactive Oxygen
ROS	Reactive oxygen species
RPE	Retinal pigment epithelium
RT	Retention time
RT-PCR	Reverse Transcriptase Polymerase Chain reaction
RXRA	Retinoid X receptor alpha
S1-P	Sphingosine 1-phosphate
S1P	Site-1 protease
S2P	Site-2 protease
SA	Stearic acid
SCAP	SREBP cleavage activating protein
SDS-PAGE	Sodium dodecyl sulphate - Polyacrylamide gel electrophoresis
sec	second(s)
siRNA	small interference RNA
SKP2	S-phase kinase associated protein – 2
SM	Sphingomyelins
SMases	Sphingomyelinases
SOD	Superoxide dismutase
SRE	Sterol responsive elements
SREBP1c	Sterol regulatory element binding protein -1c
SSC	Side Scatter
SSTR2	Somatostatin receptor 2
STZ	Streptozidin
TC_{50}	Theoretical inhibition constant
TCA	Trichloro acetic acid
TE	Thioesterase
TEMED	Tetra ethylene methylene diamine
TGF- β	Transforming Growth Factor

TGL	Triglyceride
TI	Therapeutic index
TIMP	Tissue Inhibitor of Metalloproteinases
TNF-α	Tumor necrosis factor – alpha
TOFA	5-(tetradecycloxy)-2-furoic acid
TRAIL	Tumor necrosis factor–related apoptosis-inducing ligand
TRX	Thioredoxin
USP2a	Ubiquitin specific protease 2a
VEGFA	Vascular endothelial growth factor A
WEE	WEE homolog
Symbols	
α	alpha
β	beta
γ	gamma
δ	delta
ε	epsilon
κ	kappa
μ	micro
n	nano
p	pico

CHAPTER 1: INTRODUCTION AND LITERATURE REVIEW

1.1. Pediatric Cancer

Cancer is defined as uncontrolled division of cells which spreads to the other parts of the body through blood and the lymph. Pediatric cancers represent 1% among the new cancers diagnosed every year. About 12,060 new cases are expected to be diagnosed as childhood cancers in the year 2012. National cancer institute reported the estimated deaths from cancer in the year 2012 in USA to be 5,77,000 approximately. The childhood cancers are: leukemia, neuroblastomas, cancers of the brain and nervous system, osteosarcoma, retinoblastoma, Wilms tumour, rhabdomyosarcoma. Leukemia constitutes 34% among the childhood cancers and, retinoblastoma accounts for 3% (Cancer Facts & Figures 2012, American Cancer Society). India has the highest number of RB affected children in the world; the incidence is estimated to be 1200 cases each year. A population based project was conducted by the National Cancer registry Project (NCRP) (ICMR) during the year 1999 - 2000 for estimating the incidence of RB. In New Delhi the estimated probable incidence of RB was 28 cases per million population of children, below 5 years of age (ICMR guidelines, 2010; http://icmr.nic.in/guide/RB_Guidelines.pdf)♣.

1.2. Retinoblastoma

Retinoblastoma (RB) is a malignant neoplasm of the retina, which occurs in the intraocular region of the children below the age of 5 years. The median age at diagnosis is 2 years. Rare cases have been reported at 5 years of age and in adulthood. The disease is fatal when diagnosed at an advanced stage. There are two types of RB based on whether it affects both the eyes (bilateral) and a single eye (unilateral). Unilateral RB is most common than the bilateral RB.

♣ *The Indian Council of Medical Research (ICMR) has published the 'National Guidelines in the Management of Retinoblastoma', in the year 2010, to enable the ophthalmologists and pediatricians to arrive at an early diagnosis of Retinoblastoma. The details of the guidelines are available at "http://icmr.nic.in/guide/RB_Guidelines.pdf" link.*

1.2.1. Genetics of RB

RB occurs due to the mutation in the Rb1 gene in the chromosome region 13q14, that encodes for the tumour suppressor protein Retinoblastoma protein (Rb protein). The disease occurs in two forms: hereditary and non-hereditary. Hereditary disease occurs due to the germ line mutation of RB1 gene with a positive family history. About 40% of the RB is of hereditary origin, in which predominantly bilateral RB (25%) occurs and to a lesser extent it causes unilateral disease (about 15%). Hereditary RB1 mutations are also found in all cells thereby increasing the risk of other cancers like malignant melanoma and osteosarcoma. The new onset germ line mutation can also occur without positive family history, resulting in unilateral RB tumours. The inherited RB is generally transmitted as an autosomal dominant trait. The children of hereditary RB patients have a 1 in 2 chance of carrying germ line mutation. The carriers have a chance close to 90% for developing the disease especially if the parents have bilateral RB than unilateral RB (Bakshi & Bakshi, 2007).

All human tumours in general have deregulated growth signaling pathways. The fate of the tumour cell during the proliferation is governed by the retinoblastoma protein (pRb) and p107 and p130. pRb in its hypophosphorylated state blocks the proliferation by altering the function of E2F transcription factors. E2F controls the expression of genes involved in the cell cycle transition from G1 to S phase. When the pRb is phosphorylated its action on E2F is disrupted and which leads to cycle cycle progression from G1 to S phase (Hanahan & Weinberg, 2000).

1.2.2. Clinical Manifestation

RB predominantly appears as an intraocular disease in the developed countries, where 90% of the patients present with a curable tumour. In developing nations, due to unawareness, delayed diagnosis, and aggressive biology of the tumour, the RB patients present with an advanced stage of the disease at diagnosis. Bilateral RB

occurs at an earlier age than the unilateral RB. Leukocoria (white coloured pupil) and strabismus (deviated eyes) are the common finding which urges the patients to seek medical attention. Bilateral RB patients report with poor vision.

Figure 1.1 Anatomy of the human eye

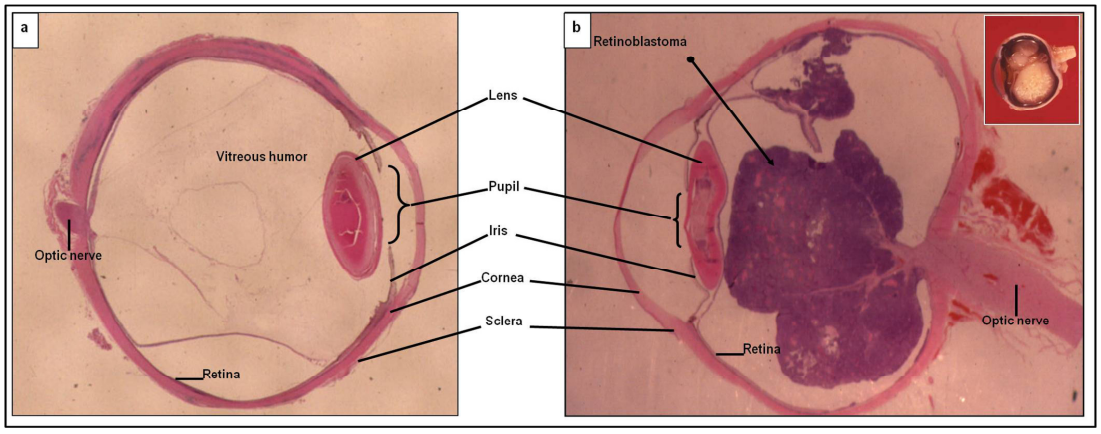

Figure 1.1: Anatomy of the human eye: Hematoxylin & Eosin stained anatomical picture of **a)** normal eye **b)** eye with retinoblastoma tumour; the pictures were obtained macroscopically from a stained section. Inset: Cut section of the RB affected globe. Pictures are taken at the Ocular Pathology Laboratory, Sankara Nethralaya, Chennai.

1.2.3. Classification

The systematic classification of RB was presented as Reese-Ellsworth classification, which is an older type of classification. The recent classification has been reported by Sastre et al., 2009. This report provides the guidelines of classification of RB and handling of the enucleated eye with RB, as per the instructions of International Retinoblastoma Staging Working Group (IRSWG). According to IRSWG the RB is classified as follows:

Choroid invasion

1. *Massive or significant* - maximum diameter (thickness or width) of invasive tumour measuring 3 mm or more in any diameter or tumours reach atleast the inner fibers of the scleral tissue.

2. *Focal invasion* - less than 3 mm in any diameter (thickness or width) of the tumour and not reaching the sclera.

Artifactual tumour seeding during fresh tumour retreival generally shows small group of tumour cells with necrotic cells present in natural spaces of the eye. The true invasion, is in contrast composed of solid nests of tumour that have usually pushed or infiltrating borders, expanding and replacing the area of invasion. Unless the tumour is extremely large, they have few necrotic cells. Optic nerve invasion is classified as prelaminar, laminar, post laminar, and tumour at surgical margin.

1.2.4. Pathology

Retinoblastoma tumour growth patterns are of four different types: endophytic, exophytic, mixed endophytic and exophytic and diffuse plaque-like tumours. Endophytic type tumours grow towards the vitreous from the retina. Small clusters of tumour cells detach from the main mass and forms tumour nodules in the vitreous. This is called as 'vitreous seeding' which also deposits on the other sites within the eye such as retina, and iris. Exophytic tumours grows from the outer retinal layers towards the choroid, they extend beyond the detached retina. Plaque like RB tumours grows diffusely within the retina without even forming the tumour mass and is often difficult to diagnose when the tumour masses are present in the vitreous and anterior chamber.

Invasion of the choroid and optic nerve have been determined as risk factors for RB metastasis. The choroid invasion is reported by many histopathologists as less than or greater than 3 mm thickness. Optic nerve invasion means presence or absence of tumour cells in the optic nerve and the extent of the invasion and the extent of lamina cribrosa involvement. This is an important aspect as the optic nerve is the primary route for tumour cells to invade the central nervous system. One should also determine the presence of tumour cells in the surgical end to ensure the likely

risk of metastasis. Frozen section examinations generally help the surgeons to find the extent of presence of tumour cells in the optic nerve region, during enucleation. Frozen section examinations are uncommon in most of the eye care centers during enucleation. Histopathological processing of the enucleated RB globes is commonly done. Optic nerve head is generally removed first as a part of the processing and the eye ball is processed separately to avoid cross contamination of tumour cells from the globe to the optic nerve head. Orbital invasion is also considered a risk factor for metastasis to other areas of the body.

1.2.5. Histopathology

Histopathological studies are general procedures that are performed with the enucleated globe. The RB cells are typically round in shape which has a basophilic nucleus and the nuclear cytoplasmic ratio is very high and the nucleus varies in its size. Viable cells appear as ribbon-like areas and they alternate the necrotic area of cells. Viable cells appear around blood vessels and areas of calcification are common in highly necrotic tumours. Differentiated tumours shows clusters of RB cells which are called as Homer-Wright rosettes and Flexner-Winter-steiner rosettes (Finger, 2002) (Figure 1.2). Another benign condition that presents with the abundant fleurettes of tumour cells is called Retinoma. Retinoma is defined as a benign, elevated, gray, translucent retinal mass with cottage cheese–like calcification and hyper-pigmented retinal pigment epithelium. The clinical presentation shows translucent intra-retinal mass with calcification and/or choroidal scarring. Retinoma is commonly seen in eyes removed for retinoblastoma, but is usually hidden under the proliferating RB tumour cells (Dimaras et al., 2009).

1.2.6. Treatment

Management of RB is based on several factors such as systemic status, metastatic disease, and risk of second cancers, laterality, size and location of the tumour. The

overall goal is to save the child's life and also to an extent the eye and vision of the child.

The various treatment strategies are:

1. Enucleation
2. External beam radiation
3. Plaque radiotherapy
4. Laser photocoagulation
5. Cryotherapy
6. Thermotherapy
7. Chemotherapy
8. Intravenous/ sub-conjunctival chemo reduction
9. Systemic chemotherapy for metastatic disease
10. Intra-arterial therapy

Figure 1.2. Cluster formation of Retinoblastoma cells in tumour tissue sections

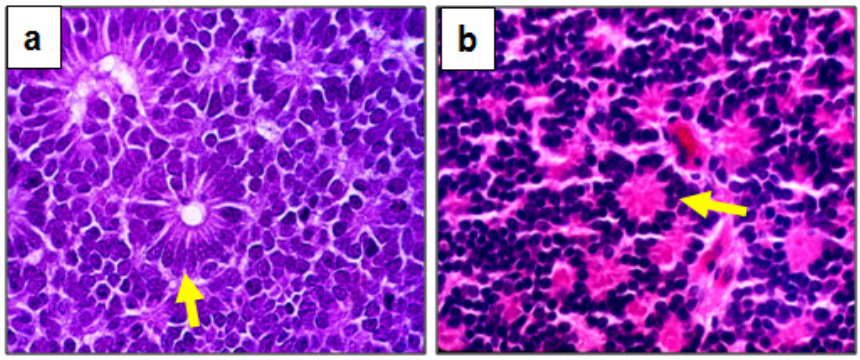

Figure 1.2: Cluster formation of RB cells in tumour tissue sections: Hematoxylin and eosin stained section of RB tumour showing a) Flexner - Wintersteiner rosettes with a clear central lumen, b) Homer-Wright rosettes (indicated by arrows). Pictures are taken at Dept. of Ocular Pathology, Sankara Nethralaya (Magnification – 100X).

1.2.6.1. Enucleation

This method is the common procedure that is generally done for managing advanced retinoblastoma. It involves the removal of the entire affected eye through surgery. It is done in advanced disease states, where the restoration of vision affected eye is less likely and/or if the tumour has invaded choroid, optic nerve and

orbit. The necessity of enucleation procedure has reduced in number with the advent of new modes of therapy.

1.2.6.2. External beam radiotherapy

External beam radiation is a method that involves irradiation of the whole eye with the radio-sensitive tumour (RB) presented with a diffuse vitreous seeding. With an improved eye preservation rate the method generally has the problem of tumour recurrence within 1-4 years of treatment. The visual outcome is poor and tumour recurrence sometimes depends on the stage of the tumour and the largest tumour size during treatment. Damage to retina, optic nerve and lens are additional effects during this procedure.

1.2.6.3. Plaque radiotherapy

This procedure involves the placing a radioactive implant in the scleral area over the base of the tumour, where the tumour irradiation occurs trans-sclerally. The method is performed as a secondary treatment procedure for first failed treatment procedures such as chemotherapy or radiation therapy.

1.2.6.4. Laser photocoagulation and cryotherapy

Tumours with base of 4.5 mm or less and a thickness of 2.5 mm or less with no evidence of vitreous seeds can be treated with laser photocoagulation. The success of this method is related to the size of the tumour. This method involves treating the posterior RB tumours with argon laser, diode laser or xenon arc. The laser delimits the tumour cells by coagulating all the blood vessels connected to it. Recurrence of tumour during this procedure is a drawback which is treated with plaque radiotherapy. Other problems during the procedure are retinal detachment and formation of retinal hole. Cryotherapy involves triple freeze thaw cycles for one or two sessions at 1 month's interval periods. This is successful only with small RBs measuring 3.5 mm or less in diameter and 2.0 mm or less in thickness (Shields, 1999).

1.2.6.5. Chemotherapy

Systemic chemotherapy uses anti-cancer drugs for destroying the tumour growth. These drugs are administered intravenously, intramuscularly or orally. Chemotherapy is often given to avoid enucleation and external beam radiation and to reduce formation of second malignancies due to the radiation therapy. It is also used after the removal of the tumour to remove any residual tumour, which is called "adjuvant therapy". Neo-adjuvant therapy is a procedure where the patient is given chemotherapy prior to enucleation under known cases of spread of tumour to the optic nerve. **Chemoreduction** is a protocol to shrink the tumour volume for the purpose of focal treatment procedures like cryo therapy and laser photocoagulation.

1.2.6.6. Chemotherapy protocol

The common drugs that are used for chemotherapy are vincristine, etoposide and carboplatin. Due to multi-drug resistance phenomenon, cyclosporine is added in the common chemotherapy regimen. There are several protocols depending on the severity and type of the disease: two drug, triple drug and four drug protocols. The number of cycles of the chemotherapy depends on the rate of tumour regression which is examined periodically.

The chemotherapy protocol administered as short infusion (Helen et al., 2005):

- Carboplatin - 22 mg/kg/dose on day 1 as a 30-minute infusion
- Vincristine - 0.05 mg/kg/dose on day 2 as a 5-minute injection
- Teniposide or etoposide, 9 mg/kg/dose on day 2 as a 25-minute infusion

1.2.6.7. Side effects of chemotherapy

Chemotherapy associated side effects are common and they are vascular and ocular toxicity, hyper sensitivity reactions, neuro toxicity, bone marrow depression, mucositis, nausea, vomiting, renal failure, and hepatic dysfunction (ICMR guidelines, 2010)

1.2.6.8. Sub-conjunctival topotecan in fibrin sealant

Topotecan (TPT) is a topoisomerase I inhibitor tested for its cytotoxic effects in RB cells, was injected by subconjunctival route in fibrin sealant. Fibrin sealant is a biodegradable surgical adhesive, used for periocular drug delivery for controlled release of drugs. Topotecan treated mice showed reduction of tumour burden and effective controlled release of drug. However the route of delivery with this system was haematogenous rather than trans-scleral route (Tsui et al., 2008).

1.2.6.9. Intra-arterial chemotherapy

Intra arterial chemotherapy is a novel alternative approach for RB treatment. To provide a high local concentration of the drug, this method employs intra-arterial route of administration. This gives efficient biological effects at the tumour site and this method also minimises systemic side effects caused by the other modes of therapy. With this approach 88% (14 out of 16 RB patients) of the advanced RB patients, were successfully treated. The success of this method needs to be validated with more subjects as the present knowledge is from a very small cohort of RB patients and with shorter follow up period. Regression of the disease to a type III calcified type appears similar to regression after chemoreduction. The ideal dose and the number of cycles are yet to be finalised. However, reasons for vision-threatening situations due to local ocular toxicities and long-term systemic toxicities that are developed during this procedure have not been understood (Shields et al., 2011).

1.2.7. Novel therapeutic targets of RB

Treatment of RB patients poses a big threat for the ophthalmologists due to multiple problems such as side effects of chemotherapy, development of secondary cancers, and the risk of metastasis which leads to a life threatening situation. Recent research on cancer therapy has brought about novel molecules, which can be targeted for treating cancers, including RB. There are several important molecules that are

reported to be prognostic and therapeutic targets. These molecules are involved in various processes involved in tumour cell proliferation and apoptosis (PRDX6 and CRYAA) (Mallikarjuna et al., 2010), cell adhesion (EpCAM) (Krishnakumar et al., 2004), angiogenesis (MMP-2 and MMP-9) (Mallikarjuna et al., 2010), genes involved in energy metabolism (FASN) (Camassie et al., 2003) and multi-drug resistance (P-gp, MRP1) (Mallikarjuna et al., 2010). Targeted therapies based on these candidate markers using RNA interference strategies, chemical inhibitors, natural compounds and their products have all been successfully tested in human cultured retinoblastoma cells cultured *in vitro* and these strategies induced apoptosis of cultured retinoblastoma cells (Mallikarjuna et al., 2010). Epigenetic mechanisms contribute to tumourigenesis in retinoblastoma. Key cancer related genes were found to be epigenetically deregulated in RB tumours. SYK (spleen tyrosine kinase) is a proto-oncogene, that is identified as important oncogene in retinoblastoma by epigenetic and gene expression analyses in RB tumour tissues (Zhang et al., 2012). Connexin 46, a gap junction protein, that has been reported to confer protection to tumour cells from hypoxic death. Gene silencing studies with connexin 46 specific siRNA in cultured cells led to apoptotic cell death, suggesting anti-connexin 46 therapy to be a potential target in RB treatment (Burr et al., 2011).

1.3. Metabolic pathways as anti-cancer targets

All cancer cells have an increased aerobic glycolysis to meet the energy requirements. Otto Warburg discovered the hallmark of cancer cell metabolism, in which increased carbon flux through the aerobic glycolysis provided growth advantage to the cancer cells. Glycolysis in cancer cells are regulated by several members of the metabolic and signaling pathways. Hexokinase of the glycolytic cycle is increasingly expressed in cancers and the signaling molecules such as PI3K (Phosphoinositide 3-kinase)/AKT (protein kinase B), MYC, HIF (bHLH transcription factors) and p53 (tumour suppressor gene) all work and regulate the increased

glycolysis in the cancer cells. Further, this leads to increased production of citrate which gets converted to acetyl CoA and malonyl CoA thus enhances the production of lipids in cancer cells. In addition to increased protein and DNA synthesis, elevated glutaminolysis is also observed in tumour cells (Figure 1.3) (Menendez & Lupu, 2007). Lipid metabolic genes that are up-regulated during carcinogenesis process are Fatty acid synthase (FASN), acetyl CoA carboxylase alpha (ACCα), ATP citrate lyase (ACLY), and Spot14 protein.

Figure 1.3. Glycolysis pathway and lipogenesis in cancer

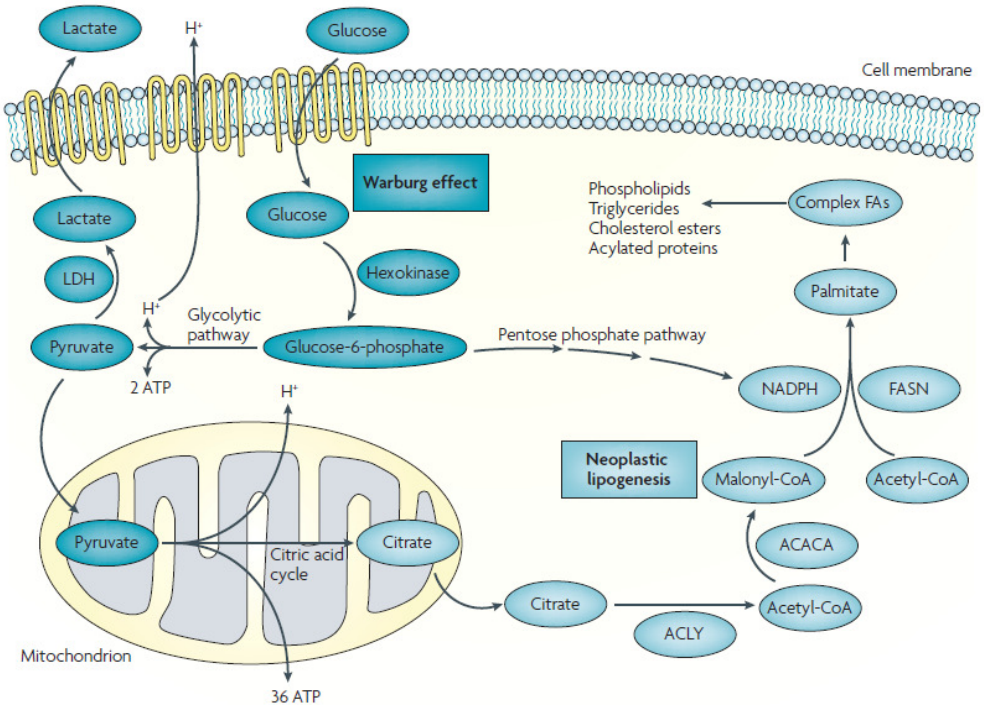

Figure 1.3: Glycolysis pathway and lipogenesis in cancer: During the metabolism of glucose to fatty acids, 25 enzymes function in an orderly fashion to help the tumour cells in proliferation. Pyruvate that is formed out of glycolysis enters the TCA cycle and gets converted to citrate and then acetyl CoA. Acetyl CoA and Malonyl CoA forms the primers for the fatty acid synthesis. The end product palmitate during fatty acid biogenesis is then utilised to form various classes of lipids in the tumour cells (Picture adapted from Menendez & Lupu, 2007).

ACCα is the rate limiting enzyme of the fatty acid synthase pathway that converts acetyl CoA to Malonyl CoA. Spot 14 is a protein that regulates the functions of both

ACCα and FASN. Anti-cancer therapy targeting several lipid metabolic genes have been reported (Dakubo, 2010).

1.4. Lipid metabolizing enzymes in cancer therapy

1.4.1. Acetyl CoA carboxylase

Acetyl CoA carboxylase (ACC) catalyses the synthesis of malonyl CoA (the pre-requisite for the fatty acid synthesis) from acetyl CoA. This enzyme is a negative regulator of fatty acid oxidation and the rate limiting enzyme for fatty acid synthesis. ACC inhibition has emerged as a target for cancer therapy. There are two isoforms for the enzyme ACC1 and ACC2. ACC1 is a cytosolic protein that supplies malonyl CoA for the fatty acid synthesis and ACC2 is associated with mitochondria that regulate the secondary pool of malonyl CoA, which in turn regulates the fatty acid oxidation through inhibition of carnitine palmitoyl transferase 1 (CPT1) enzyme. Both the ACC isoforms are over expressed in cancer cells. A previous study with 5-(tetradecycloxy)-2-furoic acid (TOFA), a classic inhibitor of ACC, showed that TOFA failed to induce apoptosis in breast cancer cells. These studies proved that malonyl CoA was responsible for the cytotoxic effects during FASN inhibition in addition to the depletion of fatty acids. Soraphen A, a natural macrocyclic polyketide that is isolated from the myxobacterium *Sorangium cellulosum*. Soraphen A binds to the biotin carboxylase domain dimer interface of the ACC enzyme, thus inhibiting its activity. At nanomolar concentrations, it blocks lipogenesis and activates fatty acid oxidation. The cells on treatment were arrested in the G0-G1 phase of the cell cycle. These studies show the importance of ACC inhibition in cancer therapy (Thupari et al., 2001; Wang et al., 2009).

1.4.2. HMG CoA reductase

HMG CoA reductase enzyme catalyses the conversion of HMG CoA to mevalonate, which is the rate-limiting step in the mevalonate pathway. The targeted therapy with

statins that inhibits this enzyme, results in decreased levels of mevalonate which critically influences many cellular functions. Statin induced depletion of geranyl geranylated proteins were responsible for induction of apoptosis. Anti-cancer effects of statins were also reported to be synergistically enhanced by the histone acetylase inhibitors during combination treatment in HeLa cells. The five commercially available HMG CoA reductase inhibitors (statins) are simvastatin, lovastatin, fluvastatin, pravastatin, and atorvastatin (Gan et al., 2008).

1.4.3. Enzymes in Sphingomyelin pathway

Enzymes of the sphingomyelin pathway such as serine palmitoyl transferase, ceramide synthase, ceramidase, sphingosine kinase, and glucosyl ceramide synthase have been reported (Kolesnick, 2002) as cancer targets and drugs that inhibit these enzymes have been developed. Combination therapy with drugs that increase ceramide levels along with chemotherapy are encouraged based on the pre-clinical data. Ceramides are synthesized *de novo* and also through the catabolism of sphingomyelins (SM) by sphingomyelinases (SMases). The pool of ceramide from both these sources adds to the possibility of apoptotic cell death during treatment with cytotoxic agents. Ceramide and sphingosine 1-phosphate (S1P) has opposite functions towards cell proliferation and cell death. Ceramide functions for anti-proliferative activity, and S1P acts as a second messenger for the cell proliferation and survival. S1P is also reported to confer protection to cells against ceramide mediated cell death. Thus the balance between ceramide and S1P levels determines the fate of the cell (Kolesnick, 2002).

1.4.4. Fatty acid synthase (FASN)

Fatty acid synthase (FASN) is a lipogenic multi-enzyme complex that is over-expressed in several types of cancer (Menendez & Lupu, 2007). FASN catalyses the synthesis of long chain fatty acids, especially the 16 carbon fatty acid palmitate,

which forms the main constituent of the lipid bilayer in the actively proliferating cancer cell membranes. FASN is basally expressed in normal cells, where the cells depend on the dietary fatty acids for their energy production. In contrast, in cancer cells it is over-expressed due to extensive cell proliferation. FASN has been targeted by various chemical inhibitors, as it possesses seven different catalytic domains that perform different functions during the fatty acid synthesis. These chemical inhibitors such as cerulenin, triclosan, orlistat and green tea polyphenols such as epigallo-catechin 3 gallate (EGCG) target specific domains of FASN. The anti-cancer potential of these inhibitors have been explored in several cancer cell lines and in xenografts models. In addition to these studies, siRNA mediated gene silencing of FASN and the resulting anti-cancer effects have been studied in breast cancer cell lines (Menendez & Lupu, 2007).

1.5. Fatty acid synthase (FASN), Protein structure and Biochemical reactions

Enzyme commission number: EC 2.3.1.85 - The enzyme belongs to the transferase class, which transfers acyl groups.

Systematic Name: acyl-CoA: malonyl-CoA *C*-acyltransferase (decarboxylating, oxoacyl- and enoyl-reducing and thioester-hydrolysing)

Fatty acid synthase (FASN) is a lipogenic multi-enzyme complex that has seven atalytic domains in a single polypeptide chain. The seven domains are β-ketoacyl synthase (KS), acetyl transacylase (AT), malonyl transacylase (MT), β-hydroxy acyl dehydratase (DH), enoyl reductase (ER) and β-ketoacyl reductase (KR), thioesterase (TE) and acyl carrier protein (ACP). The FASN enzyme structure varies with the species. There are two types of FASN.

1 Type I FASN (Contains all catalytic domains of the cyclic reaction in a single polypeptide chain)

2 Type II FASN (Each catalytic domain is a small independent protein, each of which catalyses a single step of the cyclic reaction

Fatty acid synthase (FASN) is a complex multi-functional lipogenic enzyme of molecular weight 260 kDa and contains two separate domains-seven different catalytic activities. The gene encoding for the FASN protein is located in the 17q25 region. FASN catalyses the synthesis of long-chain fatty acids from acetyl CoA and malonyl CoA, in the presence of NADPH (as the reducing equivalent). FASN is a homodimer with each monomer containing the domains of all component activities and are organized in such a way that the binding sites of the primer and the elongating malonyl groups are within bond distances. Each monomer has eight domains with six catalytic activities. The six catalytic domains are β-ketoacyl synthase, acetyl transacylase, malonyl transacylase, β-hydroxy acyl dehydratase, enoyl reductase and β-ketoacyl reductase. These enzyme activities play a major role in the fatty acid synthesis initiation and chain elongation. Seventh domain thioesterase represents the enzyme activity required for releasing the mature fatty acid from the enzyme. The eighth domain represents the acyl carrier protein, the site to which the growing fatty acid is tethered during synthesis. The prosthetic group, 4'- phosphopantetheine is located in this acyl carrier protein (ACP). This protein binds all the acyl intermediates as thioester derivatives and channels them into the synthetic pathway. The identical monomer domains are organized in a head-to-tail arrangement such that the active cysteine-SH of one monomer is juxtapositioned opposite a pantetheine-SH of the adjacent monomer, generating two identical centers. Dissociation of the dimer into monomers causes loss of the enzyme activity. This is because since the cysteine-SH is located at the active site of β-ketoacyl synthase, the two centers obtained by this arrangement constitute novel β-ketoacyl synthase (condensing) sites (Wakil, 1989).

The overall reaction is:

$$\text{Acetyl CoA} + 7\,\text{Malonyl CoA} + 14\,\text{NADPH} + 14\,H^{+} \xrightarrow{\text{FASN}} \text{Palmitate} + 7\,CO_2 + 8\,\text{CoA-SH} + 14\,NADP^{+} + 6H_2O$$

1.6. Fatty acid synthesis

The reaction starts with the attachment of acetyl group to the cysteine-SH site of the KS domain of monomer 1 (Figure 1.5) and the malonyl group to the pantetheine-SH of monomer 2 making it possible for the condensation reaction to produce β-acetoacetyl-S-pantethenyl derivative.

Figure 1.4 Schematic depiction of fatty acid synthase (FASN) enzyme complex.

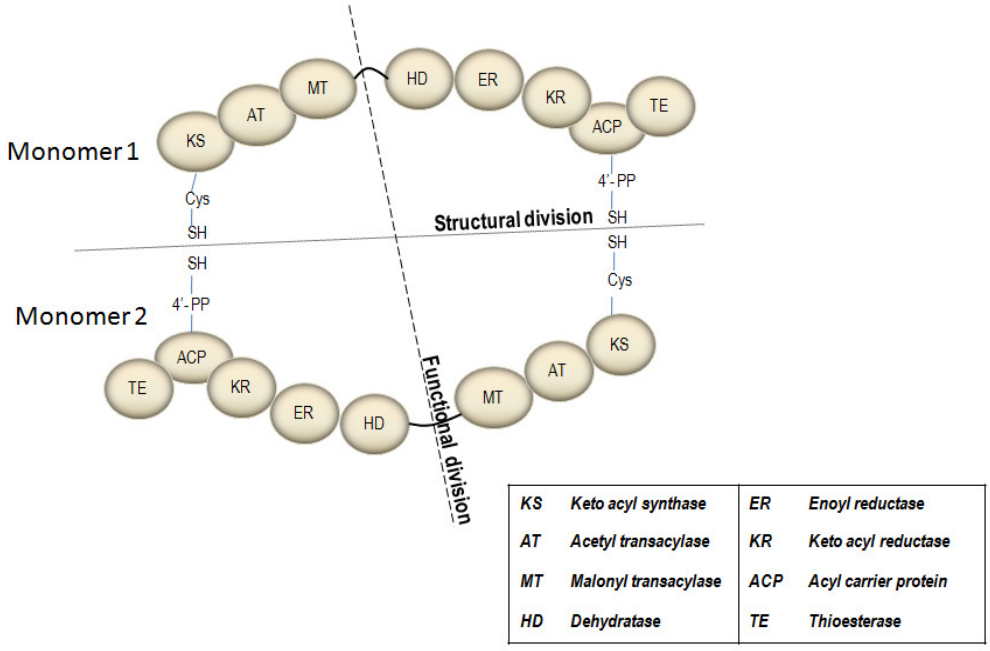

Figure 1.4: Schematic depiction of FASN enzyme complex: Presented with seven catalytic domains on both the monomers. The dotted line indicates the functional division of the enzyme where, if it is disrupted the enzyme is non-functional, whereas the structure of the enzyme is divided as monomer 1 and monomer 2 each having all the catalytic domains. Picture is adapted from Murray et al., Harper's Illustrated Biochemistry. USA: Mc Graw Hill Inc; 2003.

The cysteine-SH of the KS domain is reverted back to the free thiol state. Then it is reduced by the β-ketoacyl reductase in the presence of NADPH to the β-hydroxy butyryl derivative, which is then dehydrated by the dehydratase and reduced by enoyl reductase in the presence of NADPH to the butyryl derivative (Wakil, 1989).

This is then transferred to the cysteine-SH of the condensing enzyme in monomer I, thereby freeing the cysteamine-SH to accept a malonyl group from malonyl CoA. The butyryl and the malonyl groups condense to form a hexanoyl derivative as a final product. This whole process is then repeated five more times with the addition of C_2 unit to the acyl group finally yielding palmitoyl derivative which is then hydrolyzed by the thioesterase to form palmitic acid and cysteamine-SH (Figure 1.5).

The predominant product at the end of the reaction is palmitic acid and to a lesser extent stearic acid and myristic acid. The whole reaction takes place in the cytosol of the cell (Wakil, 1989). Figure 1.5 shows the reactions of fatty acid synthetic pathway.

1.6.1. A Historical Review of FASN molecule

Salih Jawad Wakil, the scientist behind fatty acid synthase, contributed the major part of his research to the understanding of fatty acid metabolism since the year 1950 till date. Wakil contributed several novel key findings on fatty acid oxidation and fatty acid synthesis mechanisms in a series of publications and short reports. Fatty acid oxidation was one of the other pathways that were studied by Wakil before his pioneering work on fatty acid synthesis. Among several reports, the isolation of the FASN enzyme as a crude extract from pigeon liver was noteworthy in which the properties of the extract were studied (Wakil et al., 1957). A more stable model of the purified enzyme was isolated from the chicken liver. With this extract the optimal conditions for the catalysis and cofactor requirements were optimised. The enzyme was extracted as four different fractions, which were all essential for the synthetic process. This study also determined that the palmitic, stearic and myristic acid were

the three main fatty acids synthesized by the enzymatic machinery (Teitz, 1957). Requirement of cofactors for the fatty acid synthesis process was then determined using the purified extract stated above. FASN requires Mn^{2+}, ATP, CoA, GSH, and isocitrate as cofactors for its activity.

The study also found the fact that acetate (the inactive form) is activated when it reacts with CoA in the presence of ATP and then forms the activated acetyl CoA (Porter et al., 1957). The participation of biotin in the synthetic process which does not involve the fatty acid oxidation enzymes was reported, which disproved a previous hypothesis that fatty acid synthesis involved the enzymes of fatty acid oxidation process (Wakil et al., 1958). The requirement of bicarbonate ions for the chemical reactions was also reported (Gibson et al., 1958).

Figure 1.5 Fatty acid synthesis pathway

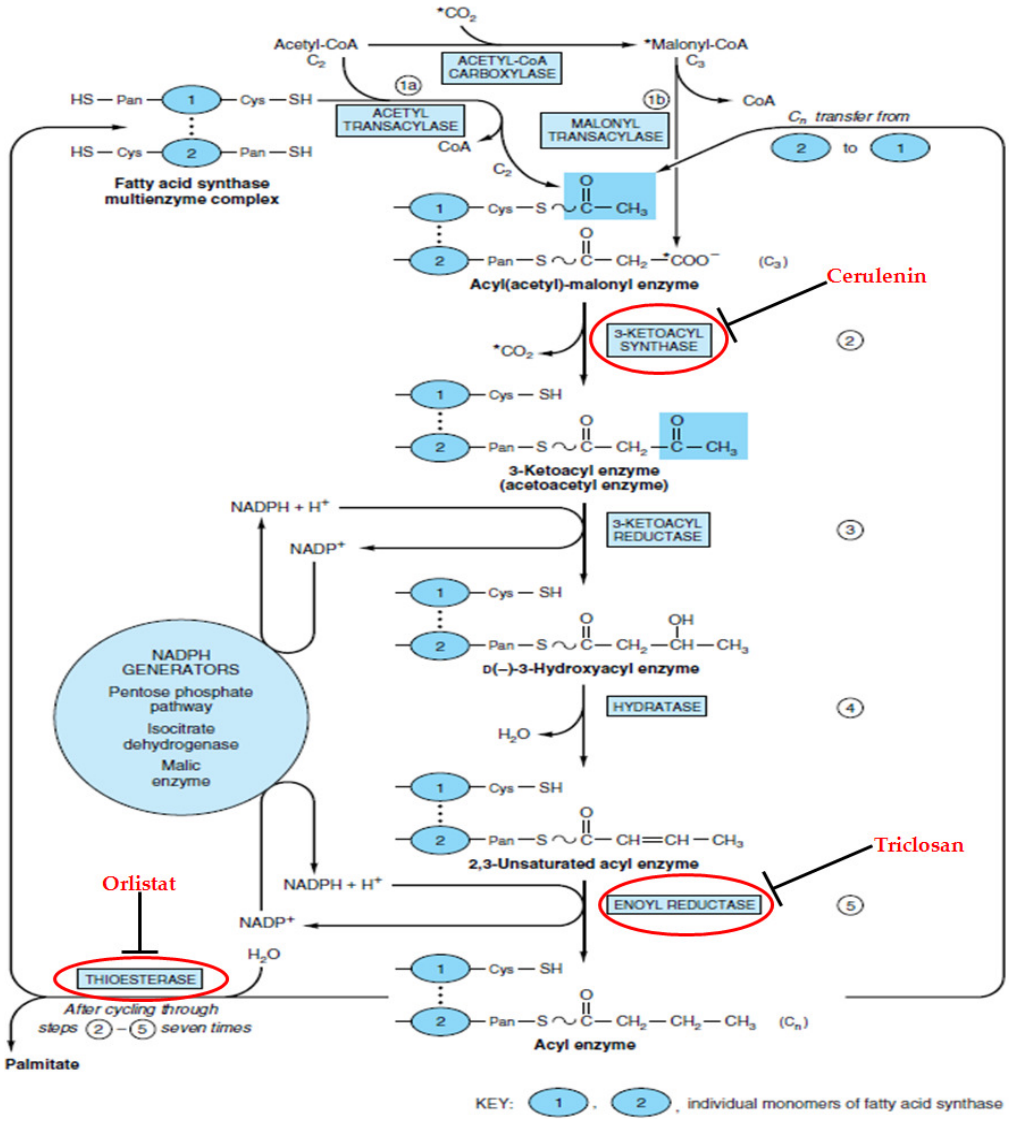

Figure 1.5: Fatty acid synthesis pathway: Fatty acid synthetic pathway chemical reactions are depicted along with the specific enzymes catalysing each step. The chemical inhibitors used under the current study are highlighted at their specific domain of action (This picture is adapted and modified from Murray et al., Harper's Illustrated Biochemistry. USA: Mc Graw Hill Inc; 2003).

1.6.2. Wakil's four classic reports on animal fatty acid synthase architecture

A series of four major findings of the animal fatty acid synthase architecture was reported in 1983. The first report was the proteolytic dissection and peptide mapping of the chicken liver fatty acid synthase by 24 proteases. These studies delineated the fact that the synthetase monomer is arranged into three major domains of molecular weight 127, 107 and 33 kDa. The sum of the fragments size generated after the proteolytic digestion corresponded to the size of the single monomer of the enzyme rather than the native enzyme. The existence of the enzyme as a homodimer, was thus evident for the first time from these results. The dimeric form of the enzyme is necessary for the inter-monomer co-operation for facilitating the condensation reaction. The dimers are arranged in a head-to-tail manner such that the active site cysteine –SH of the keto acyl synthase (KS) domain is closely juxtaposed with the phosphopantetheine-SH of the acyl carrier protein domain of the other monomer. The interaction between the KS and ACP domains thus constitutes the site of condensing activity. The molecular weight of the intact dimer was 267 (±5) kDa (Mattick et al., 1983a).

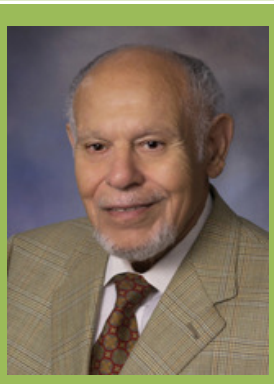

Salih J. Wakil., Ph.D

The second report demonstrated the results of chymotrypsin cleavage of the whole protein, which resulted in two fragments of molecular weight 230 and 33 kDa. The major fraction possessed all core catalytic activities required for the elongation of the fatty acid and the smaller fragment had the thioesterase activity. Amino acid sequence analysis proved that the thioesterase domain is located at the carboxyl terminus of the monomer (Mattick et al., 1983b).

Third finding was the identification of the β keto acyl reductase domain and its activity on the polypeptides generated after proteolytic digestion by 6 - 8 proteases.

This generated various fragments of size 15 – 94 kDa. The 94kDa fragment corresponded to the β-keto acyl reductase partial activity, which possessed an arginine at its active site. Another proteolytic fragment of size 36 kDa resulted from double digestion by kallikrein/subtilisin also corresponded to the β keto acyl reductase domain and activity. This domain contained phosphopantetheine prosthetic group of the acyl carrier protein that separates the KR domain from the TE domain and its location is found to be adjacent to the carboxy terminal thioesterase domain (Wong et al., 1983).

The fourth classic work showed the mapping of active centers and the mechanism of action of fatty acid synthesis. Key features of this paper is the identification of the location of ACP domain by the phosphopantetheine labeling studies, which was found to be at the end of the domain II adjacent to the thioesterase domain at the C-terminus. Both the reductases were found within the domain II, in which KR domain was identified by proteolytic cleavage and was found to be adjacent to (NH_2 terminal to ACP) ACP. The other reductase is the enoyl reductase domain which was identified by pyridoxal phosphate labelling studies as the enzyme was sensitive to proteolytic digestion. Location of acetyl/malonyl transacylase (AT/MT) was identified by binding of labelled acetyl CoA and malonyl CoA, and by their insensitivity to thiol reagent treatment due to the presence of active site serine residues. KS domain contains an active site cysteine residue and was identified by labelling studies using its reported inhibitor cerulenin. The dehydratase domain that remains unidentified was then assigned a position at the central portion of domain II, because logically the enzyme could be in between the reductase domains following the fatty acid synthesis reaction sequence (Tsukamoto et al., 1983).

This enzyme complex has different monomer division and functional division (Figure 1.4). The monomer 1 located at the amino terminal of the polypeptide chain has the β-keto acyl synthase, malonyl and acetyl transacylase activities. Monomer 2

contains enoyl reductase and dehydratase in addition to the KR and ACP active domains. The KS domain cysteine SH of monomer 1 is juxtaposed near to the cysteamine-SH of phosphopantetheine prosthetic group of ACP domain in the monomer 2. Even though each of the monomer has all the partial activities the functional unit consists of one half of one monomer interacting with the complementary half of the other monomer. This explains the requirement of the dimeric form of the lipogenic enzyme (Tsukamoto et al., 1983) (Figure 1.4).

Wakil's contributions on the understanding of fatty acid synthase structural organisation and its regulation contributed the major part for cancer therapeutic strategies targeting FASN. Having known the history of FASN, the following section elaborates the status of FASN-based management of various human cancers.

1.7. CHEMICAL INHIBITORS OF FASN

1.7.1. Cerulenin ($C_{12}H_{17}NO_3$)

Cerulenin is a potent non-competitive, irreversible inhibitor of FASN KS domain. Its chemical name is (2S, 3R) 2, 3-epoxy-4-oxo-7, 10-trans, trans-dodecadienamide. It is a natural product derived from the fungus *Cephalosporium caerulens.* Its molecular weight is 223.27. It binds covalently to the active site cysteine of the KS domain. Cerulenin's anti-proliferative effects were studied *in vitro* in various cancer cells (melanoma, cancers of the breast, colon, and prostate) (Ho et al., 2007; Liu et al., 2006; Pizer et al., 1998; Migita et al., 2009). The effect of cerulenin was limited, as it has a low chemical stability due to the presence of a highly reactive epoxide group. This reactive epoxy group interacts with other proteins and it affects processes other than FASN activity including palmitoylation (a post-translational modification allowing key signaling proteins to attach to the plasma membrane), cholesterol synthesis and/or proteolysis (Lawrence et al., 1999).

1.7.2. Cerulenin and its analogues

Cerulenin was chemically modified to a wide range of synthetic analogues, due to its low stability property. These are the first generation synthetic derivatives, a family of α- methylene -γ- butyrolactones that are named as C83, C81, C77, C75, C49, C73, and C271. Out of which C75 (trans - 4-carboxy-5-octyl-3- methylenebutyrolactone) (Figure 1.6) was exhibiting significant FASN inhibition. These analogues lack the reactive epoxide and are more stable than cerulenin. C75 treatment has been shown to induce significant anti-tumour activity in human breast cancer (Kuhajda et al., 2000), melanoma (Ho et al., 2007) and mesothelioma (Gabrielson et al., 2001) cell lines and xenografts. Later, C75 was reported to produce severe anorexia and weight loss by the fact that it induces carnitine palmitoyl transferase – 1(CPT-1) activity thus leading to increased β-oxidation of the synthesized fatty acids. Thus simultaneous FASN inhibition and activation of fatty acid oxidation leads to cellular starvation thereby leading to severe anorexia. Based on these findings several modifications of C75 led to the production of second generation synthetic derivative known as C93 which does not induce CPT-1 activation (Takahashi et al., 2004; Cha et al., 2005a).

Figure 1.6: Chemical structure of C75 ($C_{14}H_{22}O_4$; MW - 254.3)

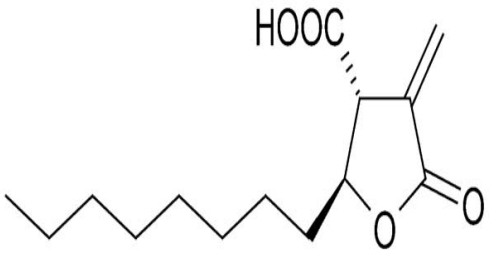

Cerulenin and C75 induced FASN inhibition is known to decrease the cyclin dependent kinase activities in cell cycle. Cerulenin and C75 induced cell death in A-375 melanoma cells by activating caspases and elevation of p21, was accompanied by cell cycle arrest at G2/M phase (Ho et al., 2007).

1.7.3. TRICLOSAN ($C_{12}H_7Cl_3O_2$; MW 289.5)

Triclosan is a lipid soluble broad spectrum antibiotic that has been widely used in soaps, toothpaste, deodorants, cosmetics etc. Its chemical name is 2, 4, 4- trichloro-2-hydroxydiphenyl ether (Bhargava & Leonard, 1996; McMurry et al., 1998). It acts as anti-bacterial by inhibiting the ER activity of the type II FASN in bacteria. Apart from its antibacterial activity it is also known for its anti-plaque and anti-inflammatory properties. Studies with breast cancer cells have shown the inhibition of type I mammalian FASN and in rat mammary tumours suggesting FASN to be a promising target for breast cancer chemoprevention (Liu et al., 2002; Lu & Archer, 2005).

1.7.4. ORLISTAT ($C_{29}H_{53}NO_5$; MW – 495.7)

Orlistat is a FDA approved anti-obesity drug. It is tetrahydrolipstatin a chemically synthesized derivative of lipstatin, a naturally occurring lipase inhibitor produced by *Streptomyces toxytricin.* It is marketed as Xenical™ by Roche S.p.A. (Milan, Italy). It acts by inhibiting the pancreatic and gastric lipases that are involved in the digestion of long chain triglycerides to form free fatty acids that are absorbed by the body. Thus it functions to prevent the fat absorption from the human diet, thereby reducing caloric intake. This provides a positive control over body weight. Its recommended therapeutic dose is 120 mg three times a day, which inhibits dietary fat absorption by about 30% (Ballinger & Peikin, 2002). The β- lactone ring of orlistat acts on the FASN by a nucleophilic attack on the active site serine of the TE domain (Kridel et al., 2004). The crystal structure of the human thioesterase (TE) domain complexed with orlistat is already available (2PX6), in which orlistat was captured in the catalytic triad. This structure now provides an excellent primer for the design of orlistat analogs and the *in silico* search for other backbone scaffolds (Kridel & Lowther, 2007).

1.7.5. NATURAL COMPOUNDS AS FASN INHIBITORS

Active ingredients from green tea have been shown to have significant anti-proliferative activity and apoptotic activity in *in vivo* & *in vitro* models of breast cancer. The green tea consumption has also shown to reduce the risk of breast cancers in Asian women. The various green tea polyphenolic compounds reported to have anti-cancer effects are – epigallocatechin gallate (EGCG), other plant derived flavonoids such as Luteolin, Taxifolin, Apigenin, Quercetin and Kaempferol (Figure 1.7). The biological activity of green tea is due to the presence of catechin and EGCG, the principal antioxidants that contributes 30% of total antioxidant capacity of green tea. The increased consumption of green tea has been related to its improved prognosis in breast cancer. EGCG inhibits the KR activity of FASN. Its galloyl moiety is indispensable for its anti-FASN activity. It resembles NADPH which is a co-factor in the fatty acid biosynthesis process. EGCG is the major compound that has been studied for anti-cancer activity which induces G1 phase arrest in the cell cycle and has been shown to reduce tumour size in animal models of breast cancer. The mechanism by which the other plant derived flavonoids act, has not yet been reported (Puig et al., 2008; Thangapazham et al., 2007).

Figure 1.7: Chemical structures of various green tea polyphenols (Kridel et al., 2007)

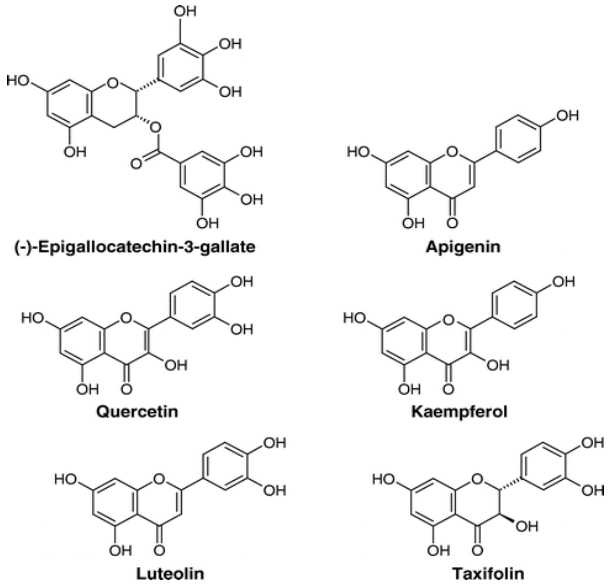

1.7.6. OTHER FASN INHIBITORS

1.7.6.1. VITAMIN D3

Vitamin D3 is reported to regulate the enzymes involved in fatty acid metabolism namely the FASN and the FACL3 (long chain fatty acyl CoA ligase 3) owing to its anti-proliferative effects in prostate cancer cell lines. Vitamin D3 activates the FACL3 which is involved in the conversion of free fatty acids to fatty acyl CoAs. The increased amounts of long chain fatty acyl CoA inhibits FASN by a feedback inhibition mechanism thus leading to growth inhibition and apoptosis (Qiaoa & Tuohimaa, 2004) (Figure 1.8).

Figure 1.8: Mechanism of vitamin D3 induced FASN inhibition (Qiaoa & Tuohimaa, 2004)

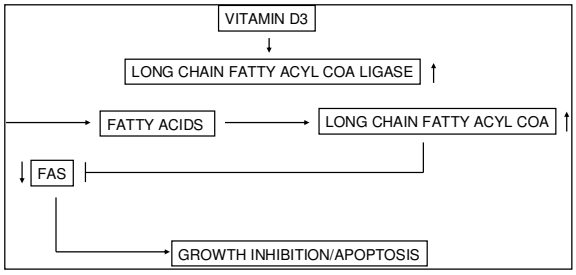

1.7.6.2. DUTASTERIDE

The prostate cancer cells develop resistance to apoptosis due to androgen independence. Dutasteride is a drug that is used for the treatment of benign prostate hyperplasia, which blocks the conversion of testosterone into active dihydrotestosterone in prostate. The effect of dutasteride in prostate cancer cell lines has been studied by microarray analysis, which showed a significant alteration of FASN mRNA and protein levels. The FASN inhibition led to apoptosis via activation of BNIP3, TNF-α pathway (Schmidt et al., 2007).

1.7.6.3. GSK837149A AND SKF-100601

GlaxoSmithKline R & D (Spain), screened about 5,50,000 compounds for their anti-FASN activity. Among all the compounds the SKF-100601 (that acts on the KR domain of FASN) was found to have significant FASN inhibition with an IC_{50} of 6.0. A chemical modification yielded a more effective derivative of SKF-100601 and is named as GSK837149A. (Figure 1.9) It forms a complex with the enzyme and acetoacetyl CoA. The activity of GSK837149A has been tested in HepG2 cells and human adipocytes. This compound has low cell permeability but still can be used as a model for designing new inhibitors for the KR domain (Vazquez et al., 2008).

Figure 1.9: Chemical structure of GSK837149A and SKF-100601 (Vazquez et al., 2008).

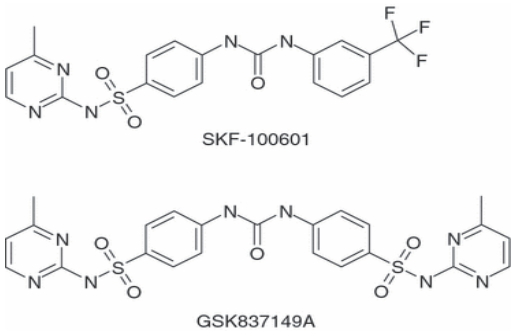

Among the various inhibitors that inhibit the specific catalytic domains of FASN, cerulenin (target: KS domain), triclosan (target: ER domain), and orlistat (target: TE domain) were evaluated for their anti-cancer effects in Y79 RB cells.

1.8. Chemical inhibition of FASN in cancer therapy

Having known about the various chemical inhibitors of FASN, this section explores the anti-cancer effects of these inhibitors on various cancer cell lines and xenografts models. Slade et al. reported the constitutive FASN protein expression and cerulenin treatment induced inhibition of FASN activity and protein expression, in pediatric cancer cell lines (Slade et al., 2003). Synergistic effects of FASN inhibition along with

conventional chemotherapeutic agent vinorelbine proved to be a newer therapeutic strategy for breast cancer therapy, which had enhanced cytotoxic effects (Menendez et al., 2004a). Cerulenin and C75 were found to retard the growth of melanoma cells by caspase 3 mediated apoptotic pathway accompanied by cell cycle arrest, which was evident from the elevation of p21 protein. The anti-proliferative activities of several FASN inhibitors cerulenin, triclosan, orlistat were compared in A-375 melanoma cells and found that the order of effectiveness in inducing cell death was cerulenin > triclosan > orlistat (Ho et al., 2007). Cerulenin and C75 were also reported to inhibit fatty acid synthesis activity, followed by DNA synthesis inhibition in colon carcinoma cells. However, the study also proved that DNA synthesis inhibition is not a direct effect and was recovered by viral oncogenes, suggesting a direct regulatory link between FASN and DNA synthesis (Pizer et al., 1998).

Triclosan inhibited the FASN II in a time- dependent manner present in *Plasmodium falciparum*, this interaction attains a stable conformation in its final stage of binding. Equilibrium binding studies suggested that triclosan undergoes a two stage binding process. The tight binding inhibitor interactions pave way for promising anti-malarial drugs against FASN II (Kapoor et al., 2004). This slow binding inhibitor also inhibited the partial activities of human and goose uropygial FASN enoyl reductase partial activity at 10 to 50μM concentrations. It also inhibits enoyl reductase partial activity of FASN in the breast cancer cells MCF-7 and SKBR3 at a similar dosage (Liu et al., 2002). Triclosan suppressed the FASN expression in the rat mammary tumour tissues and is reported to decrease the mammary tumour growth in Sprague-Dawley rats, suggesting FASN to be a promising target for breast cancer chemoprevention (Lu & Archer, 2005).

Orlistat was reported to halt the tumour cell proliferation by arresting the cell cycle at G1/S phase through the retinoblastoma protein pathway in breast cancer cells (Kridel et al., 2004). Apart from its anti-cancer effects, its FASN inhibitory action has

also been explored in the inhibition of endothelial cell proliferation and angiogenesis. It is reported to inhibit the neovascularisation during angiogenesis in human, involving VEGF and bFGF pathways. *In vitro* endothelial cell culture studies using human endothelial cells (HUVEC) showed that, orlistat inhibits angiogenesis selectively in proliferating HUVECs, thus suggesting its potential role in inhibiting angiogenesis in pathological states (Browne et al., 2006). The crystal structure of the human thioesterase (TE) domain complexed with orlistat is already available (2PX6), in which orlistat was captured in the catalytic triad. In this the human FASN TE domain was complexed with orlistat in two forms, an acyl-enzyme intermediate and the hydrolyzed product. The study had revealed the catalytic triad of Ser2308-His2481-Asp2338 (Pemble et al., 2007).

1.9. FASN Gene Silencing

Gene silencing is an epigenetic mechanism, that plays a major role in regulating gene expression, and the term is generally used to describe the 'switching off' of a gene by mechanisms other than genetic modification. Cellular components of gene silencing are:

1. Histones
2. dsRNA
3. Chromatin and heterochromatin
4. Dicer
5. MicroRNA
6. Transposon
7. siRNA

There are different types of gene silencing:

- Transcriptional gene silencing
- Post-transcriptional gene silencing
- Meiotic gene silencing

RNA interference is a conserved biological process, in which the double stranded RNA suppresses the expression of a target gene by triggering specific degradation of

the complementary mRNA sequence. It is defined as gene-silencing mechanism induced by double-stranded RNA; which can silence a gene expression at both transcriptional and post-transcriptional level. There are two types of small RNA molecules in this context; they are siRNA (small interfering RNA) and miRNA (microRNA). These small RNAs bind to the specific mRNAs and increase or decrease their activity, leading to prevention of formation of a protein from that mRNA.

Knowles & Smith, 2007 reported the genome wide changes accompanying the FASN knockdown by FASN siRNA. The inhibition of FASN was observed after 12 h of transfection and persisted till 48 h. A core set of 279 genes were differentially regulated with the FASN knockdown. Functional classification of genes revealed involvement of several pathways like cell survival, DNA replication/transcription, ubiquitin dependent protein degradation which implies the FASN inhibition mediated anti-tumourigenic activity. Gene set enrichment analysis revealed the pathways related to FASN inhibition such as fatty acid chain elongation and fatty acid metabolism. FASN controls cell division cycle evidenced by the regulation of checkpoint regulators CHEK2, WEE1 (WEE1 homolog) and PLK1 (polo like kinase 1) along with elevation of negative regulators of Rb pathway, demonstrating its regulation on G1/S transition. Up regulation of caspase 7 & 8 were observed indicating the apoptosis pathways. The differential expression of genes involved in various pathways were lipid metabolism, glycolysis, krebs-TCA cycle and oxidative phosphorylation pathways indicated that FASN plays major roles in tumour cell metabolism and in cell signaling (Knowles & Smith, 2007).

1.10. FASN INHIBITION AND SIGNALING PATHWAYS

1.10.1. FASN expression and PI3K/AKT pathways

FASN expression had a significant inverse correlation with the PTEN tumour suppressor gene in prostate cancer. The synergistic effects of the FASN siRNA and PI3- kinase inhibition have been reported to enhance the tumour cell death. This

result provides a strong rationale for exploring the therapeutic use of an inhibitor of the PTEN signaling pathway in conjunction with the FASN gene silencing in inhibiting prostate tumour growth (Bandyopadhyay et al., 2005). A recent study on epithelial ovarian cancers showed the inactivation of AKT on FASN gene silencing. Thus FASN acts as an upstream effector of AKT and its down regulation modulates the AKT mediated anti-apoptotic mechanisms. The FASN/AKT pathway mediated apoptosis induces caspase cascade and thus leads to cell death. Thus FASN/AKT pathway plays a key role in the pathogenesis of epithelial ovarian cancers (Uddin et al., 2011).

1.10.2. FASN silencing in HER-2/neu over-expressing breast cancer cells

The regulation of HER-2/neu expression and its relation with FASN have been studied by Menendez et al., 2004b. Silencing of FASN specifically down-regulated HER-2/neu mRNA expression and PEA3 (the transcriptional repressor of HER2), was up-regulated. FASN silencing caused the cytoplasmic accumulation of the HER2 protein p185. The simultaneous inhibition of FASN and HER-2/neu with chemical inhibitors showed synergistic cytotoxicity in HER-2/neu over-expressing breast cancer cells. Similar changes were observed when FASN and HER2 genes were silenced with specific siRNAs and this also synergistically increased the apoptotic cell death in HER2 over expressing breast cancer cells. Thus FASN actively plays a role in regulating the oncogenic proteins like HER-2/neu. This also suggests that HER-2/neu oncogene acts as a molecular sensor of energy imbalance after FASN inhibition (Menendez et al., 2004b).

1.10.3. Inhibition of FASN and association with c-Met kinase

In a recent study the expression of FASN in diffuse large B-cell lymphoma (DLBCL) was reported and 62% of the tumours showed FASN positivity. The FASN expression was correlated with tumours with high proliferative index. Significant

association was found between tumours expressing high FASN and c-Met tyrosine kinase and p-AKT. FASN chemical inhibition and FASN gene silencing triggered apoptosis and suppressed c-Met kinase expression in DLBCL cell lines. This shows the link between c-Met kinase and FASN. Synergistic effects on simultaneous targeting of FASN and c-Met was observed, which was evident by apoptosis of DLBCL cell lines. Thus FASN plays a critical role in the carcinogenesis of DLBCL via c-Met tyrosine kinase (Uddin et al., 2010).

1.10.4. FASN mediated drug resistance

FASN was found to be over-expressed in a drug resistant breast cancer cell line. Studies with FASN gene silencing and chemical inhibition by orlistat showed that these drug resistant cells became sensitive to drug mediated apoptosis. The same studies when conducted in the mammary epithelium, it did not show any sensitivity to drug action on FASN inhibition. FASN mediated drug resistance could be attributed to the presence and production of increasing amounts of palmitate (Liu et al., 2008).

1.10.5. FASN siRNA and lipid membrane partitioning

The fate of newly synthesized lipids in cancer cells are not studied extensively. This report has estimated the contribution of FASN to the synthesis of specific lipid classes by treating the cells with FASN siRNA. The FASN inhibition in prostate cancer cells largely decreased the synthesis of phospholipids partitioning into detergent resistant membrane micro domains. The raft-aggregates are implicated in key cellular processes including signal transduction, intracellular trafficking, cell polarization, and cell migration (Swinnen et al., 2003).

1.10.6. Synergistic cytotoxic effects of FASN siRNA and taxol in breast cancer cells

In breast cancer cell lines FASN siRNA treatment synergistically induced cytotoxicity along with Taxol™ treatment. SK-Br3 and multi-drug resistant MCF-7/AdrR cells were transiently transfected with FASN siRNA. This showed hypersensitivity to Taxol™-induced apoptotic cell death. Thus FASN blockade augments the cytotoxicity of anti-mitotic drug Taxol™ against breast cancer cells and that this chemo sensitizing effect is schedule-dependent. Under these conditions the alternate activation of both the pro-apoptotic p38 MAPK-p53 signaling and the cyto-protective MEK1/2, 3 & ERK1/2 cascade, as well as the inactivation of the anti-apoptotic AKT activity explains the enhancement of Taxol™-induced cytotoxicity that follows inhibition of FASN activity in breast cancer cells (Menendez et al., 2005a).

1.11. REGULATION OF LIPID METABOLISM IN NORMAL AND CANCER CELLS

1.11.1. Lipids in normal physiology

Lipids are the most important bio-molecules that are involved in various biochemical/biological functions: production of myelin in nervous system, surfactant in lungs, milk lipids during lactation. They form the major building blocks of membranes that separate the cellular content from the external environment, to compartmentalize many vital functions of the cell. They serve as anchors for several proteins targeting to membranes. Lipids serve as the important energy source in the human body; they also act as signaling molecules. Lipids are mostly derived from the diet and they are further modified and stored and released by liver and adipose tissue.

Lipids are carried as lipoprotein complexes (water soluble), which contains a hydrophilic surface of free cholesterol and phospholipids and a hydrophobic internal core containing the triglycerides and cholesteryl esters. These lipoprotein

complexes are hydrolysed by lipoprotein lipases, which results in release of free fatty acids. The fatty acid binds to albumin for their circulation and utilization throughout the body. The fatty acids are used for phospholipid synthesis (major constituent of membrane), triglyceride synthesis and esterification of cholesterol (storage), energy production by beta oxidation, acylation of proteins during post-translational modification (Singh & Costello, 2009).

In addition to the lipid uptake from the diet, the normal cells can synthesize lipids *de novo*. The glucose is the main carbon source for the lipid synthesis where the glucose is converted to pyruvate, and then to citrate during the Kreb's cycle in the mitochondria. The citrate re-enters the cytoplasm through the citrate – malate anti-port system, which is then converted to acetyl CoA through the action of the enzyme ATP citrate lyase. The acetyl CoA is then used up by the lipogenic enzyme fatty acid synthase (FASN) to synthesize fatty acids and further modified by HMG CoA synthase and reductase enzyme in the cholesterol synthesis pathway to mevalonate and then to cholesterol. During human embryonic development there is active fatty acid synthesis *de novo*. After development, in the adult stage the expression and activity of these enzymes reduces depending upon the specific functions and conditions [e.g. lungs (surfactant production), lactating breast (milk lipids), and cycling endometrium (during proliferation stage)]. Liver and adipose tissue convert the excess carbohydrates to fatty acids and stored as triglycerides in adipose tissue (Singh & Costello, 2009).

1.11.2. Regulation of lipid synthesis in non-neoplastic cells

Diet rich in carbohydrate lead to the stimulated synthesis of lipids and glycolysis. The genes involved in the process are glucokinase, pyruvate kinase, ATP citrate lyase, acetyl CoA carboxylase (ACC) and fatty acid synthase (FASN) regulated by modulation of their transcription rates and the enzymes are regulated by post-translational and allosteric mechanisms. These genes have the carbohydrate

responsive elements in their genes for their transcriptional regulation. The synthesis of fatty acids from glucose is nutritionally regulated by insulin. The transcription of the FASN and ACC genes is induced by insulin's action on SREBP1c, which binds to the sterol regulatory elements (SRE) sequence in the promoter region of these lipid metabolic genes. The synthesized fatty acids are partitioned into different lipids and also stored as triglycerides. In addition to SREBP1c, another member of the regulation machinery was identified, which is a basic helix-loop-helix/leucine zipper (bHLH/LZ) transcription factor called as carbohydrate-responsive element-binding protein (ChREBP). ChREBP is identified as an important transcription factor that mediates the glucose induced transcription of genes involved in lipogenesis (FASN, ACC) and the liver-pyruvate kinase (L-PK). When the glucose level rise, the ChREBP translocates to the nucleus with the help of protein phosphatase 2A-δ and then controls the gene transcription of the target genes.

The liver X receptors (LXRs) is the steroid hormone superfamily of receptors, which regulate gene expression upon ligand binding. LXRs form heterodimers with the retinoid X receptors (RXRs) and also can regulate gene expression individually by binding oxysterols (e.g. 22R-hydroxycholesterol) or 9-cis-retinoic acid. LXRs are also important regulators of the lipogenic pathway. ChREBP gene is a direct target of LXRs, where glucose activates LXRs by binding to ChREBP (Singh & Costello, 2009).

1.11.3. Regulation of FASN expression

FASN expression is generally regulated by the carbohydrate levels. During fasting FASN levels decrease in the liver, but during feeding the hepatic FASN protein levels increases. FASN expression is enhanced by various agents both nutritional and hormonal: glucose, high fat diet, dietary PUFAs, thyroid hormone, low sterol levels, insulin, glucocorticoids and progesterone increases FASN protein levels. Glucagon, leptin and cyclic AMP decrease the FASN protein levels. Studies on regulatory mechanisms of transcriptional control of FASN expression have

identified major regulatory elements in the FASN promoter, most of which are located within first 100 nucleotides of the 5' end. It also has an insulin responsive element (IRE) and an E-box in which the upstream transcription factors 1 & 2 binds, which is not regulated by the diet. The same region is also an important sterol regulation site for FASN. The SREBP binding sites flanking the E-box is an important regulatory site mediated by sterols. The human FASN gene contains two promoters and the second promoter competes with the first promoter, thus serving as a negative element. FASN is regulated both at the transcriptional level and at the translational levels in response to nutrients and hormones (Semenkovich, 1997).

SREBPs play a major role in the regulation of FASN mRNA transcription regulation on the FASN promoter. This pathway is a common mediator of nutritional, hormonal and growth factor mediated induction of FASN mRNA transcription both in normal as well as cancer cells. Hormone sensitive tissues like breast, cycling endometrium, lungs of foetus and lipogenic liver and adipose tissues respond to hormone (estrogen, progesterone, androgen) and nutritional signals (glucose, dietary fatty acids) and modify the expression and/or maturation of SREBP1c through the PI3K/AKT and the MEK/ERK1/2 pathways (Menendez & Lupu, 2007). The trigger for the tumour cells arises from the hyper-activation of growth factors/ growth factor receptors and defective functions of signaling cascades. Tumour associated FASN is generally insensitive to nutrient signals. pSREBP1c is an inactive form of the SREBP1c, which is anchored to the endoplasmic reticular membrane. SCAP is the SREBP cleavage activating protein that forms a complex with pSREBP1c and releases active SREBP1c. When the demand for fatty acids rises, pSREBP1c-SCAP complex exits the ER and goes into the golgi complex, where it is acted upon by site-1 protease (S1P). This cleavage breaks pSREBP1c into two halves, which is still bound to the membrane. Site-2 protease (S2P) cleaves the N-terminal half of SREBP1c, and then it releases the cytoplasmic portion of the SREBP1c, which travels to the nucleus and transcribes FASN (Menendez & Lupu, 2007).

1.12. REGULATION OF FASN mRNA AND PROTEIN

1.12.1. Transcriptional regulation of FASN expression

FASN transcription is induced by transcription factor specificity factor (Sp1) and the nuclear factor Y (NF-Y) which occurs through the SREBP1c. The X-box binding protein (XBP-1) increases FASN promoter activity independent of SREBP1c. Another important mediator of FASN gene transcription is ChREBP which is via the glucose mediated activation of lipogenesis. ChREBP binds to ChRE carbohydrate response elements in the FASN promoter and induces the FASN gene transcription. Glucose induces ChREBP activation and translocation, while poly unsaturated fatty acids and cAMP inhibits ChREBP activation. Apart from the direct activators the liver X receptors (LXRs) activates the FASN gene transcription indirectly by binding to the LXR elements (LXREs) in the SREBP and ChREBP promoters to induce their activation, so as to bind to FASN promoter and activate FASN transcription. Insulin response elements (IREs) in the FASN promoter are necessary for the insulin mediated activation of FASN transcription (Jensen-Urstad & Semenkovich, 2012).

1.12.2. Translational regulation of FASN expression

FASN mRNA and protein levels are quite stable, in which the sudden changes like increased transcription and translation are being dealt within a regulated fashion. Therefore the protein levels of FASN take hours to reflect the changes in the transcriptional regulation. FASN protein changes in some reports do not correlate with the FASN activity inhibition. Many cancer cells have shown changes in FASN mRNA expression without corresponding changes in the FASN protein levels. In liver, adipocytes and in cancer cells the phosphorylation of FASN by an intermediate kinase step has been reported to regulate the FASN protein levels. Phosphorylation at the serine, threonine, and tyrosine residues in the FASN protein have been reported as the modification of FASN at these amino acid residues. Changes in FASN activity in cancer cells in this context did not correlate with the FASN protein

levels. Apart from phosphorylation, acetylation of lysine residues is reported to be a novel controlling mechanism of FASN protein. The interaction of FASN with the HER2 (epidermal growth factor receptor 2) occurs in its phosphorylated state, where the FASN activity is in an induced state (Jensen-Urstad & Semenkovich, 2012).

1.13. Mechanisms of FASN inhibition mediated apoptosis of cancer cells

Several mechanisms have been proposed (Menendez & Lupu, 2007) for the induction of apoptosis mediated by FASN inhibition by chemical inhibitors and by RNA interference. They are:

1. End product starvation
2. Disturbance of membrane function (lipid rafts)
3. Accumulation of malonyl CoA (toxic substrate)
4. Inhibition of anti-apoptotic proteins
5. Inhibition of DNA replication
6. p53 regulated non-genotoxic metabolic stress
7. Peroxidative mechanisms

1.13.1. End product starvation

Cancer cells are dependent on *de novo* fatty acid biogenesis for their survival and proliferation. Addition of palmitate in the fatty acid free media reverses cerulenin mediated cytotoxicity in HL60 promyelocytic leukemia cells in a dose dependent manner. The cytotoxic effects of FASN inhibition associated decreased phospholipid synthesis is evident from the decrease in DNA content and increased apoptotic cell death. These findings provide the importance of FASN catalysed phosphatidyl choline to the extensively dividing tumour cells for their high membrane turnover. There is another notion that some of the cancer cells did not get rescued from the FASN inhibition mediated cytotoxicity, even in the presence of exogenous palmitate. The possible explanation for these findings was the involvement of other biochemical mechanisms (Pizer et al., 1996a).

1.13.2. Disturbance of membrane function

FASN synthesized phospholipids in cancer cells are partitioned into detergent resistant membrane microdomains, which are known to involve in signal transduction, intracellular trafficking, cell polarity, formation of membrane protrusions, and migration. FASN siRNA treatment in prostate cancer LNCaP cells, showed a significant 2.5 fold reduction in the label of the raft fraction compared to a 1.2 fold decrease in the non-raft fraction. Among all the lipids, phospholipids are largely affected by the altered FASN activity, and they are partitioned into the lipid raft fraction. These observations suggest the potential role of FASN in maintaining the membrane functions (Swinnen et al., 2003).

Figure 1.10: Mechanisms involving FASN inhibition mediated apoptotic cell death
Ref: Menendez & Lupu, 2007

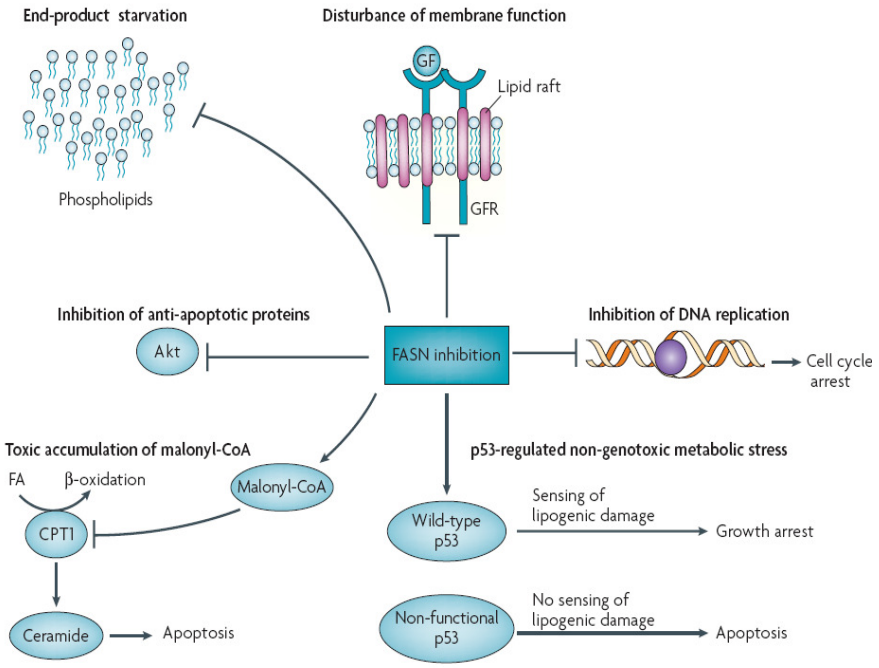

Figure 1.10: Mechanisms involving FASN inhibition mediated apoptotic cell death: Schematic representation of various mechanisms involved in FASN mediated apoptotic cell death. Figure adapted from Menendez & Lupu, 2007

1.13.3. Accumulation of malonyl CoA (toxic substrate)

Apart from the end product starvation, FASN inhibition also led to substrate accumulation which was evidently cytotoxic to the cancer cells. This was proved by several studies. FASN inhibition by cerulenin and C75 increased the malonyl CoA levels rapidly, but 5-(tetradecyloxy)-2-furoic acid (TOFA inhibitor of acetyl CoA carboxylase) reduced the malonyl CoA accumulation by 60%. Inhibition of ACC alone by TOFA was not cytotoxic. Comparing the cytotoxic effects by both these mechanisms showed that FASN inhibition to be cytotoxic and ACC inhibition did not induce cytotoxicity. Simultaneous inhibition of FASN by cerulenin/C75 and ACC by TOFA significantly reduced apoptotic cell death in breast cancer cells. Thus the accumulation of unused FASN substrate malonyl CoA, is reported to induce cytotoxicity in FASN inhibitor treated breast cancer cells and in xenografts models (Pizer et al., 2000).

1.13.4. Inhibition of anti-apoptotic proteins

Evaluation of the mechanisms behind the induction of cytotoxicity on co-exposure of C75 (FASN inhibitor) along with Taxol (microtubule interfering agent) showed cytotoxic effects on breast cancer cells. Sequential exposure of C75 and Taxol were cytotoxic to breast cancer cells in a schedule dependent manner. Apart from several other explanations for these effects, the blockade of AKT signaling activity was very prominent. Breast cancer cells treated with increasing dosages of C75 for 24 h with and without Taxol™ showed significant inhibition of phosphorylation of the pro-survival kinase protein AKT at the Ser473. The Ser473 is critical site for the activation of the AKT signals. Thus FASN inhibition enhanced apoptosis in breast cancer cells by blocking the anti-apoptotic AKT pathway (Menendez et al., 2005a).

1.13.5. Ceramide mediated apoptosis

FASN inhibition induced cell death accompanied up-regulation of several pro-apoptotic genes significantly using apoptosis specific microarray analysis. The genes were BCL2/adenovirus E1B 19 kDa protein-interacting protein 3 (BNIP3), tumour necrosis factor–related apoptosis-inducing ligand (TRAIL), and death-associated protein kinase 2 (DAPK2). Malonyl CoA accumulation leads to inhibition of carnitine palmitoyl transferase -1 (CPT-1). Inhibition of CPT-1 leads to accumulation of ceramide. The specificity of malonyl CoA in inducing ceramide accumulation was ascertained by inhibiting acetyl CoA carboxylase, which synthesizes malonyl CoA, during which the ceramide accumulation diminished. Also CPT-1 inhibitor etomoxir, led to ceramide accumulation and eventually cell death in breast cancer cells. Further studies with direct addition of C2-ceramide to the cultured breast cancer cells showed BNIP3 accumulation and ceramide synthase inhibitor, inhibited the BNIP3 induction. Thus, siRNA based specific inhibition of FASN leads to accumulation of malonyl CoA, inhibition of CPT-1, and accumulation of ceramide. These results show the involvement of ceramide in FASN mediated apoptotic cell death (Bandyopadhyay et al., 2006).

1.13.6. Inhibition of DNA replication

FASN inhibition by cerulenin accompanies inhibition of DNA synthesis concurrently. FASN synthesis inhibition occurred after 30 min of inhibitor treatment and DNA synthesis inhibition was observed after 90 min along with blockage of S phase progression. Cerulenin's DNA synthesis inhibition was however an indirect effect as the DNA damage was rescued by viral oncogenes (Pizer et al., 1998). Orlistat and FASN specific siRNA mediated inhibition of FASN activity, led to blockade of cell cycle at the G1/S phase transition, and reduced phosphorylation of Retinoblastoma (Rb) protein which governs the $p27^{kip1}$ (negative regulation of cyclin dependent kinases). FASN inhibition was also accompanied by increased levels of

$p27^{kip1}$ and reduced levels of SKP2 (S-phase kinase associate protein – 2; negative regulator of cell cycle) which is an E3 ubiquitin ligase that degrades $p27^{kip1}$ (Knowles et al., 2004). These findings provide the link between FASN and ubiquitin mediated proteolysis of cell cycle related proteins. C75 mediated FASN inhibition led to cytotoxic effects were attributed to malonyl CoA accumulation (substrate accumulation). In addition to this, C75 treatment also caused induction of apoptosis in MCF-7 breast cancer cells during S-phase progression as evident by BrdU and TUNEL labeling studies.

C75 inhibits FASN while it is also involved in induction of fatty acid oxidation by carnitine palmitoyl transferase (CPT-1), during which the cytotoxicity is believed to be malonyl CoA dependent. C75 induced apoptosis during S phase, was attributed to the decrease in production of phospholipids. Application of TOFA (inhibitor of ACC) before C75 treatment, blocked C75 induced apoptosis, but etomoxir (inhibitor of CPT-1) treatment did not. Thus CPT-1 does not play role in malonyl CoA mediated cytotoxic response and that cytotoxicity induced by C75 implies the pro-apoptotic role of malonyl-CoA independent of CPT-1 (Zhou et al., 2003).

1.13.7. p53 regulated non-genotoxic metabolic stress

p53 is generally known to induce growth arrest and apoptotic cell death. Non-genotoxic metabolic stress responses attributed to the p53 protein are hypoxia, acidosis, and disturbed protein and RNA synthesis. The DNA damage associated with FASN inhibition is an indirect effect on the cancer cells. The p53 status decides whether FASN inhibition in the cancer cells will cause cell growth arrest or apoptosis. Cells with intact p53 survive more against the malonyl CoA cytotoxicity, than the cells with the mutant p53. FASN inhibition in RKO colon cancer cells at 4 and 8 h treatment led to reduction of cyclin dependent kinase activities and at 16 h and 24 h the accumulation of p53 and p21 proteins and growth arrest in G1 and G2 phase were observed. RKO colon cancer cells with a dominant negative mutation of

p53 were sensitive to malonyl CoA cytotoxicity. Thus FASN inhibition was cytotoxic to cancer cells due to malonyl CoA and this cytostatic effect of p53 status is independent of malonyl CoA mediated cytotoxic effects. FASN inhibitors can thus be explored as therapeutic targets for cancers carrying p53 mutations (Li et al., 2001). Studies conducted with breast cancer cells with MCF-7 cell line which had intact p53 pathway indicated that, the status of p53 was the determining factor for induction of growth arrest or apoptosis, in which case after the perturbation of FASN, p53 functions to sense the energy imbalance (Menendez & Lupu, 2005).

1.13.8. Peroxidative mechanisms

FASN gene silencing with FASN specific siRNA resulted in a time dependent increase in intracellular reactive oxygen species (ROS) levels in LNCaP prostate cancer cells tested by increase in DCFH-DA staining by flow cytometry. The elevated ROS levels were reversed by the addition of palmitate to these cells. Thus depletion of palmitate is the sole reason for apoptotic cell death. Palmitate protects the cells from diffusion of ROS from the altered mitochondrial membranes out of the mitochondria (Migita et al., 2009). Another study with FASN and ACC gene silencing in breast carcinoma cell lines showed apoptotic cell death induced by increased production of ROS, and addition of α-tocopherol that scavenges free radicals decreased the ROS production. Thus palmitate depletion induced apoptosis in breast cancer cells, which involved the ROS production and mitochondrial impairment (Chajès et al., 2006).

Zecchin et al., 2011 investigated the mechanisms mediating apoptotic cell death of melanoma (B16-F10) cells, when treated with FASN inhibitors cerulenin and orlistat. Apoptosis was preceded by increase in the intracellular levels of ROS and cytosolic calcium concentrations. During FASN inhibition with orlistat, oxidative stress was evident and both cerulenin and orlistat induced cytosolic calcium levels. The involvement of mitochondria was evident by the release of cytochrome c and

activation of caspase-9 and -3. In addition, the apoptotic effects were independent of p53 and mitochondrial permeability transition (Zecchin et al., 2011).

1.14. FASN and other human diseases

Apart from the enormous work on role of FASN in human cancers, this metabolic enzyme has gained importance in other metabolic disorders as well. FASN expression is tightly regulated by hormones and nutritional signals. Expression of FASN in non-neoplastic cells is high only in certain tissues with high metabolic turnover such as liver, and adipose tissue. Metabolic disorders involving impaired liver function can thus be studied with respect to the function of FASN. The importance of FASN in diabetes mellitus and other diseases are discussed below.

1.14.1. FASN and Diabetes mellitus

FASN catalysis and lipogenesis in hypothalamus has important effects on food intake and body weight homeostasis. Liver specific FASN-knockout mice fed with a low fat/high carbohydrate diet for 4 weeks developed hepatic steatosis due to the reduction in β-oxidation, with a 3-fold increase in malonyl CoA levels in the liver. This effect was also accompanied by ketone body formation in the blood. These studies also led to novel finding of activation of peroxisome proliferator activated receptor α (PPARA) which in turn enhances the β-oxidation (Menendez et al., 2009).

FASN in the endothelial cells is regulated under diabetic conditions. FASN is required by the endothelial nitric oxide synthase (eNOS) for its palmitoylation and the absence of FASN in the endothelium led to abnormal angiogenesis and inflammation. These studies propose that FASN and eNOS contributes together for the vascular complications in diabetes and metabolic disorders. Thus FASN plays a significant role in protecting the vasculature and such studies may help in improving the vasculature in metabolic disease (Wei et al., 2011).

1.14.2. FASN: Biomarker for insulin resistance

Obesity due to its high prevalence in the community, has emerged as a diagnostic challenge, as obese patients are highly prone to risk of developing type 2 diabetes mellitus and cardiovascular diseases. Metabolic biomarkers that reflect the risk of this obesity related complications are urgently needed in order to manage the problem. Lipid metabolism is as important as the carbohydrate metabolism in diabetic individuals. Lipogenesis is tightly regulated by hormones, in which insulin is an important stimulator of FASN. Under insulin resistance FASN is markedly inactivated. Thus a biomarker that is related to lipogenesis especially FASN would be more informative in the context of level of impairment of insulin sensitivity and metabolic stress.

FASN being an intracellular protein that is over-expressed in cancers is also detected in the extracellular space of cancer cells. The excess amounts of FASN expression that is present in tumour cells beyond their metabolic needs are secreted to the extra cellular space by these cells, under severe metabolic stress. FASN may be explored as a biomarker for insulin resistance. Obesity induced insulin resistance is characterised by impaired glucose uptake by cells (glucopenia), impaired lipogenesis in adipose tissue (increased secretion of FASN in the circulation).

Studies with obese patients revealed that individuals with impaired glucose tolerance had the highest levels of serum FASN. A significant relationship between severe insulin resistance and elevated FASN levels in circulation was observed. As the circulating FASN levels increased, their intracellular levels decreased. Improving the insulin sensitivity by diet control, physical exercise and weight loss reversed the levels of FASN in circulation.

The key findings reported by Fernandez-Real et al., 2010 were:

1. Relationship between severe insulin resistance and FASN levels

2. Circulating FASN levels is inversely associated with adipose tissue FASN expression
3. Decreased circulating FASN levels correlated with improved insulin sensitivity and metabolic control
4. Plasma FASN levels is a good biomarker for insulin sensitivity in context of metabolic stress (Fernandez-Real et al., 2010).

1.14.3. FASN and non-alcoholic fatty liver disease (NAFLD)

The patho-physiology of non-alcoholic fatty liver disease (NAFLD) can be understood by modulating the levels of liver FASN. In NAFLD patients, the hepatic mRNA expression of genes such as FASN and the fructokinase (involved in fructose metabolism) were increased. In another study with NAFLD patients, FASN mRNA levels were determined in primary hepatocytes, which revealed significant elevation of FASN and which also correlated well with the degree of steatosis. Similar observation was also found in mouse models and in liver of NAFLD human subjects. Increased FASN levels were also accompanied by increased SREBP1c levels, which are the prime transcriptional regulator of FASN, both in *in vivo* and *in vitro* studies. Thus during hepatocellular lipid accumulation, FASN expression increases and is regulated at the transcriptional level through SREBP1c. However the histological inflammation status of hepatocytes did not correlate with the FASN expression. This may also be explained in the other way that under such conditions lack of FASN increase in NAFLD predisposes to hepatic inflammation. In addition, it is also true that under certain nutritional conditions, lack of FASN may lead to liver injury. Esterification of *de novo* synthesized fatty acids to triglycerides is thus considered a safety mechanism of the tissues, where they prevent the harmful effects of mitochondrial oxidation and generation of reactive oxygen species (ROS) by the accumulating fatty acids. FASN expression elevation in steatohepatitis is considered as an adaptation of the hepatocytes at the early stages of NAFLD and non-alcoholic steatohepatitis (Dorn et al., 2010).

With the knowledge of FASN structure, its chemical inhibitors and its regulatory mechanisms in both cancer cells and normal cells, this study evaluates the biochemical and molecular role of FASN in RB tumour tissues and in cultured RB cells.

CHAPTER 2: DISSERTATION OUTLINE AND RESEARCH OBJECTIVES

Retinoblastoma is a primary intra-ocular malignant tumour of the developing retina that occurs during childhood. The disease is fatal if left untreated. In the United States of America, the childhood cancers represents 1% of new cases diagnosed every year and RB accounts for 3% of childhood cancers (Cancer Facts & Figures 2012, American Cancer Society). In the Indian sub-continent the RB present with aggressive tumour biology and most of them are diagnosed only during the advanced stage of disease (Suryavanshi et al., 2011). The disease can be managed by several treatment modalities depending upon the invasion status and the laterality of the tumour (Biswas et al., 2003).

Treatment strategies for RB are several depending upon the systemic status, size and location of the tumour. Chemotherapy and enucleation are two of the several treatment options for the disease. The ultimate aim is to save the child, and to an extent the eye and his/her vision. As a general rule, cancer therapy is accompanied by toxic side effects (Shields & Shields, 1999). Pediatric cancer patients also suffer with late treatment effects such as impairment of function of specific organs and development of secondary cancers (Cancer Facts & Figures 2012. American Cancer Society). Chemotherapy associated toxic effects on the surrounding normal cells occurs both in an acute (during the chemotherapy) and chronic manner (after the chemotherapy-late effects). Novel anti-cancer molecular targets for treating cancers are emerging rapidly. The novel markers studied in RB are fatty acid synthase (FASN) (Camassie et al., 2003; Vandhana et al., 2011), epithelial cell adhesion molecule (EpCAM) (Krishnakumar et al., 2004), and multi-drug resistance protein 1 (MRP1) (Mallikarjuna et al., 2010).

Cancer therapy targeting the body's energy metabolic pathways and its key genes are emerging. Glucose metabolism and lipid metabolism are the pathways of current

importance. Lipid metabolic genes such as acetyl CoA carboxylase (ACC) (Thupari et al., 2001; Wang et al., 2009), HMG CoA reductase (HMGCR) (Gan et al., 2008), and fatty acid synthase (FASN) (Menendez & Lupu, 2007; Camassie et al., 2003) have been given importance for the targeted therapy for cancer, using various cancer cell lines and xenografts models. This lipogenic enzyme is a multi-enzyme complex that comprises seven catalytic domains, each domain catalysing a specific function during the synthesis of the 16-carbon fatty acid palmitate. Chemical inhibitors targeting specifically the catalytic domains of the microbial FASN II, have been used for anti-bacterial (Omura, 1976) and anti-malarial therapy (Surolia & Surolia, 2001). This inhibition strategy is explored for cancer therapy, as the human cancers over-expresses this lipogenic enzyme.

This dissertation explores the potential of targeting FASN in RB management. Experimental investigations were carried out in the following clinical samples and cultured cells:

(i) Clinical RB tumour tissues and donor retinal tissues

(ii) Cultured *in vitro* cancer cells [MCF-7 (breast cancer cells) and Y79 (retinoblastoma cells)] and non-neoplastic cells [3T3 (mouse embryonic fibroblasts and MIO-M1 (muller glial cells)].

Figure 2.1 Outline of present dissertation research

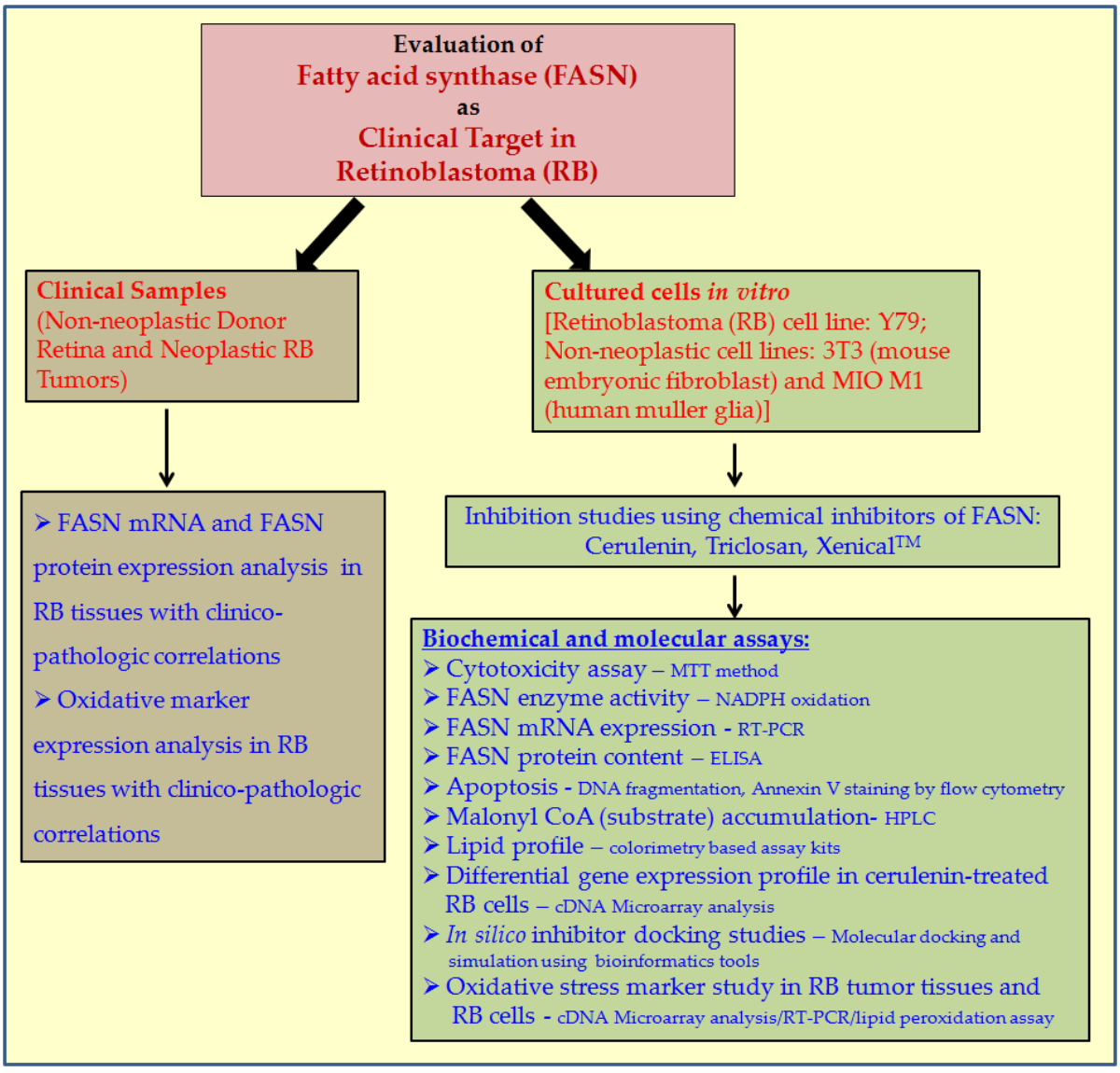

2.1. Objectives

1. To study the expression of fatty acid synthase (FASN) in retinoblastoma (RB) tumour tissues and to correlate it with the clinicopathological features of the tumours.

2. To study the role of oxidative stress in RB tumour tissues and to correlate it with the clinicopathological features of the tumours.

3. To evaluate the cytotoxic effects of FASN inhibitors [cerulenin, triclosan, and orlistat (Xenical™)] in Y79 RB cancer cells and non-neoplastic cells.

4. To investigate the biochemical effects of FASN inhibitors in cultured Y79 RB cells *in vitro*.

5. To analyse the molecular mechanisms involved in Y79 RB cancer cells treated with FASN inhibitors.

6. To explore an *in silico* approach to study FASN inhibition and validate it in a biological model.

CHAPTER 3: MATERIALS AND METHODS

3.1. Ethical clearance and patient consent

The study was reviewed and approved by the local ethics committee of our institute[♣] and the committee deemed that it confirmed to the generally accepted principles of research, in accordance with the Helsinki Declaration. Informed consent was obtained from the parents of RB children for the research use of tumour samples obtained from the enucleated eyes removed as a part of treatment.

3.2. Collection of RB tumour samples

RB tumours were freshly collected by the Ocular Pathologist from the enucleated eye balls. The samples were snap frozen in liquid nitrogen at -196°C and stored till use. The samples were thawed on ice during RNA and protein extraction. For the immunohistochemical studies the tumour tissue sections were sourced between 1997 to 2009. Fresh RB tumour tissues were collected and processed for all the biochemical assays and gene expression studies. Donor retina tissue used for comparison purposes in this study, was collected from the CU Shah eye bank, Sankara Nethralaya.

3.2.1. RNA and Protein extraction

Approximately 100 mg of the RB tumour tissue was homogenised with 1 ml of Trizol in diethyl pyrocarbonate (DEPC) treated glass tissue homogeniser. The cells were then processed further as per the RNA extraction protocol. For protein extraction the RB tumour tissues were homogenised using RIPA buffer and the homogenate was then processed for lysate preparation and protein estimation as per the protocol.

[♣] *Ethics Sub-Committee (Institutional review board), Vision Research Foundation, Sankara Nethralaya, Chennai. Study code: 16-2005-P, Study approved on: 29.10.2005*

3.3. Cell culture

3.3.1. Human retinoblastoma Y79 cells:

Y79 is a retinoblastoma cell line obtained from Cell Bank, RIKEN Bio Resource Centre (Ibaraki, Japan), the source of which is from a primary tumour (right eye) of a 2 year old Caucasian girl. It is cultured in RPMI 1640 media with 2 mM L-glutamine, 10 mM HEPES, 1 mM sodium pyruvate, 4.5 g/L glucose, 1.5 g/L bicarbonate supplemented with 15 % FBS. Cell morphology: Grape-like clusters growing as suspension culture. The doubling time is 48 h.

3.3.2. Human müller glial (MIO-M1) cells:

MIO-M1 (Müller - glial) cell line derived from neural retina of a 68-year-old female corneal donor 36 h after death. The cells were named as MIO-M1 after the institution, Moorfields/Institute of Ophthalmology-Muller 1. Cells were isolated by a slight modification of an established method. This cell line was a gift from Dr. G. A. Limb, Institute of Ophthalmology, University College, London (Limb et al., 2002). The cell grows as adherent cell culture with epithelioid morphology. It is grown in Dulbecco's minimum essential media (DMEM) with 10% FBS.

3.3.3. Mouse embryonic fibroblast (3T3) cells:

3T3 cell line was obtained from American Type Cell Culture (ATCC), USA. The cells are mouse embryonic fibroblasts. It is grown in Dulbecco's minimum essential media (DMEM) with 10% FBS.

3.3.4. Human breast cancer (MCF-7) cells:

These cells were obtained from National Centre for Cell Science (NCCS), Pune, India. The cells are maintained in DMEM supplemented with 750 μl/dl calf insulin (40 IU/ml) and 10% fetal bovine serum.

All the cell lines were cultured with the appropriate culture media along with antibiotic-antimycotic solution (Hi Media, Mumbai, India). All the cell lines were maintained at 37°C in a humidified atmosphere of 90% air and 10% CO_2.

3.3.5. Antibiotic antimycotic solution (per ml in 0.9% normal saline):

10,000 units Penicillin, 10 mg Streptomycin, 25 µg Amphotericin B

3.3.6. Trypsinisation of monolayer cultures:

Culture flasks with confluent monolayer of cells were trypsinised with sterile trypsin solution (0.02% trypsin, 0.5% dextrose and 0.03% EDTA in PBS). The flasks were incubated for 5 min after trypsin treatment and then the detached cells were removed with culture medium. The cells were used either for experiments or for further sub-culturing purpose.

3.4. Immunohistochemistry

The eye ball specimens are obtained fresh from the operation theatres and they are grossed by the pathologist. The measurements of the eye ball are reported. The tissue is then cut into two halves and the optic nerve is removed. The tissues are then processed.

3.4.1. Fixation: The tissues are fixed overnight in 10% neutral buffered formalin.

10% Neutral buffered formalin:

NaH_2PO_4	10 g
Na_2HPO_4	32.5 g
37 - 41% Formaldehyde	500 ml
Distilled water	4500 ml

3.4.2. Tissue processing:

Processing of tissues involves heat, vacuum, pressure and agitation. Tissue processor carries out these steps automatically. This uses graded alcohol ranging

from a lower to a higher concentration. The various steps involved in the tissue processing are:

Processing time 17 h (approximately)

60 % alcohol, 4 h

↓

95 % alcohol 2 changes, 1½ h each

↓

Absolute alcohol 4 changes, 45 min each

↓

Xylene 3 changes, 1 h each

↓

Paraffin wax 2 changes, 2 h each

↓

Embedding

The more satisfactory embedding material is paraffin wax. It is essential that the embedding medium thoroughly permeates the tissue in fluid form and that it solidifies with little damage to the tissue. Once the tissue is embedded into the paraffin wax, the wax is cut as blocks for making tissue sections using a microtome in silane coated glass slides. The cut sections (4 μm thick) are then processed for immunohistochemistry.

3.4.3. Coating of glass slides for immunohistochemistry with 2, 3-aminopropyltriethoxy silane (APES)

The slides are placed in a rack and immersed in acetone for 5 min. Then the slides are immersed in 2 % silane in acetone v/v for 30 min. Then the slides are rinsed in two consecutive baths of acetone for 5 min, each. The slides are allowed to dry at room temperature and were stored.

3.4.4. Deparaffinisation: Tissue section slides are processed for removing the paraffin wax from the sections as per the protocol below, prior to antigen retrieval.

The slides are dewaxed and rehydrated in successive changes of xylene and isopropyl alcohol as follows:

Table 3.1 Deparaffinisation protocol

Two changes of xylene	10 min each
100 % Alcohol	4 min
80 % Alcohol	4 min
60 % Alcohol	4 min
40 % Alcohol	4 min
Distilled water	4 min

3.4.5. Antigen retrieval:

Antigen retrieval is performed by pressure cooker method, in which the slides are placed in a slide holder and immersed in citrate buffer (0.1M citric acid and 0.1M trisodium citrate, pH 6.0) and maintained until one whistle. The cooker was then placed under running tap water for 15 min.

3.4.6. Immunostaining:

Slides were rehydrated in a moist chamber with Tris-buffered saline (TBS) (50 mM Tris and 150 mM NaCl, pH 7.6) for 5 min. Slides were subjected to 3% H_2O_2 for 10 min to block the endogenous peroxidase. Then the slides were washed with Tris buffer saline (TBS) for 3 min. After washing, the slides were incubated with the primary antibody and incubated for overnight at 4^{o}C. Next day slides were washed with TBS for 5 min. Then the biotinylated secondary antibody (Link-LSAB, DakoCytomation, Glostrup, Denmark) was added to the slides and incubated for 90 min. Slides were washed with TBS for 5 min. After washing, slides were incubated with streptavidin conjugated with HRP (horse radish peroxidase) for 90 min. Following incubation, the slides were again washed with TBS for 5 min. Diaminobenzidine (1:100 dilution) was prepared freshly and incubated for 5 min. After incubation, slides were washed with TBS, and then filtered Harris Hematoxylin was added and incubated for 30 sec. Then the slides were washed with

distilled water and allowed to air-dry. After drying, the slides were mounted with DPX mountant.

3.5. FASN enzyme activity

3.5.1. Principle: Fatty acid synthase activity was determined following the method of Dils and Carey (Dils & Carey, 1975). The method involves the measurement of malonyl CoA and acetyl CoA dependent oxidation of NADPH measured by the decrease in absorbance at 340 nm using a UV-Vis spectrophotometer.

$$\text{Acetyl CoA} + 7\,\text{Malonyl CoA} + 14\,\text{NADPH} + 14\,H^{+} \xrightarrow{\text{FASN}} \text{Palmitate} + 7\,CO_2 + 8\,\text{CoA-SH} + 14\,NADP^{+} + 6H_2O$$

3.5.2. Experimental Design:

Retinoblastoma cells were collected and washed thrice with ice-cold PBS and re-suspended in 200 µl - 300 µl of the lysis buffer (pH 7.5) containing 1 mM EDTA, 50 mM Tris HCL, 150 mM NaCl, 100 µg/ml PMSF and sonicated at 50 - 60 pixels for 1 min (thrice) and subjected to the assay. 50 µl of each lysate was taken for the reaction. Background NADPH oxidation was measured initially without the lysate for 10 min. Then the FASN dependent NADPH oxidation was measured in one ml of reaction mixture containing 200 mM potassium phosphate buffer (pH 6.6), 1 mM DTT, 1 mM EDTA, 0.24 mM NADPH, 30 µM acetyl CoA, 50 µM malonyl CoA and 50 µl cell lysate. The decrease in absorbance due to FASN dependent NADPH oxidation was monitored for 10 min at 340 nm. Enzyme activity of FASN was then calculated and expressed as nanomoles of NADPH oxidized per min per ml reaction.

3.5.3. FASN enzyme activity assay protocol:

Table 3.2 FASN enzyme activity assay protocol

Reagents	Volume (µl)
200 mM KH_2PO_4	450
1 mM Dithiothreitol (DTT)	100
1 mM EDTA	100
30 µM Acetyl CoA	100

Cell lysate	50
0.24 mM NADPH	100
50 μM Malonyl CoA	100

3.6. WESTERN BLOTTING

Western blot is a widely used analytical technique to detect specific proteins in the given sample of tissue homogenate or cell extract. It uses gel electrophoresis to separate native or denatured proteins by the length of the polypeptide (denaturing conditions) or by the 3-D structure of the protein (native/non-denaturing conditions). The proteins are then transferred to a membrane (typically nitrocellulose or PVDF), where they are probed using antibodies specific to the target protein. The nitrocellulose membrane is then soaked in blocking buffer (5% skimmed milk) to "block" the non-specific binding of proteins and further incubated with the specific antibody against the target protein. The membrane is then incubated with a secondary antibody which will typically have a covalently attached enzyme along with a chromogenic substrate, which will cause a colour reaction. The expression of the desired protein is visualized as coloured bands.

3.6.1. Cell lysate preparation

Cell lysis buffer (pH 7.6)

- 50 mM Tris – HCl
- 5 mM EDTA
- 150 mM sodium chloride
- 0.1% PMSF
- 250 μl of 1 mg/ml Protease Inhibitor Cocktail

The confluently cultured cells were collected and washed thrice with phosphate buffer saline at 5,000 rpm for 3 min. The cells were treated with radio immunoprecipitation (RIPA) buffer and sonicated at 50 - 60 cycles/min. After

sonication the lysed cells were centrifuged at 10,000 rpm at 4°C for 5 min and protein was estimated by Lowry method (Lowry et al., 1951).

3.6.2. Protein extraction from tissues

Approximately 250 mg of the tissue (retinoblastoma fresh tumour) was homogenised in a homogeniser with lysis buffer on ice cold conditions. The homogenate was then sonicated at 80 cycles/min for 60 sec. Protein was estimated using Lowry method (Lowry et al., 1951).

3.6.3. Protein Estimation

Protein estimation was done by conventional Lowry method (Lowry et al., 1951). The assay was run along with a set of standard using bovine serum albumin (BSA), ranging from 50 to 200 μg. The absorbance was read at 660 nm in DU 800 spectrophotometer (Beckman Coulter, Inc., CA, USA).

3.6.4. SDS-PAGE electrophoresis

Separating gel made of acrylamide (percentage of gel depends on size of the desired protein) was prepared. The base of the assembled glass plates were sealed with 2% agarose gel. Then the separating gel was poured onto the sealed glass plates and the gel's surface was overlayed with saturated butanol and left undisturbed for the polymerization. After the separating gel gets solidified, 4% stacking gel was poured above the separating gel by removing the butanol layer and the comb was placed carefully without any air bubble and left it aside for solidification. After the gel has been solidified the comb was removed carefully. The protein samples are mixed with 3X sample loading buffer and boiled at 100^0C for 3 min. Then the sample was loaded on the gel and run till the dye reaches the bottom of the gel. The gel was taken carefully from the glass-assembled plates.

3.6.4.1. Reagents:

Acrylamide (30%):

- Acrylamide - 14.6 g
- Bis acrylamide - 0.4 g
- Dissolved in 30 ml of water made up to 50 ml and filtered.

- **Tris-HCl Buffer (pH 8.8):**
  - Tris - 9.0 g
  - Water - 25 ml
  - Adjust the pH to 8.8 with 1 N HCl and made up to 50 ml with distilled water.

- **Tris-HCl Buffer (pH 6.8):**
  - Tris - 3.0 g
  - Water – 25 ml. Adjust the pH to 6.8 with 1N HCl and made up to 50 ml with distilled water.

- **10% Ammonium persulphate (APS):** Polymerization catalyst required for gel formation. Increasing APS concentration will make the gel set quicker.
  - Ammonium per sulphate – 10 g
  - Distilled water – 100 ml.
  - The solution if freshly prepared before use.

- **Tetramethylethylenediamine (TEMED):** Polymerization catalyst that catalyses the formation of persulphate free radicals from the APS, which in turn initiates polymerization. This is always the last reagent that is added to the gel.
- **10% Sodium dodecyl sulphate (SDS):** Binds proteins so that they become negatively charged, therefore separation is on the basis of size alone and not the intrinsic protein charges.
  - SDS – 10 g
  - Distilled water – 100 ml
- **Separating gel preparation**: This sieves and separates the proteins by size.

Percentage of gel depends upon the size of target proteins.

Acryl amide %	Range of separation (kDa)
15	12 - 43
10	16 - 68
7.5	36 - 94
5.0	57 - 212

- **10% separating gel:**
    - 30% Acrylamide - 4 ml
    - Tris HCl (pH 8.8) - 2.5 ml
    - 10% APS - 50 µl & TEMED – 5 µl
    - 10% SDS – 100 µl
    - Distilled water - 3.344 ml

- **Stacking gel:** Large pore size gel with little or no molecular sieving on the sample.
  Stacking gel (Standard 4% acrylamide)
    - 30% Acrylamide - 1.33 ml
    - Tris HCl (pH 6.8) - 2.5 ml
    - 10% APS – 50 µl
    - TEMED – 10 µl
    - 10% SDS – 100 µl
    - Distilled water - 6.01 ml.
- **Western blotting transfer buffer:**
    - Tris - 3.3 g
    - Glycine - 14.4 g
    - SDS - 1.0 g
    - The contents were dissolved in 800 ml of distilled water. The final volume was then made up to 1000 ml with methanol.

- **Ponceau stain:**
    - Ponceau S - 0.5 g
    - Glacial acetic acid - 1 ml
    - Made up to 100 ml with distilled water. Prepared just before use.

- **Electrophoresis buffer pH 8.6 (5X):**
    - Tris base - 15.1 g
    - Glycine - 72.0 g

- SDS - 5.0 g
- Distilled water - made up to 1000 ml.

- **Sample loading buffer (3X):**
  - 1M Tris HCl (pH 6.8) - 2.4 ml
  - 20% SDS - 3 ml
  - Glycerol - 3 ml
  - β-Mercaptoethanol - 1.6 ml
  - Bromophenol Blue - 0.006 g
- **Tris buffered saline – Tween 20 (TBST) (pH 7.6):**
  - Sodium chloride – 8 g
  - 1M Tris HCl - 20 ml
  - Diluted to 1000 ml with distilled water.
  - Tween 20 – 10 ml.
- **5% Skimmed milk:** 2.5 g of skimmed milk powder was dissolved in 50 ml of TBST

3.6.5. Electro-blotting

Electrophoresed gel was transferred on to the nitrocellulose membrane for 1 h under 100 V using transfer apparatus. To ensure the transfer is complete, the blot was stained with 0.5% Ponceau stain to visualize protein bands and then washed with distilled water. The transferred membrane was blocked with 5% skimmed milk for 1 h. Primary antibodies were added according the standardized dilutions and incubated for 2 h to overnight at 4°C. The blots were washed 3 times with TBST buffer 30 min each. The presence of the specific proteins was then shown by chemiluminescence of horse radish peroxidase with chemiluminescence detection using Pierce western blot detection reagents (Thermo Fisher Scientific Inc., IL, USA). The blot was exposed to X-ray film for about 5 to 10 min and then the film was developed. The band intensities were measured with densitometer using Quantity One software (BIORAD GS 800, USA). The optical densities thus obtained for FASN was normalized with respect to the loading control β-actin.

3.7. Enzyme linked immunosorbent assay (ELISA) for FASN protein content (FASN-ELISA)

3.7.1. Principle of FASN-ELISA: Estimation of FASN protein content was done by FAS-detect™ ELISA kit (FASgen Inc, Baltimore, MD) which involves sandwich ELISA method of detection. The FASN protein antigen in the test sample is sandwiched between the polyclonal capture antibody coated in the capture plate and the biotinylated monoclonal antibody in the sample diluent. After this step, the unbound antibodies are removed by washing. Then the enzyme-conjugate (HRP conjugated streptavidin) is added to the plate, which forms a complex with the biotin in the monoclonal antibody. After subsequent washing to remove the unbound enzyme conjugate, TMB substrate is added. HRP acts on the substrate to give a blue coloured product. Finally the reaction is stopped with the addition of stop solution. The colour developed is read at 450 nm.

3.7.2. Protocol: Samples and standards were processed according to the kit instructions. 100 µl of samples and standards were added to the sample dilution tray. Each sample was diluted with 100 µl of sample diluent/detection antibody. Then 150 µl of the diluted samples and standards were transferred to the FASN capture plate. The plates were incubated in a plate shaker for 90 min at room temperature. The plate was washed four times with 1X wash buffer. Then 100 µl of FASN enzyme conjugate was added to each well and incubated on a plate shaker for 60 min at room temperature. The plate was washed with 1X wash buffer for four times. Then 100 µl of TMB substrate was added to each well and incubated on a plate shaker for 15 min at room temperature. The reaction was stopped by adding 100 µl of substrate stop solution to each well and kept for an additional 10-15 sec in a shaker. The plates were then read at 450 nm using an ELISA reader (Biotek, USA). A standard calibration curve was plotted and the FASN protein content in the treated and untreated Y79 cells were calculated by interpolation from the standard curve.

3.8. Phase contrast microscopy

Cell morphology of the untreated and FASN inhibitor treated retinoblastoma cells were assessed using a phase contrast microscope (Nikon, Tokyo, Japan). To assess the toxic reactions during FASN inhibitor treatment in normal cell morphology, the non-neoplastic MIO-M1 and 3T3 cells were treated with FASN inhibitors and the morphological changes were recorded.

3.9. Cytotoxicity assay (MTT Assay)

Principle: MTT [3-(4,5-dimethylthiazol-2-yl)-2,5-diphenyltetrazolium bromide] assay, first described by Mosmann in 1983, is based on the ability of a mitochondrial dehydrogenase enzyme in viable cells to cleave the tetrazolium rings of the pale yellow MTT and form dark blue formazan crystals which is largely impermeable to cell membranes, thus resulting in its accumulation within healthy cells. Solubilisation of the cells by the addition of a detergent results in the liberation of the crystals which are solubilized. The number of surviving cells is directly proportional to the amount of the formazan product created (Mosmann, 1983).

Protocol: Y79 RB cells and non-neoplastic cells were exposed to FASN inhibitors, and incubated for specific period of exposure in 96 well plates. The test medium was carefully removed and replaced with fresh culture media. To this 10 µl of MTT (5 mg/ml) was added and incubated for 4 h at 37°C. After the incubation, the medium was discarded and the formed crystals were solubilised in 100 µl of DMSO. After the crystals have dissolved (within 5 min) the plate was read at 540 nm using ELISA reader (Biotek, USA). Cell viability (or cell survival) was calculated as: (Test OD/Control OD) x 100 (Mosmann, 1983). The 50% inhibitory concentration (IC_{50}) was calculated by polynomial regression analysis using Microsoft Excel. Similarly the IC_{30} and IC_{70} of each drug were calculated by interpolation, which indicates 30% and 70% cell growth inhibitory concentrations respectively in Y79 cells.

3.10. DNA fragmentation Assay

Principle: Cell and nuclear shrinkage, chromatin condensation, formation of apoptotic bodies and phagocytosis of neighbouring cells characterize the main morphological changes of the apoptosis. Cleavage of chromosomal DNA into oligo-nucleosomal size fragments is a biochemical hallmark of apoptosis. Several studies identified the proteins responsible for the DNA fragmentation process during apoptosis. DNA fragmentation factor (DFF) was identified as a protein that is responsible for the DNA strand breaks. DFF is a heterodimeric protein composed of two proteins- DNA fragmentation factors 45 and 40. These proteins are capable of causing chromosomal DNA breaks in the presence of an activated caspase 3. In this, the DFF40 contains an intrinsic DNase activity whereas DFF45 serves as an inhibitor of DFF40 activity. Upon activation of apoptosis, DFF45 is cleaved by caspase 3, and dissociates from DFF40. The caspase activated DNase or nuclease cleaves the DNA into oligonucleosomal size fragments. The DFF45 is also activated by caspase 7. DFF45 is required for the synthesis and folding of DFF40, thus serving also as a molecular chaperone. DFF induces chromatin condensation process (Zhang & Xu. 2000).

5×10^4 RB Y79 cells/well were seeded in 24 well plates with 500 µl of culture media and incubated at 37^0C for 24 h. The cells were then exposed to the IC_{50} dosage and a higher dosage of cerulenin, triclosan and orlistat (Xenical™) in fresh medium and then incubated for the intended time periods. DNA was extracted from the cell pellet using DNA isolation kit (Qiagen, USA) as per the manufacturer's instructions. The isolated DNA was then electrophoresed at 100 V in a 2% agarose gel with 0.5% ethidium bromide. The bands were visualized under UV light with a gel documentation system (BioDoc-It Imaging system, UVP, USA).

3.11. mRNA expression studies

3.11.1. Principle: Reverse transcription polymerase chain reaction (RT-PCR) is a variant of polymerase chain reaction (PCR), a commonly used technique in molecular biology to generate many copies of a DNA sequence, a process termed "amplification". In RT-PCR, however, an RNA strand is first reverse transcribed into its DNA complement (complementary DNA, or cDNA) using the enzyme reverse transcriptase and the resulting cDNA is amplified using traditional PCR or real-time quantitative PCR.

3.11.2. RNA extraction by Trizol method

- Cells were harvested from the cultures and collected in a vial. The harvested cells are centrifuged at 10,000 rpm for 5 - 10 min.
- To the pellet, 1 ml Trizol reagent was added and vortexed. Cells were incubated at room temperature for 5 min.
- To the cells, 500 µl of $CHCl_3$ was added and shaken well for 15 sec. Cells were centrifuged at 12,000 rpm for 15 min.
- Aqueous layer that has RNA was collected and transferred to new vial, and to this aqueous layer, 500 µl isopropanol was added and incubated at room temperature for 10 min.
- Cells were centrifuged at 12,000 rpm for 10 min and the supernatant was discarded and to the pellet 75% alcohol was added and mixed well.
- Cells were centrifuged at 12,000 rpm for 5 min and the supernatant was discarded. Pellet was air dried at room temperature for 2 min and to it 25 µl diethyl pyrocarbonate (DEPC) treated water was added.
- 5 µl of the total RNA extracted was run in 2% agarose gel to see the quality of RNA extracted and the rest was stored at -80^0C before use.

3.11.3. RNA purification

- Isolated RNA was treated by TURBO DNase (Ambion, Genetix Biotech Asia Pvt. Ltd, Chennai, India) to remove the DNA in the sample.

- 50 µl reaction containing 7.5 - 10 µg of RNA was mixed with 1 µl of TURBO DNase 1 µl (2 units) and 0.1 volume 10X TURBO DNase buffer, was incubated at 37°C for 30 min.
- To the reaction mixture, 0.1 µl of resuspended DNase inactivation reagent was added and mixed repeatedly during the incubation period of 2 min.
- The mixture was centrifuged for 1.5 min at 10,000 rpm and supernatant transferred to a fresh tube.
- The TURBO DNase treated RNA was quantified before reverse transcriptase PCR.

3.11.4. cDNA conversion

Table 3.3 cDNA conversion protocol

10X buffer	2.0 µl
DNTPs	2.0 µl
Oligo dT	2.0 µl
RNase out	1.0 µl
Sensiscript RT	1.0 µl
RNAse free water	10.0 µl
Template RNA	2.0 µl
Incubated at 37^0 C for 60 min.	

3.11.5. Semi-quantitative RT-PCR analysis

Using a housekeeping gene, glyceraldehyde-3-phosphate dehydrogenase (GAPDH), as an internal control, the gene expression of FASN in untreated and treated Y79 cells was analyzed by semi-quantitative RT-PCR. Briefly, first strand cDNA synthesis was carried and 2.0 µg of cDNA was used for PCR in the thermal cycler. PCR amplifications were performed with the specific primers designed from published human gene sequences. Semi-quantitation was established by terminating reactions at appropriate intervals for each primer pair to ensure that the PCR products formed were within the linear portion of the amplification curve. PCR products were fractionated by electrophoresis using 2 % agarose gel containing 0.5 %

ethidium bromide with molecular marker 100 bp ladder to confirm the size of the resultant product.

GAPDH primer

Forward primer: 3′ – GCCAAGGTCATCCATGACAAC – 5′

Reverse primer: 3′ – GTCCACCACCCTGTTGCTGTA – 5′

Product size: 498 bp

FASN primer

Forward primer: 3′ – AACTCCTTGGCGGAAGAGA – 5′

Reverse primer: 3′- TAGGACCCCGTGGAATGTCA- 5′

Product size: 152 bp

RT- PCR reaction cocktail

10X buffer	2.5 µl
deoxy nucleotide triphosphates (dNTPs)	2.5 µl
Forward primer	1 µl
Reverse primer	1 µl
Taq polymerase	0.3 µl
Milli-Q water	Volume adjusted to get final volume of 25 µl
cDNA	Volume corresponding to 2.5 µg of cDNA

The reaction protocol for RT-PCR for GAPDH and FASN

95°C	:	5 min	
95°C	:	30 sec	45 cycles
63°C	:	1 min	
72°C	:	1 min	
72°C	:	10 min	

3.11.6. Quantitative real-time RT-PCR (qRT-PCR)

3.11.6.1. Principle: Real time PCR is a technique used to monitor the progress of a PCR reaction in real time. At the same time, a relatively small amount of PCR product (DNA, cDNA or RNA) can be quantified. It is based on the detection of the

fluorescence produced by a reporter molecule which increases, as the reaction proceeds. This occurs due to the accumulation of the PCR product with each cycle of amplification. These fluorescent reporter molecules include dyes that bind to the double-stranded DNA (i.e. SYBR® Green) or sequence specific probes (i.e. Molecular Beacons or TaqMan® Probes). Real time PCR facilitates the monitoring of the reaction as it progresses. One can start with minimal amounts of nucleic acid and quantify the end product accurately. Real time PCR assays are now easy to perform, have high sensitivity, more specificity, and provide scope for automation. Real time PCR is also referred to as real time RT-PCR which has the additional cycle of reverse transcription that leads to formation of a complementary DNA molecule from a RNA molecule. This is done because RNA is less stable as compared to DNA.

3.11.6.2. Protocol: Control and treated Y79 cells were investigated by qRT-PCR. Total RNA was isolated from the samples and the concentration was checked by Nanodrop ND-1000 spectrophotometer (Thermo Fisher Scientific Inc, USA). 0.5 μg of total RNA from each sample was reverse transcribed using sensiscript reverse transcriptase (Qiagen, Germany). Quantification of specific gene expression was performed in triplicate in a 20 μl volume reaction mixture containing [0.5 μg of cDNA, specific primer (see table below) and SYBR green reagent] in 96-well plates on a real-time PCR system (Prism 7500; ABI Lab India Instruments, Gurgaon, India). GAPDH was used as an internal control and the detection was carried out by measuring the binding of fluorescence dye SYBR green to double stranded DNA. After cycling, relative quantitation of tested gene cDNA against the internal control was calculated using a ΔC_T method. The relative amount of gene specific mRNA to GAPDH was calculated using $2^{-\Delta\Delta Ct}$, where C_t is the number of cycles at which amplification reaches a threshold, is determined by SDS software version 1.3 (Livak et al., 2001).

3.11.6.3. Gene specific primers for qRT-PCR Gene specific primers were used to analyse the expression of few key genes by real time PCR. The primers used are listed below.

Table 3.4 Gene specific primers for qRT-PCR

Gene Name	Primer sequence	Product size (base pairs)
SKP2	FP 5′- CGTGTACAGCACATGGACCT – 3′ RP 5′- TGGATTCTCTGAATTTGCCC – 3′	199 bp
RXRA	FP 5′ – TCCTTCTCCCACCGCTCCATC – 3′ RP 5′ – CAGCTCCGTCTTGTCCATCTG – 3′	302 bp
ACACB	FP 5′- CAGAGCATCGTGCAGTTGGT-3′ RP 5′-TGCTCAACACGCAAGTATCTTCTC-3′	444bp
PPARA	FP 5'-AGATTTCGCAATCCATCGGC-3' RP 5'-GCGTGGACTCCGTAATGATA-3'	304 bp
SSTR2	FP 5′-CCCCAGCCCTTAAAGGCATGT-3′ RP 5′-GGTCTCCATTGAGGAGGGTCC-3′	234 bp
CDK2AP1	FP 5'-AGTTTCGTTTTTCCTCCCAT-3' RP 5'-AGAACACCATGGGTAACAAA-3'	250 bp
CYCS	FP 5′ – TTGGCAATCCGTCATCAGTA – 3′ RP 5′- CCCGACAGTGCCTAGAAGAG – 3′	157 bp
CAT	FP 5′- TCTGGAGAAGTGCGGAGATT-3′ RP 5′- AGTCAGGGTGGACCTCAGTG-3′	190 bp
CRYAA	FP 5'- GAGATCCACGGAAAGCACAAC-3' RP 5'- GGTAGCGGCGGTGGAACT-3'	73 bp
MMP-2	FP 5′- TCCACTGTTGGTGGGAACTCA-3′ RP 5′-TGGTCGCACACCACATCTTT-3′	121 bp
iNOS	FP 5′-GTTCTCAAGGCACAGGTCTC-3′ RP 5′-GCAGGTCACTTATGTCACTTATC-3′	127 bp
CREBBP	FP 5'-CGGTTTCTCGGCGAATGAC-3' RP 5'-CATTTCCTATTCCTGGGTTGAT-3'	206 bp
SOD1	FP 5′- GGATGAAGAGAGGCATGTTGGAGAC-3′ RP 5′- GTCTTTGTACTTTCTTCATTTCCACC-3′	186 bp
GPX	FP 5′- GCACCCTCTCTTCGCCTTC-3′ RP 5′- TCAGGCTCGATGTCAATGGTC-3′	207 bp
CDC25A	FP 5′-GCACTCGGTCAGTGTTGAAG-3′ RP 5′-CATGGGCCTTCTCTGGATTA-3′	126 bp
HMGCR	FP 5′-GGACCCCTTTGCTTAGATGAA -3′ RP 5′-CCACCAAGACCTATTGCTCTG-3′	107 bp
JUN	FP 5′-CAAAGTTTGGATTGCATCAAGTG-3′, RP 5′-TAACATTATAAATGGTCACAGCACATG-3′	45 bp

3.12. Annexin V- Fluos staining

3.12.1. Principle: In the early stage of apoptosis, changes occur at the cell surface. One of these plasma membrane alterations is the translocation of phosphpatidylserine (PS) from the inner part of the plasma membrane to the outer layer, by which PS becomes exposed at the external surface of the cell. The analysis of phosphatidyl serine on the outer leaflet of the apoptotic cell membrane is performed using Annexin V- Fluos and propidium iodide (PI) for the differentiation from necrotic or labeling with a cell surface marker for cell characterization.

3.12.2. Protocol: After the treatment of Y79 cells with the three FASN inhibitors for three different times of incubation, the cells were pelleted, washed with PBS and incubated with Annexin V apoptosis detection kit I (BD Biosciences, CA, USA) for 15 min at 15 - 25^{0}C. After the incubation period, the cells were analyzed by flow cytometry (FACS Calibur, BD Biosciences, CA, USA)

3.13. Determination of Malonyl CoA accumulation by High Performance Liquid Chromatoraphy technique (HPLC)

3.13.1. HPLC protocol

Malonyl-CoA levels were measured using the HPLC method of Corkey (Corkey, 1988; Pizer et al., 2000). CoA esters were separated and quantitated using reversed-phase HPLC (Prominence HPLC, LC-20AT, Shimadzu, Kyoto, Japan) on a Gemini 5 μm C18 110A column (Phenomenex, CA, USA) running LC solution software, monitoring at 254 nm as the maximum absorbance for CoA using diode array detector (SPD-M20A, Shimadzu, Kyoto, Japan). The following gradients and buffers were used:

1. Buffer A, 0.1 M potassium phosphate, pH 5.0;
2. Buffer B, 0.1 M potassium phosphate, pH 5.0, with 40% acetonitrile.

Following a 10-min isocratic run with 92% buffer A, 8% buffer B at 0.4 ml/min, flow was increased to 0.8 ml/min over 1 min, whereupon a linear gradient to 10% buffer B was run until 12 min and then held at 10% buffer B until 25 min, at which point a linear gradient was run to 100% buffer B at 30 min, completing at 35 min. The following CoA esters (Sigma Aldrich, USA) were run as standards: malonyl-CoA, acetyl-CoA, glutathione-CoA, succinyl-CoA, HMG-CoA, and free CoA. Standards were dissolved in 50 μl of buffer A. Quantitation of CoA esters was performed by the LC solution software.

3.14. Biochemical assay of cellular lipids

Cellular lipids such as triglyceride, phosphatidyl choline, free fatty acid and total cholesterol were measured in the Y79 RB cell extracts and in non-neoplastic 3T3 cells. The quantification of the lipids was carried out using biochemical assay kits from BioVision, CA, USA.

3.14.1. Triglyceride Assay

3.14.1.1. Principle: Triglycerides are broken down into fatty acids and glycerol, after which both can serve as substrates for energy producing and metabolic pathways. In the assay, triglycerides are converted to free fatty acids and glycerol. The glycerol is then oxidized to generate a product which reacts with the probe to generate pink colour which can be read spectrophotometrically at 570 nm.

3.14.1.2. Sample preparation: The samples were homogenized with 5% Triton-X 100 in water and were slowly heated at 80°C - 100°C in a water bath for 2 - 5 min. The Triton X-100 becomes cloudy at this point, and then the samples were slowly cooled down to room temperature. The heating was repeated again to solubilise the remaining triglyceride into solution. The samples were then centrifuged for 5 min at maximum speed. The supernatant was separated and stored and diluted 10 folds with distilled water before the assay. After incubating the samples and standards

with 2 µl lipase, 50 µl of reaction mix (as per the kit instructions) was added to each sample and incubated at room temperature for 60 min in dark. Concentration of triglycerides present in the sample was then calculated from the standard calibration curve.

3.15.2. Phosphatidyl choline Assay

3.15.2.1. Principle: Phosphatidylcholine (PC) is a phospholipid which incorporates choline as the headgroup of the lipid. PC is a major constituent of biological membranes and is involved in cell signaling through release of choline by phospholipase D leaving the second messenger phosphatidic acid. The assay kit utilizes an enzyme-coupled assay in which PC is hydrolyzed, releasing choline which is subsequently oxidized resulting in development of the OxiRed probe to generate a pink colour that can be detected at 570 nm.

3.15.2.2. Sample preparation: The samples are extracted using 4 - 10 volume of assay buffer provided in the assay kit. The samples were centrifuged at 15000 rpm for 10 min, supernatant was separated and stored. The samples and standards were mixed with 50 µl of reaction mix and incubated for 30 min at room temperature in dark. Colour developed was read at 570 nm and the concentration of phosphatidyl choline present in the samples was calculated from the calibration curve.

3.15.3. Free fatty acid assay

3.15.3.1. Principle: This method involves an enzyme-based reaction for detecting the long-chain free fatty acids in various biological samples, such as serum, plasma and other body fluids, food, growth media, etc. In the assay, fatty acids are converted to their CoA derivatives, which are subsequently oxidized with the concomitant generation of pink colour which is read spectrophotometrically at 570 nm.

3.15.3.2. Sample preparation: The samples were extracted with 200 µl of 1% Triton-X 100 in chloroform and the extract was spun at maximum speed for 5 - 10 min. The

lower organic phase was collected and air dried at 50°C to remove trace chloroform. The dried lipids were dissolved in fatty acid assay buffer and vortexed extensively for 5 min. The samples were incubated with 2 µl of ACS (Acyl CoA Synthase) and incubated at 37°C for 30 min. Then all the samples were mixed with 50 µl of reaction mix (as per the assay kit instructions) and incubated at 37°C for 30 min protected from light. Colour developed was read at 570 nm and the concentration of fatty acids present in the samples was calculated from the calibration curve.

3.15.4. Total cholesterol assay

3.15.4.1. Principle: Majority of the cholesterol in blood is in the form of cholesteryl esters which can be hydrolyzed to cholesterol by cholesterol esterase. Cholesterol is then oxidized by cholesterol oxidase to yield hydrogen peroxide which reacts with a sensitive cholesterol probe to produce pink colour that can be read at 570 nm.

3.15.4.2. Sample preparation: The samples were extracted with 200 µl of chloroform: isopropanol: NP-40 (7:11:0.1) and the extract was spun at 15000 x g for 5 - 10 min. The liquid organic phase was transferred to a new tube and air dried at 50°C to remove chloroform. The samples were vaccum dried for 30 min to remove trace organic solvent using SpeedVac (Thermo scientific, MA, USA). The dried lipids were dissolved in 200 µl of cholesterol assay buffer and vortexed to obtain a homogenous solution. The samples and standards were mixed with 50 µl of reaction mix (as per the assay kit instructions) and incubated for 60 min at 37°C, protected from light.

After the incubation, all the lipid assay plates were read at 570 nm using ELISA reader (Epoch microplate spectrophotometer, BioTek Instruments Inc, Vermont, USA). The blank reading was subtracted from all the sample and standard readings obtained. The calibration curve was plotted and the concentration of lipids in the samples was calculated from the standard curve.

3.16. Evaluation of Lipid Peroxidation

Lipid peroxide level was determined by a colorimetric reaction using thiobarbituric acid, where malondialdehyde reacts with thiobarbituric acid to generate a product that absorbs at 532 nm. The levels of malondialdehyde, an end-product of lipid peroxidation serves as an index of the intensity of oxidative stress in the RB tumour samples and cultured Y79 RB cells. Peroxidation levels was measured at basal (un-induced) and under 10 mM ferrous sulphate induced conditions.

Table 3.5 Lipid peroxidation assay protocol:

Reagents	Basal (μl)	Induced (μl)
0.15 M Tris HCl pH 7.4	350	310
10 mM Potassium dihydrogen phosphate	40	40
10 mM Ferrous sulphate	---	40
Homogenate	40	40
Incubated in shaking incubator at room temperature for 20 min		
10% Trichloro acetic acid (TCA)	220	220
1% Thiobarbituric acid (TBA)	330	330
Boiled for 15 min in a boiling water bath and then cooled for 15 min. Colour developed was read at 532 nm		

3.17. Measurement of Intracellular Reactive oxygen species (ROS) levels by 2′, 7′ Dichlorodihydrofluorescein (DCF) Fluorescence Assay:

3.17.1. Principle: The method is a cell-based assay for measuring hydroxyl, peroxyl, or other reactive oxygen species (ROS) activity within a cell, employing the cell-permeable fluorogenic probe 2′, 7′-Dichlorodihydrofluorescin diacetate (DCFH-DA). DCFH-DA is diffused into cells and is deacetylated by cellular esterases to non-fluorescent 2′, 7′-Dichlorodihydrofluorescin (DCFH), which is rapidly oxidized to highly fluorescent 2′, 7′-Dichlorodihydrofluorescein (DCF) by ROS. The fluorescence intensity is proportional to the ROS levels within the cell cytosol. The kit has a DCF detection sensitivity limit of 10 pM. Cells are cultured in a 96-well cell culture plate and then pre-incubated with DCFH-DA, which is cell-permeable. The cells are then

treated with the oxidant. After a brief incubation, the cells can be read on a standard fluorescence plate reader. The ROS or antioxidant content in unknown samples is determined by comparison with the predetermined DCF standard calibration curve.

Figure 3.1 Mechanism of DCF assay

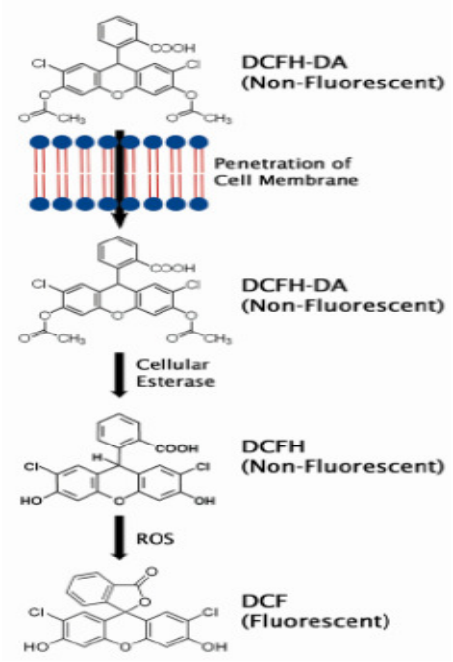

3.17.2. Preparation of DCF calibration curve

DCF stock (1 mM) was diluted with culture media to make a range of concentrations of standards as per the protocol. The concentration range is 0, 0.01, 0.1, 1, 10, 100, 1000, 10,000 nM. 100 µl of the diluted standards were transferred to 96 well plate and fluorescence was read with a fluorescence plate reader at 480 nm excitation/530 nm emission.

The intracellular ROS levels were measured using the OxiSelect ROS Assay Kit (Cell Biolabs Inc, CA, USA) as per the manufacturer's instructions. The assay measures the activity of hydroxyl, peroxyl, and other reactive oxygen species activity in a cell. 2×10^4 cells (from RB tumour tissue and donor retina) were assayed in 96-well plates

with 100 µl of culture media. 2×10^4 Y79 RB cells/well were seeded in 96-well plates with 100 µl of culture media and incubated at 37^0C overnight. The media was removed and the cells were washed with sterile PBS thrice. The cells from the RB tumour, donor retina were treated with 100 µl of 1X DCFH-DA and incubated at 37^0C for 60 min. The solution was removed and the cells were washed with sterile PBS. Then the cells were treated with 100 µM H_2O_2 for 2 h. After 2 h, the reaction was terminated by adding 100 µl of cell lysis buffer. The solutions were mixed thoroughly for proper cell lysis and incubated for 5 min. Then 150 µl of the solution was transferred to a fresh 96-well plate. The fluorescence was read with a SpectraMax M2 multi-detection micro plate reader (Molecular devices, CA, USA) at 480 nm excitation/530 nm emission. The ROS level in the tissue lysates was then calculated using the DCF standard graph.

3.18. cDNA Microarray analysis for differential gene expression profiling

3.18.1. Principle: The microarray works on the principle based on the ability of a given mRNA molecule to bind specifically to, or hybridize to, the template DNA from which it is originated. The expression levels of thousands of genes can be studied using an array by measuring the amount of mRNA bound to each spot. This can then be measured using a computer which will generate a profile of gene expression in a cell.

Base- pairing or hybridization is the underlining principle of DNA microarray.
1. A-T and G-C for DNA, 2. A-U and G-C for RNA

The study of the expression patterns of genes in several different experimental groups (for example, drug untreated/treated, normal cells/cancer cells) is called relative quantification method.

3.18.2. cDNA Microarray protocol

3.18.2.1. cDNA synthesis

Total RNA was isolated from Y79 RB cells using Trizol reagent and purified using an RNeasy Mini Kit (Qiagen, USA) combined with DNase treatment following the manufacturer's instructions. The samples for gene expression were labeled using Agilent Quick Amp Kit PLUS. 0.5 μg of sample was incubated with reverse transcription mix at 42°C and converted to double stranded cDNA primed by oligodT with a T7 polymerase promoter. The cleaned up double stranded cDNA was used as template for RNA generation. RNA was generated by *in vitro* transcription and the dye Cy3 CTP was incorporated during this step. The cDNA synthesis and *in vitro* transcription steps were carried out at 40°C. Labeled cDNA was cleaned up and quality assessed for yield and specific activity.

3.18.2.2. Hybridization, scanning and feature extraction

The labeled cDNA samples were hybridized onto a Whole Genome Human Array 4x44k. About 1650 ng of Cy3 labeled samples were fragmented and hybridized. Fragmentation of labeled cDNA and hybridization were done using the Gene Expression Hybridization kit of Agilent. Hybridization was carried out in Agilent's Surehyb Chambers at 65°C for 16 h. The hybridized slides were washed using Agilent Gene Expression wash buffers and scanned using the Agilent Microarray Scanner G Model G2565BA at 5 micron resolution. Data extraction from images was done using Feature Extraction software 10.5 of Agilent (G25677AA, Agilent Technologies, 2004). The extracted data were analyzed using GeneSpring GX version software from Agilent. Normalization of the data was done in GeneSpring GX using the recommended 'One color Per Chip and Per Gene data transformation' method. Ontology based biological analysis was done using Gene Ontology browser in GeneSpring GX. Further, biological analysis was performed using Genotype's

Biointerpreter a web-based biological interpretation tool. The present oligonuclotide microarray data were submitted to NCBI-GEO-OMNI BUS. The genes were considered for expression analysis when they satisfied the criteria: (i) $p \leq 0.05$, and (ii) log ratio of at least 2.0 for up regulation, and log ratio of 0.5 for down regulation (keeping a median log ratio of 1) in both biologic replicates.

CHAPTER 4: LIPOGENIC ENZYME FATTY ACID SYNTHASE (FASN) EXPRESSION IN RETINOBLASTOMA: CORRELATION WITH CLINICO-PATHOLOGIC FEATURES

4.1. INTRODUCTION

All cancer cells are characterised by an increased aerobic glycolysis and increased DNA and protein synthesis to meet the energy requirements. These processes also enhance the production of lipids in cancer cells. During this process, the cancer cells show up-regulated levels of lipid metabolic genes such as fatty acid synthase (FASN), acetyl CoA carboxylase (ACC), ATP citrate lyase (ACLY), and Spot14 protein. ACC is the rate limiting enzyme of the fatty acid synthesis pathway that converts acetyl CoA to malonyl CoA. Anti-cancer therapy targeting several lipid metabolic genes have been reported (Dakubo, 2010).

4.1.1. Fatty acid synthase and human cancer

The over-expression of FASN was reported first in breast cancer by Kuhajda et al in 1989. They identified the expression of haptoglobin related proteins (Hpr) in human breast cancers and the expression was associated with the breast cancer prognosis. Thus Hpr – epitope expression was considered an important predictor of early breast cancer recurrence (Kuhajda et al., 1989) Later, those molecules which expressed the haptoglobin – related protein epitopes, were named as oncogenic antigen - 519 (OA519). OA519 expression and its correlation with cancer prognosis were studied in prostate (Shurbaji et al., 1992) and colon cancer (Kuhajda et al., 1994). OA519 was then identified by peptide sequencing and enzymologic studies, as fatty acid synthase (FASN) in tumour cells. Peptide sequencing of OA519 showed sequence identity with mammalian rat FASN at residues 681 - 686 and 1208 - 1220, and this was functionally evaluated to be FASN. This was confirmed by testing the

enzyme for its ability to synthesize fatty acids in the presence of acetyl CoA, malonyl CoA and NADPH substrates. The resultant fatty acid product was identified with 80% of palmitate and 10% each of myristate and stearate. This profile was similar to liver FASN in human (Kuhajda et al., 1994).

FASN expression demonstrated in the colorectal carcinoma correlated with the elevated fatty acid synthetic activity, suggesting FASN to be a marker of early neoplastic transformation (Rashid et al., 1997). FASN over-expression was studied in various other cancer types such as those of the mesothelium (Gabrielson et al., 2001), ovary (Gansler et al., 1997), skin melanoma (Innocenzi et al., 2003), stomach (Kusakabe et al., 2002) and lung (Piyathilake et al., 2000). The over-expression in prostate tumours was compared with the corresponding normal tissues, which revealed increased FASN protein expression and very low levels of mRNA expression in 17% of the samples analysed. FASN expression correlated with the poorly differentiated tumours suggesting the importance of this molecule in aggressive form of the disease (Rossi et al., 2003). FASN expression in endometrial cancer correlated with the cancer progression and body fat distribution (Tsuji et al., 2004).

Prostate cancer tissue microarray analysis reported the amplification of FASN gene copy number and its correlation with the FASN protein over-expression in 53% of the tumour tissues tested. This gene amplification also correlated with the tumour grade (Shah et al., 2006). Another study in colorectal cancer found that, over-expression of FASN was associated with micro satellite instability (MSI) (Ogino et al., 2007). FASN is over-expressed in the normal mucosa and in the cancer cells in the ulcerative colitis patients in comparison with the negative FASN expression in the normal healthy control subjects. This study suggests that FASN could be a useful early diagnostic tool for detecting ulcerative colitis (Consolazio et al., 2006). Oral sqaumous cell carcinoma (OSCC) tissue sections showing positivity for FASN also

showed positivity for ERBB2 (HER2/neu) in 97% of the tumour sections. These tumours were also positive for Ki67, which is the hallmark of cell proliferation.

A strong positive correlation was observed with the ERBB2, FASN and USP2a mRNA expression revealed by qRT-PCR. This study showed the molecular connection between these molecules in the oral squamous cell carcinoma samples (da Silva et al., 2009). FASN over-expression in breast cancer cells such as MCF7 and MDA-MB-468 cells revealed drug resistance phenomenon and decreasing the FASN expression or by inhibiting FASN with orlistat increased the sensitivity to anti-cancer drugs. This mechanism appears to be due to the increased production of palmitic acid by FASN. These results indicated that FASN is an ideal target for chemo sensitization in breast cancer chemotherapy (Liu et al., 2008).

Haase et al., 2010 recently demonstrated the FASN expression for the first time in human meningioma tissues. Increased FASN expression was found in aggressive meningiomas tested by immunostaining. These results were confirmed by real time PCR and western blot. Studies with meningioma cell lines revealed that FASN expression was regulated by PI3K pathway, suggesting that FASN could act as a novel therapeutic target for malignant meningioma (Haase et al., 2010).

A recent report on colorectal cancer patients showed that FASN expression in three different stages of the disease was significantly different. Serum FASN levels were higher in stage III & IV compared to the enzyme levels in stages I & II of the metastatic colorectal cancer patients (Notarnicola et al., 2011). The extracellular FASN expression in cell culture supernatants of breast cancer cells and in serum of breast cancer patients was demonstrated by Wang et al., 2004. FASN was released into the extra-cellular space from cancer cells. The serum FASN levels correlated well with the disease prognosis. This study suggests that the extracellular FASN serves as a diagnostic marker in the cancer biology (Wang et al., 2004).

4.1.2. Fatty acid synthase and Retinoblastoma

Retinoblastoma (RB) is a primary intra-ocular tumour of the developing retina that often affects children, caused due to the mutation in the Rb1 gene (13q14), which encodes for the tumour suppressor Retinoblastoma protein (pRb) that inhibits cancer development in eye and throughout the body. The disease occurs both as hereditary (with a positive family history) and non-hereditary form (sporadic germline mutations). The Asian Indian RB tissues show more invasive phenotype compared to the western population (Schultz et al., 1993). These findings were correlated with the delayed referrals of the RB patients and also the different biologic behaviour of Indian RB tumours (Biswas et al., 2003; Krishnakumar et al., 2007). A study conducted at Italy with retinoblastoma tumour tissues, showed 82% FASN positivity by immunostaining. The strong expression of FASN was correlated with invasion of optic nerve, choroid, and high mitotic index (Camassie et al., 2003).

4.2 Objectives

1. To evaluate the FASN protein expression (by immunohistochemistry, western blot, and ELISA) and FASN mRNA expression (by RT-PCR) in an Indian cohort of retinoblastoma (RB) tumour tissues.

2. To correlate the expression of FASN with the clinico-pathological features of the RB tumour tissues.

4.3. Materials & Methods

In the present study, we used 65 RB tumour samples collected from 2000 to 2009 (Tables 4.3 – 4.6). Among them 24 were females and 41 were males with an average age of 1.80 yrs (range 1 month to 5 years). The clinical and pathological information and tumour-invasion were obtained from the medical records of our institute. RB sections were graded microscopically and were divided into three groups according to the predominant pattern of differentiation: well differentiated, moderately

differentiated and poorly differentiated (Finger et al., 2002). All tumour slides were reviewed and examined for invasion of choroid, optic nerve, orbit, and retinal pigment epithelium. Choroidal invasion was classified as either focal invasion or diffuse invasion of the choroid (Schilling et al., 2001; Biswas et al., 2003). The tumour invasion of the optic nerve included pre laminar invasion, post laminar invasion and invasion of the surgical end of the optic nerve.

4.3.1. Cell culture

Muller-glial (MIO-M1) cell line derived from neural retina (Limb et al., 2002) was grown in DMEM media supplemented with 10% FBS and maintained at 37°C with 10% CO_2. MIO-M1 cell line was a gift from Dr. G. A. Limb, Institute of Ophthalmology, University College, London.

4.3.2. FASN Immunohistochemistry in RB

Forty-four formalin-fixed, paraffin-embedded enucleated globes from 44 patients with RB were analyzed immunohistochemically for FASN expression. The eyeballs were from 18 female and 26 male patients with an average age of 1.97 years (range: 1 month to 5 years). The invasion and differentiation status of the RB tumours are tabulated below (Table 4.1).

Table 4.1: Immunohistochemical Analysis cohort details of RB Tumour Sections

<table>
<tr><th>Total Number</th><th rowspan="2">Tumours with No Invasion</th><th colspan="3">Tumours with Invasion of</th></tr>
<tr><td rowspan="4">44</td><td>Choroid</td><td>ON</td><td>Orbit</td></tr>
<tr><td>22</td><td>15</td><td>16</td><td>2</td></tr>
<tr><td colspan="4">Tumour Cell Differentiation</td></tr>
<tr><td>WD</td><td>MD</td><td colspan="2">PD</td></tr>
<tr><td>15</td><td>5</td><td colspan="2">24</td></tr>
<tr><td colspan="5">Abbreviations: ON – optic nerve, WD-well differentiated, MD-moderately differentiated, PD-poorly differentiated</td></tr>
</table>

Immunohistochemical detection of FASN on paraffin wax embedded tumour sections was performed using a mouse anti-FASN monoclonal antibody (1:75 dilution; Transduction Laboratories; BD Biosciences Pharmingen, USA). Staining for FASN was visualized with the streptavidin-biotin immunoperoxidase technique using the LSAB kit (DakoCytomation, Glostrup, Denmark) according to the manufacturer's instructions. The ocular pathologist analyzed the immunostaining by masking the clinical features. The FASN positivity is marked as '**+**' for intense staining and '**±**' for dull staining. Accordingly staining intensity was numbered as 1 for dull staining, and 2 for intense staining. Ten tumour fields on each tumour section were randomly scanned under high power magnification (40X) and the average percentage positivity (0% to 100%) of the tumour cells was calculated. The number of positive cells per slide was stratified into three groups based on the percentage of positive cells: group 1, <33%; group 2, 33 - 67%; group 3, 68 - 100%. Scores ranging from 1 to 6 was obtained by multiplying the staining intensity by the number of the group that represented the percentage of positive cells. (Kommoss et al., 1990; Mallikarjuna et al., 2007)

4.3.3. FASN gene expression analysis by reverse transcriptase PCR in RB

Total RNA was isolated from fresh RB tumour tissues by Trizol method. The RNA quality was checked with a 2% agarose gel. For all samples 2 µg of total RNA was used to synthesize first-strand cDNA using Sensiscript® RT kit (Qiagen) and random primers. PCR amplification of the first strand cDNA was performed using specific primer pairs (section 3.11.5), along with housekeeping gene, glyceraldehyde-3 phosphate dehydrogenase (GAPDH) as internal control. PCR products were fractionated by electrophoresis using 2% agarose gel containing 0.5% ethidium bromide with 100bp DNA ladder (Genei, INDIA) to confirm the size of the resultant product. The band intensities were semi-quantitatively measured by using the Image J 1.43 software and OD values were plotted.

4.3.4. Western Analysis of FASN protein in RB

Approximately 250 mg from 17 fresh RB tissues were homogenized in lysis buffer containing 50 mM of Tris-HCl (pH 7.6), 5 mM of EDTA, 150 mM of sodium chloride, 0.1% PMSF (Sigma), and 250 μL of 1 mg/ml Protease Inhibitor Cocktail (Sigma Aldrich, MO, USA). Tissues were then sonicated at 80 cycles/min. Protein estimation was carried out by the method of Lowry et al., 1951. 100μg of each sample was run on 8% SDS-PAGE and then electrophoretically transferred onto nitrocellulose membrane. Uniformity of transfer was checked with 0.1% Ponceau S and non-specific sites were blocked with 5% nonfat dry milk. The blots were incubated with primary antibody overnight at 4°C and then with the respective horseradish peroxidise - conjugated secondary antibody (Amersham, Buckinghamshire, UK) for 2 h. After intermittent washes with TBS-T (Tris buffered saline-Tween 20), the immunoreactive bands were detected by Enhanced Chemiluminescence (ECL; Pierce Thermo scientific, Rockford, USA). Antibodies against β- actin were used as the loading control. The FASN band intensity was measured using a densitometer (BIORAD GS 800, USA) and Quantity One software. The FASN band optical density thus obtained was then normalized with respect to the loading control β- actin.

4.3.5. FASN - ELISA in RB

Approximately 250 mg from the 5 fresh RB tumour tissues were homogenized in HEPES buffer (10mM HEPES buffer, 1mM EDTA and 10mM DTT) containing and 1 mg/ml Protease Inhibitor Cocktail (Sigma). Tissues were then sonicated at 80 cycles/min. Samples were diluted 1 in 5 with PBS and the FASN protein content was measured using FAS-detect™ ELISA, (FASgen, Baltimore, Maryland, USA) as per the manufacturer's instructions. The colour developed was read at 450 nm in an ELISA reader (Biotek, USA). The concentration of FASN protein in tumour tissues was expressed in ng/ml.

4.3.6. Statistical Analysis

Data are expressed as mean ± S.D. Student's unpaired *t*-test was used for comparisons. Differences were considered significant at $P < 0.05$.

4.4. RESULTS

4.4.1. Immunohistochemical Analysis in RB

The immunohistochemical analysis of 44 RB tissue sections is tabulated along with their respective clinico-pathologic features (Table 4.2). In the non-neoplastic donor retina, FASN immunostaining was negative in most regions except the ganglion cells that showed focal FASN positivity (Figure 4.1a). The cytoplasmic FASN immunoreactivity in representative RB samples differing in their nature of tumour invasiveness is presented in figures 4.1b - 4.1d. All the 44 tumour samples (100%) stained positive for FASN. FASN immunostaining was heterogeneous between the tumours ranging from 20% - 100% positively stained cells. This is represented as a scatter plot comparing non-invasive tumours with tumours invading choroid, optic nerve, orbit and RPE (Figure 4.2a). The percentage of cellular positivity for FASN immunoreactivity was significantly higher in the tumours with invasion compared to non-invasive tumours ($P = 0.001$). As outlined in the methods section, a numeric score for immunostaining was calculated for every sample (Table 4.2). We found that the scores for the invasive RB samples were significantly higher than the non-invasive cohort ($P = 0.027$).

On the basis of tumour cell differentiation, we found a significant increase in the FASN immunoreactivity in the poorly differentiated tumours compared to well differentiated tumours ($P=0.013$). The moderately differentiated RBs showed 60% – 90% FASN immunopositivity (Figure 4.2b). There was no significant difference in FASN expression with respect to laterality of the tumours.

Figure 4.1: Immunohistochemical analysis of FASN in RB

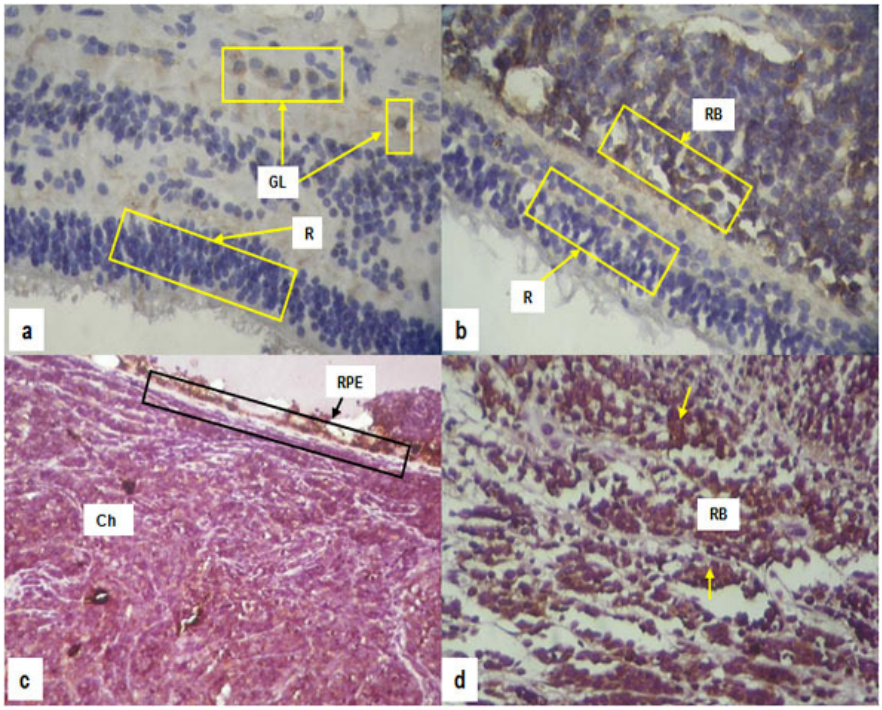

*__Figure 4.1: Immunohistochemical analysis of FASN in RB: (a)__ Photomicrograph of the non-neoplastic donor retina shows no FASN immunopositivity in most regions except a faint FASN immunoreactivity in the ganglion layer (40X). FASN immunonegativity in the retinal cells is depicted by R, and the ganglion layer positivity is indicated by GL. **(b)** RB tissue with no tumour invasion reveals positive FASN immunoreactivity in the tumour cells (indicated as RB), while the adjoining normal retinal cells are negative for FASN indicated as R (40X). **(c)** Intense FASN immunoreactivity in the RB tumour cells invading the choroid (Ch) across the retinal pigment epithelium, RPE (40X). **(d)** RB tumour tissue with prelaminar optic nerve invasion shows intense FASN immunoreactivity (indicated by arrows) in the RB cells (40X).

* *The data presented in figure 4.1 is published in: Exp Mol Pathol. 2011 Feb; 90(1):29-37. Please see the "List of publications" on Page XXIII*

Figure 4.2 Comparison FASN immunoreactivity with RB tumour invasion and differentiation status

Figure 4.2a: Dot plot of FASN immunoreactivity in RB tumour tissues

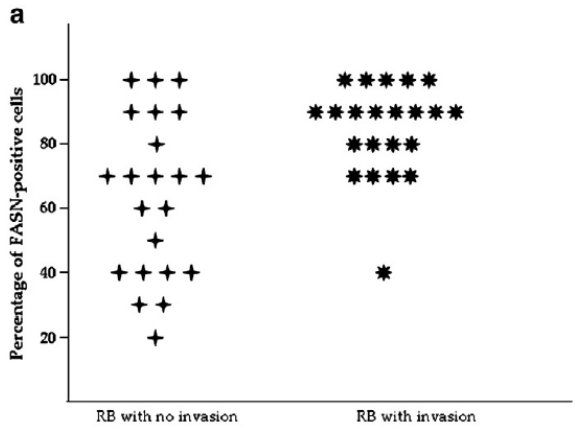

Figure 4.2b Comparison of FASN immunoreactivity relative to tumour differentiation status

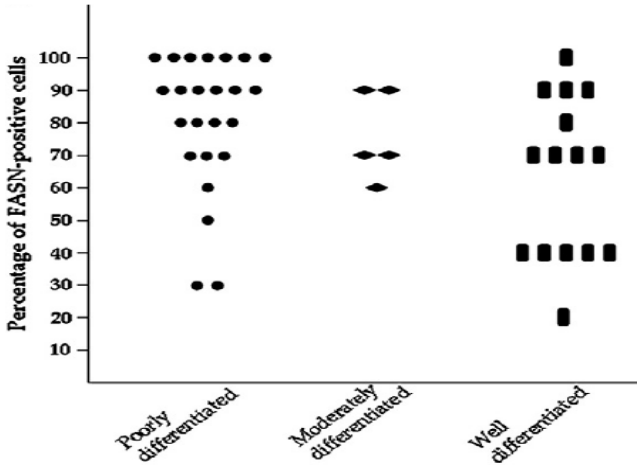

[†]**Figure 4.2 Comparison FASN immunoreactivity with RB tumour invasion and differentiation status: a)** The percentage of FASN immunopositive cells in RB with no invasion has been plotted along with RB with invasion of choroid, optic nerve, orbit and/or RPE. **b)** The percentage of FASN immunopositive cells in RB is presented with respect to tumour differentiation: poorly-, moderately-, and well-differentiated tumours.

[†]*The data presented in figure 4.2 is published in: Exp Mol Pathol. 2011 Feb; 90(1):29-37. Please see the "List of publications" on Page XXIII*

Table 4.2 Immunohistochemical analysis with clinico-pathological correlations

S. No	Age/Sex	Clinicopathological features			FASN Immunohistochemistry		
		Laterality	Differentiation	Invasion Status	% Positive cells	Staining Intensity	Score
1	2y/F	OD	PD	NI	30	±	1
2	3mon/M	OS	PD	NI	80	+	6
3	6mon/M	OD	WD	NI	90	+	6
4	18mon/F	OD	MD	NI	70	+	6
5	6mon/M	OS	WD	NI	20	±	1
6	2mon/F	OS	WD	NI	40	±	2
7	1y/F	OU	PD	NI	30	±	1
8	5y/M	OS	MD	NI	60	±	2
9	3y/F	OD	PD	NI	60	±	2
10	2y/M	OD	WD	NI	40	±	2
11	4mon/M	OS	WD	NI	70	±	3
12	8mon/F	OS	WD	NI	40	+	4
13	11mon/F	OD	PD	NI	90	+	6
14	30mon/F	OD	WD	NI	70	+	6
15	5mon/M	OD	WD	NI	100	+	6
16	12mon/M	OS	WD	NI	90	+	6
17	40mon/M	OS	PD	NI	100	+	6
18	5y/M	OS	PD	NI	>90	+	6
19	30mon/M	OU	PD	NI	50	±	2
20	1y/F	OD	WD	NI	70	±	3
21	18mon/F	OD	WD	NI	70	+	6
22	16mon/M	OD	WD	NI	40	±	2
23	2y/F	OD	PD	Focal Ch Inv (<3mm) & Post Lam ON Inv	90	+	6
24	3y/F	OD	PD	Post Lam ON Inv, Surgical end Inv	90	+	6
25	3y/M	OD	PD	Post Lam ON Inv & Orbital Inv	80	+	6
26	7mon/M	OD	PD	Rectus muscle & Orbital Inv	90	+	6
27	10mon/M	OU	WD	Diff Ch Inv and ON Inv Ant to LC	40	+	4

28	5y/F	OD	WD	Focal Ch Inv(<3mm) & Post Lam ON Inv	90	+	6
29	3y/M	OS	PD	Diff Ch, Post Lam ON Inv	70	±	3
30	3y/M	OS	PD	Diff Ch, PreLam ON Inv	80	±	3
31	3y/M	OU	PD	ON Inv & Meningeal sheath of ON Inv	100	+	6
32	42mon/M	OS	PD	Post Lam ON Inv	100	+	6
33	1y/F	OD	PD	Diff Ch Inv	100	+	6
34	4y/F	OD	MD	Focal Ch Inv (<3mm)	90	±	3
35	3mon/M	OD	PD	Ch Inv (<3mm) & PreLam ON Inv	70	±	3
36	18mon/M	OD	WD	Focal Ch (<3mm) & PreLam ON Inv	80	±	3
37	4y/M	OS	PD	Diff Ch and ON Inv	70	+	6
38	2y/F	OD	PD	Diff Ch, Post Lam ON Inv	90	+	6
39	1mon/M	OU	MD	Diff Ch Inv	90	+	6
40	7mon/F	OS	PD	Focal Ch Inv (<3mm)	100	+	6
41	15 mon/F	OD	MD	Focal Ch (<3mm) & PostLam ON Inv	70	+	6
42	2y/M	OS	PD	Diff Ch, Inv of ON up to LC	80	±	3
43	5y/M	OD	PD	Diff Ch Inv	90	+	6
44	2y/M	OU	PD	ON Inv beyond LC	100	+	6

Abbreviations: M- Male, F- Female, y- years, mon- Months, OD- right eye (unilateral), OS- left eye (unilateral), OU- both eyes (bilateral), WD- well differentiated, PD- poorly differentiated, MD- moderately differentiated, ON- optic nerve, PreLam- pre laminar, PostLam- post laminar, Inv- Invasion, NI- No Invasion, RPE- retinal pigment epithelium, LC- Lamina cribrosa, Diff- diffuse, Ch- Choroid, Ant- anterior, AC- anterior chamber.

4.4.2. Western Analysis of FASN Protein in RB: FASN expression was qualitatively assessed in 17 tumour tissue samples by immunoblotting with anti human FASN antibody. The blot showed specific band of FASN at 250 kD in the tumour samples, that varied in band intensity. Figure 4.3a shows the representative FASN bands in tumour samples whose clinico-pathologic features are tabulated (Table 4.3). The samples were tested for uniform loading with the loading control β-actin. The band intensity in 17 RB tissues was measured densitometrically and computed as a ratio with respect to β- actin (Figure 4.3b). We found the FASN expression in tumour

tissues with invasion of choroid, optic nerve, orbit and/or RPE to be significantly greater than in RB tissues without invasion (P = 0.04). The inter-tumour differences in FASN expression were clear. Yet, the overall FASN protein expression was significantly elevated in the tumours with invasion than the non-invasive tumours (P<0.05). To illustrate this, the immunohistochemical and western analysis of tumours broadly divided into invasive and non-invasive tumours has been summarized in Figure 4.3c. For this, the average immunostaining score of all the non-invasive RB cases was compared with the average immunostaining score of the RB cases with tumour invasion. Similarly the mean FASN band intensity of tumours with no-invasion was compared with tumours with invasion.

Table 4.3. Clinico-pathologic characteristics of RB samples included for Western analysis of FASN protein

Sample No.	Age/Sex	Differentiation	Laterality	Tumour Invasion Status
1	4mon/M	WD	UL	NI
2	4y/M	PD	UL	NI
3	3y/F	UD	UL	NI
4	3mon/M	UD	UL	NI
5	8mon/F	WD	UL	NI
6	16mon/M	WD	UL	NI
7	3y/F	PD	UL	NI
8	2mon/M	WD	UL	Focal RPE Inv
9	2y/F	MD	UL	Focal Ch Inv
10	1mon/M	MD	BL	Diff Ch Inv
11	5y/M	UD	UL	Full thickness Ch inv
12	3mon/M	UD	UL	Extension to ON & Ch
13	18mon/M	WD	UL	Focal Ch & PreLam ON Inv
14	2y/M	UD	UL	PostLam ON Inv, No Ch Inv
15	3mon/F	UD	UL	Extension into AC and RPE. No Ch and ON Inv
16	1y/F	WD	UL	Focal Ch, RPE & PreLam ON Inv
17	2y/M	PD	UL	PostLam ON Inv

Samples numbers 1, 2, 3, 4 & 11 correspond to lanes 1 to 5 respectively in the representative western blot (Figure. 4.3a). Abbreviations as explained in Table 4.2

Figure 4.3 Western analysis of FASN in RB tissues

Figure 4.3a

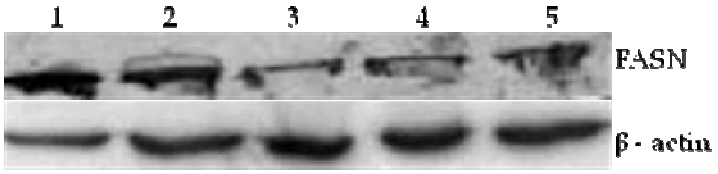

Figure 4.3b

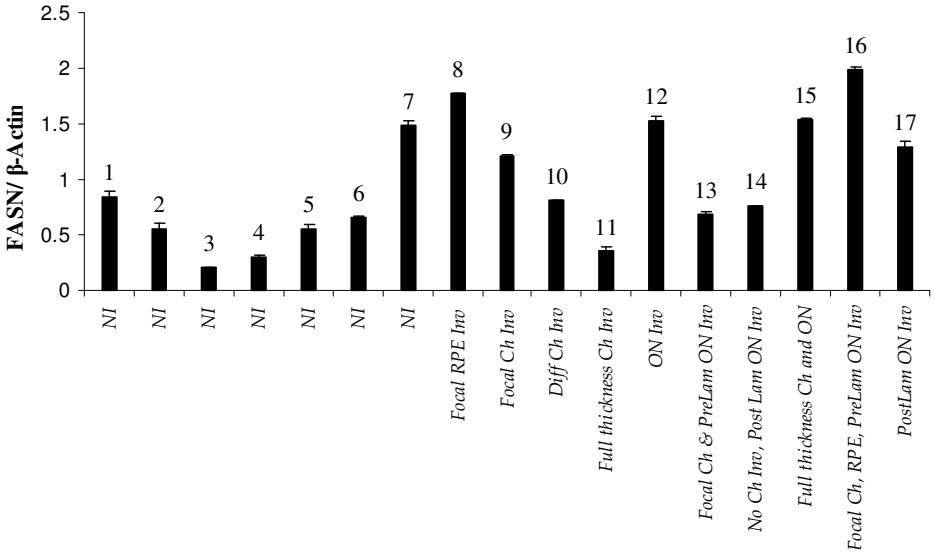

‡**Figure 4.3 Western analysis of FASN in RB tissues: a)** Western blot of FASN protein expressed in 5 representative RB samples differing in their tumour differentiation and invasion status (Table 4.3). The samples were tested for equal protein loading with β-actin. **b)** Densitometric measurement of FASN band intensity was expressed with respect to β-actin. Values are expressed as mean ± S.D. of two independent experiments.

‡*The data presented in figure 4.3 is published in: Exp Mol Pathol. 2011 Feb; 90(1):29-37. Please see the "List of publications" on Page XXIII*

Figure 4.3c

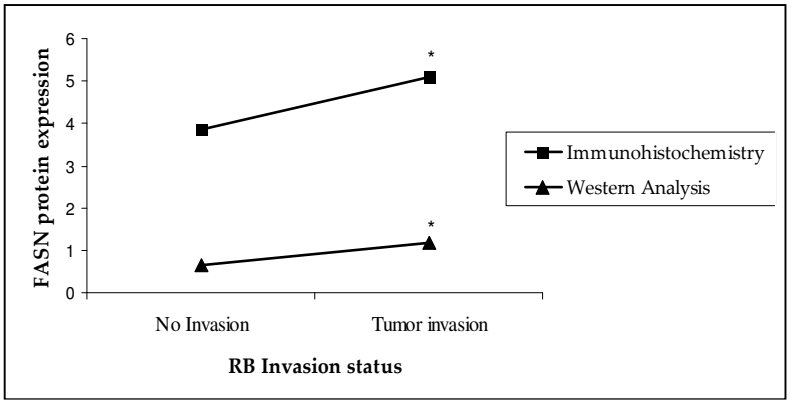

Figure 4.3c Western analysis of FASN in RB tumour samples: A comparative graph is presented to illustrate the overall increase in FASN expression evaluated by immunostaining and western analysis of RB tissues with and without tumour invasion. The average FASN/ β-actin ratio (western analysis), and immunostaining score were computed for the tumours with invasion, and for the non-invasive tumours. * indicates significantly increased FASN expression in the invasive tumours with respect to non-invasive tumours ($P<0.05$).

4.4.3. FASN – ELISA in RB

FASN protein content in 5 RB tissues and MIO-M1 cells was estimated by sandwich ELISA. The clinical and pathological features of the RB cases have been tabulated (Table 4.4). The FASN concentration was quantified in ng/ml. We found FASN concentration in the non-neoplastic MIO-M1 cells to be minimal. Therefore we used the FASN levels in muller glial cells as the basal expression of normal tissue, and expressed the FASN concentrations in tumour tissues as fold increments over MIO-M1 cellular FASN expression (Figure 4.4).

Table 4.4: Clinico-pathologic characteristics of RB samples included for FASN protein quantification by ELISA

Sample No.	Age/Sex	Differentiation	Laterality	Tumour Invasion Status
1	3mon/M	WD	UL	NI
2	2mon/M	WD	UL	Focal RPE Inv
3	2y/F	MD	UL	Focal Ch Inv
4	9mon/F	WD	UL	PreLam ON Inv
5	2y/M	PD	UL	Post Lam ON Inv

Abbreviations as explained in Table 4.2

4.4.4. RT-PCR Analysis of FASN mRNA in RB

Ten RB tissues and MIO-M1 cells were analyzed for FASN mRNA expression by RT-PCR along with the house keeping gene GAPDH. The clinical and pathological features of the RB cases have been presented in Table 4.5. All the RB tissues expressed the 152 bp FASN mRNA band (Figure 4.5a). The intensity of the bands was normalized with GAPDH. Similar to the heterogeneous FASN protein expression in RB tissues, the FASN mRNA too showed inter-tumour differences in expression. FASN mRNA in MIO-M1 cells was minimal. The over-expression of FASN mRNA in tumour tissues was then computed as increments over MIO-M1 cellular FASN expression (Figure 4.5b). The over-expression of FASN mRNA and FASN protein has been collated from two representative RB samples to illustrate the extent of up- regulation of FASN at transcriptional and translational levels (Figure 4.5c).

Table 4.5: Clinico-pathologic characteristics of RB samples assayed for FASN mRNA by RT-PCR

Sample No.	Age/Sex	Differentiation	Laterality	Tumour Invasion Status
1	2y/F	MD	UL	Focal Ch Inv
2	10mon/F	PD	UL	NI
3	2mon/M	WD	UL	Focal RPE Inv
4	6mon/M	WD	UL	NI
5	2y/M	UD	UL	PreLam ON Inv
6	2/M	MD	UL	Minimal RPE Inv
7	3/M	PD	UL	Focal RPE & Ch Inv, 20% LC Inv of ON, tumour cells seen in menengeal sheath
8	2/M	UD	UL	Focal RPE Inv, extension to ON Ant to LC
9	3/M	UD	UL	NI
10	1/M	MD	UL	ON Inv beyond LC

Sample numbers 1-5 correspond to lanes 2 to 6 respectively in the representative RT-PCR gel (Fig. 4.5a).
Abbreviations as explained in Table 4.2 in this section

Figure 4.4: Enzyme linked immuno-sorbent assay of FASN protein in RB

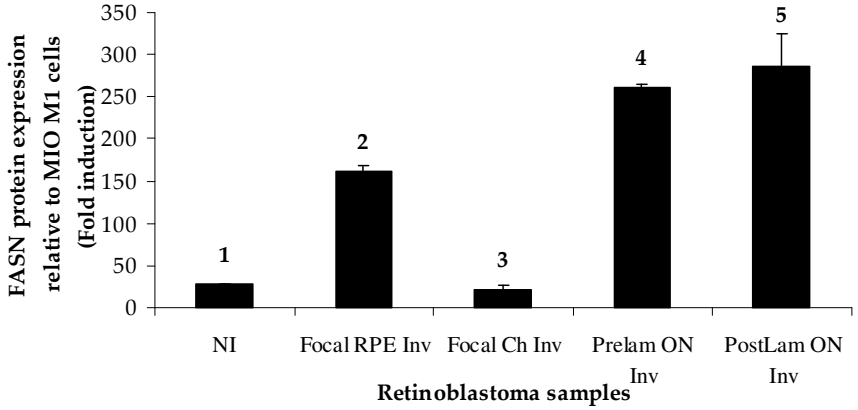

[§]**Figure 4.4: Enzyme linked immuno-sorbent assay of FASN protein in RB tissue samples:** FASN protein was quantified by sandwich ELISA in RB tissues differing in tumour-invasion status. The clinical details of the samples are presented in table 4.4. The over-expression of FASN in the tumour tissues is depicted as fold-increases with respect to the non-neoplastic muller glial cells. Values are expressed as mean ± S.D of three independent experiments.

[§]*The data presented in figure 4.4 is published in: Exp Mol Pathol. 2011 Feb; 90(1):29-37. Please see the "List of publications" on Page XXIII*

Figure 4.5 RT-PCR analysis: FASN mRNA expression in RB

Figure 4.5a

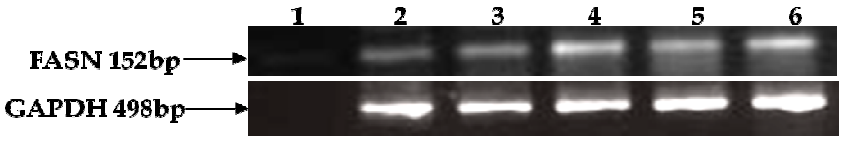

Figure 4.5b

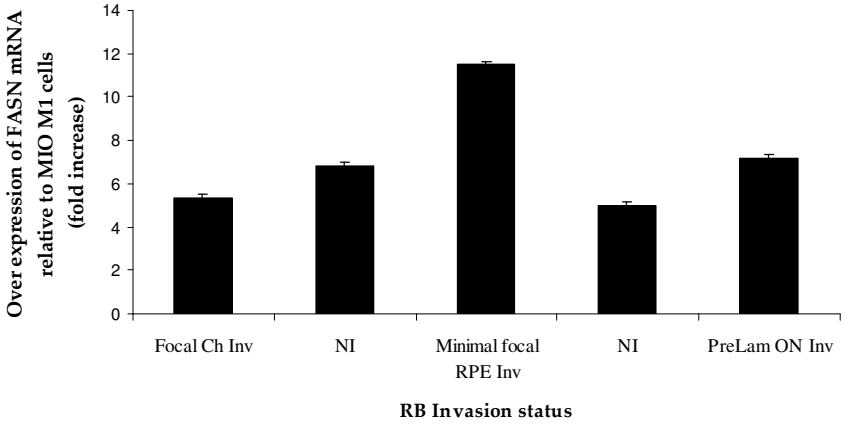

[**]**Figure 4.5 RT-PCR analysis FASN mRNA expression in RB: a)** FASN mRNA expression in RB tissues was assayed by RT-PCR. A representative RT-PCR gel depicting five samples is shown. The corresponding loading control (GAPDH, glyceraldehyde 3-phosphate dehydrogenase) is also presented. Lane 1 is a technical negative control, and lanes 2 to 6 are loaded with RB samples whose clinical details are tabulated (Table 4.5). **b)** The band intensity was measured densitometrically and calibrated with GAPDH. The FASN mRNA expression in ten tumour samples is expressed as a ratio with respect to FASN mRNA expression in MIO-M1 cells.

[**]*The data presented in figure 4.5a&b is published in: Exp Mol Pathol. 2011 Feb; 90(1):29-37. Please see the "List of publications" on Page XXIII*

Figure 4.5c: FASN mRNA and protein expression ratio in RB tissues

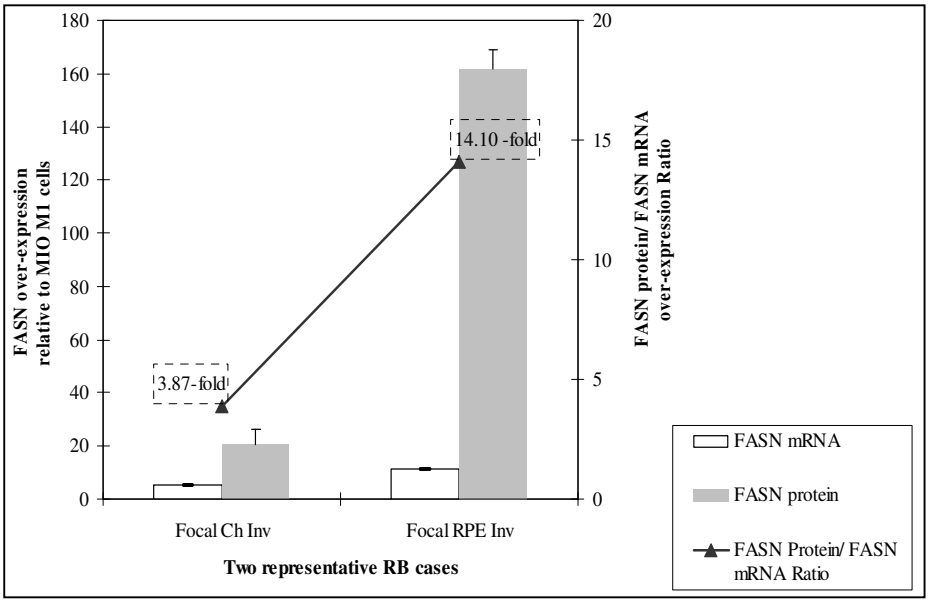

††**Figure 4.5c: FASN mRNA and protein expression ratio:** The concurrent expression of FASN mRNA and FASN protein is demonstrated in two representative RB samples (Y-axis), along with the ratio of fold induction of FASN protein to that of FASN mRNA relative to MIO-M1 cells (Y'-axis). The extent of increase of FASN protein over the corresponding FASN mRNA expression has been depicted numerically in the line graph.

4.5. Chapter Summary

FASN expression studies in RB tumour tissues revealed markedly high expression of

i. FASN protein in poorly differentiated and in invasive RB tissues;

ii. Multi-fold over-expression of FASN mRNA and protein in RB tissues, although at varying levels, indicating FASN to be a potential therapeutic target in retinoblastoma management.

††The data presented in figure 4.5c is published in: Exp Mol Pathol. 2011 Feb; 90(1):29-37. Please see the "List of publications" on Page XXIII

CHAPTER 5: OXIDATIVE STRESS IN RETINOBLASTOMA (RB): CORRELATION WITH CLINICO-PATHOLOGIC FEATURES

5.1. INTRODUCTION

The expression of fatty acid synthase (FASN) in RB tumour tissues was correlated with the RB tumour invasiveness in Chapter 4. This chapter deals with the evaluation of oxidative stress in RB tumour tissues and their role in tumour invasiveness.

5.1.1. Oxidative stress and cancer therapy

De novo synthesized palmitate (by FASN) plays an important role in the maintenance of redox balance by rescuing the cancer cells from diffusion of ROS and oxidative stress mediated cell death (Migita et al., 2009). FASN chemical inhibition in melanoma cells led to apoptotic cell death, which was preceded by increase in reactive oxygen species (ROS) production (Zecchin et al., 2011). During cancer chemotherapy, many anti-neoplastic agents produce oxidative stress in biological systems; the ROS generated during cancer therapy may interfere with the efficacy of the treatment. Some of the chemotherapy drugs that generate high levels of reactive oxygen species (ROS) levels are doxorubicin, carboplatin, and etoposide. Redox-active agents that can enhance the benefits of conventional anti-cancer therapy, without adversely affecting the normal cells, would be an effective strategy in the clinical management of RB, and other cancers (Conklin, 2004).

5.1.2. Oxidative stress

5.1.2.1. Oxidative damage to lipids

The oxidative damage is defined as the damage to tissues and cells caused by the reactive oxygen species. High concentrations of unsaturated fatty acid in the

membrane phospholipids make the cellular membranes highly sensitive to oxidative damage. Lipid peroxidation occurs in three stages namely: initiation, propagation and termination. The reactive oxygen metabolite attacks the fatty acid, in which the double bond between the hydrogen and carbon atoms weakens and the hydrogen atom is abstracted to form a fatty acid radical. The fatty acid radical undergoes reactions, rearrangements, and cyclisation process to form a series of intermediates: aldehyde, cyclic endoperoxide, and isoprostans. These reactions continue during the propagation stage. Thus one initiation step by the reactive oxygen metabolite can lead to peroxidation of all the unsaturated lipids present in the membranes. Chain termination occurs when two lipid radicals interact with each other or when it reacts with an antioxidant (Halliwell, 2011; Kohen & Nyska, 2002).

5.1.2.2. Reactive oxygen species (ROS)

The **reactive oxygen species (ROS)** is the collective term for oxygen radicals, which comprises two types: radicals and non-radicals. These species can easily generate free radicals and/or cause oxidative damage. The radical group is termed as free radicals. They are oxygen ($O^{\cdot}{}_2$), superoxide ($O^{\cdot}{}_2^-$), hydroxyl ($OH^{\cdot}$), and peroxyl ($ROO^{\cdot}$) radicals. The superscript dot in each of these represents the free radical state. Hydrogen peroxide (H_2O_2), hypochlorous acid (HOCl), ozone (O_3) and aldehyde (HCOR) are non-radicals.

An antioxidant is defined as a molecule that protects a biological target such as a cell, against the oxidative damage (Halliwell, 2011).

Oxidative stress is defined as the imbalance between the generation of reactive oxygen species and antioxidant protection in favour of the ROS, causing excessive oxidative damage to the membrane lipids and DNA thereby leading to cell death (Halliwell, 2011; Kohen & Nyska, 2002).

5.1.2.3. ROS Homeostasis

ROS plays dual roles both beneficial and harmful to the living cells. Beneficial effects are defense against infectious agents and important functions in cell signaling processes. At low concentrations ROS can induce mitogenic signals, but at higher concentrations it damages the biological molecules: proteins, lipids and nucleic acids.

All the free radicals are present in measurable concentrations in the cells. Their 'steady state' level depends on the balance between their production and the rate of removal by antioxidants. Under normal conditions, the redox state of the cells is maintained in a normal level, which under pathological states, alters to low or high values. **Redox homeostasis** is primarily maintained by GSH (reduced glutathione) and TRX (Thioredoxin). The glutathione (2GSH/GSSG) couple represents the major cellular redox buffer and acts as a redox indicator. Under oxidative stress conditions GSSG content increases and it increases the concentration of protein mixed disulphides. These proteins containing the critical thiols are involved in signaling mechanisms. Thus GSSG acts as a non-specific signaling molecule.

GSH and TRX buffering systems counteract intracellular oxidative stress, in which the ratios of reduced and oxidised GSH and TRX levels are maintained by the GSH reductase and TRX reductase activities respectively. In addition GSH and TRX are also involved in cell signaling process. Various free amino acids, peptides and proteins, when present at high concentrations contribute to the free radical scavenging activity.

5.1.2.4. Generation of reactive oxygen species

The chain of reactions that generate reactive oxygen species starts with the reduction of molecular oxygen (Figure 5.1) by oxidase enzymes such as NAD(P)H oxidases and xanthine oxidase enzymes and also by non-enzymatic redox-reactive

compounds. This results in the formation of superoxide anion radical which is called as the **'primary ROS'**. The primary ROS interacts with other molecules further to generate **'secondary ROS'**. Superoxide dismutase (SOD) enzyme dismutates the superoxide radical to hydrogen peroxide. Hydrogen peroxide is scavenged by the enzyme glutathione peroxidase (GPx) which uses GSH as the electron donor. In this process GSH (reduced) gets oxidised to glutathione (GSSG-oxidised form). The GSSG is then reduced back to GSH by the enzyme glutathione reductase (GRed) in the presence of NADPH as the electron donor. Transition metals such as Fe^{2+}, Cu^{2+} ions act on hydrogen peroxide to release the reactive hydroxyl radical. This reaction is called the **Fenton reaction**. Apart from the ROS, the reactive nitrogen, sulphur, iron, copper and chlorine species are collectively called as **'reactive species'**.

Fenton reaction:

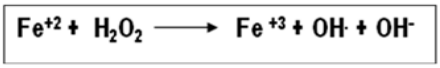

The hydroxyl radical can abstract an electron from polyunsaturated fatty acid (LH) to give rise to a carbon-centred lipid radical ($L^{\bullet}$). The lipid radical ($L^{\bullet}$) can further interact with molecular oxygen to give a lipid peroxyl radical ($LOO^{\bullet}$). This leads to **lipid peroxidation,** where the antioxidant systems do not reduce these peroxyl radicals.

5.1.2.5. Lipid peroxidation

This process involves the fast reaction of lipid hydroperoxides with Fe^{2+} to form lipid alkoxyl radicals ($LO^{\bullet}$), also in a slower reaction with Fe^{3+} to form lipid peroxyl radicals ($LOO^{\bullet}$). The cyclisation of lipid alkoxyl radical ($LO^{\bullet}$) (For e.g. arachidonic acid undergoes cyclisation reaction to form a six-membered ring hydroperoxide), and further reactions of the cyclised six-membered ring hydroperoxide (involving β-scission) leads to the formation of 4-hydroxynonenal. 4-hydroxynonenal is then

rendered unreactive into a glutathiyl adduct by glutathione S-transferase (GST). A peroxyl radical located in the internal position of the fatty acid undergoes cyclisation to produce cyclic peroxide, which reduces to a hydroperoxide, or it undergoes a second cyclisation to form bicyclic peroxide. This then undergoes reduction to form endoperoxide. This product acts as an intermediate to produce malondialdehyde (MDA). MDA then reacts with DNA bases adenine, guanine, cytosine to form M1A, M1G and M1C adducts respectively.

Then vitamin E (T-OH, reduced form) reduces the lipid peroxyl radical ($LOO^{\bullet}$) within the membrane, resulting in the formation of lipid hydro peroxide and vitamin E radical ($T\text{-}O^{\bullet}$). Vitamin E is regenerated back to its original form by Vitamin C (Ascorbate monoanion $AscH^{-}$) which leaves back ascorbyl radical ($Asc^{\bullet -}$). Vitamin E is also regenerated by GSH, where the oxidised vitamin E radical ($T\text{-}O^{\bullet}$) is reduced. In this reaction GSH gets oxidised to oxidised glutathione (GSSG). The GSSG and the ascorbyl radical ($Asc^{\bullet -}$) are reduced back to GSH and ascorbate monoanion, $AscH^{-}$, respectively, by the dihydrolipoic acid (DHLA) which is converted to α-lipoic acid (ALA). NADPH then converts the ALA back to DHLA. Lipid hydroperoxides are reduced to alcohols and dioxygen by GPx using GSH as the electron donor.

5.1.3. Other biological targets of reactive oxygen species

5.1.3.1. Protein

In addition to lipids, the proteins being the major constituents of cell membranes, also serve as possible targets for ROS attack. They are damaged by $OH^{\bullet}$, $RO^{\bullet}$, and reactive-nitrogen radicals predominantly. Hydrogen peroxide and superoxide radicals weakly affect the proteins, particularly they interact with those containing SH groups. ROS on interaction with the amino acid residues in the proteins leads to changes in tertiary structure, degradation and fragmentation of the proteins. The

biologic consequences of these changes are loss of enzyme activity, alteration of cellular functions, changes in cellular protein types and their levels. Protein oxidation usually forms aldehydes, keto compounds, and carbonyls. 3-nitrotyrosine serves as a marker for oxidative damage of protein.

5.1.3.2. DNA: Effects of ROS on DNA bases are: DNA base modifications, breaks on DNA strands, loss of purines (apurinic sites), deoxyribose sugar damage, DNA-protein cross-linkage, and damage to DNA repair system. The $OH^{\cdot}$ can attack guanine at its C-8 position to yield 8-hydroxydeoxyguanosine (8-OHdG). $OH^{\cdot}$ can also attack other bases like adenine. In addition to this, the less reactive ROS species such as $O^{\cdot}_2$ and H_2O_2 are not toxic to the cells at their physiological concentrations. But these species act as sources for other reactive intermediates to cause cell damage.

Every cell develops some defence mechanisms against the free radical induced oxidative damage. These defences are: preventive mechanism, repair mechanisms, physical defences and antioxidant defences. Antioxidant enzymes are superoxide dismutase (SOD), glutathione peroxidase (GPx), and catalase (CAT). Non-enzymatic antioxidants are ascorbic acid (Vitamin C), α-tocopherol (Vitamin E), glutathione (GSH), carotenoids and flavonoids (Valko et al., 2007).

5.1.4. Redox Signaling

Any disturbance in the 'redox balance' such as increase in ROS levels or a decrease in antioxidant activity leads to activation of 'redox signaling'. Changes in the thiol/disulphide redox state led to activation of signaling pathways:

1. Transcription factors AP-1
2. Protein tyrosine phosphatase
3. Src family kinase
4. JNK & p38 MAPK signaling pathways
5. Insulin receptor kinase

Figure 5.1: Pathways involved in the generation of reactive oxygen species (ROS) and lipid peroxidation

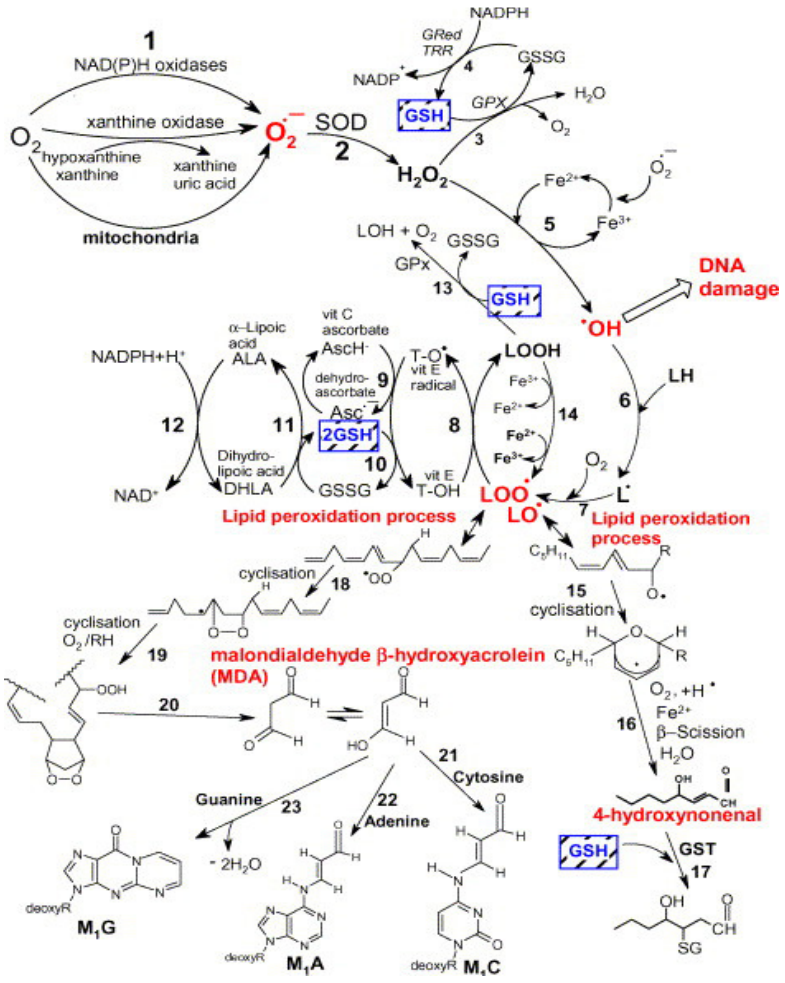

Figure 5.1 Pathways involved in the generation of reactive oxygen species (ROS) and lipid peroxidation: Figure shows the lipid peroxidation reactions and the antioxidant redox cycles (Valko et al., 2007).

Intracellular changes in GSH concentration sensitizes the redox environment of the cell, leading to a disturbed cell cycle. GSH rescues cells from apoptosis, in which the depletion of GSH renders the environment more oxidising. Elevated levels of GSH and TRX maintain a reducing environment of the cells thus stimulating cell proliferation. A slight shift towards oxidising environment leads to cell differentiation. On the other hand more oxidising environment leads to apoptosis

and necrosis. Thus the redox state of a cell determines the fate of the cell (Valko et al., 2007).

5.1.5. Oxidative stress in health

The redox regulated signaling pathways controls several physiological functions: production of NO, ROS production by NAD(P)H oxidase, ROS production in response to change in oxygen concentration, redox regulation of cell adhesion, immune response and apoptosis mechanisms.

5.1.6. Oxidative stress and diseases

Oxidative stress is implicated in pathological conditions, which are categorised into two groups:

1. Mitochondrial oxidative stress conditions (cancer, diabetes mellitus)
2. Inflammatory oxidative conditions (atherosclerosis, chronic inflammation, ischemia/reperfusion, and ageing (damage due to free radical action by lipid peroxidation, DNA damage and protein oxidation).

Table 5.1 Validated biomarkers of oxidative damage associated with human diseases.

Disease	Biomarker
Cancer	MDA, GSH/GSSG ratio, 3-Nitrotyrosine, 8-OH-dG
Diabetes mellitus	MDA, GSH/GSSG ratio, 3-Nitrotyrosine, AGE, F_2-isoprostanes, S-glutathionylated proteins
Cardiovascular disease	4-hydroxy-2-nonenal, GSH/GSSG ratio 3-Nitrotyrosine, Acrolein, F_2-isoprostanes
Rheumatoid arthritis	F_2-isoprostanes, GSH/GSSG ratio

Abbreviations: MDA- Malondialdehyde, GSH-reduced glutathione, GSSG- oxidised glutathione, AGE – advanced glycation end products

5.1.7. Oxidative stress and cancer

As already mentioned that the redox state of a cell determines its proliferation state, the extent of oxidative stress in a cancerous tissue determines its proliferation. ROS are oxidants and they have dual roles in promoting cell proliferation or cell death depending upon their concentrations (Valko et al., 2006). The redox imbalance due to oxidative stress is present more in the cancers compared to the normal cells, wherein this can be related to oncogenic stimulation. ROS induced DNA damage has been the critical factor to cause carcinogenesis, noted in various tumour tissues. Direct oxidative DNA damage can facilitate cancer development. 8-OH-dG is the extensively studied DNA lesion during tumourigenesis and it is an important oxidative biomarker for cancer progression. Various redox metals and non-redox metals induce carcinogenesis and ageing. Iron, cadmium, hexa valent chromium, arsenic, tobacco smoke has all been implicated as important sources for ROS induced carcinogenesis. Apart from the ROS, the lipid peroxidation products such as MDA, HNE have been found to be carcinogenic and affect signal transduction pathways in cancer cells (Valko et al., 2007).

Halliwell. (2007) reviewed the various stages of cancer progression in response to increasing ROS generation. Each cell is under reduced state and when gets exposed to oxidised environments, they start proliferating under mild oxidative stress which also involves release of free Ca^{2+} ions. Under greater oxidative stressed states oxidative damage at the DNA level starts and intracellular levels of Ca^{2+} increases. More oxidative stress conditions causes oxidative damage and mitochondrial damage by ROS, and mitochondrial permeability transition and release of cytochrome c from the mitochondria, and initiation of apoptosis. Eventually these processes worsen with increased oxidative insults and this leads to shutdown of caspases and halt of apoptosis. This is also accompanied by survival of damaged

cells, and necrotic cell death and spread of injury to the surrounding tissues (Halliwell, 2007).

The involvement of oxidative stress in cancer progression was studied in prostate cancer (Kumar et al., 2008). Studies in retinoblastoma (Adithi et al., 2005) correlated the expression of iNOS (inducible nitric oxide synthase) and (NT) nitrotyrosine with the RB tumour aggressiveness. The knowledge of differential gene expression and proteomic profile, and cell signaling mechanisms, in tumour cells is essential for designing the appropriate therapeutic strategy for the specific cancer. This is facilitated by cDNA microarray analysis.

5.1.8. cDNA Microarray analysis

cDNA Microarray analysis is a widely used technique for understanding the gene expression patterns. It is defined as an orderly arrangement of samples where matching of known and unknown DNA samples is done based on base pairing rules. The microarray works on the principle based on the ability of a given mRNA molecule to bind specifically to, or hybridize to, the template DNA from which it is originated. The expression levels of thousands of genes can be studied using an array by measuring the amount of mRNA bound to each spot. This can then be analysed using a computer, which will generate a profile of gene expression in a cell.

Microarray is categorized into three types based on the type of information that is obtained from them. They are: microarray expression analysis, microarray for mutation analysis, and comparative genomic hybridization.

5.1.8.1. Design of cDNA Microarray experiment

The steps involved in the microarray protocol are as follows:

1. Preparation of DNA chip using chosen target DNAs
2. Generation of hybridization mixture of fluorescently labeled cDNA
3. Incubation of hybridization mixture with the DNA chip

4. Detection of bound cDNA using LASER technology and storage of information
5. Data analysis (Zareparsi et al., 2004).

5.1.8.2. Applications of cDNA Microarray

Microarray type	Application
Comparative genome hybridization (CGH)	Tumour classification, risk assessment, and prognosis prediction
Expression analysis	Drug development, drug response, and therapy development
Mutation/Polymorphism analysis	Drug development, therapy development, and tracking disease progression

5.2. Objectives

1. To determine the lipid peroxidation marker malondialdehyde (MDA) and reactive oxygen species (ROS) levels in RB tumour tissues and to correlate with the RB tumour invasiveness.
2. To analyse the differential gene expression profile of RB Y79 cells (H_2O_2 oxidant- induced model) by cDNA Microarray technique.

5.3. Materials and methods

5.3.1. Tumour Samples

For studying the expression of malondialdehyde in RB tumour tissue sections, tumour samples from 34 patients (sourced between 1997 and 2002) were divided into two groups, A and B. Group A comprised of tumours without invasion of the choroid, optic nerve, or orbit and/or without metastasis. Group B consisted of tumours with invasion of the choroid, optic nerve, or orbit and/or with metastasis. The tumours were investigated for histopathological features and immunoreactivity of MDA.

Further the lipid peroxidation levels were biochemically analysed in fresh RB tumour samples. These samples were histologically examined, and the tumours were grouped into A (n=8) and B (n=8) as above. The reactive oxygen species (ROS) levels and gene expression studies were studied in four fresh RB tumour tissues and these samples have been labelled as 1, 2, 3 and 4. The clinical features of the tumour tissues are given in Tables 5.2 – 5.7

5.3.2. Histopathology

RB sections were graded microscopically and were divided into three groups according to the predominant pattern of differentiation (Finger et al., 2002). All tumour slides were reviewed, and the level of choroidal invasion was classified as either focal or diffuse. For the optic nerve, prelaminar invasion, post laminar invasion, and invasion of the surgical end of the optic nerve were analyzed (Finger et al., 2002). The invasion of tumour cells into the orbit was also investigated in the sections.

Table 5.2 Malondialdehyde expression analysis by Immunohistochemistry (cohort details)

<table>
<tr><th rowspan="2">Total Number</th><th rowspan="2">Tumours with No Invasion</th><th colspan="5">Tumours with Invasion of Ch, ON, Orbit</th></tr>
<tr><td colspan="2">Choroid</td><td colspan="3">ON</td></tr>
<tr><td rowspan="5">34</td><td rowspan="3">17</td><td colspan="2">11</td><td colspan="3">10</td></tr>
<tr><td>Diffuse</td><td>Focal</td><td>Prelam</td><td>Postlam</td><td>SE</td></tr>
<tr><td>8</td><td>3</td><td>4</td><td>4</td><td>2</td></tr>
<tr><td colspan="6">Tumour Cell Differentiation</td></tr>
<tr><td colspan="2">WD</td><td colspan="2">MD</td><td colspan="2">PD</td></tr>
<tr><td colspan="2">9</td><td colspan="2">6</td><td colspan="2">19</td></tr>
<tr><td colspan="7">Abbreviations: ON – optic nerve, WD-well differentiated, MD-moderately differentiated, PD-poorly differentiated, SE-surgical end of the optic nerve, Prelam & Post lam-Pre & post laminar ON Inv, Ch-Choroid</td></tr>
</table>

5.3.3. Immunohistochemistry

Primary rabbit anti-MDA polyclonal antibody (AB5524) was obtained from Chemicon International, California, U.S.A. LSAB kit and developing solution (DAB) were obtained from Dakocytomation Corp., Glostrup, Denmark.

5.3.4. Immunostaining protocol

Immunohistochemical detection of MDA on paraffin wax embedded tumour sections was performed using a rabbit anti-malondialdehyde polyclonal antibody (1:50 dilution; Chemicon International, CA, USA). Staining for MDA was visualized with the streptavidin-biotin immunoperoxidase technique using the LSAB kit (DakoCytomation, Glostrup, Denmark) according to the manufacturer's instructions. For control sections, the same procedure was performed in the absence of the primary antibody. At least one control was undertaken in each experiment.

5.3.5. Evaluation of Immunostaining

The slides were examined by two observers using conventional light microscopy. The levels of immunoreactivity and the cell types that exhibited MDA immunoreactivity was recorded for each slide. There was significantly better agreement in the interpretation of MDA expression in the invasion group with a kappa value K= 1 ($P<0.0001$) and in the no invasion group with kappa value K=0.91 ($P<0.0001$). The amount of immunostaining was evaluated as: **+** for immunostaining in > 5% but less than one-third of tumour cells, **++** for immunostaining in more than one-third but less than two-thirds of tumour cells, and **+++** for immunostaining in more than two-thirds of tumour cells (Adithi et al., 2005).

5.3.6. Assessment of lipid peroxidation in tumour tissue (Malondialdehyde quantification) Lipid peroxide level was determined in fresh RB tumour tissues by colorimetric reaction using thiobarbituric acid (TBA), (Hogberg et al., 1974) where malondialdehyde (MDA) reacts with TBA to generate a product that absorbs at 532

nm. The levels of MDA (end-product of lipid peroxidation), serves as an index of the intensity of oxidative stress in the tumour samples. Peroxidation was measured at basal and 10mM ferrous sulphate induced conditions (Devasagayam, 1986).

5.3.7. Measurement of intracellular reactive oxygen species (ROS) levels by 2′, 7′ dichlorodihydrofluorescein (DCF) Fluorescence Assay:

The intracellular ROS levels were measured using the OxiSelect ROS Assay Kit (Cell Biolabs Inc, CA, USA) as per the manufacturer's instructions. The tumour tissues were homogenized and diluted with ice cold PBS. Donor retina, was obtained from the eye bank in ice cold DMEM, and was processed immediately, by homogenizing in ice cold PBS. 2 x 10^4 cells (from RB tumour tissue (Table 5.3) and donor retina) were assayed in 96-well plates with 100 µl of culture media. 2×10^4 Y79 RB cells/well were seeded in 96-well plates with 100 µl of culture media and incubated at 37^0C overnight. The media was removed and the cells were washed with sterile PBS thrice. All the samples were then processed for the DCF assay as per the protocol given in section 3.17 in chapter 3. After incubation with oxidant, the reaction was terminated by adding 100 µl of cell lysis buffer. The fluorescence was read with a SpectraMax M2 multi-detection micro plate reader (Molecular devices, CA, USA) at 480 nm excitation/530 nm emission. The ROS level in the tissue lysates was then calculated using the DCF standard calibration curve.

Table 5.3 Clinico-pathologic characteristics of RB tumours used for studying reactive oxygen species (ROS) level determination and gene expression studies

Tumour Number	Age /Sex	Differentiation/ Laterality	Invasion status
1	6/M	FD/UL	Ch Inv >3mm
2	3/M	PD/UL	Focal Ch Inv 1.5mm, PreLam ON Inv
3	3/F	PD/UL	Focal RPE Inv, Focal Ch Inv <3mm, Pre & Post Lam ON Inv
4	5/F	UD/UL	Full thickness Ch Inv >3mm, Focal RPE Inv, Pre & Post Lam ON Inv
Abbreviations: M – male, F – female, FD-Focal differentiation, PD-poorly differentiated, UD-undifferentiated, UL-unilateral, Ch – choroid, Inv - invasion, PreLam – Pre laminar, PostLam – Post laminar, ON - optic nerve, RPE – retinal pigment epithelium			

5.3.8. cDNA microarray analysis of Y79 retinoblastoma cells (H_2O_2 oxidant-induced model)

5.3.8.1. Experimental induction of oxidative stress

Y79 RB cells (1.5 x 10^6 cells/well) were plated in 12 well plates with 1 ml of culture media and incubated at 37^0C overnight. The next day the fresh media was added and the cells were exposed to 400 μM Hydrogen peroxide (H_2O_2) and incubated for 8 h (Kase et al., 2009). The un-induced control Y79 cells had only the culture media and incubated simultaneously along with the test. At the end of 8 h the cells were collected and processed for microarray analysis.

5.3.8.2. Preparation of cDNA

Total RNA was isolated from Y79 retinoblastoma cells using TRIZOL reagent (Invitrogen) and purified using an RNeasy Mini Kit (Qiagen), combined with DNase treatment following the manufacturer's instructions as per the protocol given in the section 3.11 in chapter 3.

5.3.8.3. Hybridization, scanning and feature extraction

The labeled cDNA samples were hybridized onto a Whole Genome Human Array 4x44k as per the microarray analysis protocol mentioned in Chapter 3 (section 3.18). The present oligonuclotide microarray data were submitted to NCBI-GEO-OMNI BUS (Accession number GSE27880).

5.3.8.4. Real-Time Quantitative RT-PCR (qRT-PCR)

To confirm the expression of up-regulated or down-regulated genes after cerulenin treatment, the expression of selected genes were validated using real-time quantitative reverse transcription polymerase chain reaction (qRT-PCR). All reactions were carried in 20µl volume containing SYBR green PCR master mix (Eurogentec S.A, Belgium) as per the protocol given under section 3.11.6.2 in chapter 3.

5.3.9. Statistical Analysis

To determine associations of MDA immunoreactivity with tumour invasion and differentiation, Mann–Whitney U test was used. For statistical purposes, moderately differentiated and well differentiated tumours were grouped together and were compared with poorly differentiated tumours. The inter-observer variability of the immuno-analysis was determined using kappa statistics.

Lipid peroxidation was estimated in each tumour sample (in triplicate), and the values of each group (A and B) was expressed as mean ± S.D., and compared using unpaired *t*-test. Values of $P<0.05$ was considered significant. The analyses were performed using the SPSS software package for Windows (version 10.0; SPSS Inc., Chicago, IL).

For microarray analysis, the genes were considered for expression analysis when they satisfied the following two criteria: (i) $P \leq 0.05$, and (ii) log ratio of at least 2.0 for

up regulation, and log ratio of 0.5 for down regulation (keeping a median log ratio of 1) in both biologic replicates. Values are expressed as mean ± S.D. of duplicate values.

5.4. Results

5.4.1. MDA immunoreactivity in Retinoblastoma

The immunostaining for MDA was positive in all 34/34 (100%) tumours. Group A tumours: Among 17 non-invasive RB, the extent of immunostaining for MDA was as follows. There were 9 tumours with + staining, 6 tumours with ++ staining, and 2 tumours with +++ staining (Table 5.4). Figure 5.2a shows MDA immunoreactivity in non-invasive RB. Group B tumours: Among 17 invasive RB, the extent of immunostaining for MDA was as follows. There were 2 tumours with + staining, 11 tumours with ++ staining, and 4 tumours with +++ staining (Table 5.5). Figure 5.2b shows the MDA immunoreactivity in invasive RB.

Table 5.4 Clinicopathological features of RB along with MDA immunoreactivity in the non-invasive tumours

S. No.	Age/Sex	Clinicopathological features	MDA Immunoreactivity
1.	1Y, 6 mon/ M	OD: WD	++
2.	4Y/M	OD: PD	++
3	5Y/M	OS: PD	+
4	4mon/M	OS: WD	+
5	2Y, 2mon/M	OD: WD	+
6	3Y/F	OS: WD	++
7	3Y, 6 mon/F	OD: PD	+
8	8Y/M	OS: PD	+
9	1Y/F	OD: WD	+
10	3Y/F	OD: PD	++
11	1Y/F	OD: PD	++
12	4Y/F	OS: PD	+
13	1Y, 6 mon/M	OS: WD	+
14	1Y, 4 mon/M	OD: WD	+++
15	1Y, 6 mon/M	OD: MD	+

16	7 mon/M	OD: WD	+++
17	4Y, 6 mon/ M	OS: MD	++

Abbreviations: Y: Years; mon: months; M: Male; F: Female; OD: Right eye; OS: Left eye; OU: Bilateral; PD: Poorly differentiated; MD: Moderately differentiated; WD: Well differentiated.

5.4.2. Comparison of MDA immunoreactivity in Group A and Group B tumours

The Mann–Whitney U test was used to compare the extent of oxidative stress in the two groups, A and B. Significantly higher levels of the oxidative marker MDA were observed in group B tumours, in comparison with group A tumours ($P<0.05$). MDA immunoreactivity was compared with the differentiation and laterality of the tumours. The statistical analysis did not bring out any correlation between the MDA expression and the differentiation/laterality of the tumours.

Table 5.5 Clinicopathological features of RB along with MDA immunoreactivity in the tumours with invasion

S No	Age/Sex	Clinicopathological features	MDA immunoreactivity
1.	3Y/M	OS, PD: Diff Ch Inv, Post lam ON Inv	+++
2.	4Y/F	OS, PD: Post lam ON Inv	++
3	2Y,10mon/ M	OS, PD: Diff Ch Inv, Prelam ON Inv	++
4	21Y/F	OD, PD: Pre and post lam ON Inv, SE involved	++
5	1Y/F	OD, PD: Diff Ch Inv	+++
6	4Y/F	OD, WD: Pre lam ON Inv	++
7	7Y/M	OD, PD: Diff Ch Inv	+
8	4Y/F	OD, MD: Focal Ch Inv	++
9	4Y/F	OD, MD: Focal Ch and Pre lam ON Inv	++
10	1Y,6mon/ M	OD, PD: Pre lam ON Inv	++
11	5 mon/M	OS, MD: Focal Ch Inv	+++
12	3Y/M	OS, PD: Diff Ch and Post lam ON Inv	++
13	2Y/F	OS, PD: SE involved	+++
14	3Y, 6 mon/ M	OS, PD: Diff Ch Inv	++
15	4Y/M	OS, PD: Diff Ch Inv	++
16	7Y/M	OS, MD: Post lam ON Inv	+
17	2Y,6mon/F	OS, PD: Diff Ch Inv	++

Abbreviations: Y: Years; mon: months; M: Male; F: Female; OU: Bilateral; OD: Right eye; OS: Left eye; PD: Poorly differentiated; MD: Moderately differentiated; WD: Well differentiated. Ch: choroidal; post lam: post laminar; ON: Optic nerve, Diff-Diffuse, SE-surgical end, Inv-Invasion, Prelam-prelaminar

5.4.3. Comparison of lipid peroxidation levels in non-invasive and invasive tumours

MDA, an end product of lipid peroxidation, is a vital biomarker of oxidative stress. The tissue lipid peroxidation was expressed as nano moles of malondialdehyde formed per 100 mg tissue, in the invasive and non-invasive tumours, and their clinicopathologic features were recorded (Table 5.6). There was a 2.25 fold increase in the basal lipid peroxidation levels in the invasive group when compared with the

non-invasive group (P<0.05; Figure 5.3). Similarly, the ferrous sulphate induced lipid peroxidation system also showed a 1.58 fold rise in the malondialdehyde levels in the invasive cohort, in comparison with the non-invasive group (P<0.05).

Figure 5.2: MDA Immunoreactivity in RB tumour tissue sections

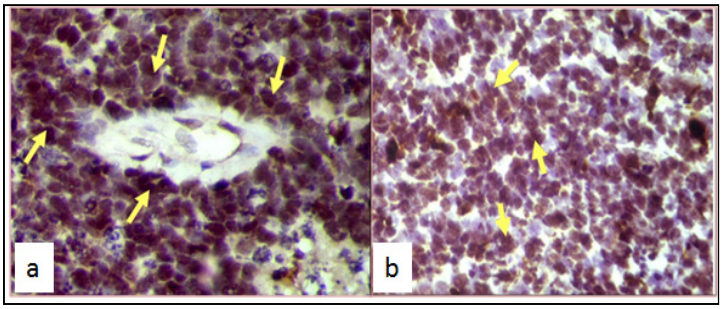

Figure 5.2 MDA Immunoreactivity in RB tumour tissue sections: Photomicrograph showing the positive MDA immunoreactivity (arrows - nuclear positivity) of the tumour cells arranged around the blood vessel, in non-invasive retinoblastoma **(a)** and in the tumour cells of retinoblastoma with diffuse choroidal and post laminar optic nerve invasion **(b)**. Magnification x 100 (DAB staining with hematoxylin counter stain)

Figure 5.3 Lipid peroxidation levels in retinoblastoma tumour tissues

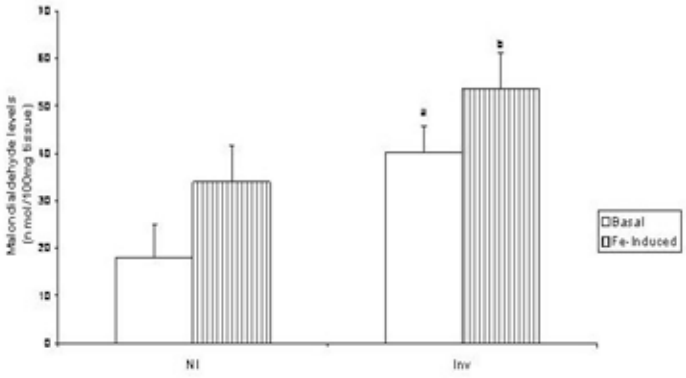

♦**Figure 5.3 Lipid peroxidation levels in retinoblastoma tumour tissues.** Values are expressed as mean±S.D. Statistical comparisons were made between the non-invasive (NI) and invasive (Inv) groups: a: significance at P<0.05 (basal); b: significance at P<0.05 (Fe-induced; $FeSo_4$ induced). MDA levels are expressed as mean ± S.D. of triplicate values.

♦ *The data presented in figure 5.3 is published in: Curr Eye Res. 2009;34(12):1011-8. Please see "List of publications on page XXIII*

5.4.4. Reactive oxygen species (ROS) levels in RB tumour tissues and cultured cells:

DCF assay was used to quantify the ROS levels in the RB tumour tissues, donor retina, and Y79 RB cells in the presence of an oxidant stress inducer 100 μM H_2O_2 for 2 h. Under these conditions we compared the oxidative levels in tumours, with respect to donor retina (Figure 5.4b). The fold increase in the ROS levels in the H_2O_2 induced tumours relative to the donor retina ranged between 32-56 folds. Figure 5.4c reveals a significant 3-fold rise in ROS levels in Y79 RB cells induced by H_2O_2 in comparison with un-induced Y79 RB cells ($P<0.05$).

Table 5.6: Clinicopathological features of RB cohort analyzed for lipid peroxidation status

S. No.	Age/Sex	Clinicopathological features	Invasion status
1	1/F	OU, extensive necrosis, calcification, few viable cells	NI
2	2/M	OD, PD	NI
3	3/M	OU, PD, tumour cells seen in AC	NI
4	2/F	OS,PD	NI
5	8/M	OS, UL, PD	NI
6	7mon /M	OS, PD, tumour cells seen in AC and angle	NI
7	4/M	PD	NI
8	3/F	OS, PD	NI
9	2/F	OS, MD, Ch inv, tumour cells seen in PreLam end of ON	Inv
10	18mon/M	OD, endophytic WD, Focal Ch, Pre lam ON Inv	Inv
11	18mon/M	OD, PD, Post Lam ON Inv	Inv
12	7mon/F	OS, PD, tumour cells seen in Ch focally	Inv
13	4/M	OD, UL, Focal Ch Inv, proximal end of ON till LC of ON invaded by tumour cells.	Inv
14	2/M	OS, endophytic, UD, extension into ON	Inv
15	3/M	OD, WD, focal RPE Inv	Inv
16	2/M	OS, MD, Focal Ch Inv and RPE, PreLam ON Inv	Inv

Abbreviations: Y: Years; mon: months; M: Male; F: Female; OU: Bilateral; OD: Right eye; OS: Left eye; PD: Poorly differentiated; MD: Moderately differentiated; WD: Well differentiated. Ch: choroidal; post lam: post laminar; ON: Optic nerve; AC: Anterior Chamber, PreLam-Prelaminar, Inv-Invasion, LC-Lamina cribrosa, UL-Unilateral, NI-No invasion

Figure 5.4 Quantification of reactive oxygen species (ROS) levels in RB tumours and Y79 RB cells by DCF Assay

Figure 5.4a. Calibration curve of 2′, 7′ – dichlorodihydrofluorescein (DCF)

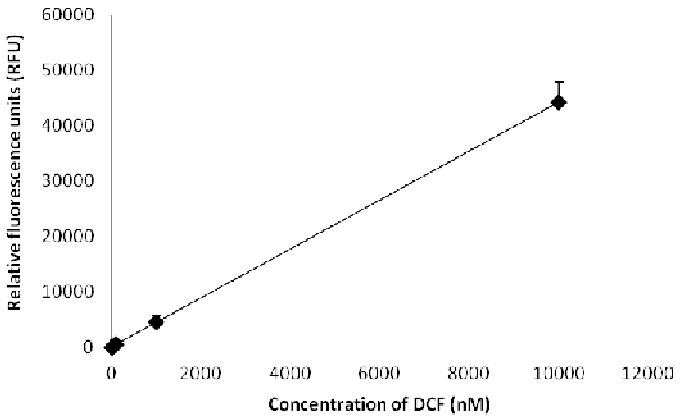

Figure 5.4a: Calibration curve of 2′, 7′ – dichlorodihydrofluorescein (DCF): Calibration curve was plotted with the DCF standard chemical provided in the assay kit. The range of concentration used was 1-10,000nM of DCF. Each point represent mean ± S.D. from triplicate values. The fluorescence was read with a SpectraMax M2 multi-detection micro plate reader (Molecular devices, CA, USA) at 480 nm excitation/530 nm emission. The ROS level in the tissue lysates were then calculated using this calibration curve.

Figure 5.4b Quantification of reactive oxygen species (ROS) levels in RB tumour tissues by DCF Assay

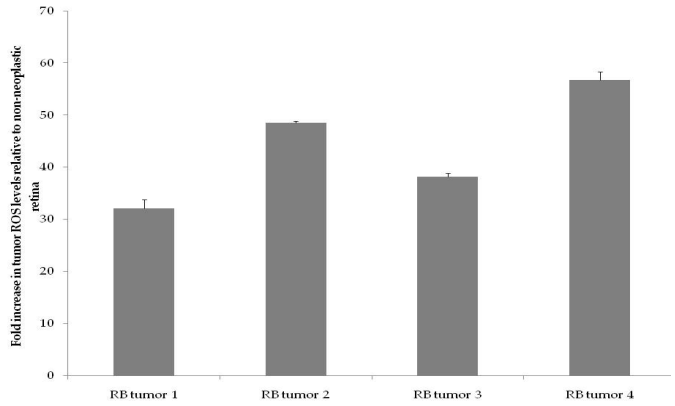

Figure 5.4b Quantification of reactive oxygen species (ROS) levels in RB by DCF Assay. We measured intracellular ROS levels in 4 RB tumour tissues induced with 100 μM H_2O_2 for 2 h and compared with the donor retina under the same conditions. The clinical features of these tumour samples are presented in Table 5.3. The level of ROS on H_2O_2 induction is depicted as fold increases with respect to non-neoplastic retina. Error bars represent S.D. from duplicate values.

Figure 5.4c Quantification of reactive oxygen species (ROS) levels in Y79 RB cells by DCF Assay.

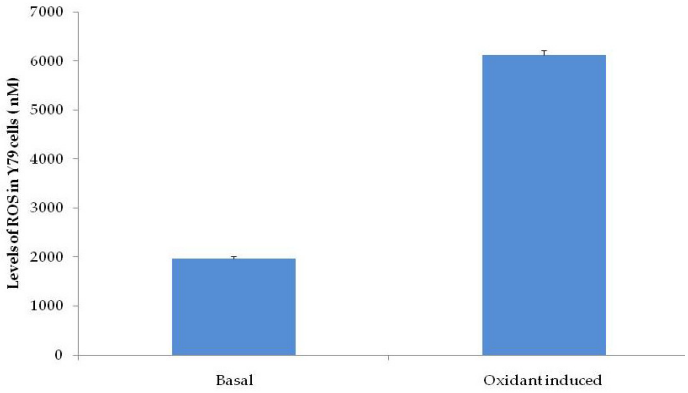

[Δ]Figure 5.4c Quantification of reactive oxygen species (ROS) levels in Y79 RB cells by DCF Assay. We measured the ROS levels in Y79 RB cells with and without H_2O_2 induction. The level of ROS is expressed as nM. Values are expressed as mean ± S.D. of triplicate values.

5.4.5. cDNA Microarray profile of gene expression in Y79 retinoblastoma cells (H_2O_2 oxidant-induced model)

We analyzed the differential expression of genes in Y79 RB cells (H_2O_2 oxidant-induced model) compared with the un-induced Y79 RB cells (control). The genes were considered for expression analysis when they satisfied the criteria: (i) $P \leq 0.05$, and (ii) log ratio of at least 2.0 for up regulation, and log ratio of 0.5 for down regulation (keeping a median log ratio of 1) in both biologic replicates. There were 2843 significantly up-regulated genes and 2533 genes were significantly down-regulated (Figure 5.5a & 5.5b).

The genes were clustered into several functional classes. The important functional classes of the genes are oncogenes, angiogenesis, tumour suppressor, lipid metabolism, cell proliferation, JAK-STAT pathway, PI3K pathway, MAPK pathways, and drug resistance (Figure 5.6; Table 5.7). The comprehensive list of genes

[Δ] *The data presented in figure 5.4b & c is published in: Curr Eye Res. 2012 Sep;37(9):830-41. Please see the "List of publications" on Page XXIII*

differentially regulated on oxidant induction, have been presented in Table A1 in Appendix 1. The data discussed here has been submitted to NCBI Gene expression OMNIBUS. The data is accessible through GEO series accession number GSE27880.

Figure 5.5 Heat map of differential expression of genes in Y79 RB cells (H_2O_2 oxidant- induced model)

Figure 5.5a & b

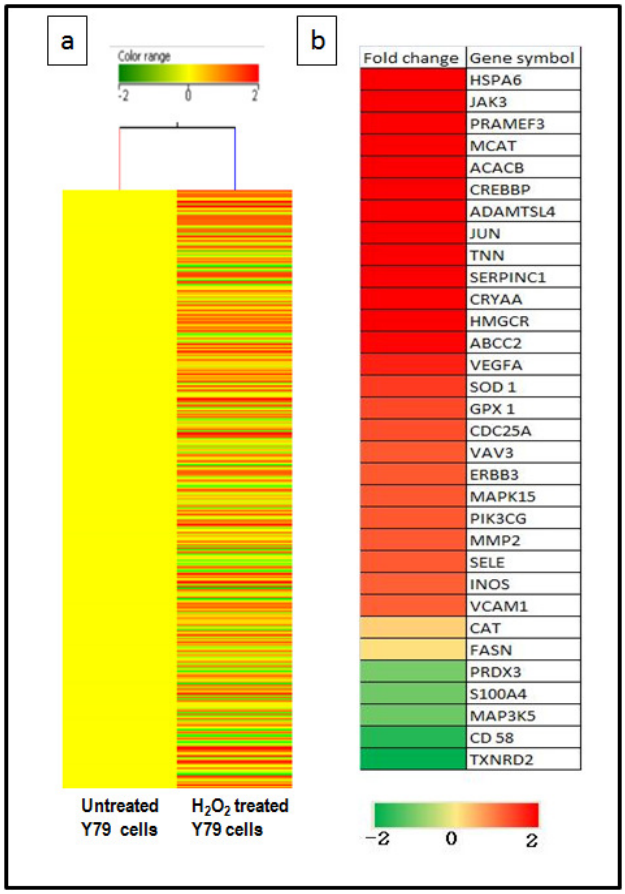

[Δ]Figure 5.5 Heat map of differential expression of genes in Y79 RB cells (H_2O_2 oxidant- induced model): a) Heat map represents the overall differential expression of genes. **b)** Heat map represents the genes of interest that are up-regulated and down-regulated significantly. Red and green colours represent the up-regulation and down- regulation of genes respectively relative to un-induced control Y79 RB cells.

[Δ] *The data presented in figure 5.5 is published in: Curr Eye Res. 2012 Sep;37(9):830-41. Please see the "List of publications" on Page XXIII*

Figure 5.6 Differentially regulated pathways in Y79 retinoblastoma cells (H_2O_2 oxidant-induced model)

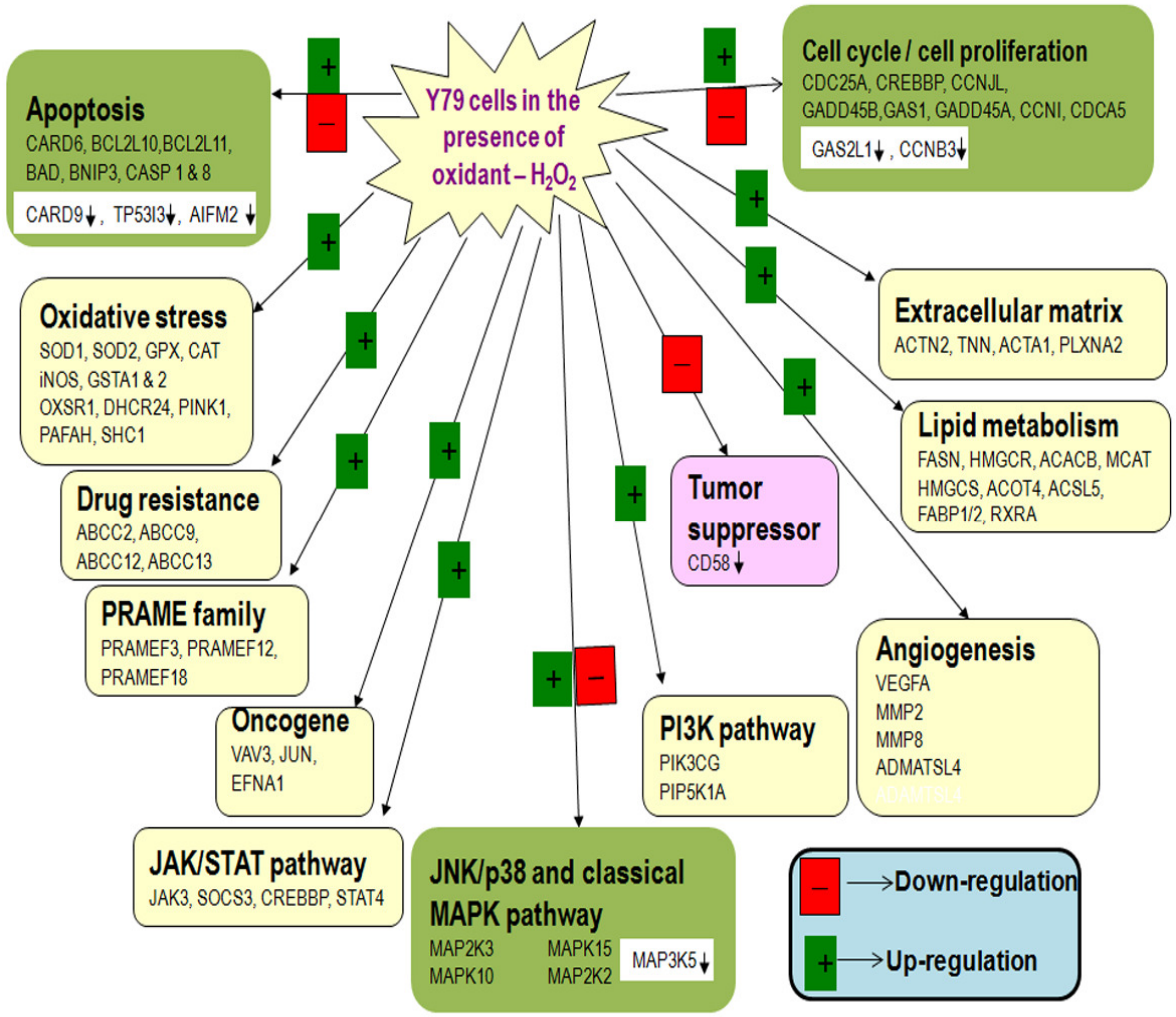

♣Figure 5.6 Differentially regulated pathways in Y79 retinoblastoma cells (H_2O_2 oxidant-induced model): The important pathways that were differentially regulated in Y79 cells on H_2O_2 induction are depicted. The gene names that are up/down-regulated in each pathway are shown. Unless indicated the genes are up-regulated. The down-regulated genes are followed by a down arrow.

♣ *The data presented in Figure 5.6 is published in: Curr Eye Res. 2012 Sep;37(9):830-41.Please see " list of publications" on page XXIII*

5.4.5.1. Validation of gene expression in oxidative stress induced retinoblastoma cells *in vitro* and in fresh RB tumour tissues by qRT-PCR:

Further to the microarray analysis, we performed real time PCR (qRT-PCR) analysis for a set of important genes for implicating their role in oxidative stress and oncogenesis. The gene expression profile obtained by microarray analysis corroborated with our qRT-PCR findings (Figure 5.7).

Figure 5.7 Validation of microarray data with qRT-PCR in Y79 cells.

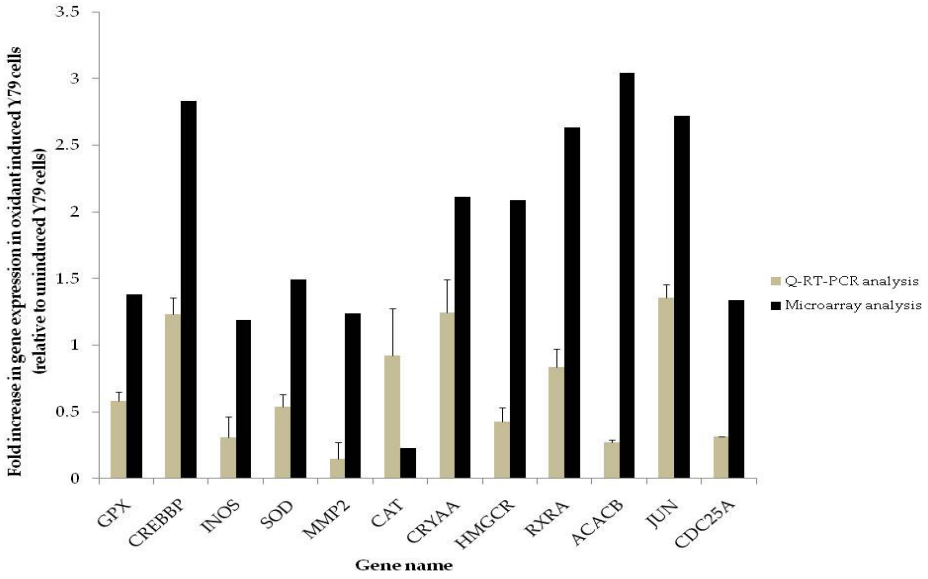

‡‡**Figure 5.7 Validation of Microarray data with Real time PCR in Y79 cells:** The microarray results were consistent with our real-time PCR analysis of gene expression in Y79 RB cells (H_2O_2 oxidant-induced model). This is indicated by the two columns presented alongside each gene (Gray: qRT-PCR; Black: Microarray analysis). The results are represented as fold change relative to un-induced Y79 cells (control). Values are expressed as mean ± S.D. of triplicate values.

In addition to the Y79 RB cells, we analyzed the gene expression of the same set of genes in four retinoblastoma tumour tissues. Figures 5.8a-e compares the fold-increase in the gene expression relative to the non-neoplastic donor retina. We compared the gene expression changes in the RB tumour no. 1 and RB tumour no. 4

‡‡ *The data presented in figure 5.7 is published in: Curr Eye Res. 2012 Sep;37(9):830-41. Please see the "List of publications" on Page XXIII.*

which had the lowest and the highest ROS levels respectively, among the 4 tumour tissues analyzed (P<0.05). The levels of first line defense antioxidant genes (♥SOD, GPX and CAT) in tumour no. 1 were high when compared with the respective gene expression in the tumour no. 4 (P<0.05) (Figure 5.8a).

Figure 5.8 Validation of microarray data with qRT-PCR in RB tumour tissues

Figure 5.8a

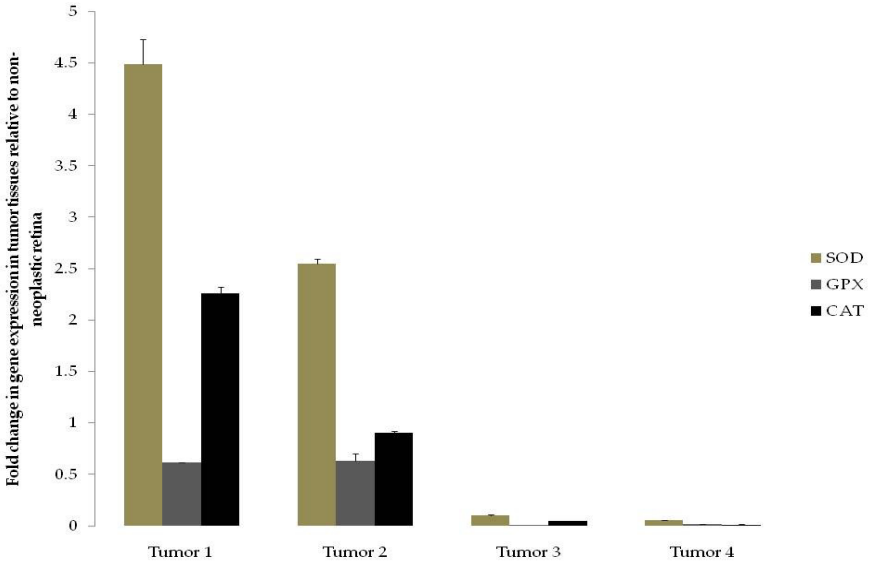

♥ *SOD – Superoxide dismutase; GPX – Glutathione peroxidise; CAT – Catalase*

•**Figure 5.8b**

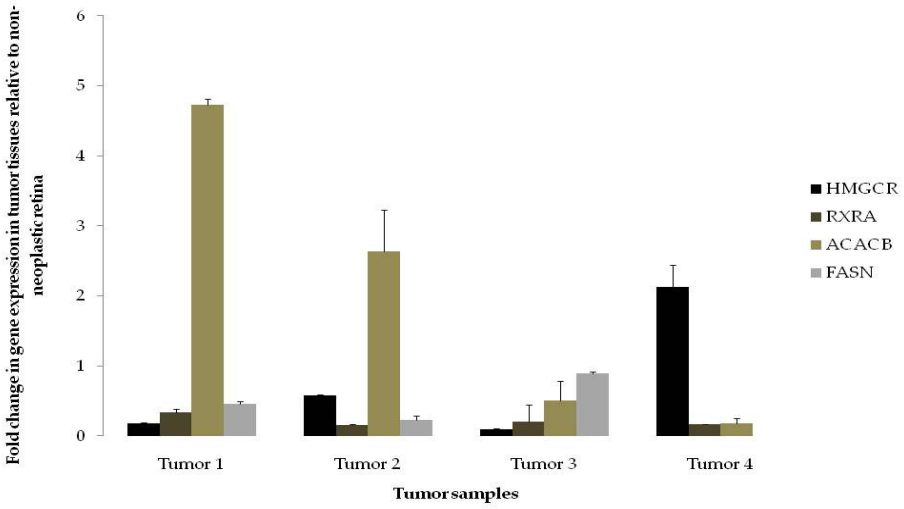

Figure 5.8c

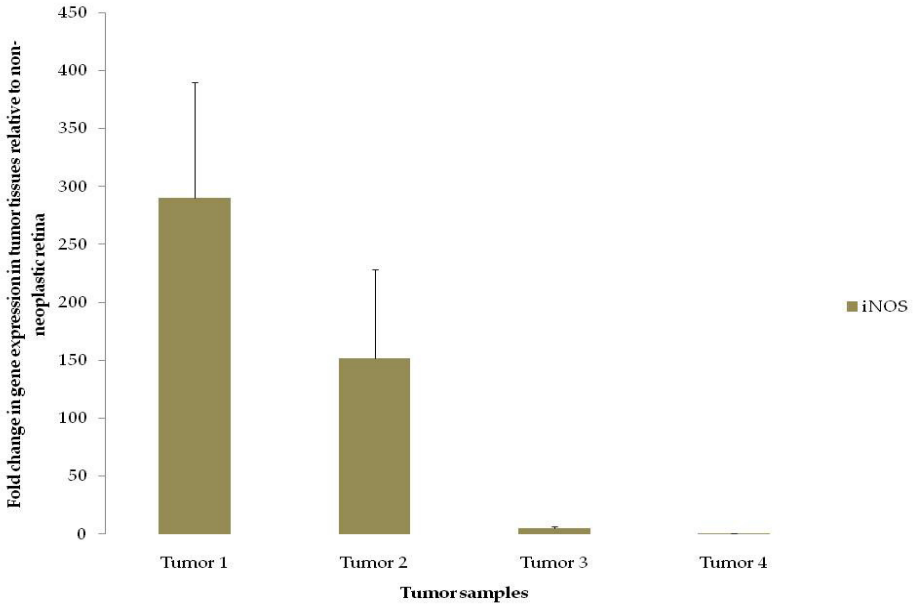

• HMGCR – HMG CoA reductase; RXRA – Retinoid X receptor alpha; ACACB – acetyl CoA carboxylase β; FASN – fatty acid synthase; iNOS – inducible nitric oxide synthase

Figure 5.8d

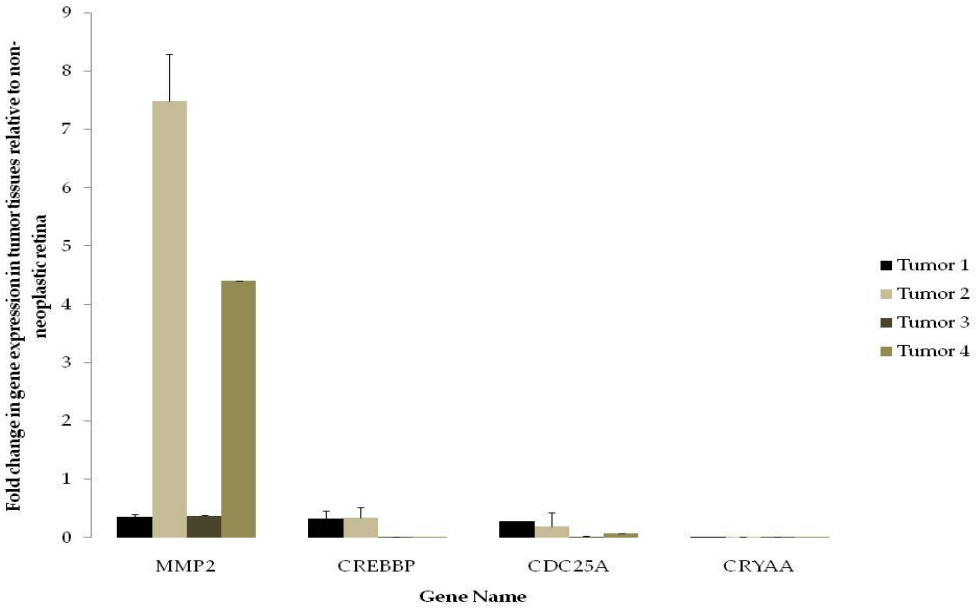

Figure 5.8e

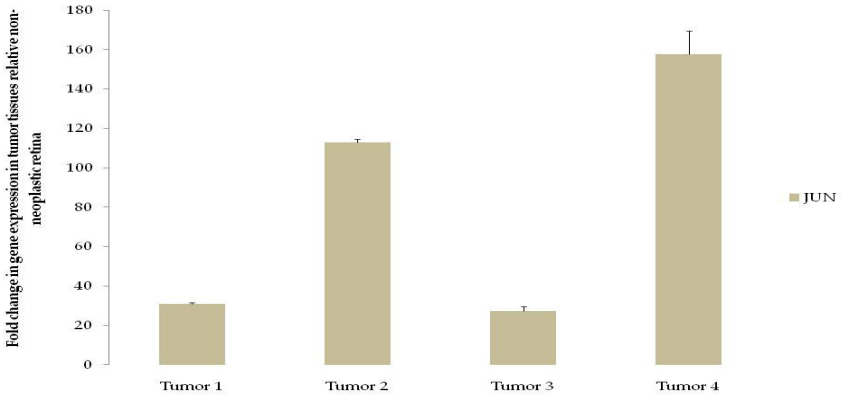

[§§]**Figure 5.8a-e Gene expression in RB tumour tissues analysed by real-time PCR:** We validated the set of genes of importance in four RB tumour tissues. The results are represented as fold change of mRNA expression relative to non-neoplastic donor retina. Values are expressed as mean ± S.D. of duplicate values.

[§§] *The data presented in Figure 5.8 is published in: Curr Eye Res. 2012 Sep;37(9):830-41. Please see the "List of publications" on Page XXIII*

Abbreviations: MMP2 – Matrix metalloprotease 2; CREBBP – CREB binding protein; CDC25A - Cell division cycle 25 homolog A; CRYAA – Crystallin alpha A; JUN – Jun oncogene

Table 5.7 List of important genes differentially regulated in Y79 RB cells (H_2O_2 oxidant-induced model)

S.No	Gene Name	Gene Symbol	Fold change
1.	Jun Oncogene	JUN	2.72
2.	Acyl-CoA synthetase long-chain family member 5	ACSL5	1.16
3.	Acyl-CoA thioesterase 4	ACOT4	1.18
4.	Retinoid X receptor, alpha	RXRA	2.63
5.	MalonylCoA:ACP acyltransferase (mitochondrial)	MCAT	3.42
6.	Acetyl-Coenzyme A carboxylase beta	ACACB	3.04
7.	Cell division cycle 25 homolog A	CDC25A	1.34
8.	CREB binding protein, transcript variant 1	CREBBP	2.83
9.	Superoxide dismutase	SOD1	1.49
10.	Glutathione peroxidise	GPX	1.38
11.	Catalase	CAT	0.23
12.	Matrix metalloprotease	MMP2	1.24
Note: The comprehensive table of the differentially expressed genes in Y79 cells (H_2O_2 oxidant-induced model) is presented in Table A1; Appendix I.			

5.5. Chapter Summary

- Biochemical indicator of lipid peroxidation - Malondialdehyde (MDA) was found in RB tumour tissues and correlated with the RB tumour invasiveness.
- A separate cohort of four tumour tissues were analysed for ROS levels. The levels of ROS in two of the tumours inversely correlated with their antioxidant enzymes (SOD, CAT, GPX) gene expression levels.
- Microarray analysis of oxidant induced Y79 RB cells showed differential expression of several cellular processes such as lipid metabolism, cell proliferation, and angiogenesis and various cell signaling pathways.
- The microarray findings presented here substantiated the pro-oxidant nature of hydrogen peroxide, leading the Y79 RB cells towards proliferation.

CHAPTER 6: EXPERIMENTAL EVALUATION OF ANTI-CANCER EFFECTS OF FASN INHIBITORS: OPTIMISATION OF DRUG DOSAGES

6.1. Introduction

Chemical inhibitors of different catalytic domains of fatty acid synthase (FASN) enzyme have been tested for their anti-proliferative potential with various cancer cell lines and xenograft models. Inhibitors for four out of seven catalytic domains have been identified and explored for the chemical inhibition of FASN using various cancer cell lines and xenograft models. They are ketoacyl synthase (KS), β-ketoacyl reductase (KR), thioesterase (TE), and enoyl reductase (ER) domain. In the present study, three FASN inhibitors (cerulenin, triclosan and orlistat) were evaluated for their anti-proliferative effects in RB cells. This introduction section briefly explains the roles played by these three inhibitors in various other cancer cells and xenograft models.

6.1.1. FASN inhibitors

6.1.1.1. Cerulenin ($C_{12}H_{17}NO_3$)

Cerulenin is a potent non-competitive, irreversible inhibitor of FASN KS domain. Cerulenin's anti-proliferative effects were studied *in vitro* in various cancer cells (melanoma, cancers of the breast, colon, and prostate) (Ho et al., 2007; Liu et al., 2006; Pizer et al., 1998; Migita et al., 2009). Cerulenin has been reported to induce apoptosis by activating the mitochondrial pathway, which is regulated in a p53 independent manner in a set of wild type p53 and mutant p53 tumour cell lines (Heiligtag et al., 2002). Cerulenin was also reported to induce apoptosis in melanoma cells through the activation of caspase 3 and the dose dependent cleavage and inactivation of poly ADP ribose polymerase (PARP) (Ho et al., 2007).

Figure 6.1: Chemical structure of cerulenin

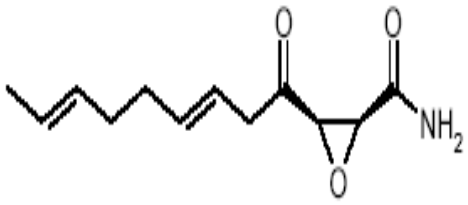

6.1.1.2. TRICLOSAN ($C_{12}H_7Cl_3O_2$; MW 289.5)

Triclosan is a lipid soluble broad spectrum antibiotic that acts as an anti-bacterial agent, by inhibiting the ER activity of the type II FASN in bacteria. Studies with breast cancer cells have shown the inhibition of type I mammalian FASN (Liu et al., 2002). There are reports showing its inhibitory action against the type I FASN in breast cancer cells and in rat mammary tumours, suggesting FASN to be a promising target for breast cancer chemoprevention (Lu & Archer, 2005). *In vitro* and *in vivo* studies with triclosan showed potent growth inhibition of *Plasmodium falciparum*. This study identified the existence of *de novo* FASN pathway in the parasite, which also served as a basis for the identification of new anti-malarials (Surolia & Surolia, 2001).

Figure 6.2: Chemical structure of triclosan

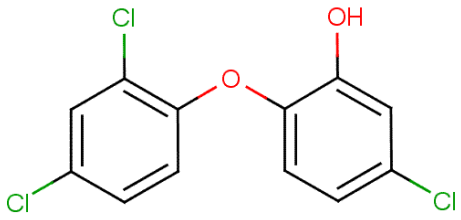

6.1.1.3. XENICAL™ (ORLISTAT)

Xenical™ (Orlistat) is an FDA approved anti-obesity drug, and acts by inhibiting the pancreatic and gastric lipases. In addition, orlistat was reported to halt the tumour

cell proliferation by arresting the cell cycle at G1/S phase through the retinoblastoma protein (pRb) pathway in breast cancer cells (Kridel et al., 2004). The β- lactone ring of orlistat acts on FASN by a nucleophilic attack on the active site serine of the thioesterase (TE) domain. The crystal structure of the human TE domain complexed with orlistat is reported (PDB: 2PX6), in which orlistat was captured in the catalytic triad.

Figure 6.3: Chemical structure of orlistat

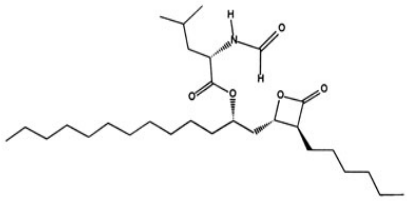

FASN inhibition by orlistat was accompanied by down-regulation of HER2/neu expression in breast cancer cell lines. This effect also led to up-regulation of PEA3, a DNA binding protein of the Ets transcription factor family, which binds to the PEA3 binding motif of the HER2/neu gene promoter. Further the effect of orlistat in combination with trastuzumab (anti-HER2/neu monoclonal antibody) showed synergistic effects when compared with the effects of either of them alone. Xenical™ has a low oral bio-availability, in its approved formulation. This present formulation can be used to treat gastric cancers when administered orally. But when the need comes to treat cancers at other distant body sites, a more stable novel formulation and/or route of administration may be required for more effective anti-cancer therapy (Menendez et al., 2005b).

6.2. Objectives:

1. To optimize solubilisation conditions for the three FASN inhibitors [cerulenin, triclosan, orlistat (Xenical™)] in order to evaluate their anti-proliferative effects in human Y79 RB cells cultured *in vitro.*

2. To evaluate the concentration- and time-dependent cytotoxic effect of FASN inhibitors in human RB Y79 cells.

6.3. Methods:

6.3.1. Solubilisation of FASN inhibitors for cell culture testing

6.3.1.1. Cerulenin – Cerulenin was dissolved in dimethyl sulphoxide (DMSO) to obtain a stock solution of 1 mg/50 μl. Working solution was prepared by diluting the stock in culture medium to obtain a final concentration of 0.5 mg/2 ml in culture medium. The working solution of cerulenin was filter sterilized and required volume was used as per the concentration required. The drug was tested for its anti-proliferative effects in cultured RB cells with dosages ranging from 0.25 - 500 μg/ml.

6.3.1.2. Triclosan - Triclosan was weighed and dissolved in DMSO and diluted in culture medium. This solution became turbid and formed precipitate which indicated that the drug did not dissolve completely. A systematic approach of finding a suitable solvent to dissolve the hydrophobic triclosan in cell culture conditions was carried out in human retinoblastoma (Y79) as well as human breast cancer (MCF-7) cells *in vitro.*

6.3.1.2a. Test of solubility and pH

Five different solvents were chosen to analyse the solubility of triclosan. They were: (i) DMSO, (ii) acetone, (iii) 55% PEG-400 + 45% ethanol mixture (PEM), (iv) absolute ethanol, and (v) 1 N NaOH. The dissolved drug solution was then diluted with the culture medium to obtain a final concentration of 1 mg/ml. The drug was considered completely solubilised when it formed a clear solution in its solvent and produced no turbidity or precipitate, when diluted with the medium. Any precipitation or turbidity observed visually in the final solution containing the drug + solvent + medium was recorded. The pH was measured with a pH meter (LI120-ELICO, India).

6.3.1.2b. Cell viability (MTT) assay

MCF-7 cells were seeded at 2.5×10^3 cells/well and Y79 RB cells were seeded at 5 x 10^3 cells/well in 96-well plates with 100 µl of culture media and incubated at 37^0C overnight and then fresh medium was added. Working standards of solvents (acetone and PEM) were prepared using appropriate dilutions with culture medium. The concentration of acetone in acetone – culture medium solution ranged between 0.02 – 0.49 mg per well for all the experiments listed in 6.3.1.2b, c, and d. Triclosan dissolved in acetone and PEM (selected after the above-mentioned preliminary screening of five different solvents) was added at a range of concentrations from 50 - 200 µg/ml to MCF-7 cells and 2.5 - 50 µg/ml to Y79 RB cells containing wells. The solvent controls contained the corresponding volumes (5 - 20 µl in MCF-7 cells and 0.25 - 5 µl in Y79 RB cells) of solvent alone, without the drug. The cells were then incubated for 48 h at 37°C. Then, the cells were treated with MTT for 4 h and the formed formazan crystals were dissolved in DMSO. The colour developed was read at 540 nm.

Cell viability (or cell survival) was calculated as: (Test OD/Control OD) x 100

The 50% inhibitory concentration (IC_{50}) of triclosan solubilized in acetone and in PEM was calculated using polynomial regression analysis using Microsoft Excel.

6.3.1.2c. Assessment of cell morphology by phase contrast microscopy

MCF-7 and Y79 RB cells treated with PEM and acetone were assessed for morphological changes using a phase contrast microscope (Nikon). The cells were exposed to these two solvents in which the volumes corresponding to the volume required to dissolve triclosan at its 50% inhibitory concentration (IC_{50}) were used.

6.3.1.2d. DNA fragmentation assay (Agarose gel electrophoresis)

MCF-7 cells were plated at 2.5×10^4 cells/well and Y79 RB cells were plated at 5 x 10^4 cells/well in 12-well plates and incubated overnight. Then the medium was removed

and fresh medium and respective solvent controls (5 – 20 µl for MCF-7 cells and 0.25 - 5 µl for Y79 RB cells) were added to the wells and incubated for 48 h. At the end of incubation, the cells were collected and pelleted and were subjected to DNA fragmentation analysis. The bands were visualized under UV light with a gel documentation system (BioDoc-It Imaging system, UVP, USA).

Based on the MTT assay and DNA fragmentation assay results, triclosan's anti-proliferative effects in cultured RB cells were tested by dissolving it in acetone. The dosages tested ranged from 0.625 - 100 µg/ml.

6.3.1.3. Xenical™ (Orlistat): The contents of the Xenical™ capsules were transferred to a sterile 1.5 ml tube under sterile conditions. A stock solution of 25 mg/ml was dissolved in a DMSO/acetone mixture. The stock was then diluted in culture medium. A range of dosages were tested for the anti-proliferative effect of Xenical™ (orlistat) in cultured RB cells. The dosage range used is: 2.5 - 2500 µg/ml.

Each capsule of Xenical™ contains 120 mg of orlistat

The concentration versus percentage (%) cell viability graph was plotted and the IC_{50} was calculated for different time periods (48, 72 & 96 h).

6.3.2. Cell Viability (MTT) assay

Y79 RB cells were seeded at 5×10^3 cells/well in 96-well plates with 100 µl of culture media and incubated at 37^0C overnight and then fresh medium was added. The cells were then treated with various concentrations of cerulenin, triclosan and Xenical™ (as stated above) and incubated for 48, 72 and 96 h at 37°C. Then the cells were treated with MTT for 4 h and the formed formazan crystals were dissolved in DMSO and the colour developed was read at 450 nm. Cell viability (or cell survival) was calculated as: (Test OD/Control OD) x 100. The 50% inhibitory concentration (IC_{50}) of all the three FASN inhibitors was calculated using polynomial regression analysis using Microsoft Excel.

6.3.3. Toxicity of solvents

A concentration of 1 % of DMSO in the final solution is considered as toxic in the cell culture studies. In the present study, less than 0.5% of DMSO was used in the final solutions of the three FASN inhibitors. Acetone concentration of 5 mg/ml was reported to be non-toxic to the human fibroblast cells (Pace & Elliott, 1962). The concentration of acetone used in the present study was well below 5 mg/ml. The concentration of acetone in acetone – culture medium solution ranged between 0.02 – 0.49 mg per well for all the experiments listed in 6.3.1.2b, c, and d.

6.3.4. Statistical analysis

In all the experiments, the untreated cells with only the culture medium served as the control. Comparisons between specific groups as mentioned in the results section were done using student's *t*-test. Differences were considered significant at $P < 0.05$.

6.4. Results

6.4.1. EVALUATION OF SUITABLE SOLVENT FOR TRICLOSAN

6.4.1.1. Solubility of triclosan

Differences in triclosan solubility were observed in the five solvents made up with the culture medium (final concentration: 1 mg/ml) (Figure 6.4). Triclosan did not dissolve completely in DMSO (bottle 1), absolute ethanol (bottle 2) and 1 N NaOH (bottle 3) when diluted with culture medium, resulting in a turbid solution. However, PEM (bottle 4), and acetone (bottle 5) solubilized triclosan diluted with the culture medium resulted in a clear solution. pH was also recorded in these triclosan + solvent + culture medium solutions. The pH of the final solutions with 1 N NaOH and absolute ethanol was unfavourable (pH 8.0) for cell culture conditions while with acetone, PEM and DMSO an optimal pH of 7.4 was obtained. Based on the solubility and pH criteria, only two solvents (acetone and PEM) were selected for further evaluation of suitability as triclosan solubilizers in cell culture conditions.

6.4.1.2. Effect of solvents on cultured MCF-7 and Y79 RB cells

Toxicity of the solvents (5, 7.5, 10 and 20 µl in MCF-7 cells and 1, 5 and 10 µl in Y79 RB cells) was evaluated in terms of percentage viability of cells incubated with the solvents only.

Figure 6.4 Evaluation of solubility of triclosan in five different solvents

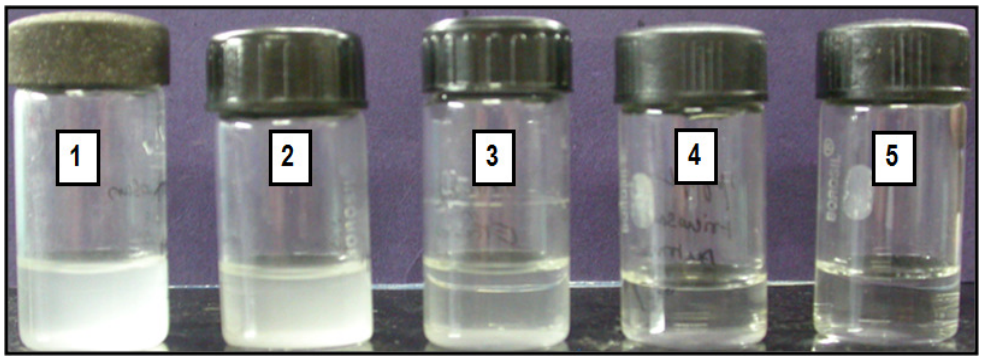

***Figure 6.4 Evaluation of solubility of triclosan in five different solvents:** Bottles 1 through 5 represent triclosan dissolved in DMSO, absolute ethanol, 1N NaOH, PEM, and acetone respectively. Triclosan did not dissolve completely in the solvents in the bottles 1 through 3 giving a turbid appearance. However, PEM (bottle 4), and acetone (bottle 5) solubilized triclosan, giving a completely clear solution.

Figure 6.5a represents MTT assay results of acetone and PEM, respectively in MCF-7 cells. A significant decrease was observed in the viability of MCF-7 cells incubated with PEM, in comparison with those incubated with acetone ($p<0.05$). At the same volume (10 µl), while acetone-incubated cells had 95.23% viable cells, PEM-incubated cells had only 49.45% viable cells, strongly indicating the cytotoxicity of PEM in MCF-7 cell culture conditions. In Y79 RB cells solvent volumes used to assess the solvent toxicity were selected on the basis of IC_{50} dosage volume and two other volumes above and below IC_{50} dosage which were flanking the IC_{50}. In all the volumes tested, acetone-solubilised triclosan showed viability above 94% in Y79 RB

*** *The data presented in figure 6.4 is published in: Indian J Biochem Biophys. 2010 Jun;47(3):166-71. Please see "List of publications on page " on Page XXIII*

cells, and PEM-solubilised triclosan showed inconsistent response and showed cytotoxicity of about 66 ± 33% at 100 μg/ml dosage volume (Figure 6.5b).

Cell morphology analysis (Figure 6.6) showed shrinkage of cells with PEM in MCF-7 cells, while there was no observable change in the morphology of cells incubated with acetone (Figure 6.6 b,c), which was comparable with the control (Figure 6.6a). Y79 RB cells showed no observable changes in morphology when treated with acetone and PEM (Figure 6.6d,e) and was comparable with the control (Figure 6.6f). Further, agarose gel electrophoresis revealed mild oligonucleosomal DNA fragmentation with PEM in both MCF-7 and Y79 RB cells (Figure 6.7 a, c), suggesting its cytotoxicity. On the other hand, acetone-incubated group in both the cells were comparable with the untreated control (Figure 6.7 b, d). From these experiments, acetone was shown to be constantly non-toxic solvent for solubilising triclosan.

6.4.1.3. Effect of solvents on anti-proliferative activity of triclosan

The anti-proliferative effect of triclosan was assessed, when solubilized in acetone and PEM by MTT assay (Figure 6.8). Panels of triclosan concentrations between 50 - 200 μg/ml for MCF-7 cells and 2.5 – 50 μg/ml for Y79 RB cells were chosen. The IC_{50} (50% inhibitory concentration of the drug over cell viability) was obtained by interpolation. IC_{50} of triclosan solubilized in acetone in MCF-7 cells & Y79 RB cells was found to be 91.09 μg/ml and 20 μg/ml, while in PEM, it was 121.25 μg/ml and 29.5 μg/ml respectively. This implied that a 1.33-fold (in MCF-7 cells) and 1.5-fold (in Y79 RB cells) increase in drug concentration were required to induce anti-proliferative effects, when triclosan was dissolved in PEM, compared to acetone-dissolved triclosan. This indicates the lesser drug-sensitivity in PEM than acetone. A significant decrease in cell proliferation was observed in MCF-7 cells at 100 μg/ml, and with 50 μg/ml of acetone-solubilized triclosan in Y79 cells, compared with their respective PEM-solubilized triclosan ($P<0.05$). These results indicate a stronger anti-proliferative effect and greater drug sensitivity of triclosan when solubilized in

acetone.

Taken together, the results from sections 6.4.1.2 and 6.4.1.3, acetone was found to be more suitable for testing triclosan in cancer cells, owing to its lack of toxicity, and in conferring improved drug sensitivity.

Figure 6.5: Assessment of cytotoxicity of solvents (acetone, PEM) on MCF-7 & Y79 RB **cells by MTT Assay**

Figure 6.5a Cytotoxicity of solvents in MCF-7 cells

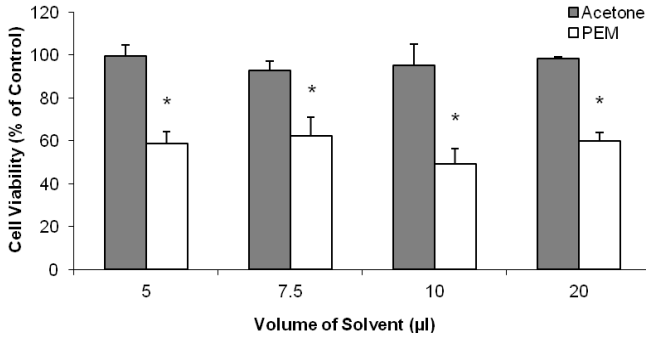

Figure 6.5b Cytotoxicity of solvents in Y79 RB cells

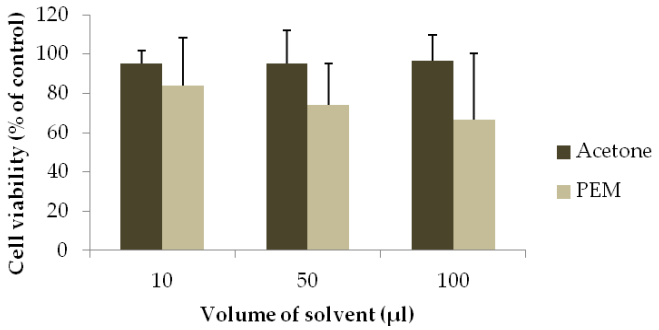

[†††]**Figure 6.5: Assessment of cytotoxicity of solvents (acetone, PEM) on MCF-7 & Y79 RB cells by MTT Assay:** Effects of the solvents (acetone, PEM) on cell viability presented as percentage of control (cells with only medium; no other solvent). MCF-7 **(a)** and Y79 RB **(b)** cells were grown for 48 h at various concentrations of the solvents. Values are expressed as the mean +/- S.D. of three separate experiments in triplicate. Differences in cell viability corresponding to acetone and PEM solvents in each concentration were compared by student's t-test. * represents significant difference at $P < 0.05$ in MCF-7 cells.

[†††] The data presented in figure 6.5a is published in: Indian J Biochem Biophys. 2010 Jun;47(3):166-71. Please see "List of publications" on Page XXIII

Figure 6.6 Cell morphology analysis of MCF-7 & Y79 RB cells treated with acetone and PEM

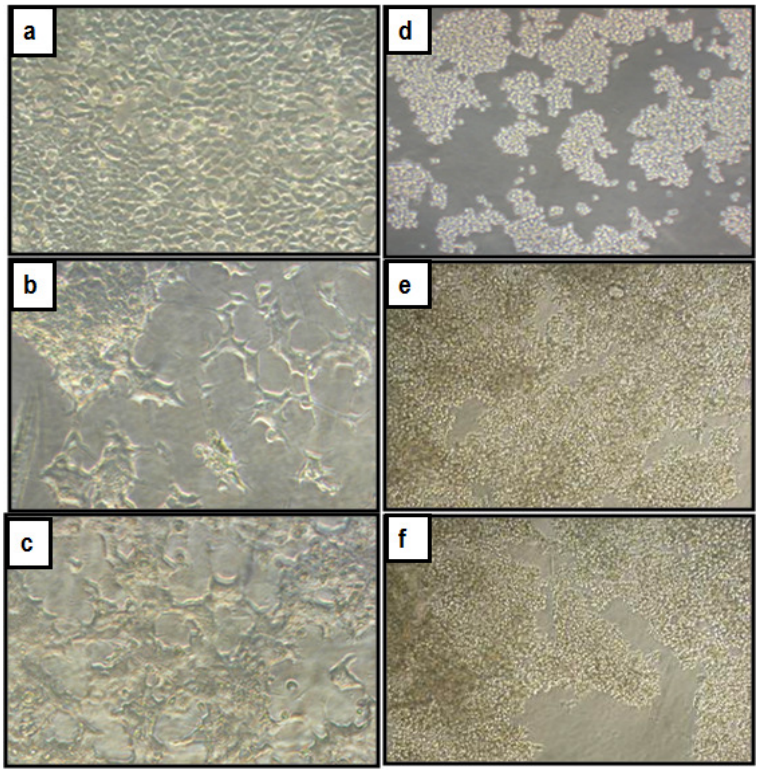

###**Figure 6.6 Cell morphology analysis of MCF-7& Y79 RB cells treated with acetone and PEM:** Effect of solvents on MCF-7 cell morphology was observed by phase contrast microscopy. **a)** untreated MCF-7 cells, **b)** MCF-7 cells exposed to acetone (volume corresponding to dissolution of triclosan at its IC_{50}) show no observable morphological changes **c)** MCF-7 cells exposed to PEM (volume corresponding to dissolution of triclosan at its IC_{50}) reveal shrinkage of cells. **d)** untreated Y79 cells, **e)** Y79 cells exposed to acetone (volume corresponding to dissolution of triclosan at its IC_{50}) show no observable morphological changes **f)** Y79 RB cells exposed to PEM (volume corresponding to dissolution of triclosan at its IC_{50}) reveal no observable morphological changes. (Magnification – 10X)

The data presented in figure 6.4a-c is published in: Indian J Biochem Biophys. 2010 Jun; 47(3):166-71. Please see "List of publications" on Page XXIII

Figure 6.7a,b Assessment of DNA damage on MCF-7 cells treated with solvents:

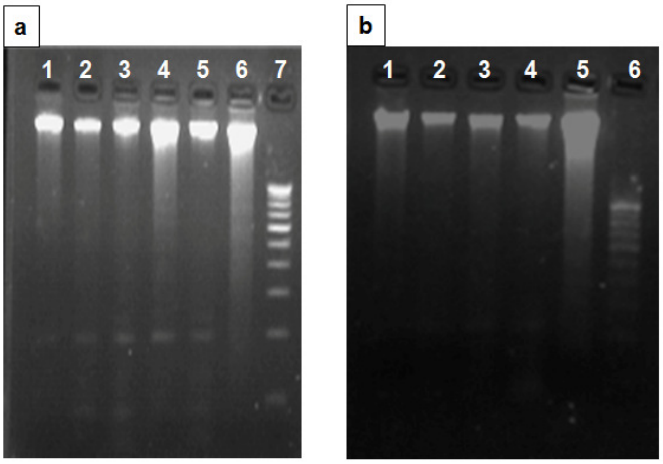

§§§**Figure 6.7a, b Assessment of DNA damage on MCF-7 cells treated with solvents: a)** Cytotoxic effect of PEM solvent on MCF-7 cells analyzed by DNA fragmentation assay. Cells treated with different volumes of PEM reveal fragmented DNA that can be compared with the positive control served by hydrogen peroxide treated cells (lane 6) and a standard marker DNA ladder (lane 7). **b)** DNA fragmentation assay on acetone solvent incubated MCF-7 cells. The DNA corresponding to different acetone volumes are comparable with the control untreated MCF-7 cells (lane 1). The volumes of solvents indicated in the figure corresponds to the solubilising volume for 50-125 µg/ml of triclosan diluted with the culture medium

§§§ *The data presented in figure 6.7 a-b is published in: Indian J Biochem Biophys. 2010 Jun; 47(3):166-71. Please see "List of publications" on Page XXIII*

Figure 6.7c, d Assessment of DNA damage on Y79 RB cells treated with solvents:

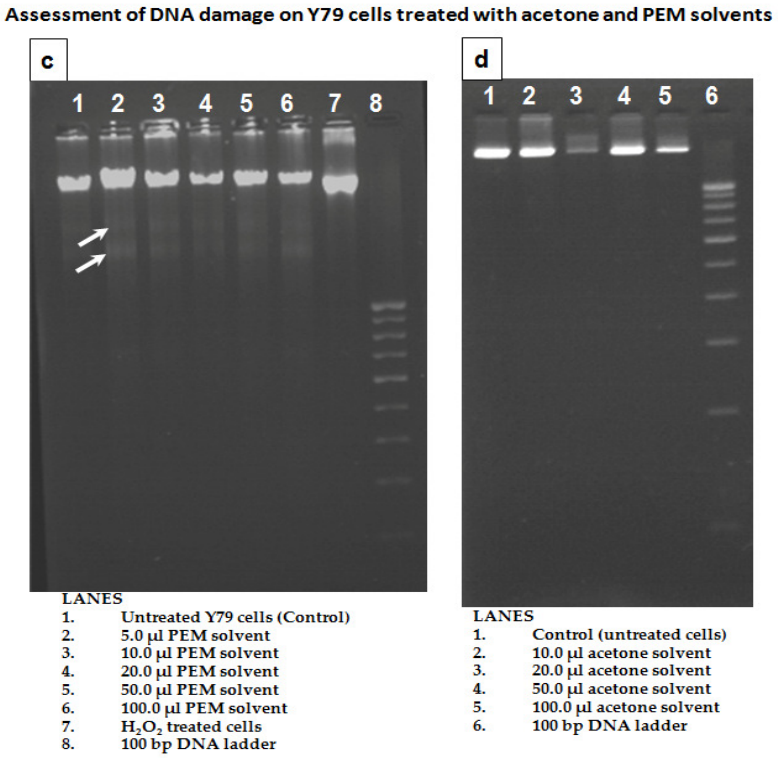

Figure 6.7c, d Assessment of DNA damage on Y79 RB cells treated with solvents c) Cytotoxic effect of PEM solvent on Y79 RB cells analyzed by DNA fragmentation assay. Cells treated with different volumes of PEM reveal fragmented DNA (arrows) that can be compared with the positive control served by hydrogen peroxide treated cells (lane 7) and a standard marker DNA ladder (lane 8). **d)** DNA fragmentation assay on acetone solvent incubated Y79 cells. The DNA corresponding to different acetone volumes are comparable with the control untreated Y79 cells (lane 1). The volumes of solvents indicated in the figure correspond to the solubilising volume for 50-100 µg/ml of triclosan diluted with the culture medium.

Figure 6.8a Differences in triclosan concentrations needed to reduce MCF-7 cell proliferation when dissolved in acetone and PEM.

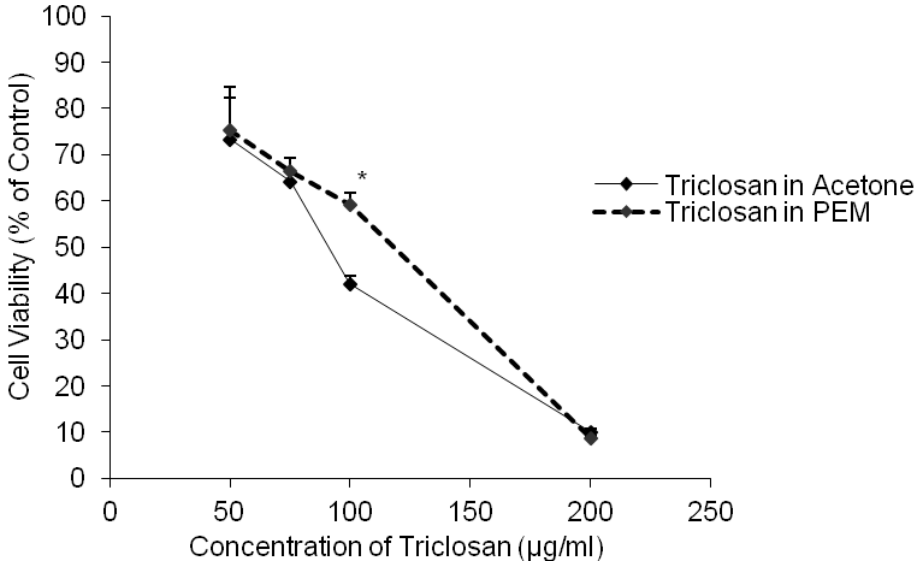

[****]**Figure 6.8a Differences in triclosan concentrations needed to reduce MCF-7 cell proliferation when dissolved in acetone and PEM:** Inhibitory concentrations of triclosan solubilized in acetone, and PEM differ, as observed by MTT assay, in MCF-7 cells incubated with triclosan for 48 h. Difference in cell viability corresponding to each concentration (50, 75, 100 and 200 µg/ml) of triclosan solubilized in acetone, and triclosan in PEM solvent, was compared by student's t-test. * represent significant difference at $P < 0.05$. Triclosan dissolved in acetone showed significantly lower percentage of cell viability than PEM-dissolved triclosan at 100 µg/ml concentration. Further, the IC_{50} value of PEM-solubilized triclosan is about 1.33 fold higher than the IC_{50} of acetone-solubilized triclosan (121.25 µg/ml and 91.09 µg/ml respectively).

[****] *The data presented in figure 6.8a is published in: Indian J Biochem Biophys. 2010 Jun;47(3):166-71.*

Figure 6.8b Differences in triclosan concentration needed to reduce Y79 RB cell proliferation when dissolved in acetone and PEM

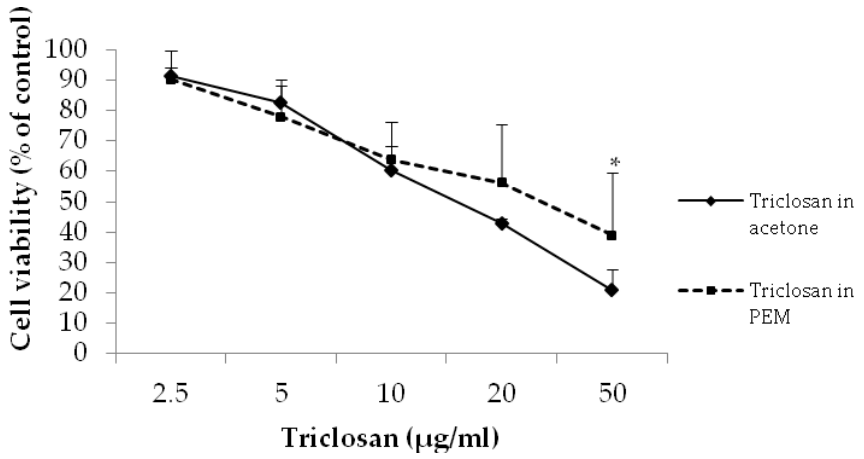

Figure 6.8b Differences in triclosan concentration needed to reduce Y79 RB cell proliferation when dissolved in acetone and PEM: Inhibitory concentrations of triclosan solubilized in acetone, and PEM differ, as observed by MTT assay, in Y79 RB cells incubated with triclosan for 48 h. Difference in cell viability corresponding to each concentration (2.5, 5, 10, 20 and 50 µg/ml) of triclosan solubilized in acetone, and triclosan in PEM solvent, was compared by student's *t*-test. * represent significant difference at $P<0.05$. Triclosan dissolved in acetone showed significantly lower percentage of cell viability than PEM-dissolved triclosan at 50 µg/ml concentration. Further, the IC_{50} value of PEM-solubilized triclosan is about 1.5 fold higher than the IC_{50} of acetone-solubilized triclosan (29.5 µg/ml and 20 µg/ml respectively).

6.4.2. Inhibition of viability of Y79 RB cells by FASN inhibitors: Determination of IC_{50}

Figure 6.9 demonstrate the effect of different concentrations of cerulenin, triclosan, and Xenical™ (orlistat) on viability of Y79 RB cells treated at 48, 72 and 96 h respectively. The three drugs showed both dose- and time-dependent decrease in cell viability. The IC_{50} (50% inhibitory concentration) values of cerulenin, triclosan, and Xenical™, decreased when the time of treatment was increased from 48 h to 96 h.

Figure 6.9 Cytotoxic effects of FASN inhibitors in Y79 RB cells at 48, 72 & 96 h

Figure 6.9a

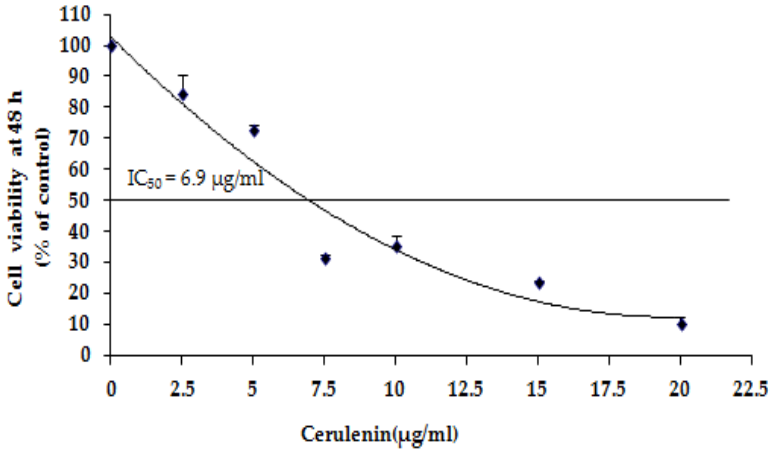

Figure 6.9b

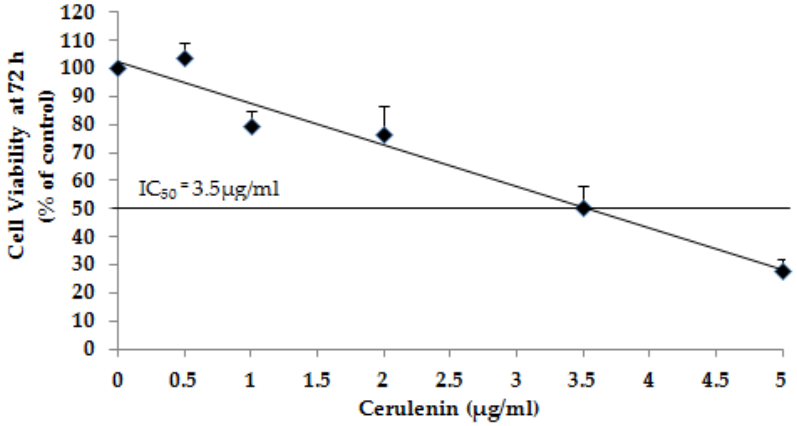

Figure 6.9c

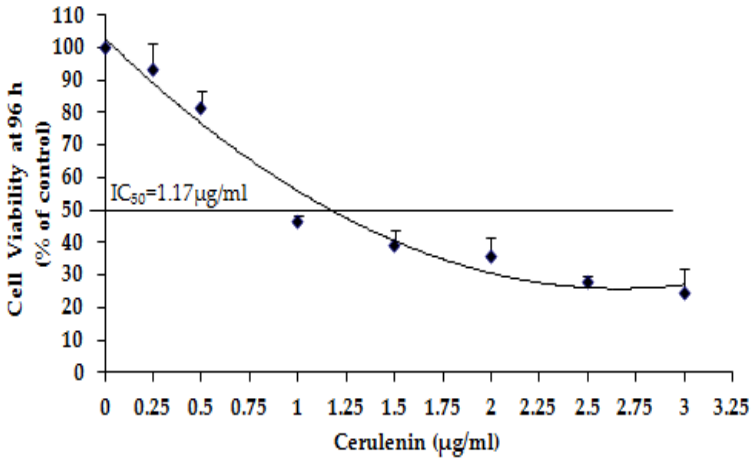

Figure 6.9 a-c Cytotoxic effects of cerulenin in Y79 RB cells at 48h (a), 72h (b), 96h (c): Cytotoxic effect of cerulenin on retinoblastoma cells was evaluated by MTT Assay. IC_{50} was calculated using polynomial regression analysis by Microsoft excel. Values are expressed as mean ± S.D of three separate experiments in triplicate.

Figure 6.9d

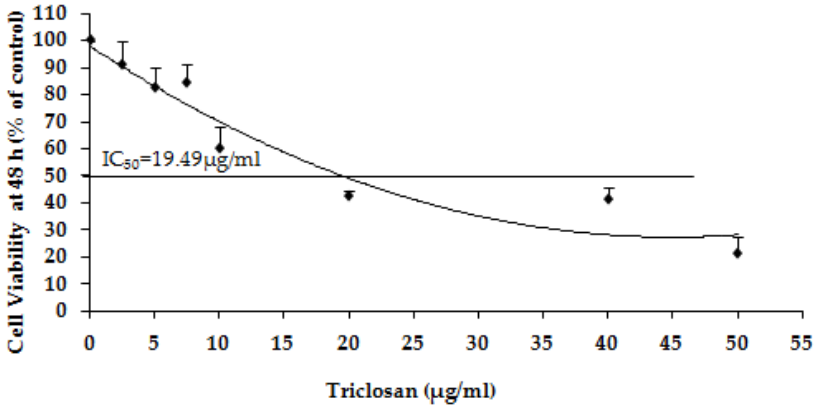

Figure 6.9e

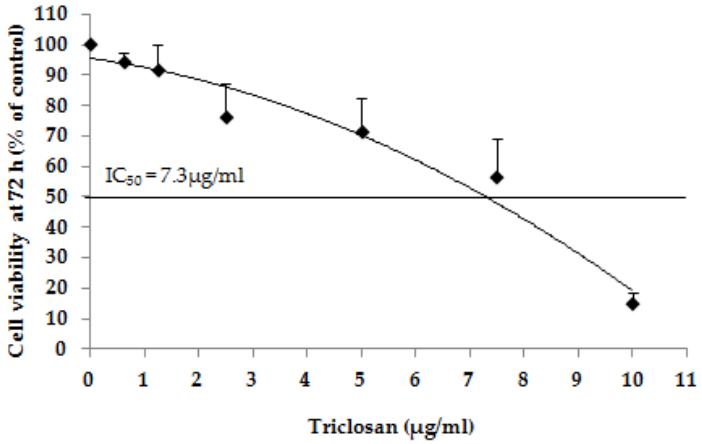

Figure 6.9f

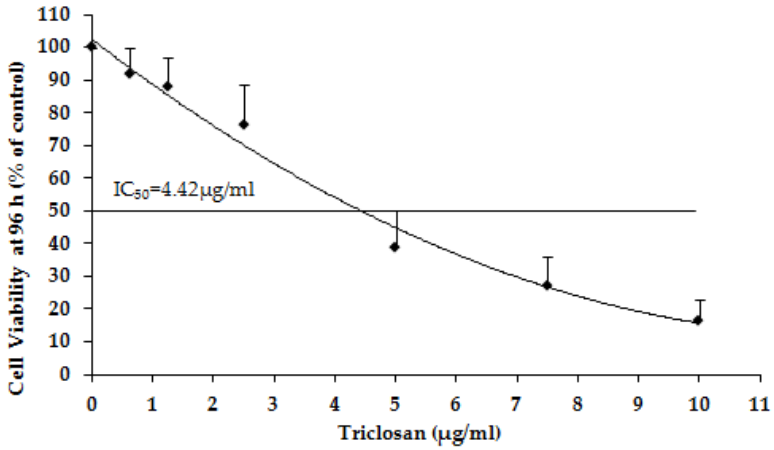

Figures 6.9 d-f Cytotoxic effects of triclosan in Y79 RB cells at 48h (d), 72h (e) and 96h (f): Cytotoxic effect of triclosan on retinoblastoma cells was evaluated by MTT Assay. IC_{50} was calculated using polynomial regression analysis by Microsoft excel. Values are expressed as mean ± S.D of three separate experiments in triplicate.

Figure 6.9g

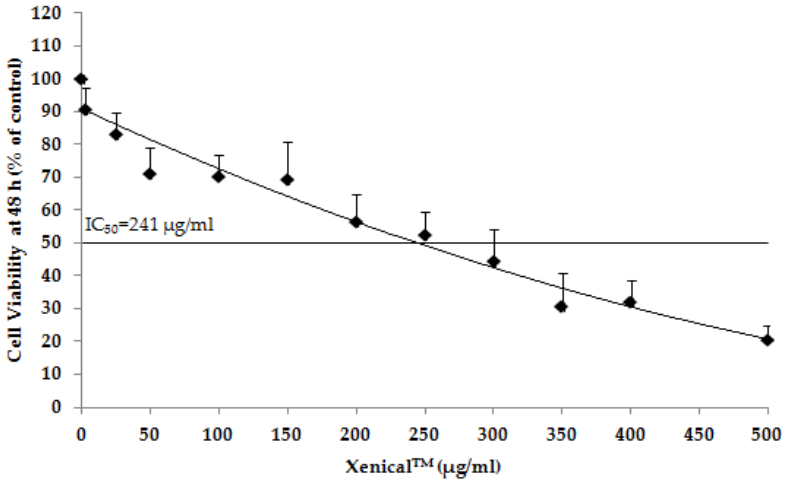

Figure 6.9h

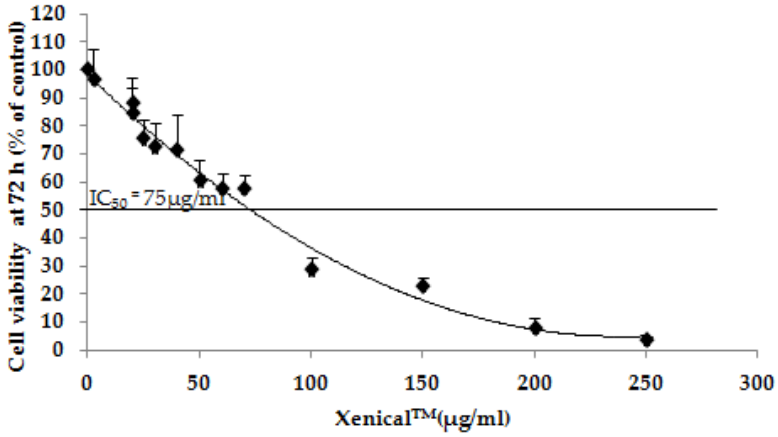

Figure 6.9i

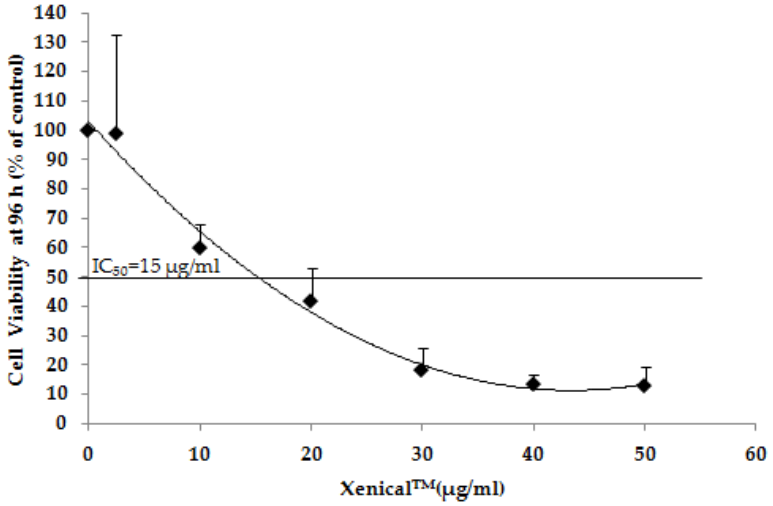

††††**Figures 6.9 g-i Cytotoxic effects of Xenical™ in Y79 RB cells at 48h (g), 72h (h), 96h (i):** Cytotoxic effect of orlistat (Xenical™) on retinoblastoma cells was evaluated by MTT Assay. IC_{50} was calculated using polynomial regression analysis by Microsoft excel. Values are expressed as mean ± S.D of three separate experiments in triplicate.

6.4.3. Differences in growth inhibitory response in neoplastic cells treated with specific concentration of FASN inhibitors for 48, 72 and 96 h.

A series of concentrations flanking the IC_{50} of FASN inhibitors at 48 h of incubation were identified. Corresponding to these concentrations, we plotted the percentage viability of Y79 RB cells treated with FASN inhibitors at 48, 72 and 96 h. Figure 6.10a reveals the growth inhibition by cerulenin in a dose- and time- dependent manner. At the lower end of the concentration series, the difference in the inhibitory response is extremely high with respect to time of treatment (45% at 72 h and 55% at 96 h when compared to the cell viability at 48 h with 5 µg/ml cerulenin), while at a concentration much higher than the IC_{50} the time of treatment has marginal effect on the cell viability (difference in viable cells compared between each of the 3 different

†††† The data presented in figures 6.9 a-i is published in: Basic & Clin Pharmacol & Toxicol, 2012, 110, 494-503 & J Ocul Biol Dis Inform. 2010; 3(4): 117-12. Please see "List of publications" on Page XXIII

time periods at 20 µg/ml treatment was less than 10%). On similar lines, triclosan's cytotoxicity on Y79 RB cells (Figure 6.10b) was highly time-dependent on the lower end of the concentration series at 5 µg/ml, wherein about 43.5% difference in viable cells was observed between the time periods, 48 h and 96 h and 11% difference in viability between 48 h and 72 h.

Figure 6.10 Differences in growth inhibitory response in neoplastic cells treated with specific concentration of FASN inhibitors for 48h, 72h and 96h.

Figure 6.10a

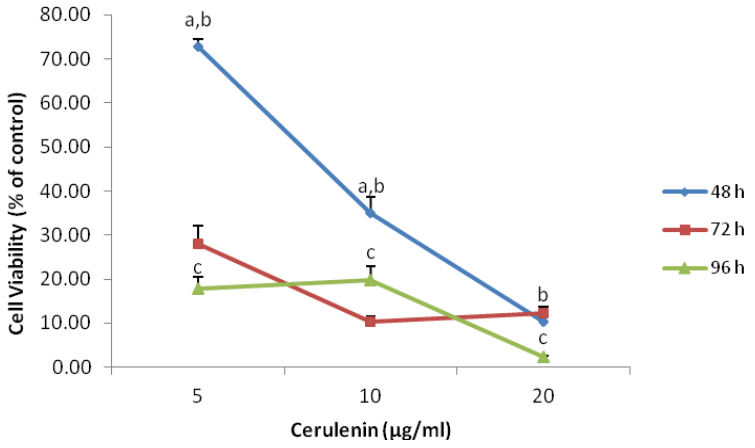

###**Figures 6.10a Differences in growth inhibitory response in neoplastic cells treated with specific concentration of cerulenin for 48h, 72h and 96h.** At specific concentrations of cerulenin the relative cell viability was measured at increasing times of incubation (48h, 72h & 96h). Student's *t*-test was used for comparisons between the experimental groups, $P<0.05$ is considered statistically significant. [a]indicates statistically significant difference relative to 72 h incubated cells, [b] indicates statistically significant difference relative to 96 h incubated cells, and [c] indicates statistically significant difference relative to 72 h incubated cells. Values are expressed as mean + S.D of three separate experiments in triplicate.

The data presented in figure 6.10 a is published in: Basic & Clin Pharmacol & Toxicol, 2012, 110, 494-503. Please see "List of publications" on Page XXIII

Figure 6.10b

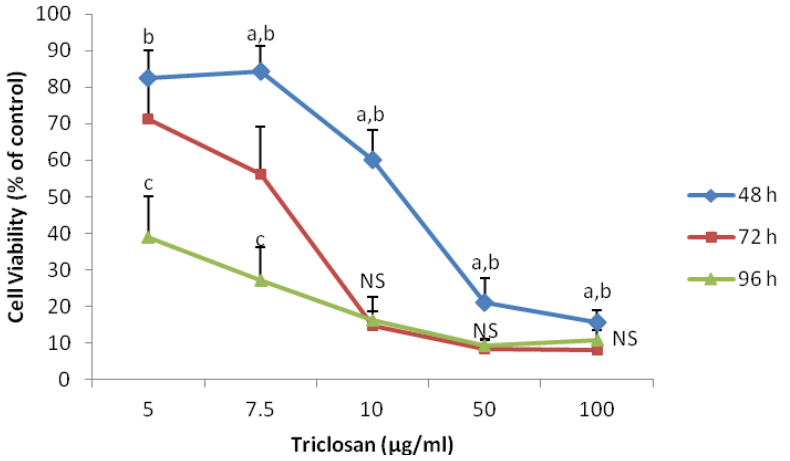

Figure 6.10c

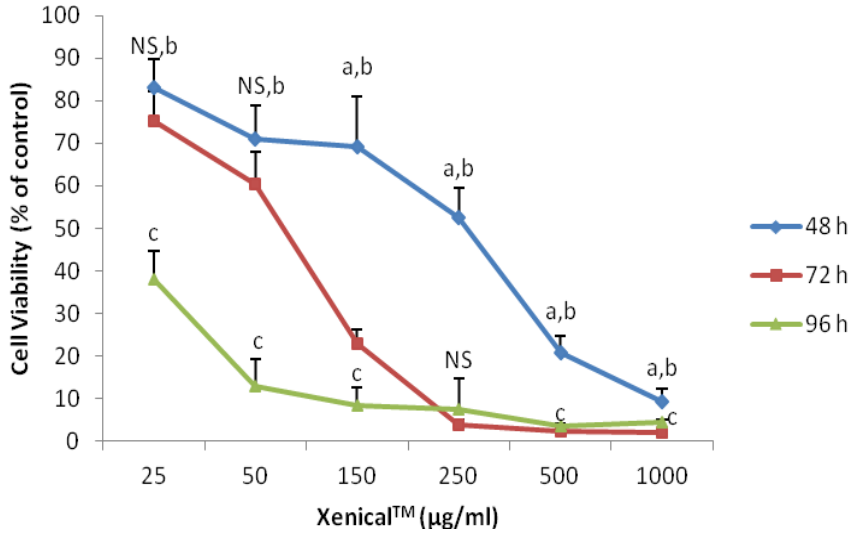

§§§§**Figures 6.10 b,c: Differences in growth inhibitory response in neoplastic cells treated with specific concentration of triclosan (6.10b) and Xenical™ (6.10c) for 48 h, 72 h and 96 h.** At specific concentrations of triclosan and Xenical™ the relative cell viability was measured at increasing times of incubation (48, 72 & 96 h). Student's *t*-test was used for comparisons between the experimental groups, $P<0.05$ is considered statistically significant. [a] indicates statistically significant difference with respect to 72 h incubated cells, [b] indicates statistically significant difference with respect to 96 h incubated cells, and [c] indicates statistically significant difference with respect to 72 h incubated cells. NS indicates no significance at that particular dosage. Values are expressed as mean + S.D of three separate experiments in triplicate.

§§§§ *The data presented in figure 6.10 b, c is published in: Basic & Clin Pharmacol & Toxicol, 2012, 110, 494-503. Please see "List of publications" on Page XXIII*

This difference in cell viability tapered at concentrations higher than 50 μg/ml, (difference in cell viability between 48 h and 96 h of incubation with 100 μg/ml was only 4.8%, and between 48 h and 72 h the difference was only 7%). At 10 μg/ml the difference in viability between 48 and 72 h was 45%, and between 48 h and 96 h the difference was 43%. These results indicated lesser sensitivity to time beyond these concentrations of triclosan. The IC_{50} of orlistat in Y79 cells treated for 48 h was 250 μg/ml. At 150 μg/ml concentration (that is lesser than this IC_{50}) the cells were greatly sensitive to time of incubation, wherein 150 μg/ml dosages induced reduction in cell viability to only about 69% at 48 h in contrast to 23% and 8% cell viability after 72 h and 96h of treatment respectively (Figure 6.10c). However at a dosage higher than the IC_{50} (250 μg/ml), we observed the impact of time of incubation becoming minimal (9%, 2% and 4.5% cell viability at 48 h, 72 h and 96 h respectively at a drug dosage of 1000 μg/ml). At 250 μg/ml (IC_{50} at 48 h) and 500 μg/ml Y79 RB cell viability was less than 7% both at 72 and 96 h, indicating saturating effect on time- dependent toxicity of Xenical™ (orlistat) to Y79 RB cells.

6.4.4. Sensitivity of Y79 RB cells to increasing concentrations of FASN inhibitors

Figure 6.11 presents the sensitivity of Y79 RB cells treated with FASN inhibitors [cerulenin (Fig.6.11a-c), triclosan (Fig.6.11d-f), and Xenical™ (Fig.6.11g-i)] at increasing dosages higher than their respective IC_{50} at 48, 72 and 96 h of treatment. It is clear from the graph that the cancer cells respond sharply to increasing concentrations beyond the IC_{50}. However, this dose dependent sensitivity of the cancer cells diminishes beyond a particular concentration. Cerulenin at 48 h showed a significant decrease between consecutive dosages 15 and 20 μg/ml, the higher dosage (30 μg/ml and beyond till 500 μg/ml) did not show significant difference. At 72 h the threshold was 20 μg/ml, beyond which the cell viability was not significantly varying. IC_{50} of cerulenin at 96 h was 1 μg/ml and beyond this dosage the decrease in cell viability was very marginal. Triclosan showed significant

difference at 72 h between consecutive dosages (7.5, 10 and 50 μg/ml). However, a two-fold higher dosage, 100 μg/ml, did not significantly decrease the cell viability. A two fold higher dosage of 40 μg/ml than its IC_{50} of 20 μg/ml at 48 h showed an insignificant response and beyond this, the higher dosages were significantly cytotoxic to Y79 cells. At 96 h of treatment higher dosages (10, 50 and 100 μg/ml) showed viability of less than 20%, in which 100 μg/ml was not significantly different than the next lower dosage 50 μg/ml. The sensitivity of the cancer cells to increasing dosages of orlistat (Xenical™) at 48 h was in the range 250 - 350 μg/ml, at 400 μg/ml viability had reached 31% beyond which increase in dosage of orlistat attained saturation and the response was variable. A significant sensitivity between consecutive dosages of orlistat was observed at 72 h (till 250 μg/ml) and at 96 h (till 30 μg/ml). Increasing drug treatment beyond the threshold upto 1000 μg/ml at 72 h and 500 μg/ml at 96 h showed no variation of cytotoxicity to Y79 cells.

Figures 6.11: Sensitivity of FASN inhibitors with multi-fold increase in dosages of drug exposed for 48, 72 & 96h on cultured retinoblastoma cells

Figure 6.11a

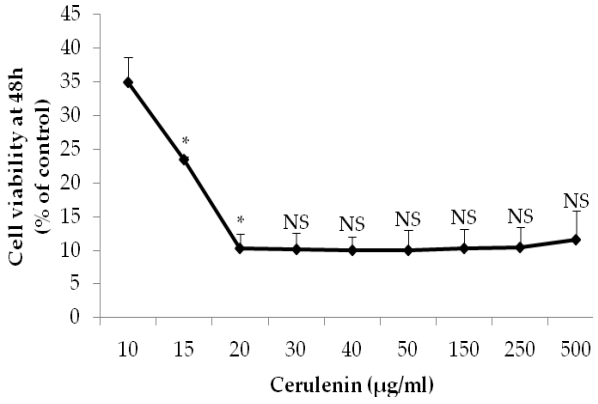

Figure 6.11b

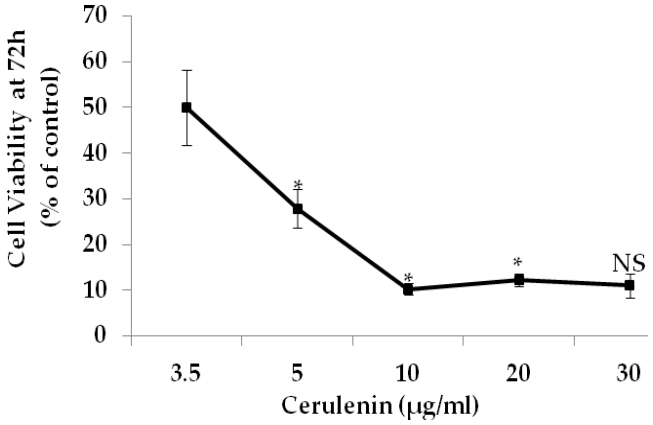

Figure 6.11c

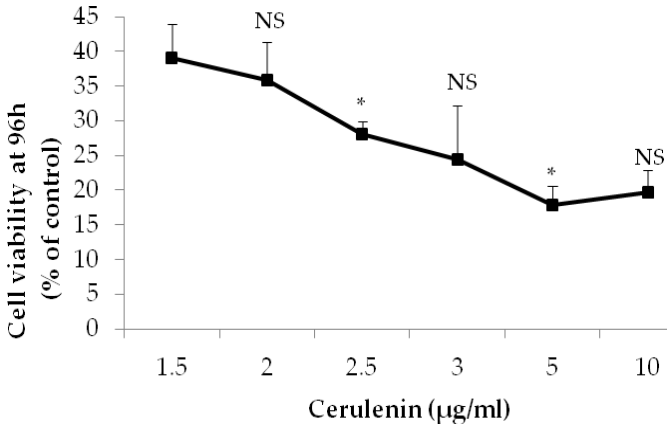

Figure 6.11a-c Sensitivity of cerulenin with multi-fold increase in dosages of drug exposed for 48, 72 and 96 h on cultured RB cells: Cultured RB Y79 cells were treated with multi-fold increase in dosages of cerulenin at 48 h **(a)**, 72 h **(b),** 96 h **(c).** Dose dependent decrease in cell viability was observed only till a threshold concentration beyond which the cells were less sensitive to increase in drug concentration. Student's *t*-test was used for comparisons between the experimental groups, $P<0.05$ is considered statistically significant. * indicates significant difference between consecutive dosage of the inhibitor and NS indicates no statistically significant difference.

Figure 6.11d

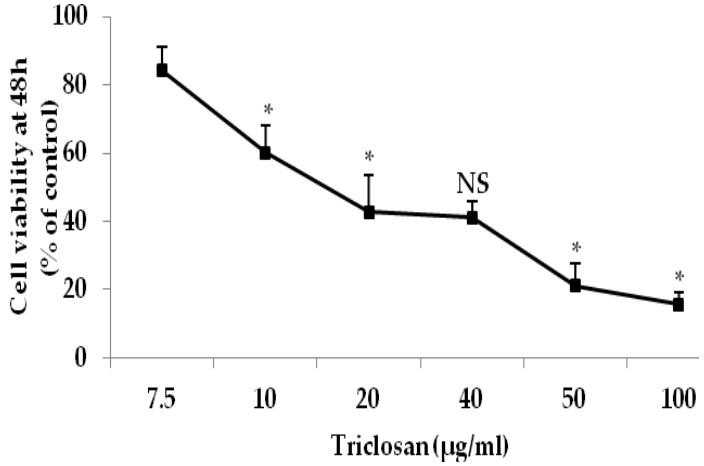

Figure 6.11e

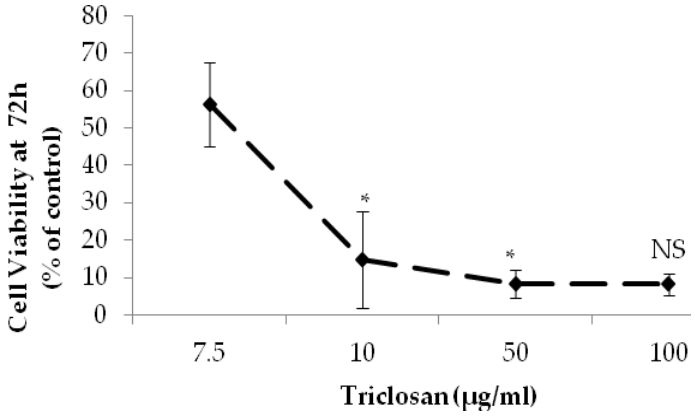

Figure 6.11f

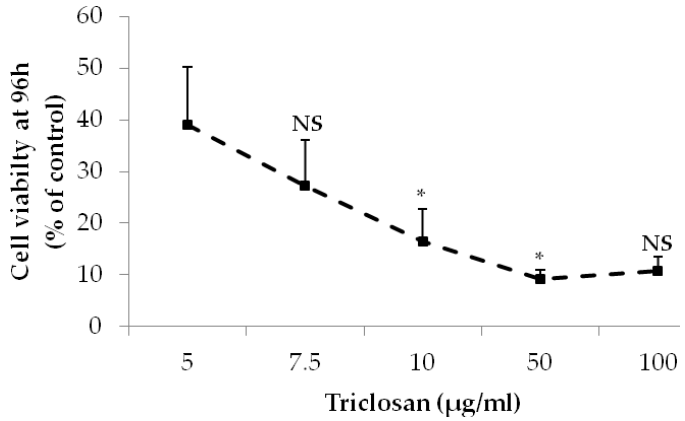

Figure 6.11d-f: Sensitivity of triclosan with multi-fold increase in dosages of drug exposed for 48h, 72 and 96h on cultured retinoblastoma cells: Cultured retinoblastoma Y79 cells were treated with multi-fold increase in dosages of triclosan at 48h **(d),** 72h **(e)**, and 96h **(f)**. Dose dependent decrease in cell viability was observed only till a threshold concentration beyond which the cells were less sensitive to increase in drug concentration. Student's *t*-test was used for comparisons between the experimental groups, P<0.05 is considered statistically significant. * indicates significant difference between consecutive dosage of the inhibitor and NS indicates no statistically significant difference.

Figure 6.11g

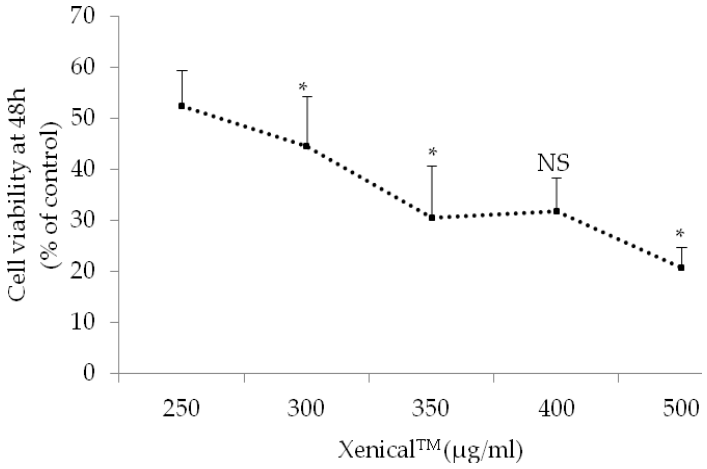

Figure 6.11h

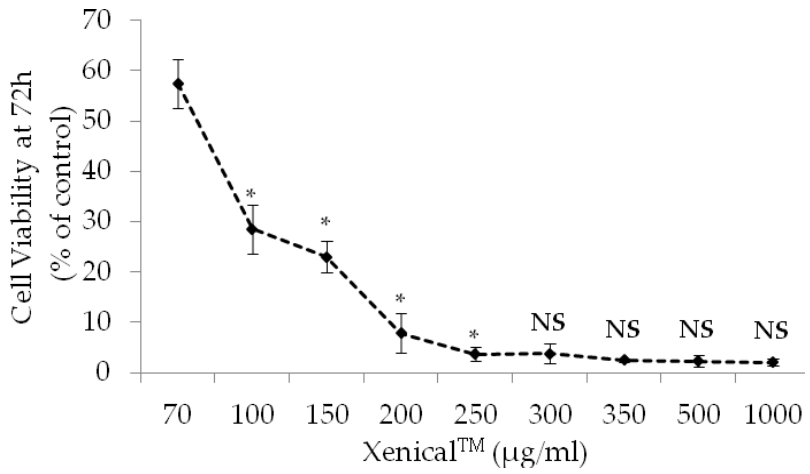

Figure 6.11i

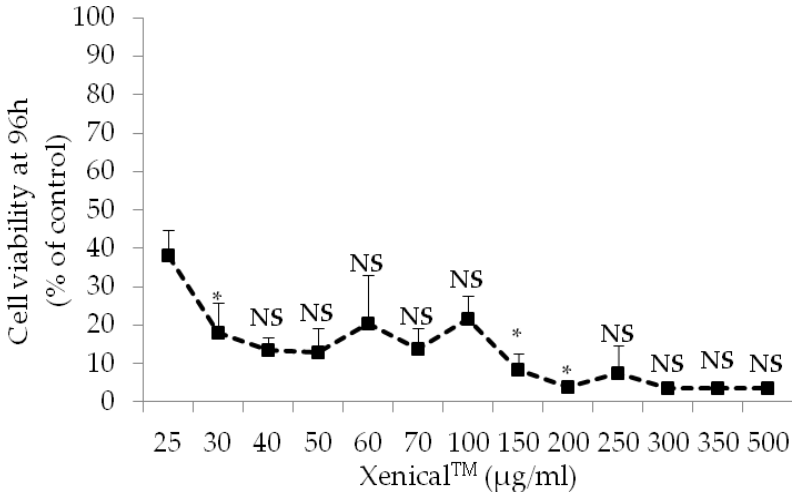

[*]**Figure 6.11i: Sensitivity of orlistat (Xenical™) with multi-fold increase in dosages of drug exposed exposed for 48h, 72h & 96h on cultured retinoblastoma cells:** Cultured retinoblastoma Y79 cells were treated with multi-fold increase in dosages of Xenical™ at 48h **(g)**, 72h **(h)** and for 96h **(i)**. Dose dependent decrease in cell viability was observed only till a threshold concentration beyond which the cells were less sensitive to increase in drug concentration. Student's *t*-test was used for comparisons between the experimental groups, $P<0.05$ is considered statistically significant. * indicates significant difference between consecutive dosage of the inhibitor and NS indicates no statistically significant difference.

[*] *The data presented in figure 6.11b,e,h is published in: J Ocul Biol Dis Inform. 2010; 3(4): 117-128. Please see "List of publications" on Page XXIII*

6.4.5. Response of Y79 RB cells to cytotoxic (IC_{70}) and cytostatic (IC_{30}) concentrations of the FASN inhibitors at different times of treatment

Comparison of the concentration increments required by each FASN inhibitor to decrease viability of Y79 RB cells from 70 % to 30% was then performed (Figure 6.12). For this the IC_{30} (cytostatic) and IC_{70} (cytotoxic) (30% & 70% inhibitory concentration respectively) of the three FASN inhibitors were determined (Menendez et al., 2007). The IC_{30}/ IC_{70} ratio was calculated to indicate the fold increment in drug concentration needed to produce the drug-response (inhibition of cell viability). The basis of this comparison was that if the ratio was higher, the concentration of the drug required to diminish cell viability to 30% was also higher, thereby indicating lesser sensitivity of the cancer cells to the anti-proliferative effect of the drug.

Figure 6.12 Response of Y79 RB cells to cytotoxic (IC_{70}) and cytostatic (IC_{30}) concentrations of the FASN inhibitors at different times of treatment

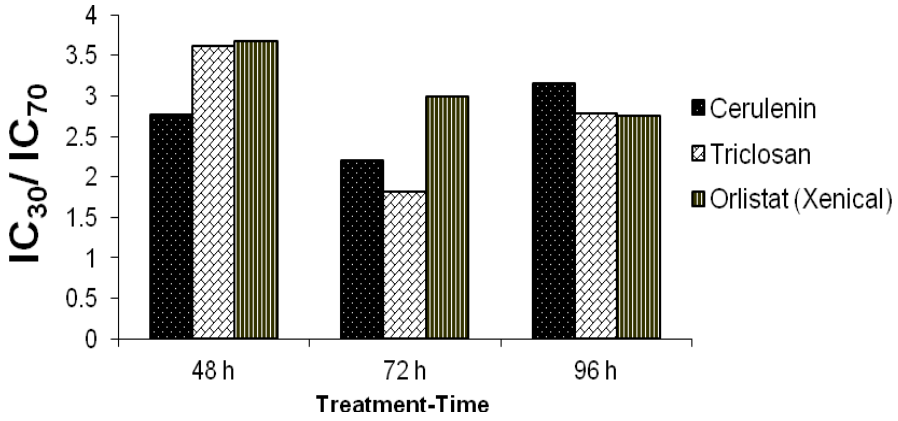

*__Figure 6.12 Response of Y79 RB cells to cytotoxic (IC_{70}) and cytostatic (IC_{30}) concentrations of the FASN inhibitors at different times of treatment:__ Drug dosage increments required to induce cytotoxicity in cultured Y79 RB cells was evaluated by computing the IC_{30} and IC_{70} for each drug at specific treatment-duration. Figure shows the fold increase in drug dosage required to inhibit cell viability from 70% to 30% at 48, 72 & 96h.

* *Data presented in figure 6.12 is published in: Basic & Clin Pharmacol & Toxicol, 2012, 110, 494-503. Please see "List of publications" on Page XXIII*

Here it was found that cells after 48 h of treatment showed greater sensitivity to cerulenin treatment, wherein a 2.77 fold increment in dosage resulted in 30% cell viability. However to achieve the same 30% cell viability an increment of 3.6 fold and 3.7 fold of triclosan and orlistat (Xenical™) respectively was required. When Y79 cells were treated for 72 h with FASN inhibitors, cells were more sensitive to triclosan, wherein an increment of 1.8 fold decreased viability of cells to 30%. In contrast, a 2.2 fold increase in cerulenin and a 3.0 fold increase in Xenical™ concentrations were required to produce 30% cell viability. The cells treated for 96 h were least sensitive to cerulenin (3.15 fold increment) in comparison with triclosan and Xenical™ (2.78 and 2.75 fold increment). To sum up, the neoplastic Y79 RB cells were more sensitive to cerulenin at 48 h, and to triclosan at 72 h, while at 96 h treatment, their sensitivity were comparable to both orlistat (Xenical™) and triclosan.

Figure 6.13 Cell morphology analysis on FASN inhibitor treated Y79 RB cells

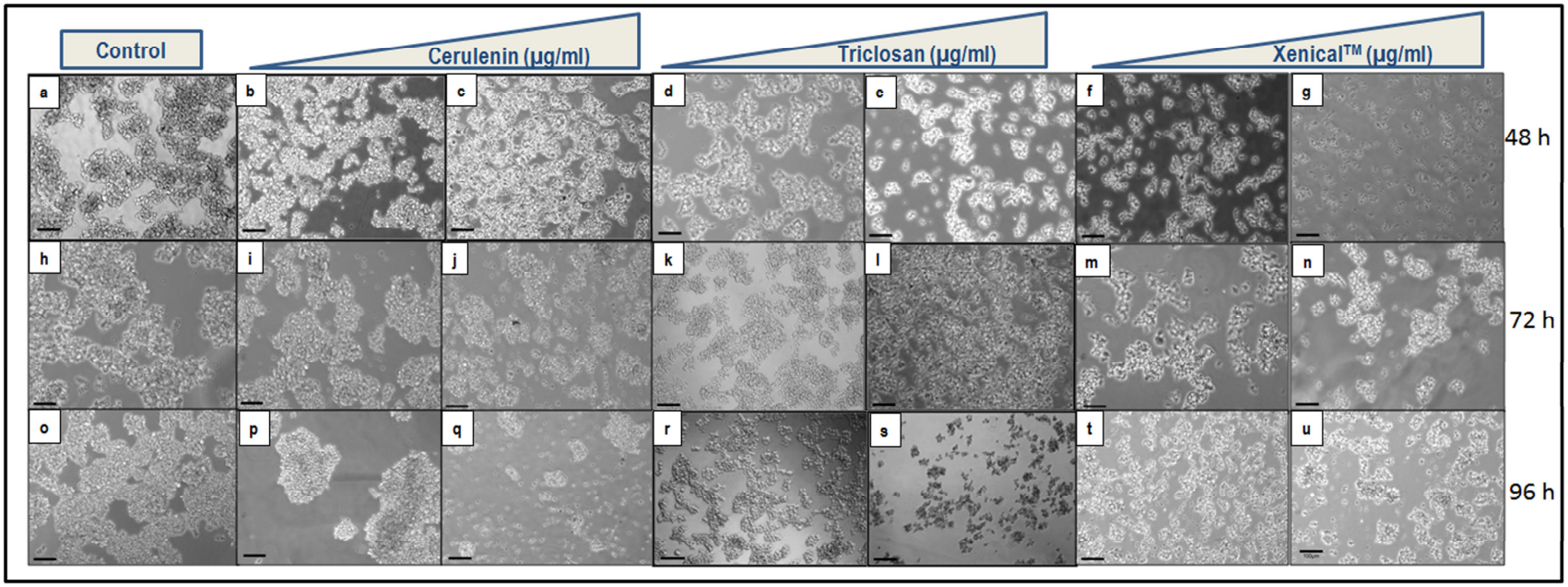

*__Figure 6.13: Cell morphology analysis on FASN inhibitor treated Y79 RB cells at 48h, 72h & 96h:__ Cultured RB Y79 cells were treated with IC_{50} and a higher dosage (selected based on MTT assay) of each inhibitor at 48 , 72 & 96 h. a, h & o – untreated control Y79 cells at 48, 72 and 96h respectively, and b, c – 7, 20 µg/ml cerulenin; d, e – 20, 100 µg/ml triclosan; f, g – 250, 1000 µg/ml Xenical™ (orlistat) treated at 48 h, and i, j – 3, 20 µg/ml cerulenin; k, l – 7.5, 100 µg/ml triclosan; m, n – 75, 250 µg/ml Xenical™ (orlistat) treated at 72h, and p, q – 1, 20 µg/ml cerulenin; r, s – 5, 100 µg/ml triclosan; t, u – 15, 70 µg/ml Xenical™ (orlistat) treated at 96h. Magnification: 10X (Scale bar: 100µm).

* *The data presented in figures 6.13 is published in: Basic & Clin Pharmacol & Toxicol, 2012, 110, 494-503 & J Ocul Biol Dis Inform. 2010; 3(4): 117-128. Please see "List of publications" on Page XXIII*

6.4.6. Cell morphology analysis

The morphology of Y79 RB cells were evaluated after treatment with the IC_{50} dosage and a higher dosage of each FASN inhibitor at three different times of exposure: 48, 72 and 96 h. Cell shrinkage was observed with the higher dosage of treatment. However, the cells treated with the respective IC_{50} dosages were comparable with the untreated control, which did not induce any observable morphology changes (Figure 6.13).

6.5. Chapter Summary

- The solubilisation conditions for testing the anti-proliferative effects of FASN inhibitors (cerulenin, triclosan and orlistat (Xenical™) in cell culture conditions were optimised.
- FASN inhibitors (cerulenin, triclosan and orlistat) showed dose- and time-dependent cytotoxic effects in Y79 RB cells, and their respective IC_{50} was determined.
- Sensitivity of each inhibitor in causing cytotoxic effects with respect to time of exposure and concentration were compared and analysed.

CHAPTER 7: SAFETY PROFILE OF FASN INHIBITORS IN NON-NEOPLASTIC CELLS

7.1. Introduction

Cancer therapy in general, besides their anti-cancer effect has also been reported to affect the growth of the surrounding normal cells in the tumour environment. Clinical successfulness of novel therapeutic targets depends on their differential expression in cancer cells and non-neoplastic cells, such that the treatment procedures can be specifically targeted to the cancer cells without affecting the normal cells. Pediatric cancer patients also suffer with late treatment effects such as impairment of function of specific organs and development of secondary cancers (Cancer Facts & Figures 2012, American Cancer Society). Chemotherapy associated toxic effects on the surrounding normal cells occurs both in an acute (during the chemotherapy) and chronic manner (after the chemotherapy-late effects). Normal cells and tumour cells react differently to the radiation therapy that is administered. The tumour cells are sensitive to the radiation compared to the surrounding normal cells in tumours that are treatable with radiation therapy. Likewise the cancer cells and the non-neoplastic cells cultured *in vitro* also behave differently towards the anti-cancer agents.

Recently developed novel anti-cancer treatment strategies ensure that the anti-cancer agents are non-toxic to the non-tumour regions (Cukier et al., 2005). Likewise the potential tumour targets that are explored for anti-cancer therapy are differentially expressed in normal and cancer cells. In this context fatty acid synthase (FASN) is over-expressed in cancer cells and expressed very minimally or not expressed in the non-neoplastic cells. The enzyme has different functions in normal and cancer cells, which makes the regulation mechanisms between normal and cancer cells distinct. The normal cells rely on the dietary fatty acids for their energy and the cancer cells rely on the *de novo* lipogenesis for their increased proliferation. The role of FASN

being distinct in the normal and cancer cells, this chapter explores the role of FASN in normal and cancer cells and the effects of FASN inhibitors in two non-neoplastic cells.

7.1.1 Role of FASN in non-neoplastic cells

Fatty acid synthase (FASN) in normal cells is very minimally expressed as the dietary fatty acids fulfil the cellular requirement, making the cells independent of *de novo* lipogenesis. Few normal tissues such as liver, adipose tissue, lactating breast and the cycling endometrium in the adults have high metabolic turnover, and thereby express FASN in significant amounts. The FASN in these tissues perform specialized physiological functions including the production of milk lipids in lactating breast tissue and surfactant in infant lung.

7.1.2. Regulation of FASN in non-neoplastic cells

Under normal conditions the expression and function of FASN is tightly regulated by various mechanisms such as the environmental, hormonal and nutritional signals. In normal liver, FASN and fatty-acid synthesis are up-regulated by carbohydrate ingestion, thyroid hormone (T3), insulin, "spot 14" protein, and glucocorticoids. FASN is down-regulated by polyunsaturated fatty acids, cyclic-AMP, and glucagon. Leptin up-regulates FASN expression acutely but causes marked decrease in expression with chronic administration. FASN expression is also regulated by the various signaling pathways such as the PI3K and Akt pathways. The sterol level also regulates FASN expression, in which the FASN mRNA transcription is regulated by the binding of sterol regulatory element binding protein (SREBP1c) in the sterol response elements (SRE) domain of the FASN promoter. The FASN expression in the lactating breast, foetal lung, and cycling endometrium is under tight hormonal control of estrogens, progesterone, prolactins and androgens, which drives the FASN gene expression and the biosynthetic pathway through the PI3K/Akt and

MAPK/ERK1/2 signaling pathways. The resultant activity of FASN is thus in minimal to undetectable levels in all the normal adult tissues except for those few tissues with high metabolic turnover. In well-nourished adults, FASN is responsible primarily for energy storage by converting excess carbohydrate to fatty acids that are then esterified to be stored as triacylglycerols. FASN normally functions in the liver to make lipids for exporting to metabolically active tissues and for storage in adipose tissue (Singh & Costello, 2009; Quinn & Wang, 2008) (Figure 7.1).

7.1.3. Role of FASN in cancer cells

Cancer cell has a highly proliferative metabolic machinery to meet the requirements in the tumour micro-environment. In doing so there are high levels of carbon flux through aerobic glycolysis providing growth advantage to the cancer cells. There are about 25 enzymes involved in the synthesis of fatty acids from glucose. The main synthetic machinery has four important enzymes. 1) acetyl CoA carboxylase 2) citrate lyase 3) malic enzyme and the HMP shunt 4) FASN. A second hallmark is high rate of energy-consuming processes driving increased protein synthesis and active DNA synthesis. The third pathway is the increased *de novo* fatty acid synthesis with the help of FASN. Supporting this notion, FASN which is also called as the oncogenic antigen (OA519) is over-expressed in many of the human malignancies and their pre-neoplastic lesions. The endogenously synthesized fatty acids in the cancer cells are predominantly esterified to phospholipids, which are partitioned into detergent insoluble lipid rafts. In contrast the fatty acids synthesized in the normal cells are esterified into triglycerides for storage (Menendez & Lupu, 2007; Swinnen et al., 2003).

7.1.4. Regulation of FASN in cancer cells Aberrant activation of PI3K/AKT and MAPK, ERK1/2 signaling pathways respond to a variety of oncogenic stimuli such as over production of growth factors and hyper- activation of growth factor receptors.

Figure 7.1: FASN regulation in normal and cancer cells mediated by SREBP1c

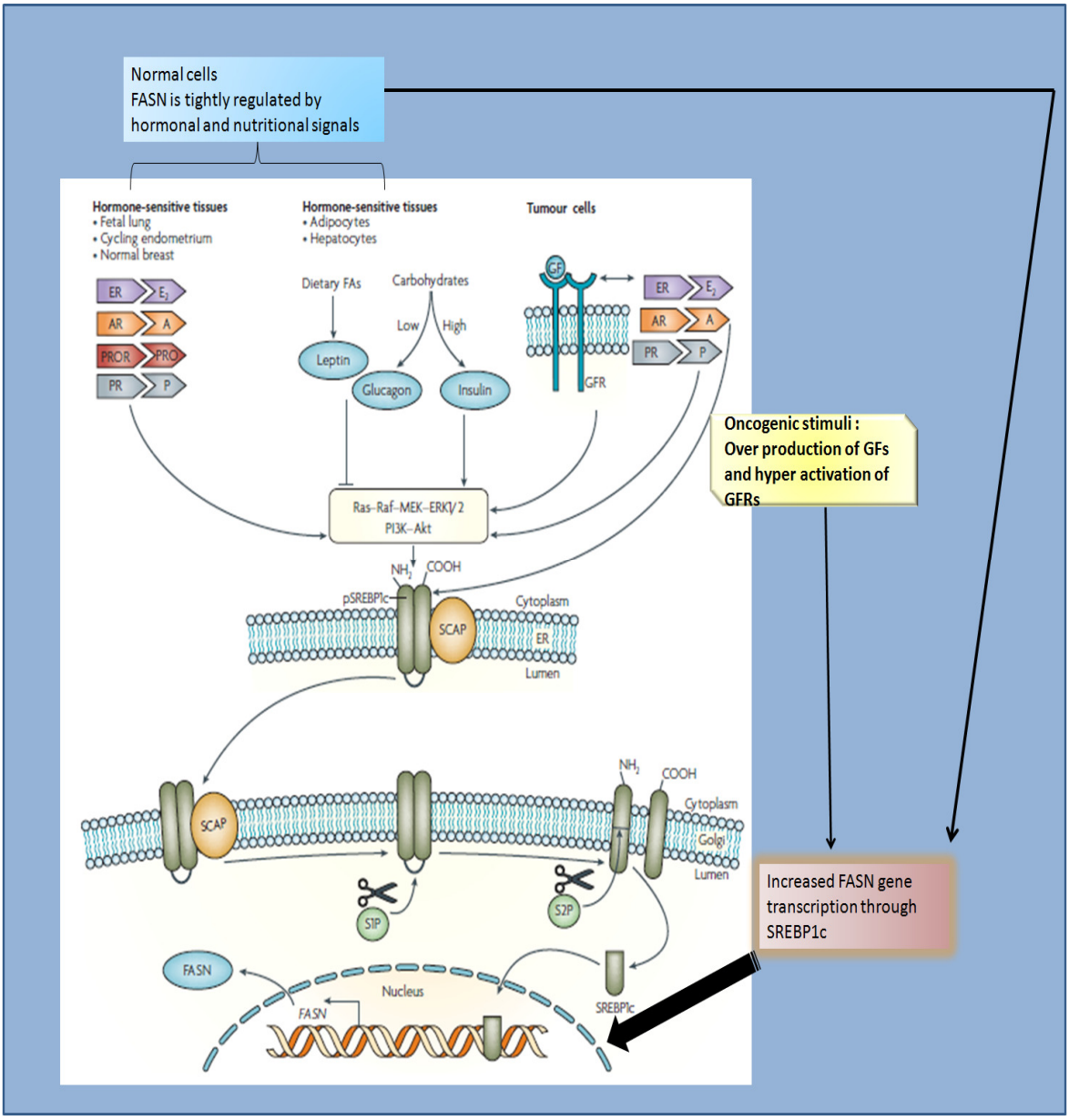

Figure 7.1 FASN regulation in normal and cancer cells mediated by SREBP1c: Schematic representation of FASN regulation at the transcriptional level in normal and cancer cells. The up-stream signals that stimulate FASN gene transcription is distinct from each other and both the signals converge at the common point SREBP1c to stimulate FASN gene transcription. This picture is adapted and modified from Menendez & Lupu, 2007. **Abbreviations:** A - androgens; AR - androgen receptor; E2 - oestradiol; ER-oestrogen receptor; P - progestins; PR - progesterone receptor; PRO - prolactin; PROR - prolactin receptor; SREBP1c - Sterol regulatory element binding protein 1c, GF – Growth factors, GFRs – growth factor receptors.

This response leads to increased FASN gene transcription via the SREBP1c. Tumour associated FASN is insensitive to nutritional signals. FASN regulation has been reported by various studies. Steroid hormones and their receptors are also responsible for over-expression of FASN through the similar pathway. In hormone responsive cancers the steroid hormone and the growth factor mediated effects converges at the PI3K/MAPK pathway, thus amplifying FASN gene (Swinnen et al., 1997; Swinnen et al., 2000). FASN protein interacts with the ubiquitin specific protease (USP2a) which removes the ubiquitin from the protein and thus stabilizes the FASN enzyme (Graner et al., 2004). FASN gene (17q22-17q24) is prone to gene amplification at a high level. This leads to high copy number gain of the FASN gene. Recent study in prostate tumour tissues, showed the FASN gene copy number gain (Shah et al., 2006). These are the mechanisms that are reported to be regulating the over-expression of FASN in tumour cells.

The anti-proliferative effects of the FASN inhibitors in Y79 RB cells were evaluated in the previous chapter. This chapter evaluates the safety of the FASN inhibitors in non-neoplastic cells.

7.2. Objectives

1. To study the cytotoxicity (if any) of fatty acid synthase inhibitors [cerulenin, triclosan and orlistat (Xenical™)] in non-neoplastic cells [3T3 (mouse embryonic fibroblast) and MIO-M1 (Muller-glial)] by cell viability assays and cell morphology assessment.
2. To compare the safety and therapeutic efficacy of each FASN inhibitor by calculating their therapeutic index in human RB Y79 cells with respect to the two non-neoplastic cells.

7.3. Materials and methods

7.3.1. Cell viability (MTT) Assay

MIO-M1 and 3T3 cells were seeded at a cell density of 5×10^3 cells/well in 96-well plates with 100 µl of culture media and incubated at 37^0 C overnight. The cells were then exposed to varying concentrations of cerulenin, triclosan and orlistat (Xenical™) in fresh medium and then incubated for 48 h. At the end of the incubation, the cells were treated with 10µl of MTT (3-(4, 5-dimethylthiazol-2-yl)-2, 5-diphenyltetrazolium bromide; 5 mg/ml) with fresh medium and incubated for 4 h at 37^0C. The formazan crystals formed was dissolved in 100µl of DMSO. Colour developed was read at 570 nm. Cell viability (or cell survival) was calculated as: (Test OD/Control OD) x 100. The 50% inhibitory concentration (IC_{50}) of the three drugs [cerulenin, triclosan & orlistat (Xenical™)] was calculated using polynomial regression analysis using Microsoft Excel.

7.3.2. Therapeutic index

The IC_{50} of cerulenin, triclosan, and orlistat (Xenical™) was determined independently in 3T3, and MIO-M1 cells. The therapeutic index for each drug was then calculated as follows (Cha et al., 2005b):

Therapeutic Index = (IC_{50} non-neoplastic cell line) / (IC_{50} neoplastic cell line)

where, non-neoplastic cell lines are: 3T3 and MIO-M1, and neoplastic RB cell line is: Y79.

7.3.3. Assessment of cell morphology by phase contrast microscopy

Y79 RB cells, MIO-M1 and 3T3 cells treated with the three FASN inhibitors were assessed for morphological changes using a phase contrast microscope (Nikon, Tokyo, Japan). The IC_{50} dosage of FASN inhibitors corresponding to Y79 RB cells was

administered to the non-neoplastic MIO-M1 and 3T3 cells to assess any toxic reactions in normal cell morphology.

7.3.4. Statistical analysis

Comparisons between specific groups as mentioned in the results section were done using student's *t*-test. Differences were considered significant at $P < 0.05$. The results are expressed as mean ± S.D. of values obtained from a minimum of three independent experiments, each performed in triplicate. In all the experiments, the untreated cells with the culture medium served as the control.

7.4. RESULTS

7.4.1. Assessment of safety of anti-FASN drugs in non-neoplastic cells

Most anti-cancer agents exert cytotoxic side effects on the normal cells. To ascertain the safety of the FASN inhibitors (cerulenin, triclosan and orlistat (Xenical™) in normal cells, we tested their anti-neoplastic IC_{50} dosage in two non-neoplastic cell lines (MIO-M1 and 3T3). Mean cell viability greater than 75% was considered non-toxic to the non-neoplastic cells. We observed that, the respective (IC_{50}) dosage of cerulenin (7.0 μg/ml), triclosan (20 μg/ml), and orlistat (Xenical™) (250 μg/ml) that induced 50% inhibition of viability of neoplastic Y79 RB cells, were not toxic to both the non-neoplastic cells, 3T3 and MIO-M1 when incubated for 48 h (Figure 7.2).

7.4.2. Determination of IC_{50} dosage for cerulenin, triclosan and orlistat (Xenical™) in non-neoplastic (3T3 and MIO-M1) cells

The anti-neoplastic IC_{50} dosage (from Y79 RB cells) for the three FASN inhibitors showed no toxicity in both non-neoplastic cells as mentioned in the previous sub-section. Further the non-neoplastic cells were treated with different dosages of each of the three FASN inhibitors and the IC_{50} for both the non-neoplastic cells MIO-M1 (Figure 7.3 a-c) and 3T3 (Figure 7.4 a-c) were determined.

Figure 7.2 Assessment of safety of anti-FASN drugs in non-neoplastic cells

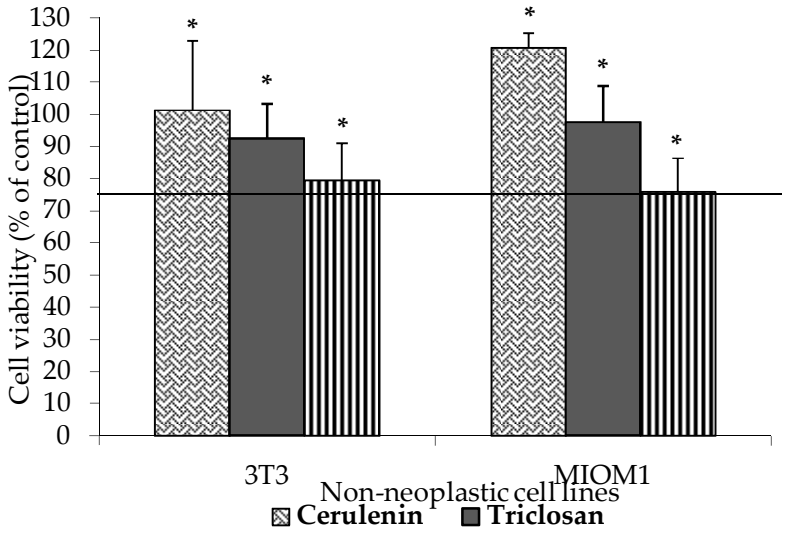

[*]**Figure 7.2 Assessment of safety of anti-FASN drugs in non-neoplastic cells:** The safety of the FASN inhibitors in normal cells, were tested with their anti-neoplastic IC_{50} dosage [cerulenin (7.0 μg/ml), triclosan (20 μg/ml) and orlistat (Xenical™) (250 μg/ml)] in two non-neoplastic cell lines (MIO M1 and 3T3). MTT assay revealed that all the three FASN inhibitors tested here were not toxic to non-neoplastic cells. The horizontal line at 75% cell viability indicates the cut-off for minimum mean cell viability that would denote safety of the drugs on normal cells. The drugs were significantly toxic to cultured RB cells. * indicates statistically significant difference with respect to Y79 cells ($P<0.05$). Error bars indicate S.D. from triplicate values each from three independent experiments.

7.4.3. Therapeutic index (TI)

Any compound that is administered to the host, as an anti-neoplastic agent should not be equally toxic to both neoplastic and non-neoplastic cells. Therapeutic index (TI) is defined here as the ratio of the drug-concentration which inhibits 50% viability of the normal cells to the concentration which inhibits 50% viability of tumour cells (Cha et al., 2005b). The therapeutic indices of the three FASN inhibitors differed between each other. In both the normal cell types (MIO-M1 and 3T3) tested

[*] *The data presented in the figure 7.2 is published in: Basic & Clinical Pharmacology & Toxicology, 2012, 110, 494-503. Please see "List of publications" on Page XXIII*

here, the TI values were in the order: Cerulenin > Triclosan > Orlistat (Xenical™) (Figure 7.5).

Figure 7.3 Determination of IC_{50} of FASN inhibitors (cerulenin (7.3a), triclosan (7.3b) and orlistat (Xenical™) (7.3c)) in MIO-M1 cells.

Figure 7.3a

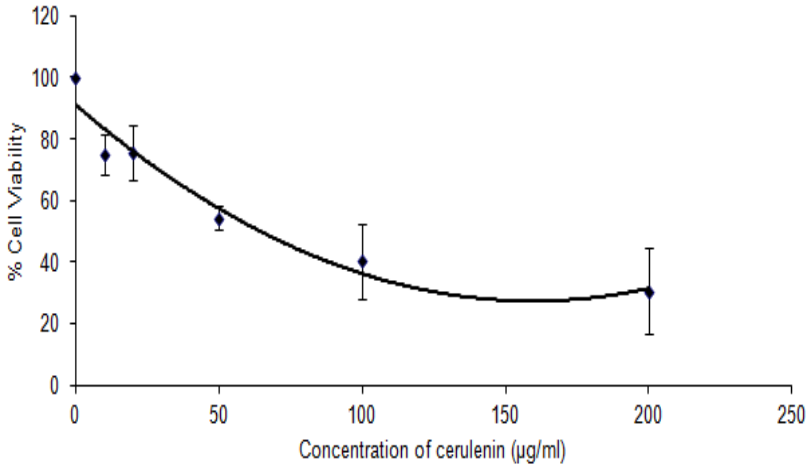

Figure 7.3b

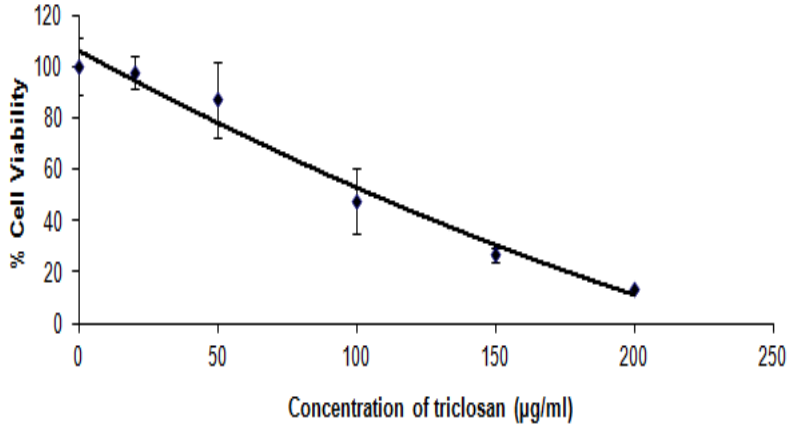

Figure 7.3c

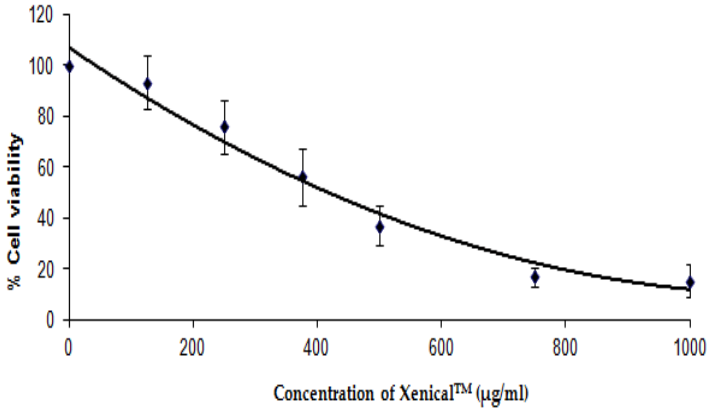

Figure 7.3: Determination of IC_{50} of FASN inhibitors (cerulenin (a), triclosan (b), & orlistat (Xenical™) (c) in MIO-M1 cells: The three inhibitors were tested for their cytotoxic effects in MIO-M1 cells at 48 h. IC_{50} was determined for each drug by polynomial regression analysis using Microsoft Excel. Values are represented as mean ± S.D. from three independent experiments.

Figure 7.4 Determination of IC_{50} of FASN inhibitors (cerulenin (4a), triclosan (4b) and orlistat (Xenical™) (4c)) in 3T3 cells.

Figure 7.4a

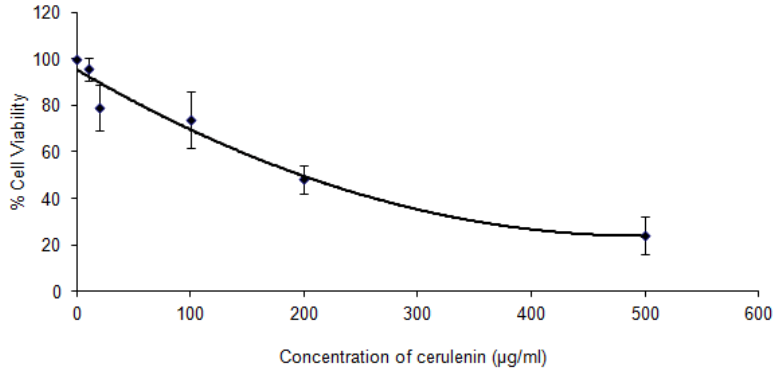

Figure 7.4b

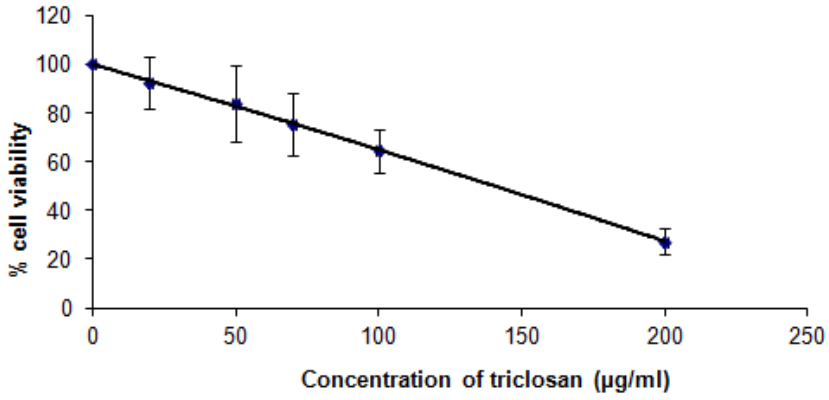

Figure 7.4c

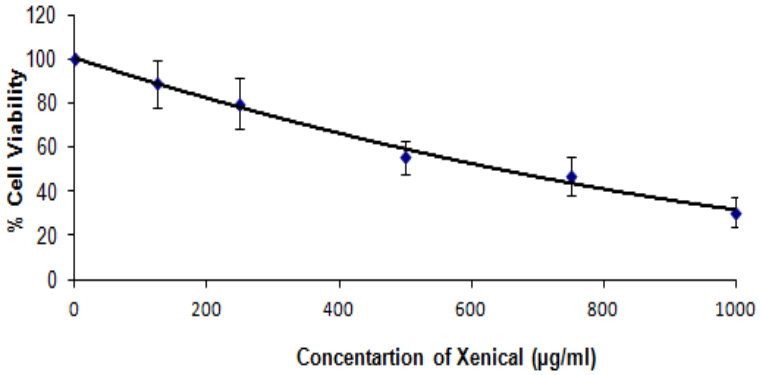

Figure 7.4: Determination of IC_{50} of (cerulenin (a), triclosan (b) and orlistat (Xenical™) (c)) in 3T3 cells: The three inhibitors were tested for their cytotoxic effects in 3T3 cells at 48 h. IC_{50} were determined for each drug by polynomial regression analysis using Microsoft Excel. Values are represented as mean ± S.D. from three independent experiments.

Figure 7.5 Comparison of Therapeutic Indices of FASN inhibitors

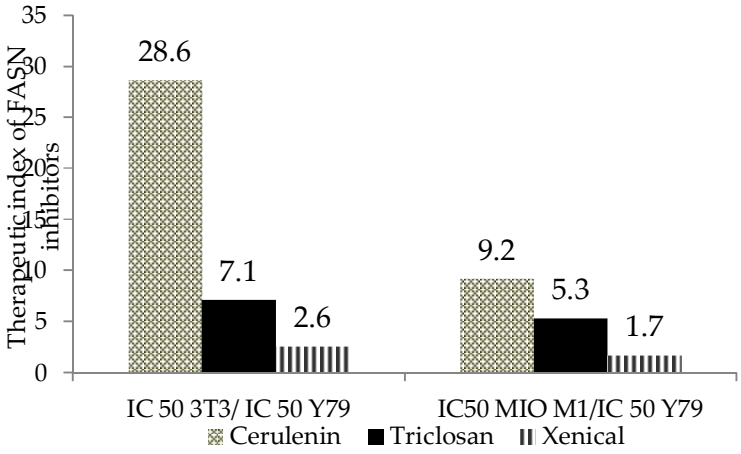

[†]**Figure 7.5 Comparison of Therapeutic Indices of FASN inhibitors:** Therapeutic index for each FASN inhibitor in retinoblastoma Y79 cells was calculated as mentioned in section 7.3.2 with respect to two non-neoplastic cells (3T3 & MIO-M1). Bars represent the therapeutic index of the three drugs. The absolute values of therapeutic indices are given above each bar.

The therapeutic index for cerulenin was higher (28.6 and 9.2 with respect to the normal cells 3T3 and MIO-M1 respectively) in comparison with the other two FASN inhibitors. Triclosan showed TI of 7.1 and 5.3 relative to 3T3 and MIO-M1 cells respectively, while Orlistat (Xenical™) showed the lowest TI among the three FASN inhibitors tested here, with values of 2.6 and 1.7 relative to 3T3 and MIO-M1 cells respectively (Figure 7.5).

7.4.4. Effect of FASN inhibitors on cell morphology studied in 3T3 and MIO-M1 cells

The morphology of the two normal cell types studied here [MIO-M1 (Figure 7.6 a-d) and 3T3 (Figure 7.6 e-h)] when treated with the anti-neoplastic IC_{50} dosages of FASN inhibitors, showed no major change in their cell morphology.

[†] *The data presented in figure 7.5 is published in: Basic & Clinical Pharmacology & Toxicology, 2012, 110, 494-503. Please see "List of publications" on Page XXIII*

Figure 7.6 Morphology of non-neoplastic cells treated with FASN inhibitors for 48 h

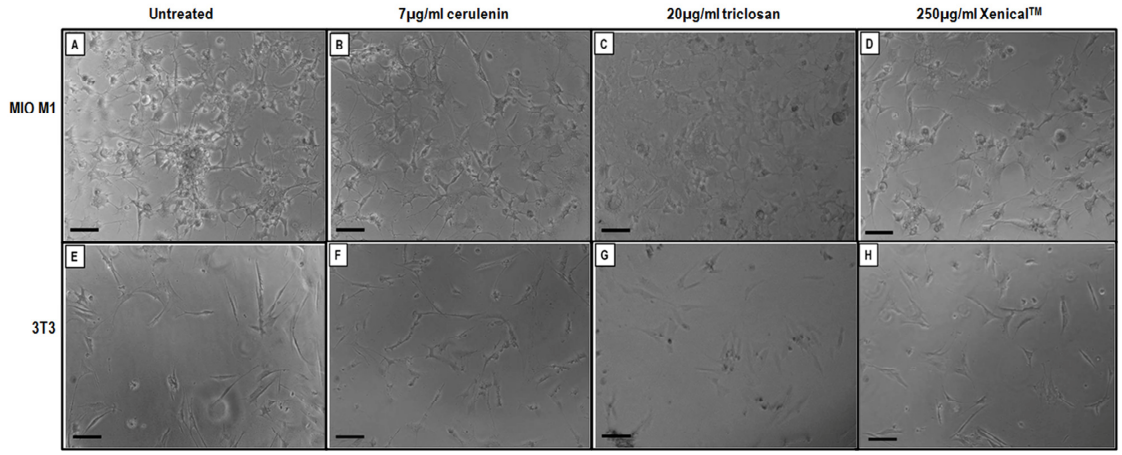

‡**Figure 7.6 Morphology of non-neoplastic cells treated with FASN inhibitors for 48 h:** MIO-M1 (panels: B, C, D) & 3T3 (panels: F, G, H) cells were treated with the anti-neoplastic IC_{50} (in Y79) concentrations of cerulenin, triclosan and orlistat (Xenical™) respectively for 48 h. The drugs showed no observable changes in cell morphology at this concentration on both the non-neoplastic cell types**.** (A) & (E) are untreated MIO-M1 and 3T3 cells respectively Magnification – 10X (Scale bar: 100µm).

7.5. Chapter Summary

- FASN inhibitors [cerulenin, triclosan and Xenical™ (orlistat)] were tested for their safety in two non-neoplastic cells (MIO-M1 and 3T3) and were found to be non-toxic to these cells at their anti-neoplastic IC_{50} dosage.

- The relative efficacy of the three inhibitors were analysed by computing the therapeutic index of each drug and the order of efficacy was cerulenin > triclosan > orlistat (Xenical™)**.**

‡ *The data presented in figure 7.6 is published in: Basic & Clinical Pharmacology & Toxicology, 2012, 110, 494-503. Please see "List of publications" on Page XXIII*

CHAPTER 8: BIOCHEMICAL EVALUATION OF FASN INHIBITORS IN CULTURED RETINOBLASTOMA CANCER CELLS

8.1. Introduction

Dose- and time- dependent cytotoxicity of fatty acid synthase (FASN) inhibitors and their safety aspects on non-neoplastic cells were determined (as discussed in Chapters 6 and 7). In the present chapter, effect of FASN inhibitors on FASN enzyme activity, mRNA and protein expression will be evaluated. The biochemical and molecular mechanisms during FASN inhibition have been studied extensively using various cancer cells and xenograft models. The following section will present key aspects of inhibition of FASN enzyme activity, FASN mRNA and protein expression, in cancer cells and their implications in inducing apoptosis.

8.1.1. Inhibition of FASN enzyme activity, mRNA and protein expression

Triclosan, a slow binding inhibitor inhibited both human and goose FASN enzyme activity, and at similar concentrations, triclosan caused cell death in human breast cancer cells (MCF-7 & SKBr3) (Liu et al., 2002). Magnitude of FASN enzyme activity inhibition was dependent on FASN enzyme content. High FASN expressing SKBr3 and MCF-7 cells showed a 90% reduction of FASN enzyme activity with 10μg/ml of C75, but MDA-MB-231 showed a less marked decrease with about 60% reduction with the same concentration of C75 which has low FASN expression (Menendez et al., 2005a). FASN activity inhibition was not accompanied by changes in FASN protein content. C75 and EGCG treated SKBR3 breast cancer cells showed no difference in the FASN immuno-reactive band intensity (Puig et al., 2008).

Cerulenin was reported to suppress the FASN protein expression in two murine colorectal cancer cells (colon 26 and CMT 93). This decreasing effect was accompanied by deactivation of Akt and activation of caspase 3 thus leading to

apoptotic cell death (Murata et al., 2010). Cerulenin treatment in IOMM-Lee (human meningioma) cells decreased the FASN protein expression along with the modulation of Akt phosphorylation, suggesting FASN to be novel therapeutic target in malignant meningioma (Haase et al., 2010).

8.1.2. Induction of apoptosis by FASN enzyme activity inhibition

During FASN inhibition, accumulation of un-used substrate malonyl CoA, was observed and which was cytotoxic to breast cancer cells and in xenograft models (Pizer et al., 2000). In addition to this mechanism, malonyl CoA inhibits fatty acid oxidation by inhibiting carnitine palmitoyl transferase -1 (CPT-1), which was cytotoxic to cancer cells (Thupari et al., 2001), which was also accompanied by increased levels of ceramide causing cancer cell death (Bandyopadhyay et al., 2006). FASN gene silencing in breast cancer cells, revealed significant up regulation of pro-apoptotic genes: BNIP3, TRAIL and DAPK2[€].

8.1.3. Anti-cancer agents inducing apoptosis via FASN pathway (without inhibiting FASN enzyme activity)

Some anti-cancer agents have been reported to induce apoptosis through FASN mediated pathways, where the enzyme activity of FASN is not primarily targeted for inhibition. One among this is the effect of Hoechst 33342**,** a compound that induces apoptosis through many intracellular events including mitochondrial dysfunction, disruption of DNA cleavable complexes involved in DNA replication processes, and induction of apoptosis by increasing the intracellular concentrations of E2F-1 and nitric oxide. The inhibitory effect of Hoechst 33342 on fatty acid synthesis is attributed to the degradation of FASN protein content via caspase activation, rather than inhibition of FASN mRNA and enzyme activity (Zhang et al., 2006).

[€] *BNIP3 - adenovirus E1B 19-kDa-interacting protein; mitochondrial associated cell death protein; TRAIL tumour necrosis factor–related apoptosis-inducing ligand; DAPK2- death-associated protein kinase 2*

Malonyl CoA decarboxylase (MCD) regulates the malonyl CoA levels by decarboxylating it back to acetyl CoA. Inhibition of MCD increases the malonyl CoA levels and is cytotoxic to cancer cells. This potentiates the cytotoxicity induced by FASN inhibition. Pharmacological inhibition of both MCD and FASN significantly increased the malonyl CoA levels by 162%, compared to the inhibition of either FASN or MCD alone. Increase in malonyl CoA levels as a result of this effect, however increased the fatty acid synthesis by 20%, and no reduction in fatty acid oxidation was observed.

Cancer cells are thus reported to exhibit different regulatory mechanisms between fatty acid synthesis and oxidation. Normal cells are under tight regulation by hormonal/nutritional signals, where during increased fatty acid synthesis, the fatty acid oxidation is inhibited to avoid a futile cycle. The increased malonyl CoA levels can participate in the cytotoxic effects mediated through inhibition of both FASN and MCD. There are several possible mechanisms underlying this phenomenon: 1) malonyl CoA reduces the fatty acid oxidation by inhibiting CPT-1, 2) Increase in malonyl CoA levels increases fatty acid synthesis and depletes the ATP and NADPH levels, 3) Inhibition of succinyl CoA dehydrogenase (electron transport chain – complex II) and thereby causes apoptosis (Zhou et al., 2009).

In addition to the various mechanisms involved in FASN inhibition mediated apoptosis, the FASN and the associated lipid synthesis and their fate in cancer cells and normal cells needs to be understood.

8.1.4. Lipid metabolism and cancer

The important genes involved in lipid metabolism that are targeted for cancer therapy are: fatty acid synthase (FASN), acetyl CoA carboxylase alpha (ACCα), ATP citrate lyase (ACLY), and Spot14 protein. The importance of these molecules has been explained in detail in section 1.4. The role of FASN in tumour progression and its inhibition by various strategies have led to development of various novel anti-

cancer agents. In this context it is important to know the difference between lipids and its components in normal and cancer cells, and the fate of fatty acids synthesized by tumour associated FASN.

8.1.5. Synthesis of lipids

Liver is the primary site of lipid metabolism and it has several functions in metabolising lipids. They are: 1) synthesis of phospholipids and lipoproteins, 2) saturation and desaturation of fatty acids, 3) synthesis, esterification, and degradation of cholesterol (cholesterol is oxidised to bile acids, secreted into bile and excreted through the intestines, 4) ketogenesis, 5) biosynthesis of fatty acids (both cytoplasmic and mitochondrial), 6) synthesis of triacyl glycerols from fatty acids (Postic et al., 2004).

8.1.6. Differences in lipids in normal cells and cancer cells

Meng et al., 2004 had reported the different composition of fatty acids in cultured normal and cancer cells. Different cell lines showed varying abilities to incorporate the linoleic acid and arachidonic acid. The cancer cells showed more longer chain fatty acids (saturated) which were eventually formed from the elevated palmitic acid synthesis by FASN in these cells. But the cancer cells produced more mono- and poly- unsaturated fatty acids when compared to long chain saturated fatty acids which reduced the fluidity of the membrane, and hence decreased material exchange. The stearic acid (SA) to oleic acid (OA) ratio is considered an important solid tumour marker. This ratio was above 0.7 for all normal cells and the malignant cancer cell lines had a SA/OA ratio lesser than 0.7 (Meng et al., 2004). Previous studies by Gülcan et al., 1993 had reported the composition of phospholipids, fatty acids that are present in the retina and in the RPE, choroid, and macular regions of the normal eye analysed by HPLC technique. The major fatty acids that are predominant in these tissues were palmitic acid (16:0), stearic acid (18:0), and oleic

acid (18:1). The different tissues isolated from the same region had different fatty acid and phospholipid composition. In retina, the phospholipids were the predominant lipids. The Bruch's membrane/choroid and the RPE contained almost three times higher amounts of neutral lipids compared to the retina (Gülcan et al., 1993).

8.1.7. Fate of *de novo* synthesized fatty acids in normal and cancer cells

The fate of fatty acids synthesized by FASN differs between normal cells and cancer cells. During surplus energetic states the palmitate synthesized by FASN esterifies to storage lipid as triglycerides. But FASN is inactivated during starvation thereby activating fatty acid oxidation. In contrast, fatty acids synthesized in cancer cells are esterified predominantly to phospholipids, not triglycerides (Kuhajda, 2006). Thus the fate of the fatty acids synthesized by FASN in cancer cells leads to phospholipid synthesis, formation of cell membrane, and formation of lipid rafts.

FASN over-expression and the deregulation of membrane composition has been correlated. FASN gene silencing decreased the ^{14}C incorporation into the phospholipids by 40% - 60%. This was accompanied by marked reduction in triglycerides, but the free cholesterol levels did not decrease. The predominant amounts of phospholipids synthesized during FASN inhibition are mainly saturated and mono-unsaturated type. Sucrose density gradient centrifugation separates the low density detergent resistant micro-domains from the high density detergent soluble fractions. The membrane micro-domains perform several functions such as: signal transduction, intracellular trafficking, cell polarization, migration, and formation of membrane protrusions. On FASN inhibition, the amount of lipid fractions in raft decreased considerably when compared to the non-raft lipid fractions. These studies indicated that FASN mediated phospholipid synthesis is mainly involved in the formation of the lipid raft fractions (Swinnen et al., 2003).

8.1.8. Lipid rafts, its important components, and role in cell signaling

Lipid rafts are defined as micro-domains within the plasma membrane-lipid bilayer which are resistant to cold detergent treatment. They have a distinct lipid composition than the rest of the membrane, with trans-membrane or GPI-anchored proteins and lipids (cholesterol and phospholipids). There are two types of lipid rafts: planar lipid rafts (non-caveolae) and Caveolae. Planar lipid rafts are non-invaginated micro-domains, and caveolae are tube-like invaginations containing specific scaffolding proteins called "caveolins". Caveolin-1 is an important protein that play major role in caveolae mediated endocytosis and transport. The lipid rafts are primarily involved in signal transduction, intra-cellular trafficking, cell polarity and migration. Caveolin-1 regulates the signal transduction pathways such as the RTK-mediated pathways, adenylate cyclase isoforms, G proteins, endothelial nitric oxide synthase and a series of tyrosine kinases by interacting with the caveolin scaffolding domains (CSD) (Staubach & Hanisch, 2011; Swinnen et al, 2003). Caveolin-1 is reported to be responsible for the up-regulation of FASN during prostate cancer progression. Caveolin negative tumours did not show up-regulation of FASN and did not metastasize. These studies proved that caveolin acts upstream of FASN during tumour progression (Di Vizio et al., 2007).

8.1.9. Differential lipid contents in two major RB cell lines

Lipid bilayer in the mammalian cell membrane is primarily composed of phospholipids and cholesterol. Proteins involved in important functions like receptors, transporters and enzymes are embedded in this bilayer (Spector & Yorek, 1985). Phosphatidyl choline (PC) represents nearly 48% - 50% of the membrane phospholipids in mammalian cells (Tercé et al., 1994; Spector & Yorek, 1985). Increased phospholipids are synthesized during the induction of G0 to G1 transition and during S phase (Tercé et al., 1994). Thus for normal progression through G1 and S phases of the cell cycle, PC serves as an important requirement.

Y79 and Weri Rb-1 cells (retinoblastoma cell line derived from RB tumour of a 1 year old Caucasian female) were characterised for their lipid content and their lipid content differed. Y79 cells had higher phospholipid and Weri Rb-1 cells contained more triglycerides. Although these two cell lines have been derived from the same retinal tumour type, their origin is from two functionally different neurons. Their metabolic properties and biochemical functions diverged during cell culture propagation. Y79 possessed more capacity to elongate and desaturate the poly unsaturated fatty acids, which property presents Y79 as a better experimental model for studying the retinal fatty acid metabolism (Yorek et al., 1985).

8.1.10. FASN and oxidative stress

Recent studies with prostate cancer tumour tissues showed increased FASN levels along with an increased saturation of phospholipids. The nature and the degree of unsaturation of fatty acids determined their sensitivity to lipid peroxidation process. Tumour associated FASN contributes more saturated and monounsaturated fatty acids which are less sensitive to lipid peroxidation, thereby it confers protection to tumour cells from oxidative stress induced apoptotic cell death. During FASN and ACC inhibition with siRNA and soraphen A respectively, the poly-unsaturation level increased and mono unsaturation decreased, which led to lipid peroxidation and cell death due to oxidative stress induced apoptosis. FASN inhibition also altered the membrane dynamic properties due to the shift in saturation levels. FASN inhibitors are suggested to be anti-neoplastic agents and chemosensitizers (Rysman et al., 2010). In addition, several other studies reported the induction of ROS mediated apoptotic cell death during pharmacological and siRNA mediated FASN inhibition in prostate, melanoma, and breast cancer cell lines (Migita et al., 2009; Chajès et al., 2006; Zecchin et al., 2011).

8.1.11. Molecular pathways regulated during FASN inhibition analysed by Microarray technique

The cDNA microarray analysis of cerulenin-treated breast cancer cells had resulted in up-regulation of several genes such as TGF-β2, genes of insulin signaling pathway, caspase 7 in apoptosis and down regulation of GRB7 (HER2 pathway), FGF5, inhibin and IL-11 (Vazquez-martin et al., 2004). Dutasteride, is an inhibitor of 5-alpha reductase caused death of prostate cancer cells and reduced the FASN mRNA and protein expression levels along with significant inhibition of FASN enzyme activity. The genes that were affected are ♠SREBP1a, SCAP, INSIG 1 & 2 and SREBP1c (Schmidt et al., 2007).

Differentially regulated genes during silencing of FASN in MDA MB 435 breast cancer cells were classified into several pathways such as cell survival/proliferation, DNA replication/transcription, and protein degradation by ubiquitination and apoptosis pathways. ♠SGPL1 (involved in sphingosine 1-phosphate metabolism) was up- regulated, which is reported to increase the amounts of pro-apoptotic molecule ceramide. FASN knockdown also decreased the tumour cell energy metabolism by affecting the genes involved in glycolysis, lipid metabolism, TCA cycle and oxidative phosphorylation pathways. Apoptosis of breast cancer cells on FASN inhibition involved up-regulation of cell cycle arrest pathways and death receptor mediated apoptotic pathways (Knowles & Smith, 2007).

8.2. Objectives

1. To evaluate the effect of cerulenin, triclosan and orlistat (Xenical™) on FASN molecular expression and enzyme activity in human RB Y79 cells

---

♠ *SREBP1a – sterol regulatory element binding protein -1; SCAP – SREBP cleavage activating protein; INSIG 1 & 2 – Insulin induced gene 1 & 2; SGPL1-Sphingosine-1-phosphate lyase 1*

2. To study the substrate (malonyl CoA) accumulation and product (palmitate) depletion in FASN inhibitor treated Y79 RB cells.

3. To investigate the nature of cell damage (apoptosis) induced by FASN inhibitors in human RB Y79 cells

4. To measure lipid peroxidation levels in human RB Y79 cells treated with FASN inhibitors (cerulenin, triclosan and Xenical™) using MDA as the biochemical indicator.

5. To compare the levels of cellular lipids (phospholipid, cholesterol, and triglycerides) in FASN inhibitor treated Y79 cancer cells and 3T3 normal cells.

6. To analyse the differential gene expression during lipogenic inhibition in Y79 RB cells.

8.3. Methods

8.3.1. FASN protein content measured by FASN-ELISA

FASN protein content in human Y79 RB cells treated with FASN inhibitors were quantified by FASN specific ELISA. Briefly, 5 x 10^4 Y79 cells were treated for 48, 72 & 96 h with varying dosages (IC_{50} and higher dosage) of the three FASN inhibitors. After the intended incubation periods, the cells were collected and washed with ice cold PBS thrice and re-suspended in 200µl - 300µl of the HEPES buffer (10mM HEPES buffer, 1mM EDTA and 10mM DTT) and sonicated at 50-60 pixels for 1min (thrice). 100µl of samples and standards were added to the sample dilution tray. Each sample was diluted with 100µl of sample diluent/detection antibody and subjected to ELISA, as per the protocol in the section 3.7. After the colour development the plate was read at 450 nm using an ELISA reader (Biotek, USA). A standard curve was plotted and concentration of FASN protein content in the treated

and untreated samples was calculated from the calibration curve. The amount of FASN protein in the samples was expressed as ng/ml.

8.3.2. Evaluation of FASN mRNA expression in FASN inhibitor treated Y79 RB cells by Real time quantitative PCR (qRT-PCR)

FASN mRNA expression in human Y79 RB cells treated with FASN inhibitors were quantified by real time quantitative PCR method as per the protocol in the section 3.11.6. Briefly, 5 x 10^4 Y79 cells were treated for 48 h with the IC_{50} dosages of the three drugs. Total RNA was isolated by Trizol method and the RNA quality was checked with a 2% agarose gel. For all samples 2 μg of total RNA was used to synthesize first-strand cDNA using Sensiscript® RT kit and random primers. The quality of the first strand cDNA was assured by checking the presence of the housekeeping gene, glyceraldehyde-3 phosphate dehydrogenase (GAPDH). Quantification of FASN gene expression was performed in triplicate in a 20 μl volume reaction mixture containing [0.5 μg of cDNA, specific FASN primer (section 3.11.6.3) and SYBR green reagent] in 96-well plates on a real-time PCR system (Prism 7500; ABI Lab India Instruments, Gurgaon, India) as per the protocol in Chapter 3 (section 3.11.6).

8.3.3. Biochemical assay of free fatty acids

Approximately 1 x 10^7 Y79 RB cells were treated with the IC_{50} dosage of the three FASN inhibitors, and then the cells were washed thrice with PBS and pelleted. Then the pellet was processed as per each assay kit's instruction to measure the levels of free fatty acids as per the protocol in Materials and Methods Chapter (section 3.15).

8.3.4. Biochemical assay of FASN enzyme activity (NADPH oxidation method)

Approximately 5 x 10^4 Y79 RB cells were treated for 48, 72 and 96h with varying concentrations of the three drugs (IC_{50} and higher dosage). The cells were then processed for FASN enzyme activity determination as per the protocol given in section 3.5. Briefly, the collected cells were lysed with lysis buffer (pH 7.5) containing

1 mM EDTA, 50 mM Tris HCl, 150 mM NaCl, 100 μg/ml PMSF. 50 μl of each lysate was taken for the reaction. Background NADPH oxidation was measured initially without the lysate for 10 min. Then the FASN dependent NADPH oxidation was measured in a one ml of the reaction mixture containing 200 mM potassium phosphate buffer (pH 6.6), 1 mM DTT, 1 mM EDTA, 0.24 mM NADPH, 30 μM acetyl CoA, 50 μM malonyl CoA and 50 μl cell lysate. Enzyme activity of FASN was then calculated and expressed as nanomoles of NADPH oxidized per minute per ml. Enzyme activity in the inhibitor treated cells was compared with the untreated Y79 RB cells, and expressed as inhibition percentage.

8.3.5. HPLC analysis of malonyl CoA accumulation

Y79 RB cells (1 x 10^5 cells/well) were treated with IC_{50} and a higher dosage of FASN inhibitors for 48, 72 and 96 h. At the end of respective incubation periods the cells were collected and were pelleted and the pellet was treated with 0.5 ml of 10% trichloroacetic acid and centrifuged at maximum speed at 4°C for 5 min. The pellet mass was recorded, and the supernatant was washed six times with 0.5 ml of diethyl ether and reduced to dryness using vaccum centrifugation at 25°C. The samples were reconstituted with 50 μl of Buffer A and injected into the HPLC system. During experimental analysis of experimental groups, the standard malonyl CoA was simultaneously read, along with the test samples. The HPLC protocol is explained in detail in the Materials and Methods Chapter (section 3.13.1).

8.3.6. Analysis of cellular lipids in cancer (Y79) and normal (3T3) cells

Approximately 1 x 10^7 Y79 cells and 2.5 x 10^5 3T3 cells were treated with the IC_{50} dosage of the three FASN inhibitors, and then the cells were washed thrice with PBS and pelleted. Then the pellet was processed as per each assay kits instruction to measure the concentrations of triglyceride, total cholesterol and phosphatidylcholine respectively as per the protocol in Materials and Methods Chapter (section 3.15).

8.3.7. Assessment of cell damage by DNA fragmentation assay

Y79 RB cells were plated at 5 x 10^4 cells/well in 12-well plates and incubated overnight. Then the medium was removed and fresh medium with the respective drug concentrations (IC_{50} and higher dosage) of FASN inhibitors were added to the wells and incubated for 48 h. At the end of incubation, the cells were collected and pelleted and were subjected to DNA fragmentation analysis. The bands were visualized under UV light with a gel documentation system (BioDoc-It Imaging system, UVP, USA).

8.3.8. Assessment of cell viability and cell death by Annexin V Assay

About 5 x 10^4 Y79 RB cells were treated for 48 h with varying dosages (IC_{50} and higher dosage) of the three FASN inhibitors. After the intended incubation periods, the cells were collected and washed with ice cold PBS thrice. Then the cells were subjected to Annexin V staining with Annexin V apoptosis detection kit (BD Biosciences, CA, USA). The staining was performed as per the manufacturer's instructions and subjected to FACS analysis with FACSCalibur (BD Biosciences, CA, USA) using 'CELL QUEST PRO' software. Cytograms were plotted by taking into account the percentage of live, early and late apoptotic, and necrotic cells. Untreated cells were taken as control.

8.3.9. Analysis of lipid peroxidation marker malondialdehyde (MDA) in FASN inhibitor treated Y79 RB cells

About 1 x 10^5 Y79 RB cells were treated with IC_{50} and a higher dosage of FASN inhibitors for 48 h. At the end of 48 h the cells and the supernatant were collected and processed for lipid peroxidation marker analysis as per the protocol mentioned in section 3.16 in Chapter 3. Lipid peroxide level was determined by a colorimetric reaction using thiobarbituric acid (TBA), where malondialdehyde reacts with TBA to

generate a product that absorbs at 532 nm. Peroxidation levels were measured at basal (un-induced) conditions.

8.3.10. cDNA Microarray analysis

8.3.10.1. Cerulenin treatment of Y79 RB cells

Approximately 6 x 10^5 Y79 RB cells were exposed to the 7 μg/ml (IC_{50}) of cerulenin and incubated for 48 h. At the end of incubation the cells were removed and were processed for cDNA microarray analysis.

8.3.10.2. Preparation of cDNA

Total RNA was isolated from Y79 RB cells using Trizol reagent (Invitrogen) and purified using an RNeasy Mini Kit (Qiagen), combined with DNase treatment following the manufacturer's instructions as per the protocol given in the in Chapter 3 (section 3.11).

8.3.10.3. Hybridization, scanning and feature extraction

The labeled cDNA samples were hybridized onto a Whole Genome Human Array 4x44k as per the microarray analysis protocol mentioned in in Chapter 3 (section 3.18). The present oligonuclotide microarray data were submitted to NCBI-GEO-OMNI BUS (Accession number GSE16999).

8.3.10.4. Real-Time Quantitative RT-PCR (qRT-PCR)

To confirm the expression of up-regulated or down-regulated genes after cerulenin treatment, the expression of selected genes were validated using real-time quantitative reverse transcription polymerase chain reaction (qRT-PCR). All reactions were carried in 20 μl volume containing SYBR green PCR master mix (Eurogentec S.A, Belgium) as per the protocol given in Chapter 3 (section 3.11.6.2).

8.3.11. Statistical Analysis

Comparisons between specific groups as mentioned in the results section were done using student's *t*-test. Differences were considered significant at $P < 0.05$. The results are expressed as mean ± S.D. of values obtained from a minimum of three independent experiments, each performed in triplicate. In all the experiments, the untreated cells with the culture medium served as the control.

For microarray analysis, the genes were considered for expression analysis when they satisfied the following two criteria: (i) $P \leq 0.05$, and (ii) log ratio of at least 2.0 for up regulation, and log ratio of 0.5 for down regulation (keeping a median log ratio of 1) in both biologic replicates. Values are expressed as mean ± S.D. of duplicate values.

8.4. Results

8.4.1. MOLECULAR EXPRESSION OF FATTY ACID SYNTHASE (FASN) PROTEIN AND mRNA POST-CHEMICAL INHIBITION

8.4.1.1. Effect of FASN inhibitors on FASN protein content

The inhibition of FASN protein content in Y79 RB cells that were treated with cerulenin, triclosan, and Xenical™ for 48, 72 & 96 h were analysed by FASN-ELISA. The amount of FASN protein in the untreated and FASN inhibitor treated Y79 cells were calculated by interpolation from the calibration curve (Figure 8.1a). The three FASN inhibitors showed variable effects on FASN protein content in each of the treated cells compared to the untreated control samples. The extent of the protein content inhibition by cerulenin was significant at 72 h (1.6 and 2.8 ng/ml compared to untreated control with 19.1 ng/ml) and 96h (not detected in IC_{50} and 3.2 ng/ml against the untreated sample with 9.5 ng/ml). At 48 h cerulenin showed decrease in FASN protein expression although it was not statistically significant. After treatment with triclosan, the protein content significantly reduced at all three durations of

treatment. Orlistat (Xenical™) showed significant inhibition only at higher dosage of treatment at 48 h (4.8 ng/ml at 1000µg/ml of Xenical™ relative to 9.9 ng/ml in untreated control) and after 96 h (4.3 ng/ml at 70µg/ml of orlistat relative to 9.5 ng/ml of FASN protein in untreated control) (Figure 8.1 b-d). Thus, FASN enzyme inhibitors showed different effects on FASN protein expression, depending on the time of incubation, inhibitor-concentration, and the type of inhibitor.

Figure 8.1.Effect of FASN inhibitors on FASN protein content and mRNA expression in Y79 RB cells

Figure 8.1a FASN protein calibration curve

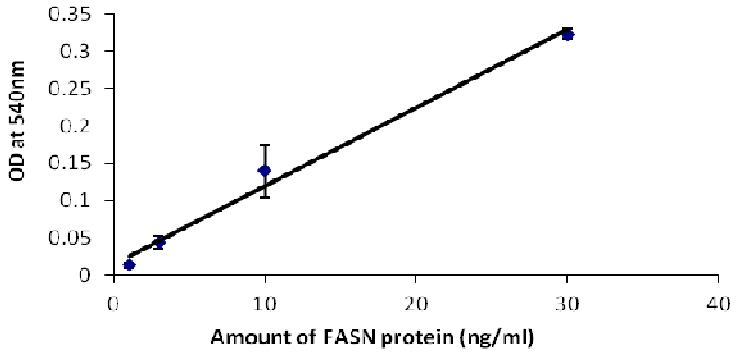

Figure 8.1a FASN protein calibration curve: Standard curve was plotted using varying concentrations of FASN protein standard provided in the assay kit. The samples were processed according to the manufacturer's instructions. The concentration of FASN protein is expressed as ng/ml. Values are expressed as mean ± S.D. of triplicate experiments.

Figure 8.1 b-d Inhibition of FASN protein content by FASN-ELISA

Figure 8.1b

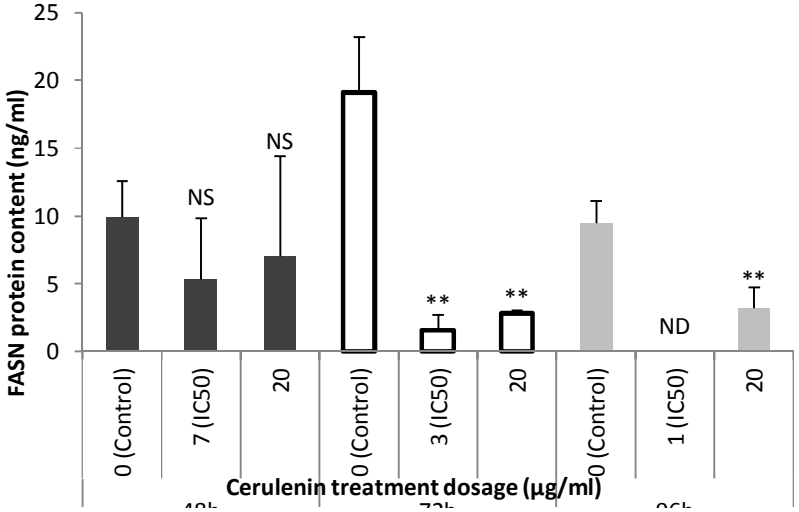

Figure 8.1c

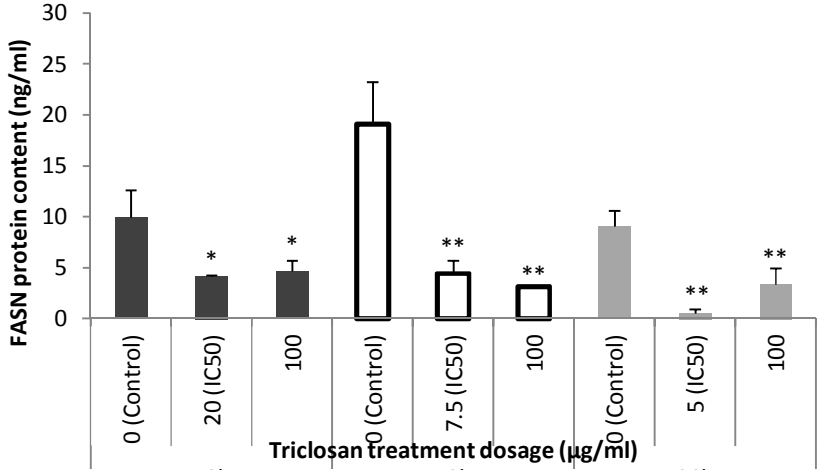

Figure 8.1d

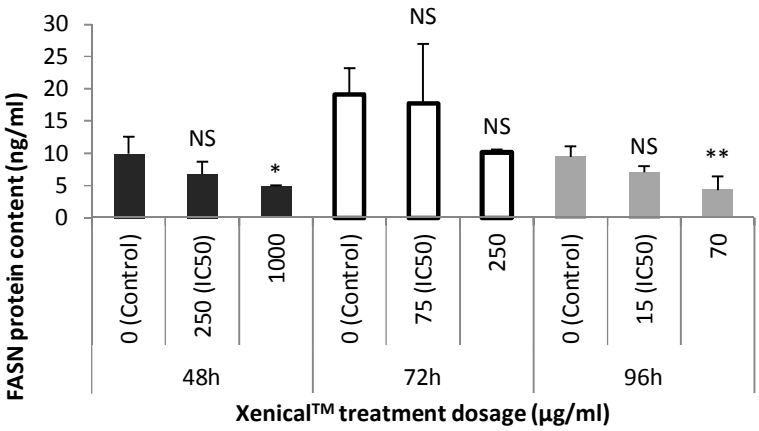

Figure 8.1b-c Inhibition of FASN protein content by FASN-ELISA: FASN protein content on Y79 RB cells treated with the IC_{50} and a higher toxic dosage of cerulenin **(b),** triclosan **(c),** and orlistat (Xenical™) **(d)** was measured by FASN-ELISA. The amount of FASN protein content in the treated and untreated control samples were calculated by interpolation from the calibration curve and expressed as ng/ml. Each bar represents mean ± S.D. obtained from triplicate values. Student's *t*-test was used to compare the FASN protein content in the treated cells relative to untreated control. P value is indicated as: * $P<0.05$, ** $P<0.01$, NS-Not statistically significant, ND-Not detected

8.4.1.2. FASN mRNA expression changes induced by FASN inhibitors

The inhibition of FASN mRNA expression in Y79 retinoblastoma cells that were treated with cerulenin, triclosan, and Xenical™ at their IC_{50} dosages for 48h were analysed by qRT-PCR. All three anti-FASN drugs showed decrease in FASN mRNA expression. Cerulenin decreased the FASN mRNA by 1.68 fold, triclosan showed 1.67 fold decrease and orlistat decreased the FASN mRNA expression by 2.6 folds (Figure 8.1e). FASN inhibitors acting as non-competitive inhibitors at the protein level also are effective to a lesser extent in modulating the FASN mRNA expression at the gene level.

Figure 8.1e Inhibition of FASN mRNA expression in cultured Y79 RB cells

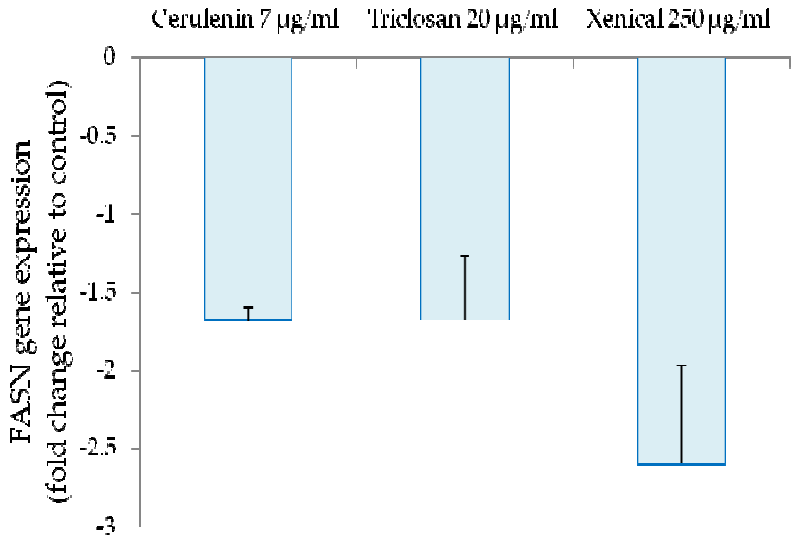

Figure 8.2 Inhibition of FASN mRNA expression in cultured Y79 RB cells: FASN mRNA expression on Y79 RB cells treated with the IC_{50} dosage of cerulenin, triclosan, and Xenical™ was measured by qRT-PCR. FASN mRNA expression in the treated samples are expressed as fold change of relative to untreated control, calculated from ΔΔCt method. Each bar represents mean ± S.D. obtained from triplicate values.

8.4.2. BIOCHEMICAL AND METABOLIC BASIS FOR CHEMICAL INHIBITION OF FATTY ACID SYNTHASE (FASN)

8.4.2.1. Profile of free fatty acid levels in the neoplastic Y79 (treated and untreated) RB cells

FASN inhibitor induced inhibition of the enzyme activity, also led to decrease in the cellular free fatty acid levels. The levels of free fatty acids in Y79 cells were quantified using fatty acid assay kit and the levels in the cell lysates were calculated from the standard curve (Figure 8.2a). Fatty acids being the breakdown product of triacylglycerols and they may be formed as intermediate during the redistribution as phospholipids, cholesterol esters. Therefore the fatty acid profile was recorded prior to the experimental incubation period of 48 h. Thus the fatty acid levels in the untreated control Y79 cells were determined at zero time and it was found to be 0.98 ± 0.15 nmol/ 10^5 cells.

Figure 8.2 Determination of free fatty acid levels in Y79 RB cells after 48 h treatment with FASN inhibitors

Figure 8.2a Palmitic acid calibration curve

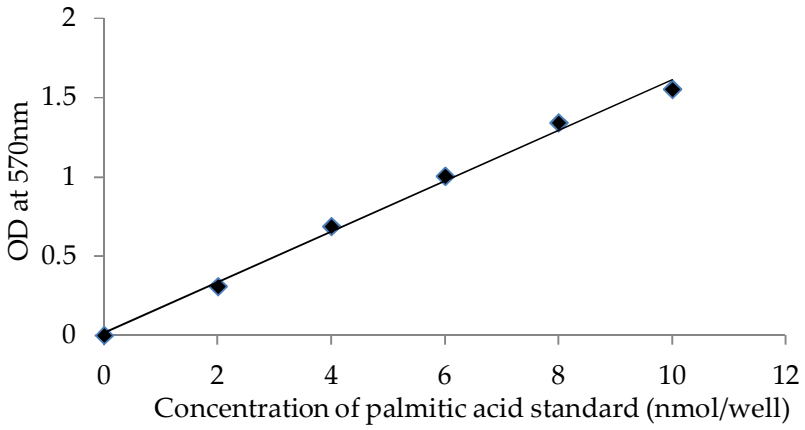

Figure 8.2a Palmitic acid standard curve Standard curve was plotted using varying concentrations of palmitic acid standard provided in the assay kit. The samples were processed according to the manufacturer's instructions. The concentration of free fatty acids is expressed as nmol/well.

The FASN inhibitor treated Y79 RB cells showed lower levels of free fatty acids compared to the zero hour control. The inhibition percentage of the treated groups was 63, 58, and 59% with cerulenin, triclosan and Xenical™ respectively (Figure 8.2b).

Figure 8.2b Decrease in free fatty acid levels in Y79 RB cells after 48 h treatment with FASN inhibitors

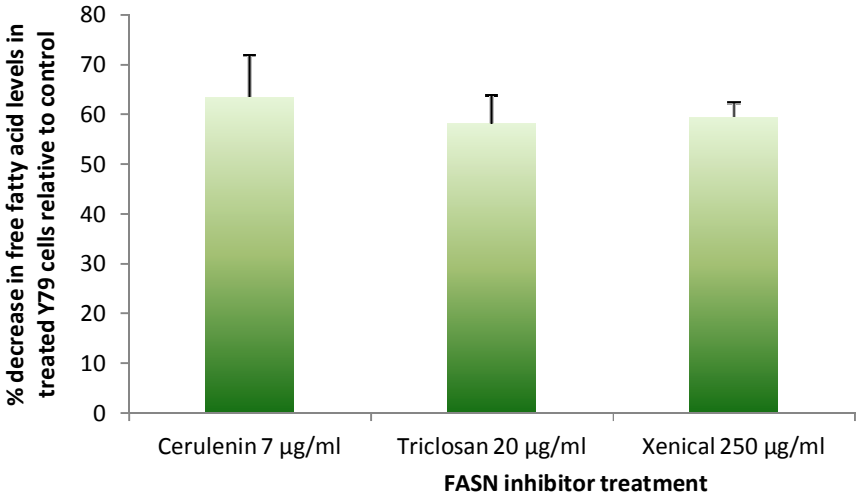

Figure 8.2b Inhibition of free fatty acid levels in Y79 cells at 48h: Free fatty acid levels were determined on Y79 RB cells treated with the IC_{50} FASN inhibitors by colorimetric method. The levels of free fatty acids were calculated using the palmitic acid standard curve and were depicted as nmol/10^5 cells. The inhibition of free fatty acid levels are depicted as percentage inhibition relative to untreated control Y79 cells at zero time. Error bars represent S.D values obtained from three independent experiments.

8.4.2.2. Effect of FASN inhibitors on FASN enzyme activity

The inhibition of FASN enzyme activity in Y79 RB cells that were treated with cerulenin, triclosan, and orlistat (Xenical™) for 48, 72 & 96 h were analysed by NADPH oxidation method. All the three anti-lipogenic agents inhibited the FASN enzyme activity in a dose-dependent manner when treated at their respective IC_{50} and higher concentrations, in comparison with the untreated control. The extent of

inhibition at 48 and 72 h by cerulenin exceeded that of triclosan, which in turn showed greater degree of inhibition compared to orlistat [Cerulenin (50 & 64%) > triclosan (37 & 45%) > orlistat (Xenical™) (29 & 23%)] at their 50% inhibitory concentrations respectively). At 96 h treatment Xenical™ showed increased inhibition of 59% followed by cerulenin with 53% and triclosan with 44% (Figure 8.3).

Figure 8.3 Inhibition of FASN enzyme activity by FASN inhibitors in Y79 RB cells

Figure 8.3a

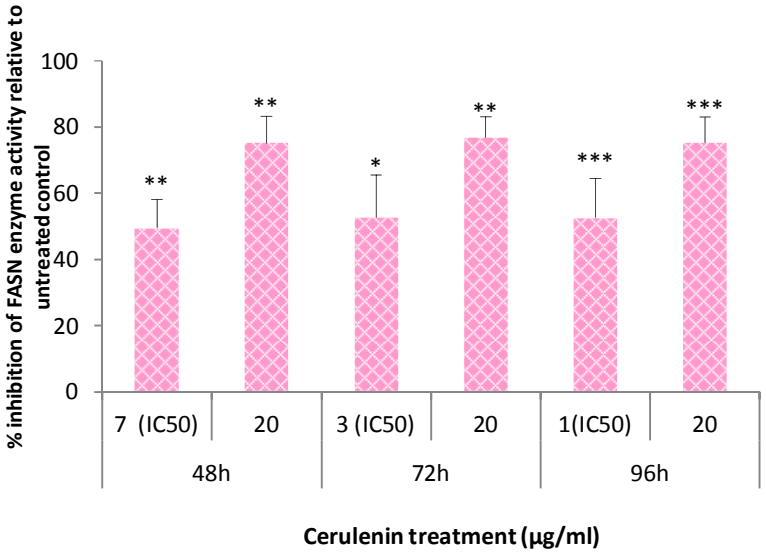

Figure 8.3b

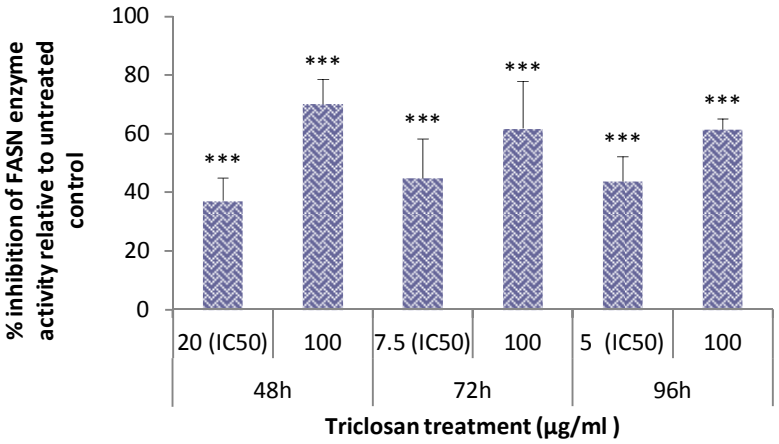

Figure 8.3c

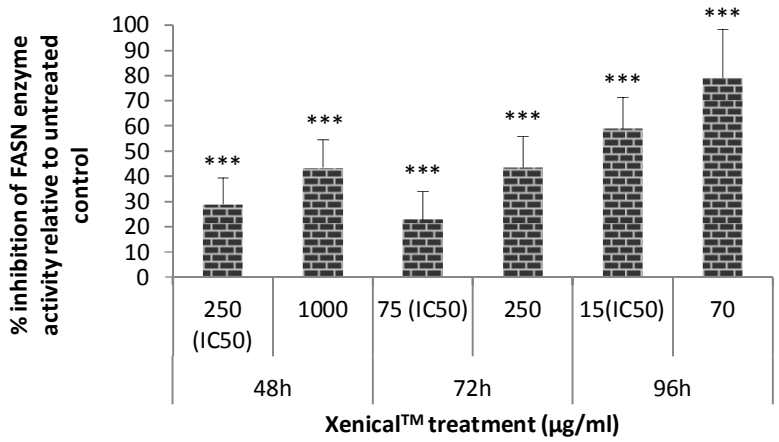

§**Figure 8.3 Inhibition of FASN enzyme activity by FASN inhibitors in Y79 RB cells** FASN enzyme activity on Y79 RB cells treated with the IC_{50} and a higher toxic dosage of cerulenin **(a),** triclosan **(b),** and Xenical™ **(c)** was measured by NADPH oxidation method at 340 nm. The enzyme activity was calculated as nano moles of NADPH oxidized per minute per ml reaction, obtained from three independent experiments performed in duplicates. FASN activity inhibition was then expressed as percentage decrease in enzyme activity in the inhibitor-treated cells relative to the untreated control RB cells. Error bars represent S.D values obtained from three independent experiments (each with duplicate values). Student's *t*-test was used to compare the percentage decrease in FASN enzyme activity in the treated cells when compared with the untreated control. P value is indicated as: * $P<0.05$, ** $P<0.01$, *** $P\leq0.001$.

§ *The data presented in Figure 8.3 is published in: J Ocul Biol Dis Inform. 2010; 3(4): 117-12. Please see List of publications on page XXIII*

8.4.2.3. Analysis of malonyl CoA (substrate) accumulation induced by FASN inhibitors in Y79 RB cells

FASN inhibitor treatment in Y79 RB cells led to accumulation of its substrate malonyl CoA. Malonyl CoA levels in the treated and untreated Y79 RB cells were calculated from the standard values run along with the test samples. Figure 8.4 c-e shows the differential accumulation of malonyl CoA when treated with different concentrations and three different periods of exposure to cerulenin, triclosan and orlistat.

Figure 8.4 Analysis of malonyl CoA (substrate) accumulation on FASN inhibitor treatment in Y79 RB cells by HPLC

Figure 8.4a Malonyl CoA calibration curve

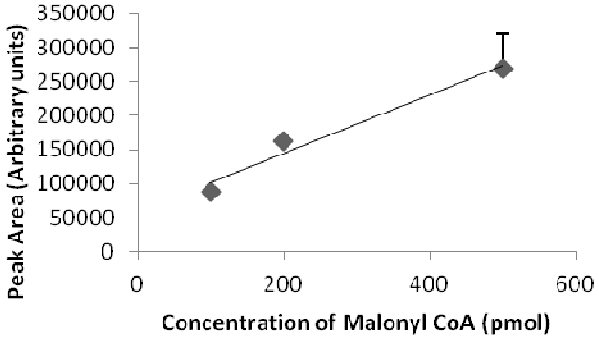

Figure 8.4b HPLC Chromatogram of Malonyl CoA standard

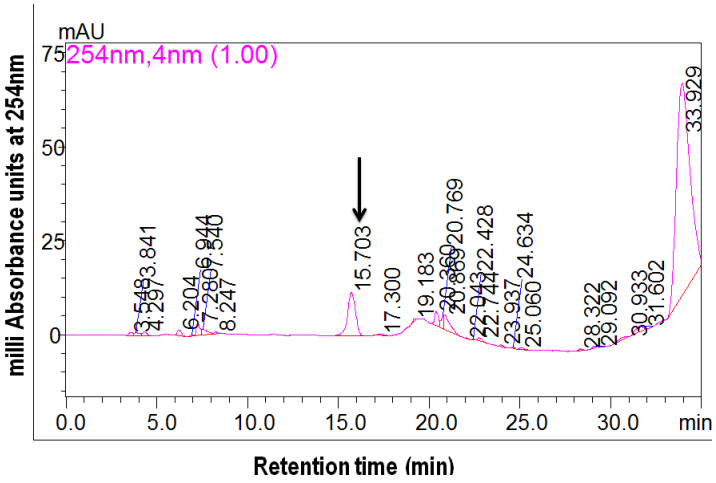

Figure 8.4 Malonyl CoA standard: a) Standard curve was plotted using increasing concentrations of malonyl CoA standard. The amount of malonyl CoA is expressed as pmol. Error bars represents mean ± S.D. obtained from triplicate values. **b)** Representative HPLC chromatogram of malonyl CoA standard run at 500 pmol concentration is presented. Malonyl CoA standard was eluted at 15.8 ± 0.8 min. Down arrow indicates malonyl CoA peak at 15.7 min retention time.

Figure 8.4c-e Analysis of malonyl CoA (substrate) accumulation on FASN inhibitor treatment in Y79 RB cells by HPLC

Figure 8.4c

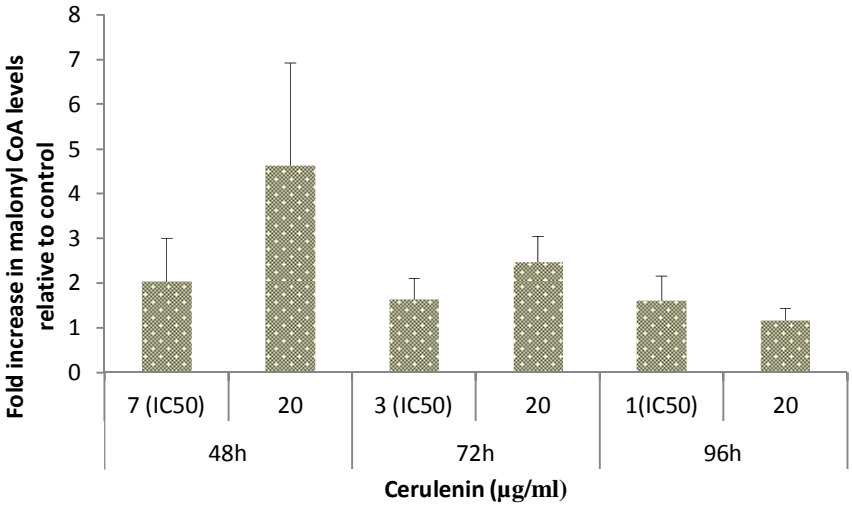

Figure 8.4d

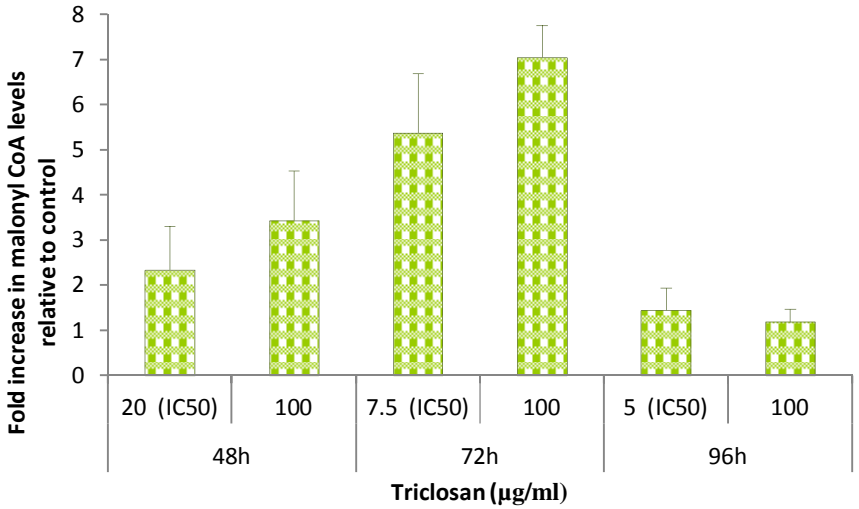

Figure 8.4e

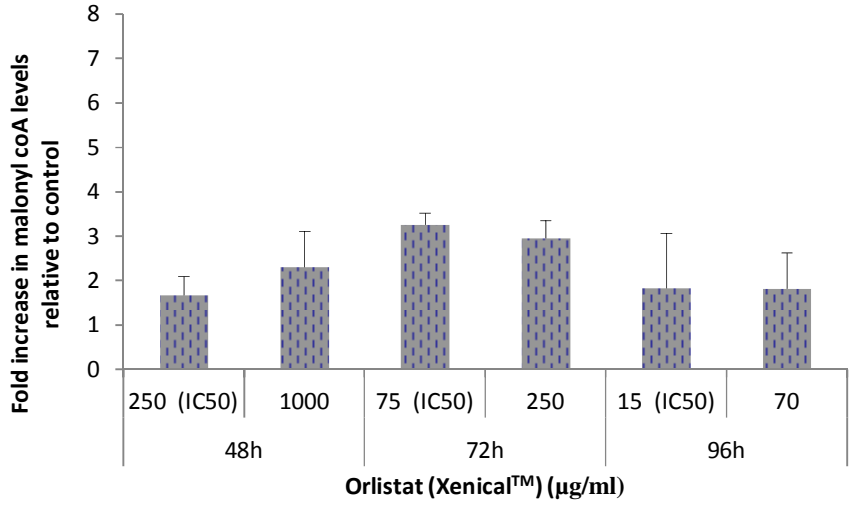

Figure 8.4c-e Analysis of Malonyl CoA (substrate) accumulation on FASN inhibitor treatment in Y79 RB cells by HPLC: RB cells were treated with the three FASN inhibitors cerulenin **(c),** triclosan **(d),** orlistat (Xenical™) **(e)** at 48h, 72h & 96h. Concentration of malonyl CoA was determined by HPLC. Values are expressed as fold increase in malonyl CoA in the treated samples relative to their respective untreated control RB Y79 cells. Each bar represents mean ± S.D. obtained from three independent experiments.

After 48 h of cerulenin treatment, malonyl CoA level increased between 2 folds to 4.6 folds at 7 and 20 µg/ml dosages. The representative chromatograms for the malonyl CoA levels in the experimental groups are presented in figure 8.4 f-h. Malonyl CoA in these treated groups was detected at 14.0 – 14.3 min retention time in a gradient elution with a flow rate of 0.4ml/min detected at 254 nm in a diode array detector.

Figure 8.4 HPLC chromatogram of Malonyl CoA on FASN inhibitor treated Y79 RB cells

Figure 8.4f & g

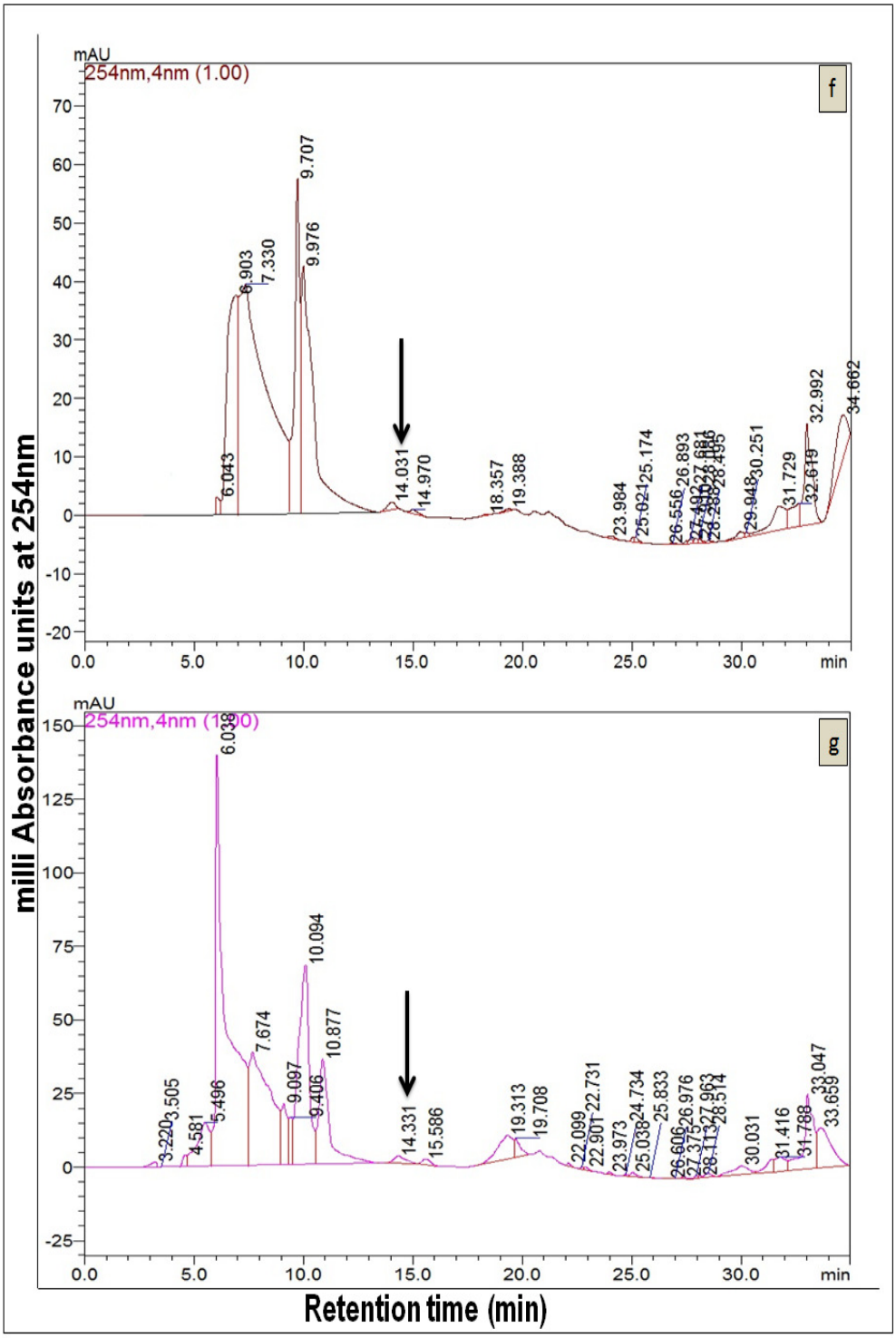

Figure 8.4h

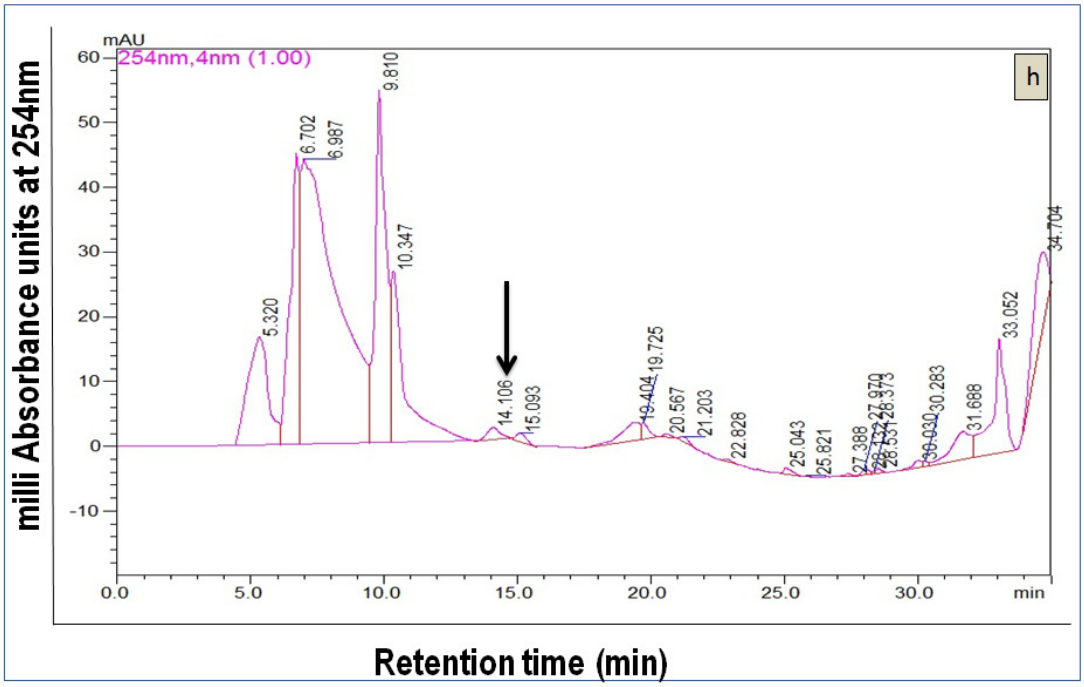

Figure 8.4 f-h HPLC elution profiles of malonyl CoA in cerulenin treated human Y79 RB cells: Representative HPLC chromatograms obtained for cerulenin at 48 h are presented. Malonyl CoA was detected at 14.6 ± 0.9 min retention time (indicated by down arrow in each chromatogram), in a gradient elution with a flow rate of 0.4ml/min detected at 254 nm in a diode array detector. Chromatograms: control **(f),** cerulenin treatment: 7 µg/ml **(g),** & 20 µg/ml **(h).**

After 72 h of triclosan treatment, malonyl CoA level increased between 5 folds to 7 folds at 7.5 and 100 µg/ml dosages. The representative chromatograms for the malonyl CoA levels in the experimental groups are presented in figure 8.4 i-k. Malonyl CoA in these treated groups was detected at 15.5 – 16.5 min retention time in a gradient elution with a flow rate of 0.4ml/min detected at 254 nm in a diode array detector.

Figure 8.4i & j

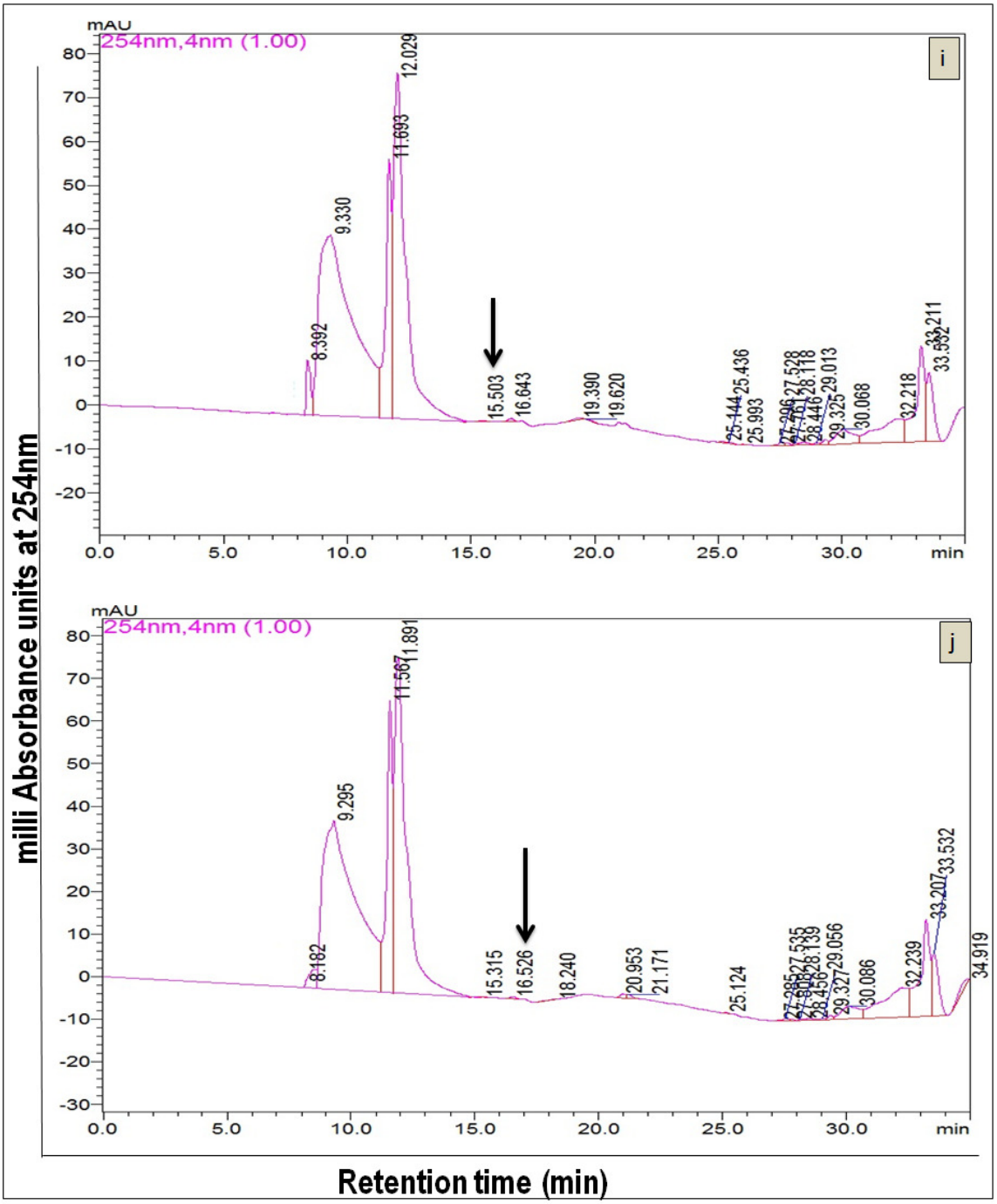
mAU
254nm,4nm (1.00)
i
12.029
11.693
9.330
8.392
15.503
16.643
19.390
19.620
25.436
33.211
33.532
min
mAU
254nm,4nm (1.00)
j
11.891
11.567
9.295
8.182
15.315
16.526
18.240
20.953
21.171
25.124
33.532
33.207
34.919
min
milli Absorbance units at 254nm
Retention time (min)

Figure 8.4k

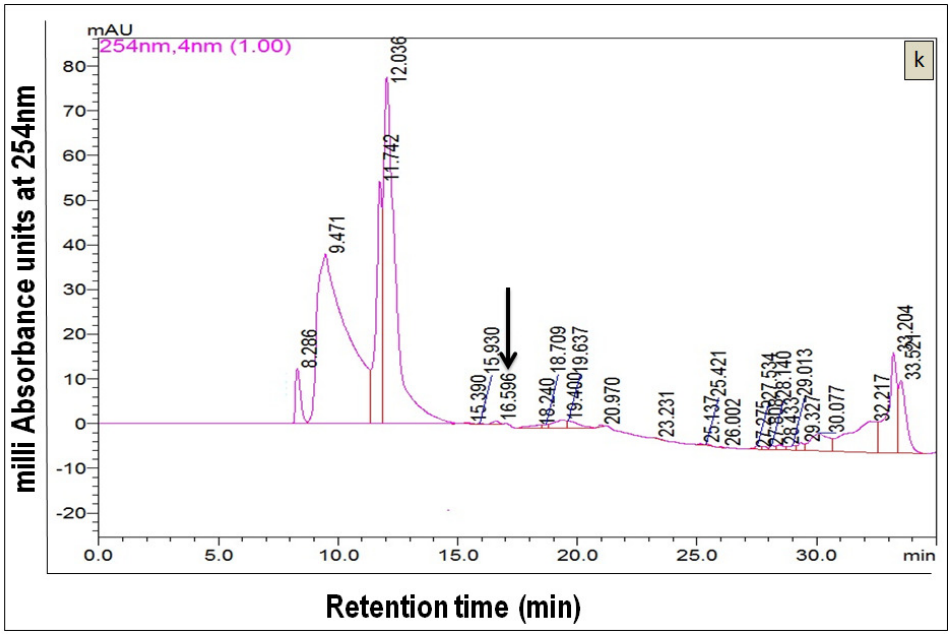

Figure 8.4i-k HPLC elution profiles of malonyl CoA in triclosan treated human Y79 RB cells: Representative chromatograms obtained for triclosan at 48h are presented. Malonyl CoA was detected at 14.6 ± 0.9 min retention time (indicated by down arrow in each chromatogram), in a gradient elution with a flow rate of 0.4ml/min detected at 254 nm in a diode array detector. Chromatograms: control **(i),** triclosan treatment: 20 µg/ml **(j),** & 100 µg/ml **(k).**

After 72 h of orlistat (Xenical™) treatment, malonyl CoA level increased about 3 folds at 75 and 250 µg/ml dosages. The representative chromatograms for the malonyl CoA levels in the experimental groups are presented in figure 8.4 l-n. Malonyl CoA in these treated groups was detected at 14.6– 14.9 min retention time in a gradient elution with a flow rate of 0.4 ml/min detected at 254 nm in a diode array detector.

Figure 8.4 l & m

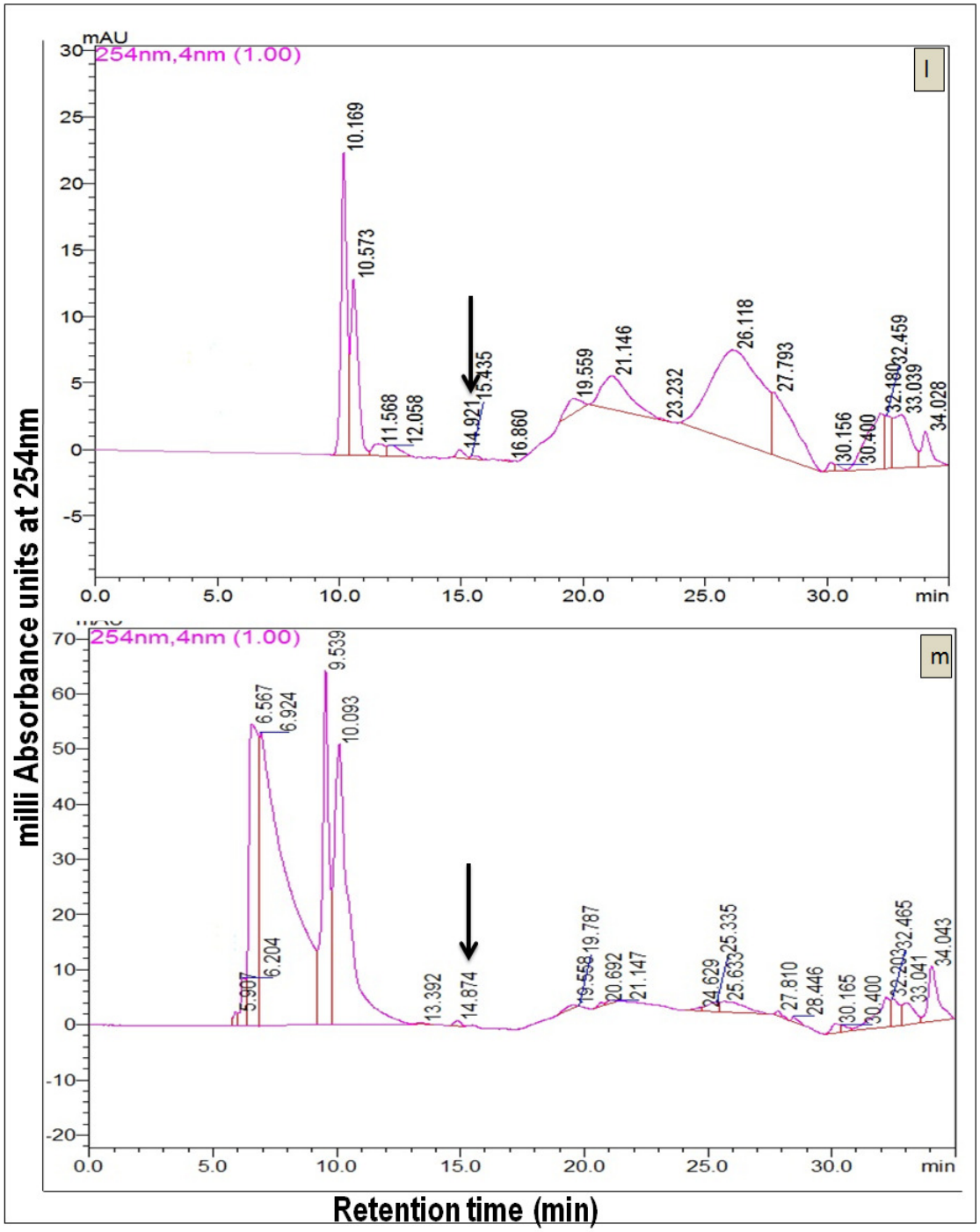
mAU
254nm,4nm (1.00)
l
10.169
10.573
11.568
12.058
14.921
15.435
16.860
19.559
21.146
23.232
26.118
27.793
30.156
30.400
32.180
32.459
33.039
34.028
min
254nm,4nm (1.00)
m
5.907
6.204
6.567
6.924
9.539
10.093
13.392
14.874
19.558
19.787
20.692
21.147
24.629
25.633
25.335
27.810
28.446
30.165
30.400
32.293
32.465
33.041
34.043
min
milli Absorbance units at 254nm
Retention time (min)

Figure 8.4n

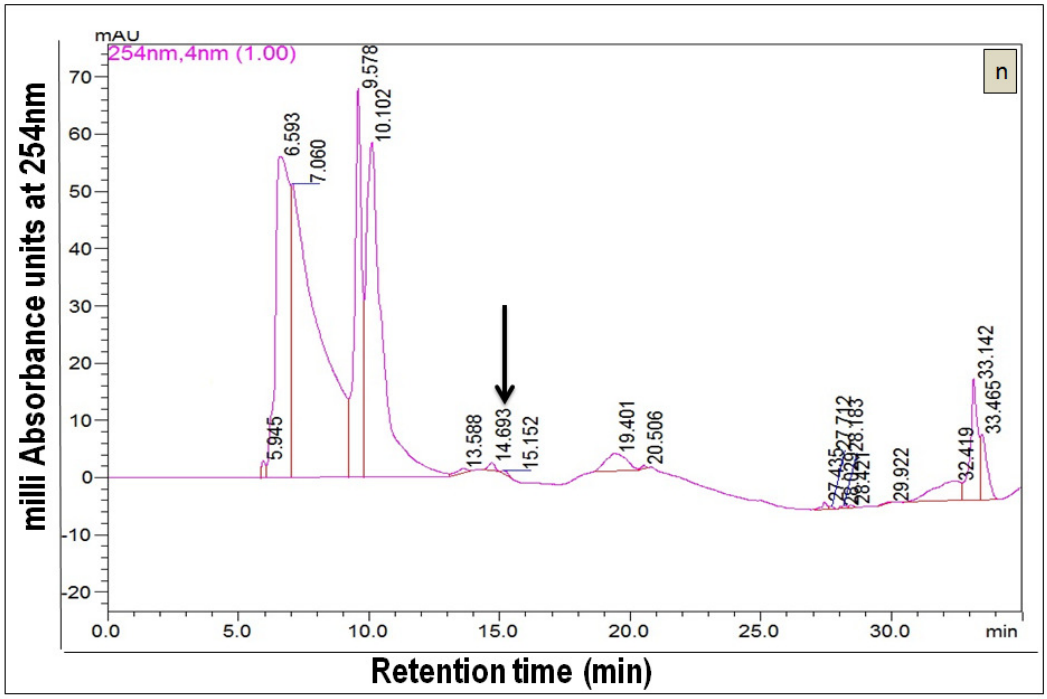

Figure 8.4l-n HPLC elution profiles of malonyl CoA in Xenical™ (orlistat) treated human Y79 RB cells: Representative chromatograms obtained for Xenical™(orlistat) at 48 h are presented. Malonyl CoA was detected at 14.6 ± 0.9 min retention time (indicated by down arrow in each chromatogram), in a gradient elution with a flow rate of 0.4ml/min detected at 254 nm in a diode array detector. Chromatograms: control **(l),** Xenical™ **(**orlistat) treatment: 250 µg/ml **(m),** & 1000 µg/ml **(n).**

8.4.2.4. Assay for cellular lipids in cancer (Y79) and normal (3T3) cells: Metabolic effect of FASN inhibition

8.4.2.4a. Standard calibration curves for quantification of cellular lipids

Cellular lipid content in Y79 RB cells and 3T3 cells were quantified from the standard curve of each type of lipid (Figure 8.5a-c).

Figure 8.5. Calibration curves for cellular lipids

Figure 8.5a Triglyceride calibration curve

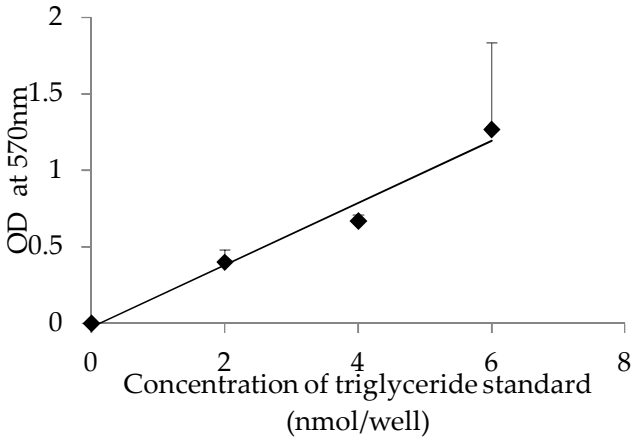

Figure 8.5b Phosphatidyl choline calibration curve

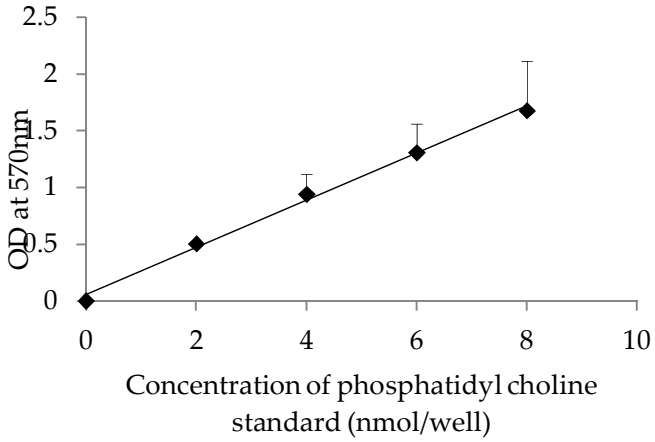

Figure 8.5c Cholesterol calibration curve

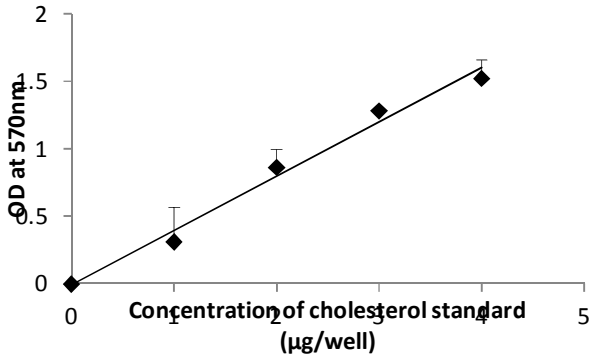

Figure 8.5 Standard curves for cellular lipids: Standard curve was plotted using varying concentrations of triglyceride **(a),** phosphatidyl choline **(b),** and cholesterol **(c)** standards provided in the assay kit. The samples were processed according to the manufacturer's instructions. The amount of each lipid is expressed as nmol. Values are expressed as mean ± S.D. of triplicate values.

8.4.2.4b. Distribution of cellular lipids in Y79 RB cancer and 3T3 normal cells

The cellular lipid [triglyceride (TGL), phosphatidyl choline (PC) and total cholesterol (TC)] levels were determined in Y79 RB and 3T3 cells treated with the anti-neoplastic IC_{50} dosage of FASN inhibitors at 48 h exposure. The untreated control Y79 RB and 3T3 cells were compared for their TGL, PC, and TC content and the distribution was determined. Figure 8.6a shows the profile of phosphatidyl choline, triglyceride, and total cholesterol levels in 3T3 cells compared to Y79 RB cells. The phospholipid to neutral lipid ratio was computed for each of the cells to understand the relative proportion of phosphatidyl choline (representative of phospholipids) to neutral lipids (triglyceride and cholesterol) at 48 h. For this phosphatidyl choline was considered as a representative of phospholipids, as PC constitutes 50% of the total phospholipids (Terce et al., 1994; Spector & Yorek, 1985). Triglycerides and total cholesterol, the mainly esterified lipids are considered as representative of neutral lipids. Y79 RB cells showed a ratio of 3.3 in contrast to 1.3 for 3T3 cells indicating that, the relative proportion of phosphatidyl choline to neutral lipids (TGL+TC) was high in cancerous Y79 RB cells compared to the non-neoplastic 3T3 cells (Figure 8.6b).

Figure 8.6: Distribution of phosphatidyl choline, triglyceride and total cholesterol in Y79 RB cells and 3T3 cells

Figure 8.6a Lipid profile in Y79 RB and 3T3 cells

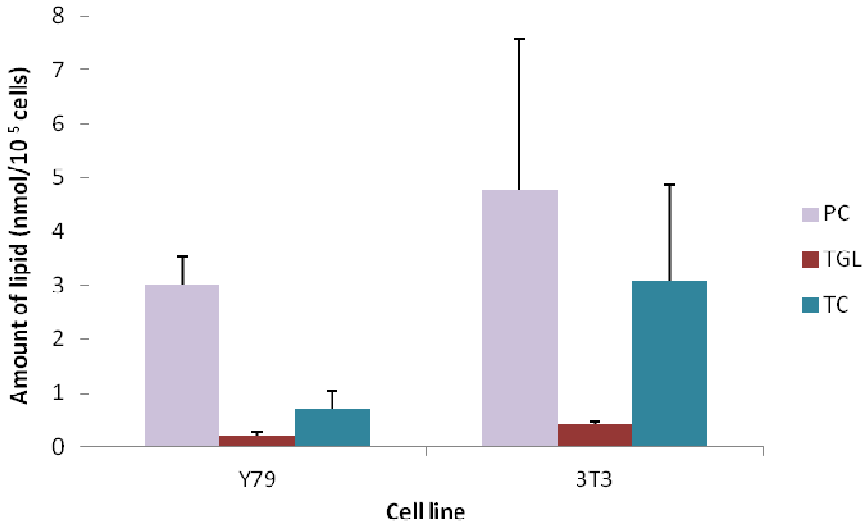

Figure 8.6b Phospholipid to neutral lipid ratio in Y79 RB and 3T3 cells

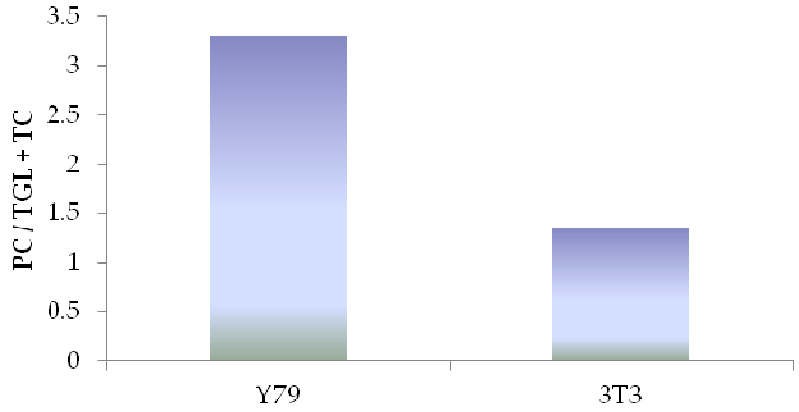

Figure 8.6 Distribution of phosphatidyl choline and triglyceride in Y79 RB and 3T3 cells: Phosphatidyl choline (PC), triglyceride (TGL), and total cholesterol (TC) levels were measured by colorimetric assays and levels were expressed as nmol/10^5 cells. **(a)** Amount of respective lipid in Y79 RB and 3T3 cells expressed in nmol/1 lac cells. **(b)** Ratio of phospholipid (Phosphatidyl choline as representative) to neutral lipid (represented by commonly esterified lipids - triglycerides and total cholesterol) is computed for each cell type. The relative proportion of phosphatidyl choline to neutral lipids (triglyceride + total cholesterol) in Y79 cancer cells was higher than the non-neoplastic 3T3 cells (N=3).

8.4.2.4c Determination of cellular lipids in Y79 and 3T3 cells treated with FASN inhibitors

The inhibition of cellular lipids - phosphatidyl choline (PC), triglyceride (TGL) and total cholesterol (TC) levels were measured in Y79 and 3T3 cells treated with FASN inhibitors. Treatment with FASN inhibitors showed decrease in the concentration of each lipid-type, in both cancer (Y79) and normal (3T3) cells.

Cerulenin and triclosan showed similar trend in reducing the lipids in Y79 cancer cells. Relative to the three lipid types analysed here, cerulenin and triclosan showed a greater decrease in triglyceride levels (cerulenin - by 46%, triclosan – by 34%). This was followed by total cholesterol (decreased by 31% and 20% with cerulenin and triclosan respectively), and then phosphatidyl choline (decreased by 16% and 14% with cerulenin and triclosan respectively). Orlistat treatment in Y79 cells reduced cholesterol levels by 48%, followed by a 25% decrease in TGL, and 20% decrease in phosphatidyl choline.

Triclosan and orlistat treatment in 3T3 fibroblast cells showed a similar profile of reducing the lipids. Marked inhibition of triglycerides by 62% and 74% was observed with triclosan and orlistat treatment respectively. This was followed by decrease in phosphatidyl choline and total cholesterol levels with triclosan treatment (by 34% and 23%) and with orlistat treatment (by 38% and 13%) respectively. Cerulenin treatment decreased the phosphatidyl choline levels by 28%, which was followed by TGL (24%) and total cholesterol (18%) (Figure 8.7).

Figure 8.7a Decrease in cellular lipid levels in FASN inhibitor treated cancer (Y79 RB) cells

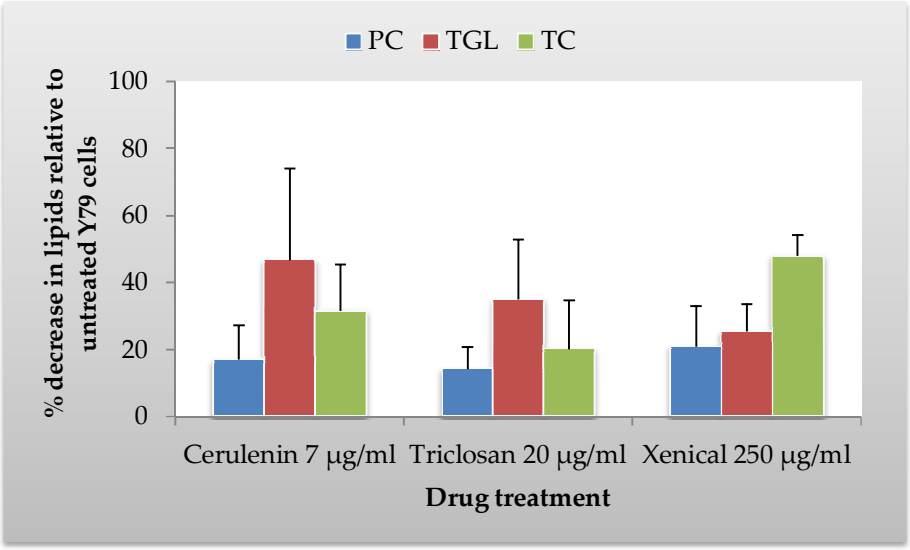

Figure 8.7b Decrease in cellular lipid levels in FASN inhibitor treated non-neoplastic (3T3) cells

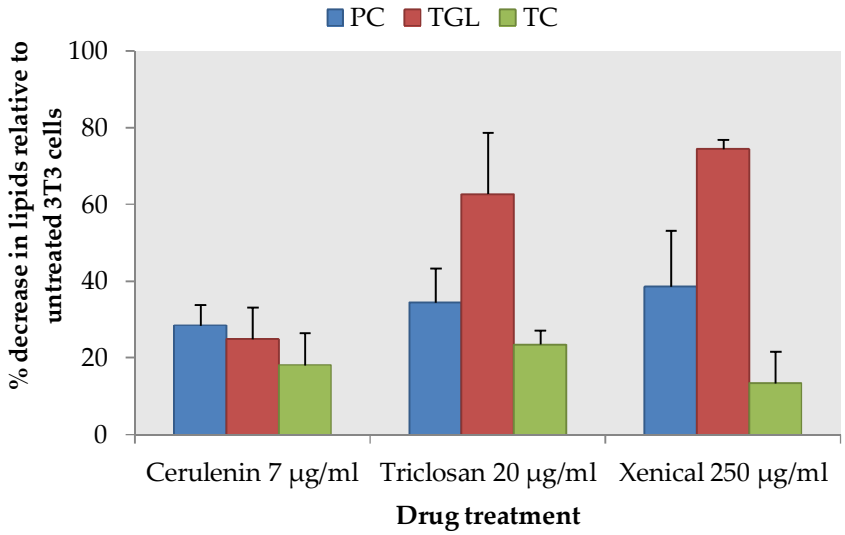

Figure 8.7 Inhibition of cellular lipid levels in FASN inhibitor treated Y79 RB and non-neoplastic (3T3) cells: Intracellular lipid content [phosphatidyl choline **(PC),** triglyceride (TGL), and total cholesterol **(TC)]** were measured by colorimetric assay in FASN inhibitor treated Y79 retinoblastoma cells **(a)** and normal 3T3 cells **(b)** at 48 h treatment. Lipid levels were calculated using standard curves and the values were expressed as nmol/10^5 cells. Each bar represents percentage inhibition of lipid levels relative to untreated control obtained from duplicate values.

8.4.3. LIPOGENIC INHIBITION AND APOPTOTIC EFFECTS

8.4.3.1. DNA fragmentation analysis of FASN inhibitor-treated Y79 RB cells

To ascertain whether each of the FASN inhibitor studied here showed its anti-cancer activity through apoptotic DNA damage, DNA fragmentation assay was performed. Figures 8.8 clearly indicate apoptotic DNA damage after treatment with cerulenin, triclosan, and Xenical™. This is evident from the DNA smearing and laddering observed on the agarose gel. Further, toxic dosages of the inhibitors, resulted in almost negligibly quantifiable genomic DNA which is evident in lane 7 of figure 8.8b, and lanes 3 and 5 in figure 8.8c. This can be attributed to the very low number of viable cells (notably 10%, 9%, 3% respectively) in these dosages as assessed by cell viability assay.

Figure 8.8 DNA fragmentation analysis of FASN inhibitor treated Y79 RB cells

Figure 8.8a

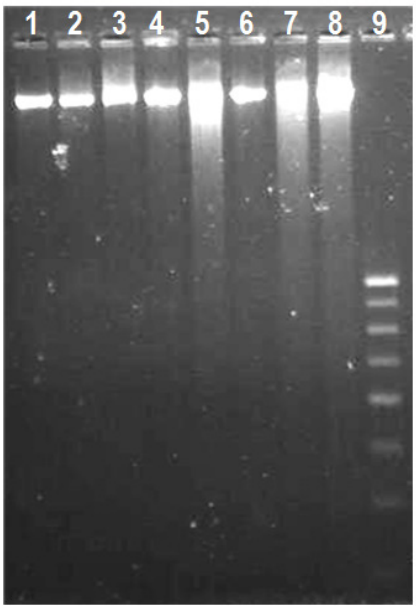

LEGENDS
1. Untreated Y79 cells
2. 7µg/ml cerulenin for 48 h
3. 20µg/ml cerulenin for 48 h
4. 3µg/ml cerulenin for 72 h
5. 20µg/ml cerulenin for 72 h
6. 1µg /ml cerulenin for 96 h
7. 20 µg/ml cerulenin for 96 h
8. Positive control H_2O_2 treated cells
9. 100 bp DNA ladder

Figure 8.8b

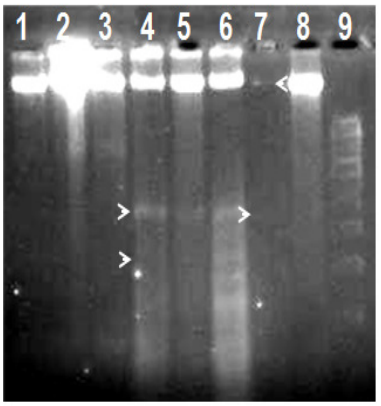

LEGENDS
1. Untreated Y79 cells
2. 20 µg/ml triclosan for 48 h
3. 100 µg/ml triclosan for 48 h
4. 7.5 µg/ml triclosan for 72 h
5. 100 µg/ml triclosan for 72 h
6. 5 µg/ml triclosan for 96 h
7. 100 µg/ml triclosan for 96 h
8. Positive control H_2O_2 treated cells
9. 100 bp DNA ladder

Figure 8.9c

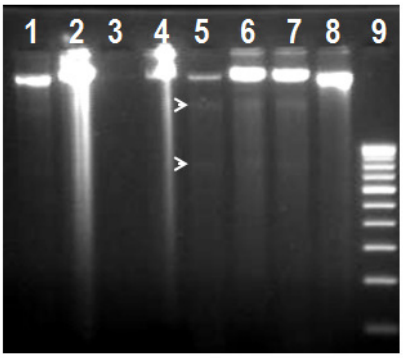

LEGENDS
1. Untreated Y79 cells
2. 250 µg/ml Xenical™ for 48 h
3. 1000 µg/ml Xenical™ for 48 h
4. 75 µg/ml Xenical™ for 72 h
5. 250 µg/ml Xenical™ for 72 h
6. 15 µg/ml Xenical™ for 96 h
7. 70 µg/ml Xenical™ for 96 h
8. Positive control H_2O_2 treated cells
9. 100bp DNA ladder

[**]**Figure 8.8 DNA fragmentation analysis of FASN inhibitor treated Y79 RB cells:** Cytotoxic effect of FASN inhibitor cerulenin **(a),** triclosan **(b)** and orlistat (Xenical™) **(c)** on Y79 RB cells was analysed & confirmed by evaluating the presence of DNA fragmentation in agarose gel electrophoresis. Y79 RB cells were treated with the three FASN inhibitors at specified time periods and DNA was extracted and electrophoresed in agarose gel. Presence of DNA fragments (indicated by arrow heads) on drug treatment indicates the drug mediated DNA damage.

[**] *The data presented in figure 7.4 is published in: Basic & Clin Pharmacol & Toxicol, 2012, 110, 494-503.*
Please see "List of publications" on page XXIII.

8.4.3.2. Assessment of apoptosis in FASN inhibitor-treated Y79 RB cells by Annexin V assay

The apoptotic effects induced by the three anti-FASN drugs were also ascertained by Annexin V staining using Flow cytometry. Figure 8.9 shows the percentage of apoptotic cells after treatment with cerulenin, triclosan, and orlistat (Xenical™) indicating that FASN inhibition induced apoptosis in treated Y79 RB cells. The percentage of apoptotic cells increased in the treated cells compared to the control cells as indicated by apoptotic cells.

Figure 8.9: Assessment of apoptosis in FASN inhibitor-treated retinoblastoma Y79 cells by Annexin V assay

Figure 8.9a Cytogram of FASN inhibitor treated Y79 retinoblastoma cells by Annexin V assay

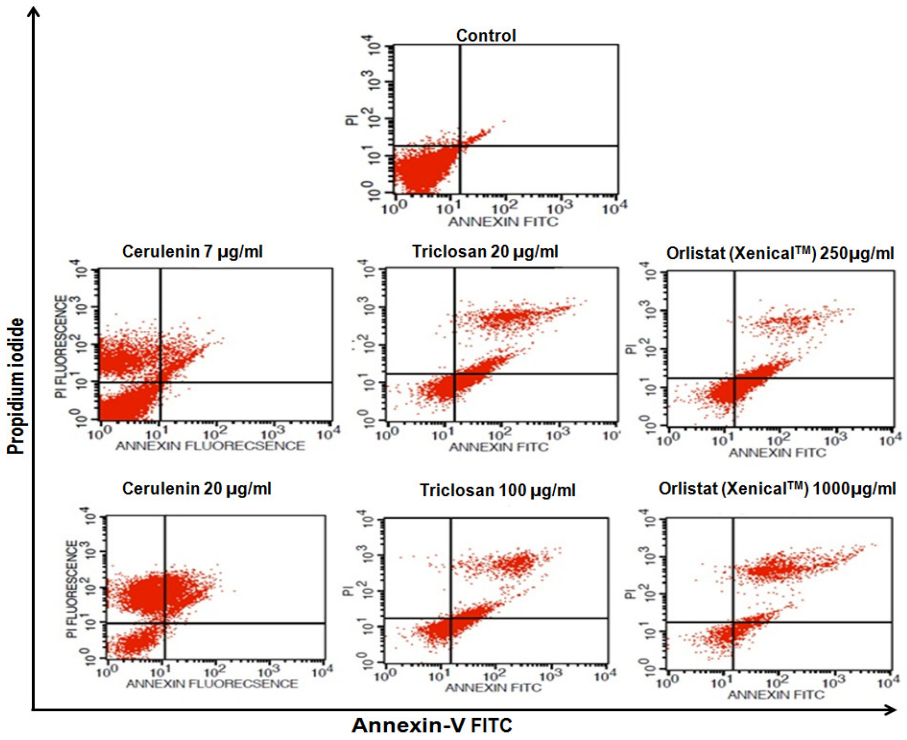

Figure 8.9a Cytogram of FASN inhibitor treated Y79 RB cells by Annexin V assay: Apoptosis was evaluated after treating Y79 RB cells with FASN inhibitors at their IC_{50} and higher dosage after treatment for 48 h. Flow cytometry cytogram represents Annexin-V-FITC staining in x-axis and Propidium iodide (PI) in y-axis. Quadrants portions indicates: lower left: Live cells (Annexin and PI –ve), lower right: early apoptotic (Annexin +ve and PI –ve), upper right: late apoptotic (Annexin +ve and PI +ve), upper right: necrotic cells (Annexin –ve and PI +ve).

Figure 8.9b & c Assessment of apoptosis on FASN inhibitor treated Y79 RB cells by Annexin V assay

Figure 8.9b

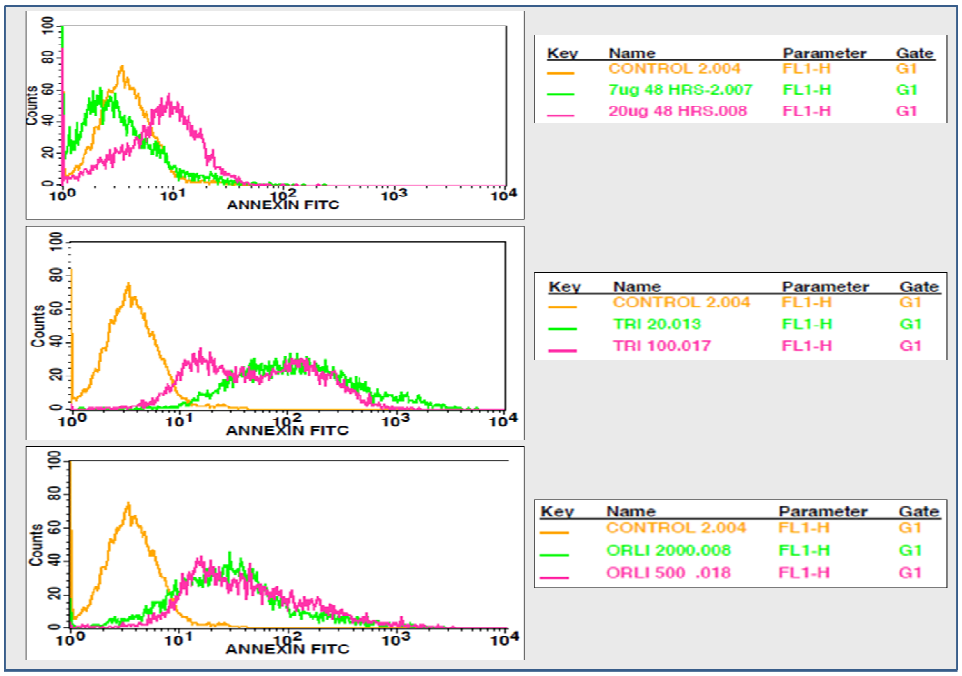

Figure 8.9c

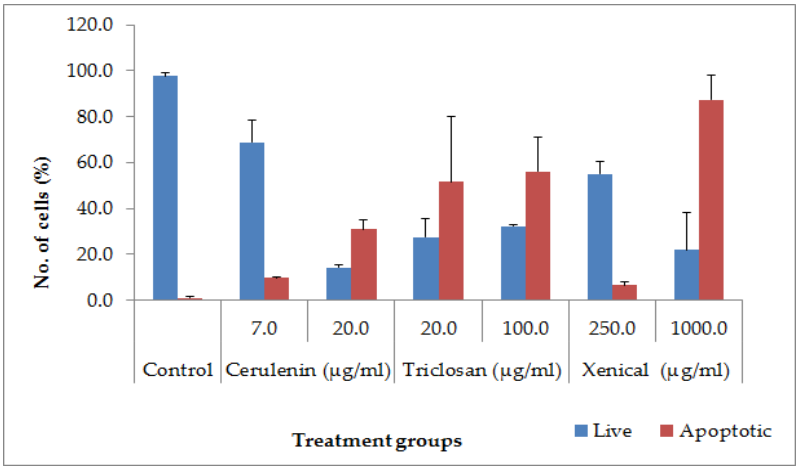

Figure 8.9 b,c Assessment of apoptosis on FASN inhibitor treated Y79 RB cells by Annexin V assay: RB cells were treated with the three FASN inhibitors at 48h and the binding of Annexin V to the apoptotic cells were measured by flow cytometry. 10,000 gated cells for each sample were analysed for the extent of apoptosis. **b)** Overlay plots for untreated and treated groups showing counts of annexin binding [Upper panel: cerulenin, middle right panel: triclosan and lower left panel: orlistat (Xenical™) treatment]. Colour codes for each sample is as indicated within each panel. **c)** Graph represents total number of cells that are annexin negative (live) and annexin positive (early + late apoptotic). Each bar represents mean ± S.D. from triplicate experiments.

8.4.3.3. Assessment of malondialdehyde (MDA) levels in Y79 RB cells treated with FASN inhibitors

Lipid peroxidation marker malondialdehyde (MDA) was measured in Y79 RB cells treated with FASN inhibitors at their IC_{50} dosages at 48 h treatment. The biochemical indicator of lipid peroxidation, MDA on FASN inhibition increased with respect to untreated control, when measured in the supernatant [medium from each well (control and treated) taken after 48 h of treatment] and in cell lysate (Figure 8.10). The increase in MDA levels were then depicted as fold change in absorbance at 532 nm relative to untreated control Y79 RB cells.

Figure 8.10 Assessment of MDA levels in FASN inhibitor treated Y79 RB cell lysates and in supernatant

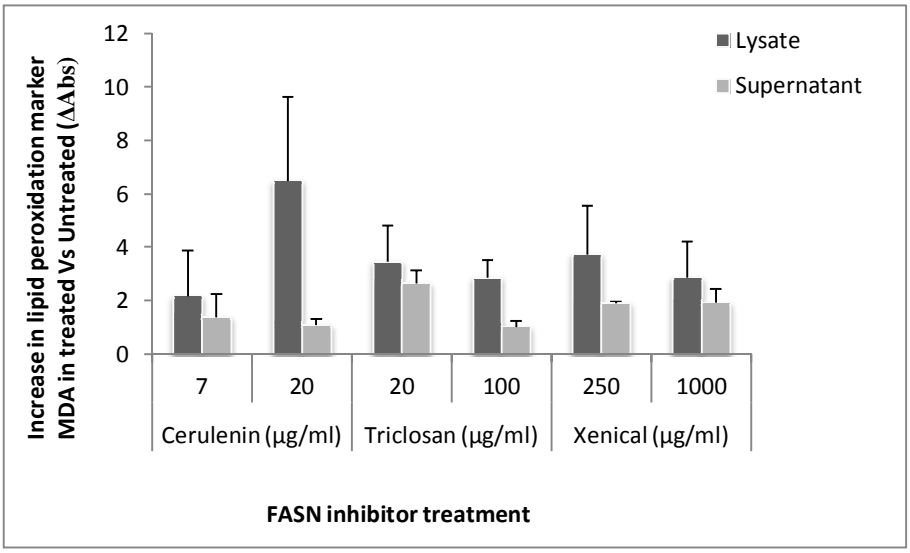

Figure 8.10 Assessment of MDA levels in FASN inhibitor treated Y79 RB cells: Y79 RB cells were treated with cerulenin, triclosan and orlistat at their IC_{50} dosages at 48 h. Lipid peroxidation marker (MDA) levels were measured colorimetrically in the cell lysates (dark grey bars) and supernatant (light grey bars) from each sample obtained after 48 h of incubation. The difference in absorbance at 532 nm in treated cells relative to the respective control cells were measured and plotted. Each bar represents mean ± S.D. of absorbance change from three independent experiments.

8.4.3.4. Cerulenin treatment in Y79 RB cells: Gene expression profile and validation of microarray analysis

The inhibition of FASN enzyme activity, protein and mRNA expression and induction of apoptosis by the three FASN inhibitors has been confirmed. Further to this, the differential gene expression profile of the cerulenin treated Y79 RB cells at its IC_{50} (7 μg/ml) at 48 h treatment were analysed and reported below.

The microarray analysis of cerulenin-treated Y79 RB cells, has revealed differential expression of several categories of genes involved in various cellular pathways/processes (Table 8.1) — lipid metabolism, cell cycle, cell proliferation, apoptosis and carbohydrate metabolism (Figure 8.11c). We validated the genes of current interest by qRT-PCR (FASN, SKP2, CYCS, PPARA, RXRA, CDK2AP1, ACACB, SSTR2). The real time PCR findings (Figure 8.11b) were consistent with that of the microarray analysis. The comprehensive list of genes differentially regulated on cerulenin treatment is presented in Tables A2 & A3 in Appendix I.

Table 8.1 List of important genes differentially regulated in retinoblastoma cancer cells treated with cerulenin

S.No	Gene Name	Gene Symbol	Fold change
1.	Cytochrome c	CYCS	1.2089
2.	Rapamycin-insensitive companion of mTOR	RICTOR	-1.9256
3.	Retinoid X receptor, alpha	RXRA	-1.831
4.	Peroxisome proliferator activated receptor	PPARA	-1.8007
5.	S-phase kinase-associated protein 2	SKP2	-1.5964
6.	Acetyl CoA carboxylase beta	ACACB	-1.4978
7.	Fatty acid synthase	FASN	-0.1119
8.	CDK2-associated protein 1	CDK2AP1	1.2177
9.	Growth factor receptor bound protein 10	GRB10	-1.065
10.	Bim-alpha1	BCL2L11	-1.1578
11.	Somatostatin receptor 2	SSTR2	1.2157
The comprehensive list of genes differentially regulated on cerulenin treatment is presented in Tables A2 & A3 in Appendix I.			

Figure 8.11: Cerulenin treatment in Y79 RB cells: Gene expression profile and validation of microarray analysis

Figure 8.11a Heat map of differential expression of genes in cerulenin treated Y79 RB cells

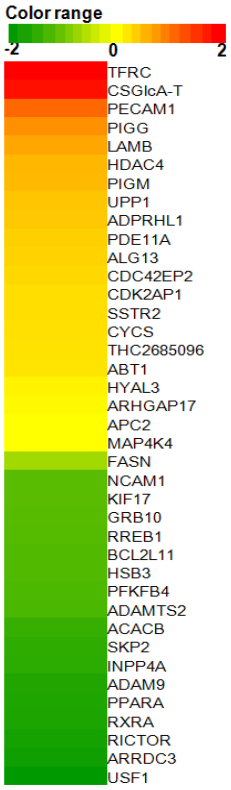

[††]**Figure 8.11a Differential gene expression profile analysis.** a) Heat map represents the overall differential expression of genes in Y79 RB cells when subjected to cerulenin treatment. Red and green colours represent the up-regulation and down-regulation of genes respectively relative to untreated control Y79 cells.

[††]*The data presented in figure 8.11a-c is published in: Nutrition and Cancer, 2013,65(2),1-6. Please see "List of publications" on page XXIII. Please see "List of publications" on page XXIII*

Figure 8.11b: Cerulenin treatment in Y79 RB cells: Validation of microarray analysis findings.

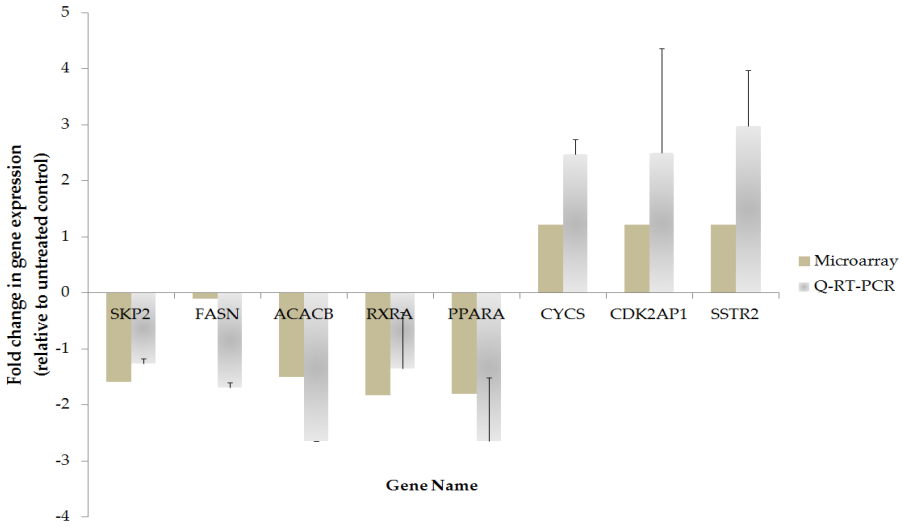

Figure 8.11b Cerulenin treatment in Y79 RB cells: Validation of microarray analysis findings: The real-time PCR findings were consistent with microarray results of gene expression in Y79 RB cells treated with cerulenin. This is represented by the two columns presented alongside each gene (Grey: qRT-PCR (mean ± S.D. of duplicate values); Brown: Microarray analysis). The results are expressed as fold-change in cerulenin-treated cells, relative to untreated Y79 cells (control). *SKP2: S-phase kinase-associated protein 2; FASN: Fatty acid synthase; ACACB: Acetyl CoA carboxylase beta; RXRA: Retinoid X receptor, alpha; PPARA: Peroxisome proliferator activated receptor alpha; CYCS: Cytochrome c; CDK2AP1: CDK2-associated protein 1; SSTR2: Somatostatin receptor 2.*

Figure 8.11c Schematic representation of various pathways/genes differentially regulated on cerulenin treatment in Y79 RB cells

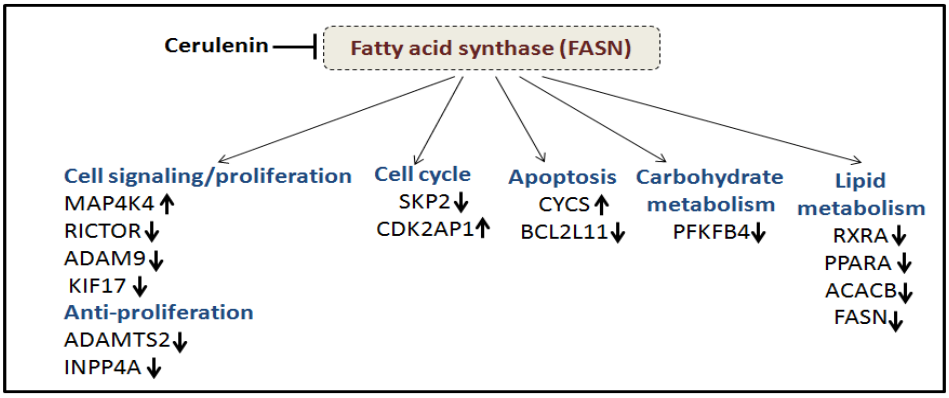

Figure 8.11c Schematic representation of various pathways/genes differentially regulated on cerulenin treatment in Y79 RB cells: The important genes that were differentially regulated in Y79 RB cells on cerulenin treatment are depicted. The gene names that are up/down-regulated in each pathway are shown. The up/down-regulated genes are followed by up/down arrows.

8.5. Chapter Summary

- The differential effects of FASN inhibitors (cerulenin, triclosan, and orlistat) on FASN protein content and mRNA levels was analysed in RB Y79 cells.
- Y79 RB cells treated with cerulenin, triclosan and orlistat showed accumulation of malonyl CoA (substrate) and depletion of free fatty acid (end-product).
- Significant decreases in FASN enzyme activity, along with modulation of free fatty acid levels were observed.
- FASN inhibition resulted in accumulation of malonyl CoA (substrate). FASN inhibitor treated Y79 retinoblastoma cells and fibroblast cells showed decrease in the cellular lipids (triglyceride, cholesterol and phosphatidyl choline) levels.
- Cytotoxicity of FASN inhibitors may be mediated via apoptotic mechanisms (indicated by Annexin V analysis and DNA fragmentation assay) with concomitant increase in lipid peroxidation.
- cDNA microarray analysis of cerulenin treated Y79 RB cells revealed differential expression of genes involved in various cellular processes such as lipid metabolism, cell cycle/apoptosis, cell signaling/proliferation.

CHAPTER 9: MOLECULAR DOCKING ANALYSIS OF FASN WITH CHEMICAL INHIBITORS

9.1. INTRODUCTION

Fatty acid synthase (FASN) is a lipogenic multi-enzyme complex that comprises seven catalytic domains within a single polypeptide chain. The enzyme's structural make-up differs with species. There are two types of FASN which are:

1 **Type I FASN** (Contains all catalytic domains of the cyclic reaction in a single polypeptide chain)

2 **Type II FASN** (Each catalytic domain is a small independent protein, each of which catalyses a single step of the cyclic reaction)

Figure 9.1 Types of Fatty acid synthase (FASN)

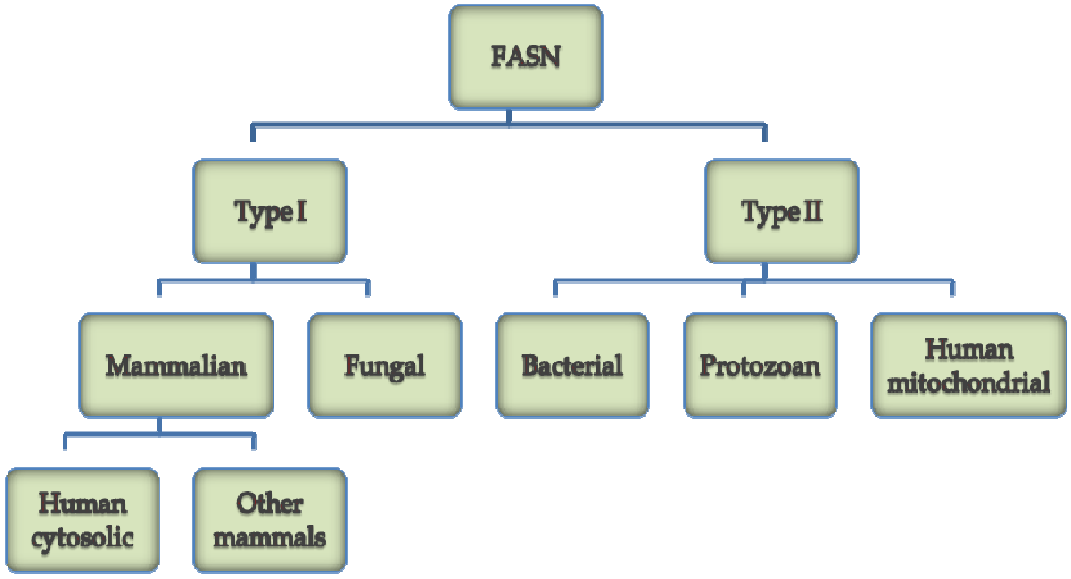

Figure 9.1 Flow chart of types of FASN: The type and structure of FASN differs with each species. Human cytosolic FASN belongs to type I whereas the human mitochondrial FASN is of type II.

9.1.1. Bacterial type II FASN:

The bacterial, plant and the human mitochondrial FASN are of type II. In these proteins, the catalytic domains are present as separate domains. Fatty-acid synthesis in bacteria is of great interest as a target for the discovery of anti-bacterial compounds. The addition of a new acetyl moiety to the growing fatty-acid chain, an

essential step, is catalyzed by ketoacyl-ACP synthase (KS). Natural antibiotics such as cerulenin and thiolactomycin inhibit the KS domain of FASN II and are explored as anti-bacterial agents. FASN II has been proposed as a possible therapeutic target for treating tuberculosis, in which FASN II can be targeted by pyrazinamide to inhibit the mycolic acid biosynthesis. Genes related to lipid metabolism and other pathways critical for amino acid synthesis and mycothiol synthesis that are critical for mycobacterial survival are short listed as promising candidates for anti-tubercular drug discovery by computational approaches using novel algorithms (Raman et al., 2008).

A novel small molecule inhibitor - 2-phenylamino-4-methyl-5-acetylthiazole, was reported to bind to the active-site Cys163 along with hydrophobic residues of the fatty-acid binding pocket in the FASN II complex. The crystal structure of this complex was resolved at 1.35 Å resolution, which revealed non-covalent interactions. The active site of KS domain in FASN II possessed a Phe392 side chain and no conformational changes were induced at the active site when the ligand was bound. These interactions differed from the mode of binding of cerulenin and thiolactomycin (Pappenberger et al., 2007).

9.1.2. Fungal FASN (Type I FASN with $\alpha_6\beta_6$ dodecamers)

Yeast FASN is a 2.6MDa protein that has a barrel shaped structure. It has 6 α and 6 β chains. The α- and β-chains define three reaction chambers per dome and contain eight catalytic centers. Of these, the α-chain contributes the phosphopantetheinyl transferase (PPT), ACP, ketoacyl synthase (KS), ketoacyl reductase (KR), and part of the malonyl-palmitoyl transferase (MPT) domain. The β-chain contributes the acetyl-transferase (AT), enoyl reductase (ER), dehydratase (DH), and the major part of the MPT domain. The AT domain participates in the initiation of fatty acid chain synthesis. The MPT, KS, KR, DH, and ER domains each carry out different steps in

the chain elongation cycle. The growing fatty acid chain is attached to the carrier domain, which shuttles between the successive catalytic sites, until it is released into the cytosol by attachment to CoA after having reached a C-16 or C-18 chain length. In yeast, fatty acid synthesis is carried out in the confined environment of a catalytic cage. This makes the process more efficient compared to prokaryotic type II FASN. This study reported the complete structure of yeast FASN unlike the earlier studies in which the structures of the PPT and KS domains were not elucidated (Gipson et al., 2010).

Figure 9.2: The crystal structure yeast FASN

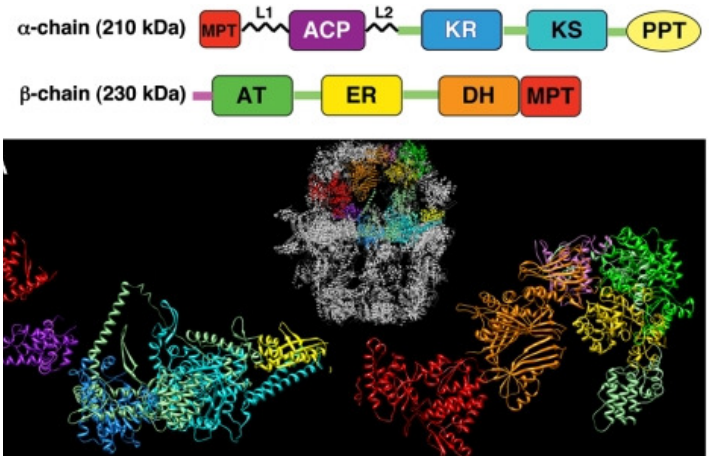

Figure 9.2: The crystal structure of yeast FASN: Domain organization of the fungal FASN α chain (Left) and β chain (Right) with the domains colored according to the colours shown in the scheme in the upper panel. A barrel shaped structure with 6 α and 6 β chains in a heterododecamer arrangement (Gipson et al., 2010).

9.1.3. Mammalian FASN

Mammalian FASN comprises α_2 homodimers in which the seven domains are arranged in a head-to-tail fashion in a single polypeptide chain. Till date the complete crystal structure of the human FASN is not yet reported. Individual crystal structures of human FASN domains: keto acyl synthase (KS), thioesterase (TE), keto acyl reductase (KR), acyl carrier protein (ACP), malonyl transacylase (MT)/acetyl transacylase (AT) domains have been elucidated and are available in the protein data bank (PDB). The near-complete crystal structure of mammalian porcine FASN

was reported, in which the enoyl reductase, keto acyl reductase and the linker regions were not reported.

9.1.3.1. Porcine FASN

Maier et al., 2008 reported the near-complete crystal structure of porcine FASN. The structure determination has been done and reported for free FASN and FASN as a complex with cofactor $NADP^+$ at a resolution of 3.2 - 3.3 Å (Figure 9.3). The ACP and TE domains and linker regions that connect these domains to the other domain complex have not been elucidated.

Highlights of the mammalian FASN complex crystal structure in comparison with the bacterial and yeast FASN structures:

1. Mammalian FASN complex is architecture of alternating linkers and domains.
2. Two non-enzymatic domains – pseudo keto reductase and pseudo methyl transferase
3. The KS domain structure remains similar to those of the prokaryotes, but the active site is designed to bind large acyl chain substrates.
4. The MAT domain of the mammalian FASN has dual specificities for both the substrates acetyl CoA and malonyl CoA
5. The KR domain of the mammalian FASN resembles the prokaryotic KR domain
6. In the DH domain the catalytic sites has three important amino acid residues His878 in N terminal and Asp1033, His1037 in the C terminal. The bacterial FASN also has the same residues in its active site in the DH domain
7. The ER domain of the mammalian FASN has a different fold from the prokaryotic counterparts. Overall comparison with the prokaryotes reveals the fact that the mammalian FASN has all the catalytic domains more similar to the poly ketide synthase model than the bacterial FASN.

Figure 9.3: Crystal structure of mammalian FASN from porcine model.

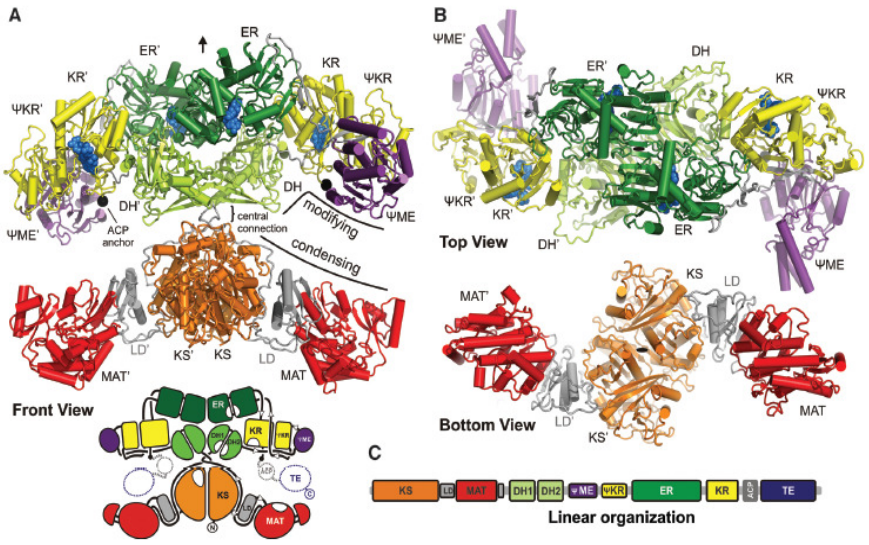

Figure 9.3: Crystal structure of mammalian FASN from porcine model: Crystal structure of mammalian FASN from porcine model. **A-** Shows the cartoon representation of the overall structure of FASN with its linker domains depicted in gray color. **B-** Top and bottom view of the FASN structure which gives an S shape to the molecule. **C-** Linear domain representation of FASN at approximate sequence scale (Maier et al., 2008).

9.1.3.2. Human FASN

Salient features of the individual domains which have been crystallized are discussed below. Table 9.1 shows the amino acids sequence length of each catalytic domain of FASN and their crystal structure availability.

Table 9.1 Details of human fatty acid synthase (FASN) crystal structures

Domain	Amino acid region	Crystal structure
KS	1-414	+
MT/AT(part of DH)	429-817 (818-980)	+
Linker	981-1630	-
ER	1635-1863	-
KR	1864-2118	-
ACP	2123-2511	+
TE	2207-2511	+
Note: + indicates crystal structure predicted, - indicates crystal structure not yet elucidated		

9.1.3.2a Human thioesterase (TE) domain

The TE domain catalyzes the termination step by hydrolyzing the thioester bond between palmitate and the 4'-phosphopantetheine moiety of the acyl-carrier protein (ACP) domain. The release of the TE from FASN by limited proteolysis, however, results in the production of fatty acids containing 20 to 22 carbons. Chakravarthy et al., 2004 reported the crystal structure of the recombinant TE domain, which reports that the TE domain is composed of two sub domains each with different size and folding motifs. The sub domain A is larger and consists of α/β motif and the smaller sub domain B is helical. Sub domain A contributes to the catalytic triad with the Ser, His and Asp residues. The long groove between the two sub domains acts as a fatty acid binding site. This groove measures the chain length of growing fatty acid product. Thus, the TE domain is essential in regulating the length of the fatty acid chain.

Crystal structure of the TE domain in complex with its inhibitor Orlistat was resolved at 2.3 Å resolution. Orlistat binds to the catalytic triad in the Ser2308 region in the Sub domain A with a covalent attachment. Orlistat is captured as a covalent complex with the acyl enzyme and as a hydrolysed product.

The binding specificities of Orlistat are (Figure 9.4):

1. The peptidyl moiety of Orlistat binds to the interface between the two sub-domains
2. The palmitic core predominantly binds to the hydrophobic specificity channel
3. The hexanoyl tail interacts with the Gly2339, Thr2342, Tyr2343 and Tyr2462

Figure 9.4: Structure of orlistat and its binding regions (Pemble et al., 2007)

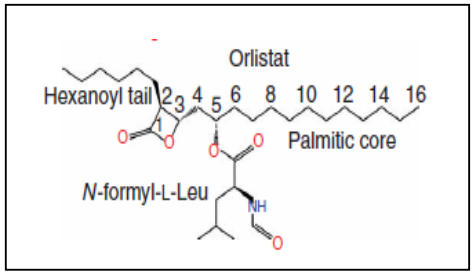

The orlistat covalent complex serves as a model for the interactions and reactivity of presumably all β-lactone containing compounds designed for the TE domain and the C16 hydrocarbon backbone of orlistat that mimics palmitate enables rationalization of substrate specificity. The nucleophilic attack occurs at the C1 carbonyl atom of orlistat, leading to the formation of an unusually stable acyl-enzyme intermediate (Pemble et al., 2007). These studies enhance the importance of further studies with the FASN complex protein crystal structure for designing newer effective drugs.

Wei et al., 2011 recently reported the crystal structure of TE domain at 1.48Å resolution which was covalently modified and inactivated by methyl γ-linolenylfluoro phosphonate.

9.1.3.2b Human acyl carrier protein (ACP) domain and malonyl transacylase (MT)/ acetyl transacylase (AT) domain

The crystal structure of human ACP in complex with the group II phosphopantetheinyl transferase (PPT) and Mg^{2+} ions and CoA was elucidated by Bunkoczi et al., 2007. Hydrophobic interactions between the ACP and the PPTs play an important role in their catalysis. Bunkoczi et al., 2009 reported the MT and AT domain structures of the human fatty acid synthase both in the cytosolic and in the mitochondrial fractions. The type I acyl transferase transfers both the malonyl and acetyl moieties during the initial step of the reaction. But the type II mitochondrial

FASN transfers only the malonyl group. The difference in this function is accounted in the structure.

9.1.3.2c Human keto acyl synthase (KS) domain

Pappenberger et al., 2010 reported the human FASN KS-MAT didomain structure and reported it as a framework for the design of inhibitors. The KS domain is characterised by a buried surface area larger than the porcine KS domain. A stretch of 28 (825-852) amino acid residues that completes the KS domain, acts as linker between the domains and forms the integral part of KS domain. This region is specifically present in mammals and absent in the FASN of other lower organisms. The active site of KS domain is characterised by cysteine residue, which is flanked by two conserved histidine residues. This is similar to the *E. coli* KS active sites.

The availability of FASN crystal structures has multi-fold advantages in the *in vitro* studies of FASN for anti-cancer treatment strategies. The structure is useful for identifying and studying the newer chemical inhibitors, dynamics of the enzyme-inhibitor complexes and their chemical interactions. The complete crystal structure of human FASN is thus much essential for anti-FASN therapy (Pappenberger et al., 2007). Bioinformatics is an *in silico* tool that enables the understanding and organisation of information associated with biologic macromolecules. The following sub-section briefs the definition and applications of bioinformatics.

9.1.4. Bioinformatics: This tool is defined as the understanding and organisation of information associated with biological macromolecules by applying informatics techniques derived from maths, computer science and statistics.

There are several aims for bioinformatics studies: 1) organisation of data in such a way that it can be accessed by researchers, and to submit new entries into the database [e.g., storage of information on macromolecule structures in the protein data bank (PDB)], 2) development of tools and resources to analyse the available

data, 3) analysis of the data and interpretation of results in a biologically meaningful manner. The primary data sources for the bioinformatics analysis are protein and DNA sequences, macromolecules and their structures and functional genomics.

9.1.4.1. Practical Applications:

1. **Identification of protein homologues:** comparison of structures of two related proteins – which helps in drug designing, prediction of tertiary structures of proteins, checking the energetic viability of the predicted structure.
2. **Rational drug designing:** docking algorithms design molecules that bind to the modelled structure, and testing the biological activity of the molecule by biochemical assays.
3. **Large-scale Censuses:** databases efficiently stores the information related to genomes, structures and expression datasets. This information is condensed into understandable facts helpful to the users (Luscombe et al., 2001).

9.2. Objectives:

1. To optimize the structures of human FASN KS and TE domains using their reported crystal structures, for the present docking studies with their specific inhibitors cerulenin and orlistat, respectively.
2. To predict and optimize the structure of human FASN ER domain (modelled on the porcine FASN I crystal structure) that will be further used in docking studies with triclosan (as human ER crystal structure is not available).
3. To study the docking characteristics of the FASN inhibitors (cerulenin, triclosan and orlistat) with their specific catalytic domains *in silico*.
4. To validate the *in silico* docking inhibition constant (Ki) of each inhibitor, by comparing with the experimental IC_{50} values obtained from *in vitro* studies in human Y79 RB cells.

9.3. Materials and Methods

9.3.1. Molecular Modelling and Optimization of FASN domains

The crystal structure of human FASN domains: KS (PDB ID: 3HHD) and TE (PDB ID: 2PX6) domains were obtained from protein data bank. The crystal structure of porcine FASN I (PDB ID: 2VZ8) [http://www.pdb.org/pdb/home/home.do] was used for modelling the ER domain structure, using the MODELLER9v7 program (Fiser & Sali, 2003). All the procured structures were subjected to geometry optimization using Gromos 43a1 force field through Gromacs4.0 molecular dynamics package (Summa & Levitt, 2007). The optimized structures before and after the minimization was validated with Structural Analysis and Verification Server which implements PROCHECK validation (Laskowski et al., 1996). For further docking studies, these optimized and refined structures were used as input.

9.3.2. Optimization of Inhibitors:

The FASN inhibitors cerulenin [Pubchem: 5282054], triclosan [Pubchem: 5564] structures in their three dimensional (3D) SDF - file format were downloaded from NCBI-Pubchem compound (http://www.ncbi.nlm.nih.gov/pccompound) database. They were then converted to PDB format using Babel (http://sourceforge.net/projects/openbabel/). The structural coordinates of the hydrolysed form of orlistat [PDB ID: 2PX6] were retrieved from the PDB. The obtained 3D structures were further geometry minimized in PDB format using ProDRG SERVER (http://davapc1.bioch.dundee.ac.uk/prodrg/).

9.3.3. Docking studies of FASN inhibitors:

AUTODOCK 4.0 suite, a molecular docking tool was used to perform the docking simulations. This tool implements Lamarckian genetic algorithm. This study uses a semi-flexible docking procedure, in which inhibitors are made flexible and the protein is treated as a rigid molecule. The respective catalytic domains of FASN

(pertaining to the inhibitor binding) under study were covered by the docking grid, based on the documented *in vitro* and *in silico* studies. The grid box size in x-, y-, and z- axis were set in accordance to the drug binding site (Pappenberger et al., 2010; Zeng et al., 2011; Maier et al., 2008; Pemble et al., 2007). The spacing between grid points was fixed as 0.375 Å. 100 conformations were considered for each inhibitor for Lamarckian genetic algorithm search during the docking procedure. The population size was set to 150 and the individuals were initialized. Maximum number of energy evaluation was set to 2500000, with 27000 as maximum number of generation and maximum number of top individual that automatically survived was set to 1 with mutation rate of 0.02 and over rate of 0.8 (other parameters were set to default). AUTO DOCK 4.0 was compiled and run under Linux operating system (Morris et al., 1998). According to the root mean square deviation (RMSD) criterion, the results were clustered.

To ascertain the correlation between experimentally-determined IC_{50} value in cancer cells and the predicted binding energy, the best docked conformation of inhibitors was selected based on cluster rank, binding energy and RMSD. The docking results were visualized using Pymol [http://www.pymol.org]. Interactions between enzyme domain and inhibitor were investigated with Ligplot using PDB sum server [http://www.ebi.ac.uk/thornton-srv/database/pdbsum/generate.html].

The Ki or TC_{50}, defined as the theoretical inhibitory constant. It was calculated using autodock from the equation: Ki = exp(deltaG/(R*T)), where: Ki – inhibitory constant or TC_{50}, deltaG – binding energy, R – universal gas constant, T – temperature (Jenwitheesuk et al., 2005).

9.4. Results

9.4.1. Homology modeling of ER domain:

The three dimensional model for human ER domain was obtained from a suitable template using MODELLER9v7. The stereo chemical properties of generated models were validated by Ramachandran plot using PROCHECK tool.

9.4.2. Validation and refinement:

Loop refinement studies were performed with the crystal structures of KS, TE domains and generated best homology model of ER domains using MODELLER9v7. Further, to optimize the protein geometry, steepest descent energy minimization was performed using the GROMOS 43a1 force field. The refined and optimized models were again validated by Ramachandran plot. The optimization results are tabulated (Table 9.2). To further examine the refined structures of FASN domain, QMEAN tool was used, which scores the structure quality as a function of linear combination of 6 structural descriptors (Benkert et al., 2009). QMEAN score ranges between (0-1), higher values are suggestive of plausible models. The root mean square deviation (RMSD) between the main chain atoms of models with its respective templates was also calculated by structural superimpositions by PYMOL, and the corresponding RMSD values are presented in Table 9.2.

9.4.3. Docking studies of FASN inhibitors:

The three inhibitors were found to dock on the documented active sites of FASN, suggestive of predictive accuracy of the semi-flexible docking protocol (Pappenberger et al., 2010; Zeng et al., 2011; Maier et al., 2008; Pemble et al., 2007). Table 9.3 shows the results of the docking experiments, wherein, binding energy, theoretical K_i (TC_{50}) between the FASN domains and their inhibitors are compared with the experimental IC_{50} in the ocular cancer cells incubated for 72 h *in vitro*. For

the purpose of direct comparison, the IC_{50} values of cerulenin and triclosan were converted from μg/ml to μM unit of expression.

The hydrophobic interactions and the hydrogen bonding patterns between the FASN catalytic subunit and its respective inhibitor are detailed below.

9.4.3.1. Molecular Docking with Cerulenin

Cerulenin was found to dock into the reported active site of KS domain of FASN (Pappenberger et al., 2010; Zeng et al., 2011) (Figure 9.5). A careful examination of the binding pocket indicated that cerulenin adopted a position in hydrophobic cage surrounded by Gln78, Ser112, Ser114, Ala160, Cys161, Asn189, Phe200, Glu333 residues. Gly113, Glu115, Val190, Arg224 were found to form five hydrogen bonds with cerulenin. These hydrogen bond and hydrophobic interactions stabilized the binding of cerulenin.

9.4.3.2. Molecular Docking with Triclosan

An *in silico* human model for the ER domain of FASN was developed for performing molecular docking studies with triclosan (Figure 9.6) (Maier et al., 2008). Triclosan was placed in the binding cavity encased by hydrophobic core: Ser1635, Val1636, Ala1645, Val1648, Pro1649, Ser1653, Trp1807, Arg1808, Asp1635, Gln1815 and Ile1818. In addition, triclosan also formed a hydrogen bond with Trp1811.

9.4.3.3. Molecular Docking with Orlistat

The results of orlistat (hydrolyzed form) docking into the reported active site of TE domain (Pemble et al., 2007) is shown in Figure 9.7. The results reveal the hydrophobic interactions between TE domain and orlistat mediated by the following residues: Ile2250, Tyr2307, Asp2338, Glu2366, Ala2367, Phe2370, Phe2423 and leu2427. Four hydrogen bonds were found to be formed with the following residues: Ser2308, Tyr2343, His2481 and Arg 2482.

[*]**Table 9.2: Structural optimization and validation analysis using PROCHECK, Gromacs, QMEAN and Pymol.**

FASN model domain	Ramachandran plot analysis			Energy calculations for models using GROM0S96 Potential Energy (Kcal/mol)	QMEAN Score	RMSD
	Favourable	Allowed	Disallowed			
KS	91.8%	7.9%	0%	-6.40918	0.677	0.075Å
ER	82.5%	16%	0%	-1.50306	0.617	0.058Å
TE	91.0%	8.9%	0%	-2.95823	0.733	0.067Å

Abbreviations: KS – Ketoacyl synthase, ER – Enoyl reductase, TE – Thioesterase, RMSD – Root mean square deviation

[*] *Data presented in table 9.2 is published in: J Ocul Biol Dis Inform. 2010; 3(4): 117-128. Please see List of publications in page XXIII*

Figure 9.5: *In silico* docking studies of FASN KS domain with cerulenin

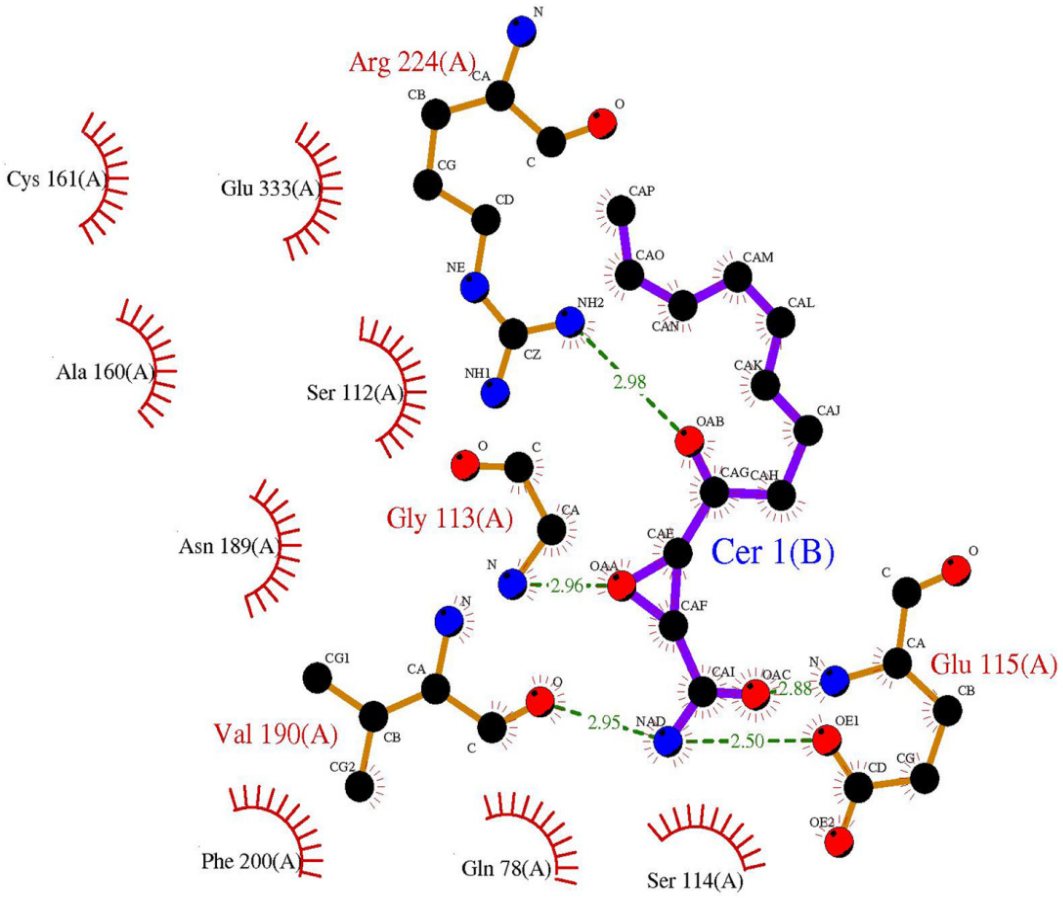

•**Figure 9.5 *In silico* docking studies of FASN KS domain with cerulenin:** The docked complex of human FASN KS domain with Cerulenin. The atoms of the enzyme and the chemical inhibitor involved in the catalysis are shown as coloured spheres: carbon in **black**, oxygen in **red**, and nitrogen in **blue**. Intermolecular hydrogen bonds are shown as **green** dashed lines with their respective bond distances in Angstrom units. The cerulenin is depicted with its chemical structure and labelled as: Cer1 – cerulenin. Image was generated using PDBSUM server.

• *Data presented in figure 9.5 was published in: J Ocul Biol Dis Inform. 2010; 3(4): 117-128. Please see List of publications in page XXIII*

Figure 9.6: *In silico* docking studies of FASN ER domain with triclosan

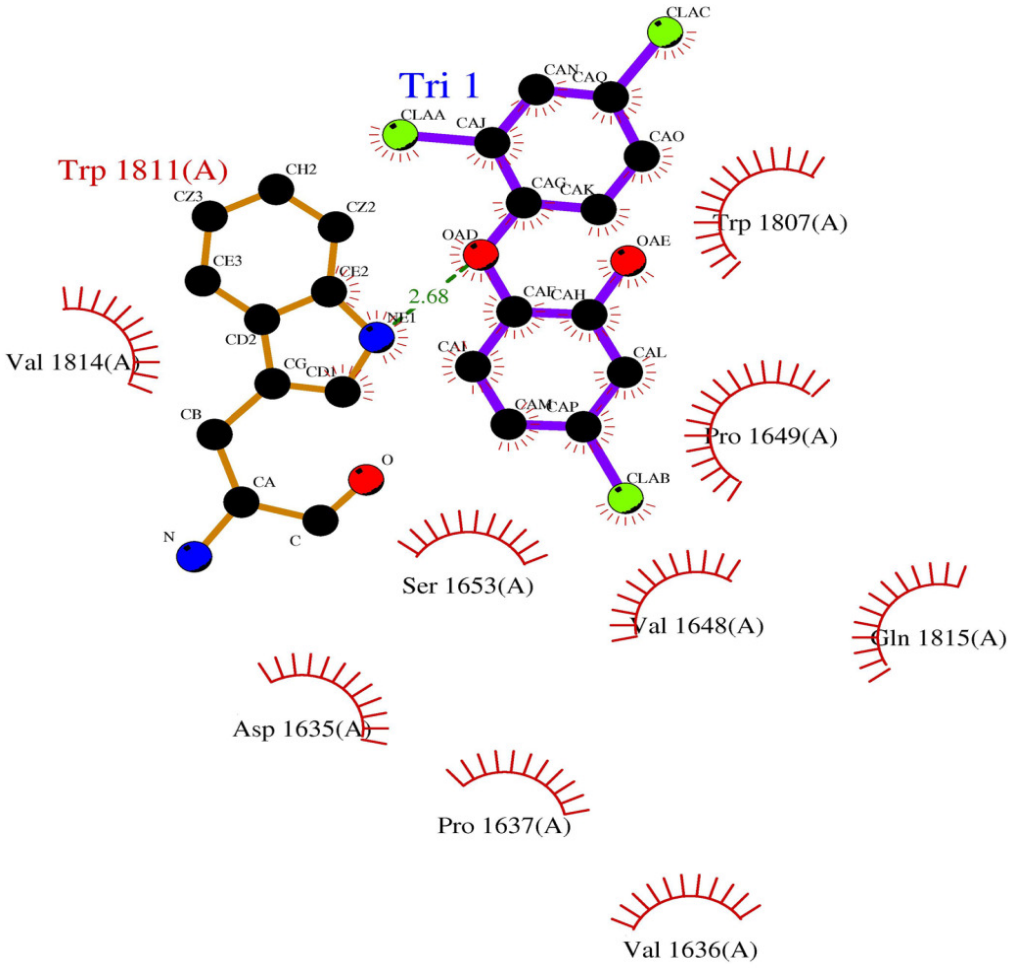

•**Figure 9.6 *In silico* docking studies of FASN ER domain with triclosan:** The docked complex of human FASN ER domain with triclosan. The atoms of the enzyme and the chemical inhibitor involved in the catalysis are shown as coloured spheres: carbon in **black**, oxygen in **red**, nitrogen in **blue** and chlorine in **light green**. Intermolecular hydrogen bonds are shown as **green** dashed lines with their respective bond distances in Angstrom units. The triclosan is depicted with its chemical structure and labelled as: Tri1 – triclosan. Image was generated using PDBSUM server.

• *Data presented in figure 9.6 is published in: J Ocul Biol Dis Inform. 2010; 3(4): 117-128. Please see List of publications in page XXIII*

Figure 9.7: *In silico* docking studies of FASN TE domain with orlistat

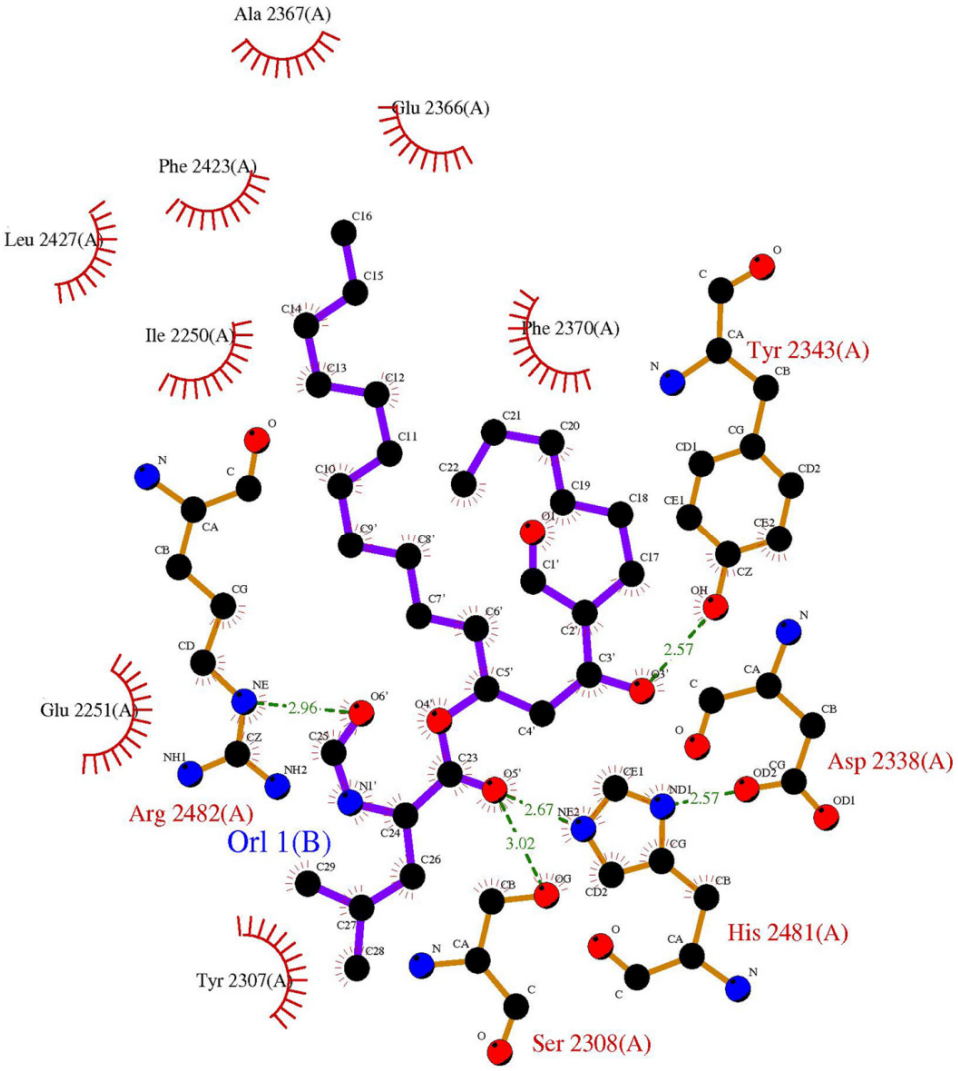

Figure 9.7 *In silico* docking studies of FASN TE domain with orlistat: Docked complex of human FASN TE domain with orlistat. The atoms of the enzyme and the chemical inhibitor involved in the catalysis are shown as coloured spheres: carbon in **black**, oxygen in **red**, and nitrogen in **blue**. Intermolecular hydrogen bonds are shown as **green** dashed lines with their respective bond distances in Angstrom units. The orlistat is depicted with its chemical structure and labelled as: Orl1 (hydrolyzed form) – orlistat. Image was generated using PDBSUM server.

Data presented in table 9.2 was published in: J Ocul Biol Dis Inform. 2010; 3(4): 117-128. Please see List of publications in page XXIII

[*]Table 9.3: Docking characteristics of enzyme – inhibitor interactions compared with cytotoxic IC_{50} obtained in cancer cells *in vitro*.

	***In silico* findings**		***In vitro* findings**	
Docked Complex	**Binding energy (Kcal/mol)**	**Docking inhibition constant (Ki or TC_{50})**	**Experimental IC_{50} at 72h (μM)**	**% Decrease in FASN activity at IC_{50} dosage/72 h of FASN inhibitor treatment (Relative to Control)**
KS – Cerulenin	-5.82	53.93 μM	15.67	64%
ER – Triclosan	-5.73	62.73 μM	25.17	44%
TE – Orlistat	-2.97	6.6 mM	72.5	23%

9.5. Chapter summary

- Human FASN KS and TE domains were optimized and the human ER domain was modelled and predicted based on porcine FASN I crystal structure and was optimised.
- FASN inhibitors were docked with their specific catalytic domains using the above models and the docking characteristics were studied.
- *In silico* docking inhibition constant (Ki) correlated well with the biochemical IC_{50} and FASN enzyme activity in Y79 cells treated with FASN inhibitors.

[*] *Data presented in table 9.3 was published in: J Ocul Biol Dis Inform. 2010; 3(4): 117-128. Please see List of publications in page XXIII*

CHAPTER 10: DISCUSSION

Retinoblastoma (RB) is a primary intra-ocular neoplasm arising from the retinal neuro epithelium that can differentiate into almost any type of outer or inner retinal cell, including photoreceptors (Bakhshi & Bakhshi, 2007). The initiating genetic event in retinoblastoma is the biallelic mutational inactivation of the RB1 gene (chromosome 13q14) in a susceptible retinal cell. This RB1 gene encodes an important tumour suppressor protein that normally functions to inhibit cancer not only in the eye but also throughout the body (Finger et al., 2002). Dimaras et al., 2012 recently reviewed the current status of RB in developing countries, wherein mortality from retinoblastoma is about 40 - 70%, compared with 3 – 5% in Europe, Canada, and the USA. 9000 newly diagnosed RB patients die every year due to delayed progress in creating public and medical awareness and delayed diagnosis (Dimaras et al., 2012). The RB cases in India present with an advanced tumour stage at the time the children are referred to the ophthalmologist, due to delay in diagnosis. In addition RB tumours in India are characterised by aggressive tumour biology (Biswas et al., 2003; Krishnakumar et al., 2007). Zhang et al., 2012 reported the epigenetic deregulation (histone modification and altered DNA methylation of oncogenes and tumour suppressor genes) of multiple cancer pathways in RB tumour samples, as a direct or indirect result of RB1 gene loss.

FASN also known as oncogenic antigen 519 plays a central role in the maintenance of the malignant phenotype by enhancing cancer cell survival and proliferation (Shurbaji et al., 1992). The expression of FASN in RB tumour tissues was studied in Italy by Camassei et al. in the year 2003. This report showed 82% positivity of FASN in RB tumour tissues. Expression of FASN correlated with the RB tumour aggressiveness (Camassie et al., 2003). In this context, the present study evaluated the expression status of the lipogenic enzyme in Indian RB tumour tissues for the first time, so as to evaluate FASN as a clinical target for management of RB by *in*

vitro studies using FASN chemical inhibitors. The results presented in Chapter 4 confirmed that FASN is over-expressed in RB tumour tissues when compared to the non-neoplastic donor retina.

10.1. LIPOGENIC ENZYME FATTY ACID SYNTHASE (FASN) EXPRESSION IN RB TUMOUR TISSUES: CORRELATION WITH CLINICO-PATHOLOGIC FEATURES

RB tumour tissues analysed for FASN immunoreactivity were positive for FASN (100% positivity). However, the expression of FASN was heterogenous within the tumours (Table 4.2). The heterogenous FASN expression in RB tumours is also evident by the presence of varying intensity of the bands in the western analysis of RB tumour tissues (Figure 4.3a). Recognizing the cellular heterogeneity in FASN expression within tumour samples, and the inter-tumour differences in FASN expression levels, the extent of up-regulated FASN expression were quantified in atleast five RB tissues of varying clinical features (Figure 4.4). For comparison, non-neoplastic muller glial cell line, MIO-M1 was used.

Limb et al., 2002 characterized a cell preparation (MIO-M1) derived from human retina, which after several passages *in vitro* retained the characteristic muller cell morphology. This human cell line was suggested to be useful in understanding of normal and pathologic retina, including retinal proliferative diseases (Limb et al., 2002). FASN protein and mRNA was expressed minimally in MIO-M1 cells, and this was used to represent the non-neoplastic cellular FASN expression in the retinal milieu.

With respect to the non-neoplastic muller glial cells, FASN protein over-expression was found to vary between 20- and 287- fold in the RB tumour samples. Similar to the protein expression patterns, FASN mRNA over-expression too varied between the tumour samples (Figure 4.5a). Further, FASN mRNA expression was several folds higher in RB tissues with different clinico-pathological characteristics when

compared with the non-neoplastic muller glial cells. In comparison with the FASN protein over-expression, quantitatively lesser degree of up-regulation of FASN mRNA levels was observed (that is, over-expression of FASN mRNA by 5 – 13 fold, whereas FASN protein over-expressed by 20 – 287 fold). To illustrate this point, two representative RB cases were analyzed for their corresponding FASN protein to mRNA ratio (Figure 4.5c). Here, the increase in FASN protein expression coincided with an increase in mRNA expression in both the RB cases, but the protein expression was multiple folds higher than its corresponding mRNA levels (nearly 4-folds in the focal choroidal invasion and 14- folds in focal RPE invasion sample).

The cellular heterogeneity in FASN immunostaining in RB sections analysed here, corroborated with the FASN expression in mammary tumours (Lu & Archer, 2005). The regulation of FASN may occur atleast in part through post-transcriptional mechanisms that may involve downstream targets of the PI3K pathway (Van de Sande et al., 2002). Rossi et al. (2003) found consistent over-expression of FASN in prostate carcinoma that strongly correlated with prostate tumour initiation and progression. Interestingly, they observed that while most cases showed transcriptional FASN regulation, a subset of cases exhibited post-transcriptional regulation of FASN wherein there was no concordance between FASN mRNA and protein levels (Rossi et al., 2003). FASN expression in both non-invasive and invasive RB indicates that this lipogenic enzyme could be associated with the pathogenesis and progression of retinoblastoma.

10.2. OXIDATIVE STRESS IN RETINOBLASTOMA: CORRELATION WITH CLINICO-PATHOLOGIC FEATURES

Lipogenesis is one of the three major pathways (lactate dehydrogenase, the respiratory chain, and lipid synthesis) that are involved in the maintenance of redox balance of the tumour, during hypoxic states (Chajes et al., 2006). Gonenc et al., 2005 analysed the breast cancer patient serum samples for their oxidative stress marker

levels, antioxidant and lipid content. Malondialdehyde (MDA) levels increased relative to the healthy controls irrespective of the stage of the tumour. In addition serum triglyceride levels were elevated in breast cancer serum samples compared to controls. The elevated cellular lipids were associated with elevated lipid peroxidation in both normal and cancer patient serum samples (Gonenc et al., 2005). Oxidative stress is an important condition that has gained enormous attention, in cancer pathogenesis. Valko et al., 2007 illustrated the dose-dependent effect of the levels of oxidative stress (Low→Moderate→High) on (i) the tumour promotion process, (ii) the process of mutagenesis, and (iii) the process of apoptosis/necrosis. Oxidative stress thus plays favourable and adverse roles during tumour progression (Valko et al., 2007). Studies have shown the elevated levels of lipid peroxidation products in various human cancers (Ray et al., 2000; Manju et al., 2002). The following section discusses the oxidative stress phenomenon in RB tumour tissues and correlation with tumour aggressiveness.

The status of oxidative stress in RB tumour tissues were evaluated by studying the presence of malondialdehyde (MDA) and levels of reactive oxygen species (ROS) in RB tumour tissues. The immunostaining revealed 100% positivity for MDA in all the 34 tumour samples and demonstrated significantly higher levels of MDA in the invasive RB compared to RB with no invasion ($P<0.05$) (Figure 5.2; Table 5.4 & 5.5). Biochemical analysis of lipid peroxidation levels further confirmed that oxidative stress was significantly higher in the invasive tumour tissues when compared with the non-invasive tumours ($P<0.05$) (Figure 5.3; Table 5.6). An earlier report, showed increase in iNOS and nitrotyrosine levels in retinoblastoma (Adithi et al., 2005).

When the intracellular ROS levels in RB tumour tissues were compared with the donor retina (measured in H_2O_2-induced condition), all the tumours showed significantly ($P<0.05$) elevated ROS levels in comparison with the donor retina. Taking into account the clinico-pathologic features of the tumours (Table 5.3), these

results relate the tumour invasion status with the ROS levels. Tumour sample labelled as 1 with choroid invasion alone, had a significantly ($P<0.05$) lower ROS levels in comparison with the tumour sample no. 4 which had invasion of tumour to multiple ocular tissues beyond the optic nerve (Figure 5.4b). This finding was in line with the MDA levels in RB, which correlates oxidative stress with tumour aggressiveness (Figure 5.2).

Oxidant stress environment in Y79 RB cells was induced by H_2O_2 treatment and the resultant gene expression changes (Figure 5.5 & 5.6) were analyzed by microarray and real-time PCR analysis. The differential gene expressions in tumour tissues with respect to donor retina (control) were also investigated. Hydrogen peroxide is an oxidizing agent that is used for experimental evaluation of oxidative stress mechanisms and antioxidant effects (Anantharam et al., 2007). Potential actions of ROS on tumour cells towards proliferation, involves various steps such as cell proliferation, invasiveness, angiogenesis, metastasis and suppression of apoptosis (Halliwell, 2007) (Table A1 & A2; Appendix I). The following section discusses the findings pertaining to the pathways relevant to RB pathogenesis in the presence of oxidants.

10.2.1. Oxidative stress: Oxidative stress can be defined as a serious imbalance between the generation of reactive oxygen species (ROS) and antioxidant protection, where the pro-oxidant nature is favored, causing oxidative injury to cells and tissues (Halliwell, 2011). Oxidative stress induces the gene expression of first line defense antioxidant enzymes glutathione peroxidase (GPX), catalase (CAT) and superoxide dismutase (SOD). These three genes were up-regulated in Y79 RB cells in the presence of H_2O_2, and in all the four tumour tissues studied here.

The genes analyzed by qRT-PCR in Y79 RB cells were also investigated in RB tumour tissues, and compared with non-neoplastic donor retina. The first line antioxidant defense enzymes (SOD, GPX and CAT) act in response to oxidative

stress and scavenge the reactive species. The tumour sample no. 4 with invasion of multiple ocular tissues (Table 5.3) expressed low levels of antioxidant enzyme genes and showed the highest intracellular ROS levels. On the other hand, tumour sample no. 1 with only choroid invasion exhibited higher expression of the antioxidant enzyme gene expression and the lowest ROS levels among the 4 tumours analyzed. Taken together, these results point out the role of oxidative stress in cancer progression, with a breakdown in the innate antioxidant defences.

qRT-PCR analysis of iNOS over-expression in the four RB tumour tissues, showed a range of 9 - 281 fold increase in iNOS mRNA expression (Figure 5.8c), compared to non-neoplastic donor retina. iNOS expression reported in RB and several other tumour tissues correlated with the tumour aggressiveness (Adithi et al., 2005). Nitric oxide (NO) modulates the expression of matrix metalloproteases, MMPs. This correlates well with the present finding of the up-regulation of matrix metalloprotease-2 (MMP2) by an average 7.4 fold increase in four RB tumour tissues indicative of oxidative stress induced promotion of neo-angiogenesis process in RB (Figure 5.8d).

10.2.2. Lipid metabolism: *De novo* lipid synthesis is abnormally elevated in cancer cells accounting for the high membrane turnover in tumour cells, leading to fatty acid accumulation, and impacting cell signaling and gene expression (Mashima et al., 2009). It is also reported that lipid accumulation is stimulated by ROS in HepG2 cells via the activation of SREBP1c, a principal regulator of transcription of lipid metabolic genes. H_2O_2 treatment in HepG2 cells induced the SREBP1c transcriptional activity dose- dependently (Sekiya et al., 2008).

*The present study reports the up-regulation of several genes involved in lipid metabolism such as ACACB with 3.04 fold, MCAT with 3.42 fold up regulation, and

* ACACB - acetyl CoA carboxylase- β; MCAT - malonyl CoA:ACP acyltransferase; HMGCR - HMG CoA reductase; ACOT4 - acyl-CoA thioesterase 4; FABP1/2 - fatty acid binding protein -1/2; ACSL5 - Acyl-CoA synthetase long-chain family member 5; RXRA - retinoid X receptor alpha

other members are HMGCR, ACOT4, FABP1/2, ACSL5, and RXRA were also found to be up-regulated in Y79 cells (Table 5.7; Table A1-Appendix I). Figure 5.8b demonstrates the over-expression of the lipid metabolizing enzymes in RB tumour tissues relative to donor retina (control).

10.2.3. Cell signaling: ROS induced stress in cancer cells activates the various cell signaling pathways such as stress associated kinases (SAPK) and mitogen activated protein kinases (MAPK) pathways (Valko et al., 2007; Davies, 1999; Thannickal & Fanburg, 2000; Benhar et al., 2002; Valko et al., 2006).

♠In the present study, we found that Y79 RB (H_2O_2 oxidant – induced model) cells altered several genes involved in various signal transduction pathways. The up-regulated genes were: MAPK10, MAPK15, MAP2K2 and MAP2K3 in the MAPK pathway; SOCS3, JAK3, STAT4, and CREBBP in the JAK-STAT pathway; and PIK3CG, PIP5K1A in the PI3K signaling pathway (Table A1 & A2; Appendix I), while the microarray analysis revealed the down-regulation of MAP3K5 gene in the MAPK pathway. The up-regulation of CREBBP gene was confirmed by the real-time PCR analysis (Figure 5.7).

Earlier microarray analyses of differential gene expression in retinoblastoma tumor tissues in comparison with non-neoplastic donor retina have suggested the involvement of several pathways including DNA damage and response, AHR signaling and p53 signaling pathways (Ganguly & Shields, 2010) and a dysregulated PI3K/AKT/mTOR pathway (Chakraborty et al., 2007). The current study thus suggests a potential role for ROS in mediating cellular processes in cancer progression.

♠ *MAPK – Mitogen activated protein kinase; SOCS3 - Suppressor of cytokine signaling 3; JAK3 - Janus kinase 3 (a protein tyrosine kinase; STAT4 - Signal transducer and activator of transcription 4; CREBBP - CREB binding protein, transcript variant 1; PIP5K1A - Phosphatidylinositol-4-phosphate 5-kinase, type I, alpha; PIK3CG - Phosphoinositide-3-kinase, catalytic, gamma polypeptide*

10.2.4. Genes involved in cell proliferation, drug resistance and protection against oxidative stress: Crystallin alpha A up-regulation counteracts the oxidative stress mediated cell death. Here, crystallin alpha A was up-regulated 2.11 fold when compared to control. These findings are in line with another report in RB tumor tissues and Y79 cells (Kase et al., 2009). The differential proteomic profiling with RB tumor tissues had revealed a 1.41 fold up-regulation of CRYAA protein expression compared to non-neoplastic retina (Mallikarjuna et al., 2010). Likewise CDC25A essential for cell cycle progression is also found to be up-regulated (Chakraborty et al., 2007) (Figure 5.7). Significant elevation of three members in the HSP70 family, HSPA6, HSPA2 and HSPA1A was observed (Martindale & Holbrook. 2002). Heat shock protein 70 (Hsp 70) family is reported to protect the oxidative stress mediated cell damage, by promoting cell proliferation, reducing the intracellular ROS levels (Jennifer et al., 2002). CREBBP, involved in cell division and cell proliferation is also found to be up-regulated in the oxidant-induced Y79 cells (Figure 5.7) (Chakraborty et al., 2007).

10.2.5. Genes involved in Apoptotic pathway: Several genes in the apoptotic pathway were differentially regulated in Y79 cells (H_2O_2 oxidant – induced model). Few of the up-regulated apoptotic genes are CARD6, BCL2L10, BCL2L11, BAD, BNIP3, and CASP 1 & 8. The down-regulated genes are CARD9, TP53I3, and AIFM2♦ indicating the association of oxidative stress and apoptotic mechanisms in Y79 cancer cells.

Thus, oxidative stress plays a critical role for redox signaling in the pathogenesis of RB. The results here clearly indicate that oxidative stress impacts several cellular processes, including cell cycle progression and apoptotic pathways. Since many anti-neoplastic agents produce oxidative stress in biological systems, the ROS generated during cancer therapy may interfere with the efficacy of the treatment (Conklin, 2004).

♦*CARD6 & 9 - caspase recruitment domain family, member 6 & 9; BCL2L10 & 11 - BCL2-like 10 & 11 (apoptosis facilitator); BAD - BCL2-antagonist of cell death; BNIP3 - BCL2/adenovirus E1B 19kDa interacting protein 3 (BNIP3); CASP 1 & 8 – Caspase 1 & 8; TP53I3 - tumor protein p53 inducible protein 3; AIFM2 – apoptosis-inducing factor, mitochondrion-associated, 2*

Figure 10.1 Lipid and oxidative metabolism in RB tumour pathogenesis – Summarizing our findings

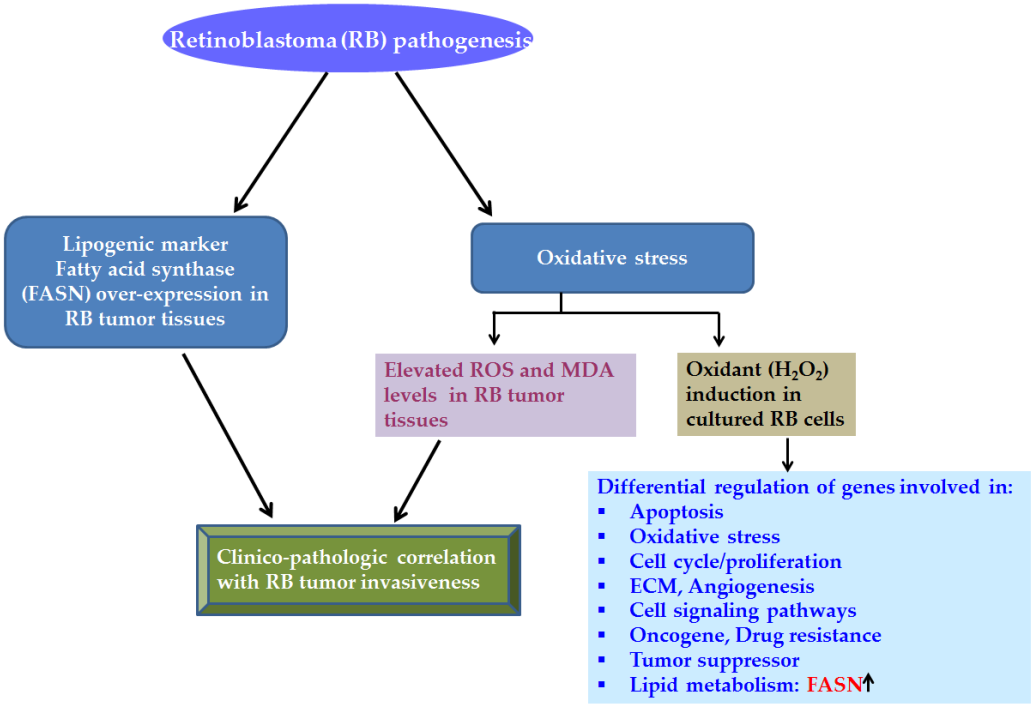

10.3. EVALUATION OF SUITABLE SOLVENT FOR TESTING ANTI-PROLIFERATIVE EFFECTS OF THE HYDROPHOBIC FASN INHIBITOR, TRICLOSAN, IN CANCER CELL CULTURE

Through the chapters 4 & 5 the expression of FASN and the status of oxidative stress in RB tumour tissues and their role in RB tumour pathogenesis were demonstrated. *In vitro* cell culture studies were conducted to analyse the cytotoxic effects of the three FASN inhibitors [cerulenin, triclosan and Xenical™(orlistat)] in cultured RB cancer cells. The optimal solubilization conditions such as, type of the solvent for dissolving the drugs, to use them in cell culture studies were optimised. Being a lipophilic organic molecule, solubilizing triclosan in a solvent followed by culture medium posed some difficulties in testing triclosan's anti-proliferative activity in

cells grown *in vitro* as outlined in Chapter 6. Triclosan has been known for its broad-spectrum anti-microbial activity for nearly three decades (Jain & Pento, 1991) and is also reported to exhibit anti-inflammatory effects (Vischer & Regos, 1974).

The present study reported that, although triclosan was completely soluble in DMSO, NaOH, and ethanol, dilution with culture medium ideal for growing MCF-7 & Y79 cells resulted in turbidity (Figure 6.4) or unfavorable pH change that was not conducive for further testing in cultured cells. On the other hand, both in acetone, as well as in polyethylene glycol-ethanol mixture (PEM), we could obtain a clear solution of solubilized triclosan in culture medium. However, it was verified that, amongst these two solvents, if any of them interfered with the biologic function of triclosan in inhibiting proliferation of MCF-7 and Y79 cells *in vitro*.

Our results clearly indicated that acetone was shown to be a non-cytotoxic solvent in contrast with the cytotoxicity of PEM solvent on both MCF-7 cells & Y79 RB cells (Figure 6.5). This was also confirmed by the apoptotic fragmented DNA induced by PEM solvent on agarose gel electrophoresis, compared to presence of intact DNA in acetone-treated cells (Figure 6.7). The anti-proliferative effect of triclosan in both the solvents on MCF-7 and Y79 RB cells revealed that the IC_{50} in PEM solvent was 1.33- and 1.5- fold higher than acetone solubilised triclosan respectively (Figure 6.8).

The higher IC_{50} of triclosan in PEM implies a decreased drug-sensitivity in PEM solvent, which may be due to the large molecular size of polyethylene glycol (PEG 400) known to form micelle-like structures. These may bind with the triclosan molecule, thus rendering it less available for biological activity (Skaare et al., 1997). The relatively lower IC_{50} of triclosan in acetone indicates its higher biological activity of countering the proliferation of cancer cells grown *in vitro* in comparison with the PEM solvent.

Factors such as the solvent volume required for solubilizing the drug, duration of incubation with the cells, and the specific chemistry of the solvent and the drug (alone and in combination) would determine the choice of the solvent. For instance, Pace and Elliott (1962) found that various cell lines grown *in vitro* showed differences in their degree of sensitivity to different chemicals such as acetone and phenol. They found that the skin cells were more sensitive to acetone's effects than the fibroblast cells, wherein a concentration of 5.0 mg/ml was not toxic to fibroblasts within a 10-day period, although it was noticeably toxic to the skin cells (Pace & Elliott, 1962).

In the present finding, acetone demonstrated favorable physico-chemical and biologic characteristics to solubilize triclosan, and to study its anti-proliferative effects further in Y79 RB cells. A systematic approach for choosing a solvent that not only dissolves the hydrophobic drug but is also compatible biologically for experimentation with triclosan on cells grown *in vitro* was thus investigated and standardised. Further inhibition studies with triclosan were performed with acetone solubilised triclosan.

10.4. ANTI-PROLIFERATIVE EFFECTS OF FASN INHIBITORS [CERULENIN, TRICLOSAN AND ORLISTAT (XENICAL™)] IN CULTURED Y79 RB CELLS

Anti-proliferative effects of FASN inhibitors [cerulenin, triclosan, and Xenical™(orlistat)], were evaluated by optimising the drug dosages in cancerous Y79 RB cells in chapter 6. Cytotoxicity assays with cerulenin, triclosan, and Xenical™ in Y79 RB cells showed dose- and time- dependent decrease in cell viability at 48, 72 and 96 h. The IC_{50} values decreased with increasing time of exposure (Figure 6.9). Further, the sensitivity of RB cells to the FASN inhibitors at 48, 72, and 96 h of exposure was evaluated by increasing the dosage, multifolds higher than their IC_{50}. All the three FASN inhibitors showed a dose-dependent decrease in cell viability

until a particular concentration beyond which increments in concentration did not have any significant effect on cancer cell growth (Figure 6.11).

Cerulenin's cytotoxic effects was most evident at 48 h of treatment, wherein a 2.77-fold increment of the drug dosage induced growth inhibition from 70% to 30%, while triclosan and Xenical™ required increments of 3.6- and 3.7- folds respectively for a similar response. Anti-proliferative effects of triclosan in Y79 RB cells was more sensitive at 72 h, wherein the concentration of triclosan required to decrease cell viability from 70% to 30% after 72 h incubation, was the least (1.8 fold) among the three FASN inhibitors. Similar to the other two FASN inhibitors, Xenical™ also induced dose- and time- dependent anti-proliferative effect in the ocular cancer cells, without adversely affecting the normal cell viability (Figure 6.12). Sensitivity of Y79 RB cells varied for each FASN inhibitor treatment, at the three different times of exposure. Y79 RB cells exhibited more sensitivity to cerulenin at 48 h and to triclosan at 72 h. At 96 h the sensitivity was comparable to both orlistat and triclosan.

In human breast cancer ZR-75-1 cells, cerulenin inhibited fatty acid synthesis and reduced the clonogenic potential within 6 h of treatment, followed by induction of apoptotic cell death, in a dose-dependent manner (Kuhajda et al., 1994). In melanoma cells, triclosan exhibited its anti-proliferative effects at 48 h more effectively than at 24 h (Ho et al., 2007).

Phase contrast microscopy analysis of cell morphology, showed cell shrinkage more evidently at higher dosages of FASN inhibitors and the cells treated with the IC_{50} were comparable to untreated control. This observation was in line with the fact that, FASN inhibitors exhibit their anti-proliferative effects as tumour stasis rather than shrinkage of the cells (Ross et al., 2008) (Figure 6.13).

10.5. SAFETY PROFILE OF FASN INHIBITORS IN NON-NEOPLASTIC CELLS

FASN inhibitors were also evaluated for their toxicity (if any) on two non-neoplastic cells (MIO-M1 and 3T3) (Chapter 7). FASN inhibitors at the IC_{50} dosage of the neoplastic RB cells did not produce comparable toxicity on the normal 3T3 and MIO-M1 cells (Figure 7.2). The cytotoxicity of FASN inhibitors is induced only in FASN over-expressing cancer cells and in the non-neoplastic cells they did not produce comparable toxicity. Thus, FASN non-expressing non-neoplastic 3T3 cells (Lee et al., 2009) and FASN minimally expressing non-neoplastic MIO-M1 cells (section 10.1) served as the normal cells to rule out any non-specific toxicity exerted by the FASN inhibitors, wherein the former was of non-retinal origin, and the latter was of retinal origin.

In order to compare the relative anti-proliferative effects of the three FASN inhibitors on neoplastic versus non-neoplastic cells, therapeutic index (TI) of the three inhibitors were determined. TI was computed as the ratio of the concentration which inhibits 50% viability of the normal cells to the concentration which inhibits 50% viability of tumour cells (Cha et al., 2005b). Inhibitors with high TI are preferred which will be more effective in killing cancer cells at a lower concentration than the inhibitors with a low TI. TI also provides a simple index for evaluating the safety and efficacy of a drug. Cerulenin's highest therapeutic index value (28.6 in 3T3 cells and 9.1 in MIO-M1 cells) among the three FASN inhibitors analysed suggested its effectiveness as an anti-cancer agent (Figure 7.5).

10.6. BIOCHEMICAL EVALUATION OF FASN INHIBITORS IN CULTURED RB CANCER CELLS

10.6.1. Molecular expression of fatty acid synthase (FASN) protein and mRNA post-chemical inhibition

FASN enzyme inhibitors **-** cerulenin, triclosan and orlistat, were evaluated for their anti-FASN effects in Y79 RB cells (Chapter 8). FASN inhibitors showed variable

effect on FASN protein content in Y79 RB cells. This impact on FASN protein content varied with respect to the FASN inhibitor type, inhibitor concentration, and time of exposure with the FASN inhibitor (Figure 8.1).

Cerulenin was reported to decrease the FASN protein expression in colorectal cancer cells and human meningioma cells. This effect was accompanied by deactivation of Akt and apoptotic cell death (Murata et al., 2010; Haase et al., 2010). An earlier report with mammary carcinoma cells had indicated that orlistat showed no effect on FASN protein levels, but it significantly affected the TE domain activity (Knowles et al., 2004). C75, an analogue of cerulenin down-regulated FASN protein levels along with inactivation of Akt in papillary thyroid carcinoma cells (Uddin et al., 2008).

Figure 8.1e reflect the effects of FASN inhibitors on the FASN mRNA expression at their IC_{50} dosages. Inhibition of FASN mRNA expression was by about 2.6 folds with orlistat treatment, while both cerulenin and triclosan showed 1.6 fold decrease in FASN mRNA expression. Sabrina et al., 2003 reported the multiple levels of regulation of FASN at the transcriptional, post-transcriptional levels in prostate tumour tissues. This was also evident in the present work of FASN over-expression in RB tumour tissues (section 10.1). Hunt et al., 2007 suggested that, FASN mRNA is stabilized in the breast cancer cell lines and this led to over-expression of the enzyme. The stable message at the mRNA level, thus promotes translation of more protein (Hunt et al., 2007). These studies suggest the differential effects of FASN inhibitors on FASN protein content and FASN mRNA levels.

In addition to the transcriptional and post-transcriptional regulation, FASN is also regulated at the post-translational level. Several previous studies have observed FASN activity inhibition or activation, without corresponding changes in the FASN protein levels. These changes have also been attributed to the phosphorylation, and acetylation of tyrosine and lysine residues respectively in the FASN protein, which could be the possible regulatory mechanism of the lipogenic enzyme's protein

expression. The phosphorylated FASN (at the tyrosine residue) is detected in mammary cancer cells in contrast to the mammary epithelium. The phosphorylated FASN may represent a cancer-specific isoform of the human FASN enzyme. The role of this isoform in human cancers needs to be identified (Jensen-Urstad & Semenkovich, 2012). In the present study, the consistent effect of FASN inhibitors was the decrease in FASN enzyme activity, while the FASN protein content modulation varied.

10.6.2. Biochemical and metabolic basis for chemical inhibition of fatty acid synthase (FASN)

10.6.2.1. Product (palmitate) depletion:

FASN inhibitors were tested for their effect on the cellular free fatty acid content. Small amounts of free fatty acid may be formed through continuous turnover of membrane lipids for redistribution as phospholipids, cholesterol esters (Spector & Yorek, 1985). Therefore the fatty acid profile on untreated Y79 RB cells was recorded prior (at 0 h) to the experimental incubation period of 48 h. In the present study, all the three FASN inhibitors inhibited the free fatty acid levels markedly (Figure 8.2b).

Kuhajda et al., 2000 measured the biochemical changes in cellular lipids during C75 treatment, prior to the onset of early apoptotic events at 4 h of exposure, in HL 60 leukemia cells. The U-^{14}C acetate incorporation into the free fatty acid pool was reported to reduce by 44% with C75 treatment (Kuhajda et al., 2000).

10.6.2.2. FASN enzyme activity:

FASN inhibitors being irreversible inhibitors of FASN enzyme activity, interact with the FASN enzyme complex. In the present investigation, all the three FASN inhibitors showed marked reduction in FASN enzyme activity, at the IC_{50} and higher dosages, as well as at the three different periods of treatment. The extent of inhibition of FASN enzyme activity in the Y79 RB cells treated with FASN inhibitors

for 48 h and 72 h was found to decrease in the order: cerulenin > triclosan > Xenical™ (Figure 8.3). These findings, showed an order of sensitivity of cerulenin > triclosan > orlistat, which is in line with our observations with the cytotoxicity assay discussed in section 10.4. After 96 h of treatment with the inhibitors, order of decreasing enzyme activity was Xenical™> cerulenin> triclosan.

A previous report in HCT116 colon carcinoma cells correlated the time-dependent effects of FASN inhibitors on inhibition of FASN enzyme activity and DNA replication. In that report, cerulenin and C75 was reported to show 50% inhibition of FASN enzyme activity within 30 min of treatment and inhibition of DNA synthesis by 90 min in HCT116 colon carcinoma cells (Pizer et al., 1998).

10.6.2.3. Substrate (malonyl CoA) accumulation:

FASN inhibitor treated Y79 RB cells were evaluated for malonyl CoA accumulation at 48, 72 and 96 h and malonyl CoA levels were found to increase in treated cells when compared to untreated Y79 RB cells (Figure 8.4). Cerulenin showed highest malonyl CoA accumulation at 48 h, and triclosan and orlistat was more effective at 72 h, proving the consistent sensitivity, exhibited by the three FASN inhibitors similar to their anti-proliferative effects and anti-FASN action. Malonyl CoA accumulation at 96 h treatment with FASN inhibitors was very marginal and ranged between 1.1 – 1.8 fold. Among the three inhibitors orlistat was more effective at 96 h treatment.

FASN inhibition by siRNA in breast cancer cells was reported to result in malonyl CoA accumulation. This was accompanied by inhibition of β-oxidation by inhibiting CPT-1 and accumulation of ceramide (Bandyopadhyay et al., 2005). Ceramide is a sphingolipid that has been associated with death inducers and causes apoptotic cell death. Cerulenin is reported to induce malonyl CoA levels in breast cancer cells by 930%, assayed at 30 min (within the time frame of fatty acid synthesis inhibition).

The increase in malonyl CoA levels is marked in these studies, as the changes during FASN inhibitor treatment are measured prior to the onset of apoptosis of the breast cancer cells.

The present study reports the malonyl CoA accumulation at three different times of exposure – 48, 72, and 96 h. The inhibitory concentrations were their IC_{50} dosages, and a higher dosage where the cell viability was less than 10%. The associated apoptotic events in FASN-inhibited Y79 RB cells under similar conditions, is evident from section 10.6.3, indicating cytotoxicity caused by malonyl CoA accumulation.

10.6.2.4. Lipid profile in non-neoplastic and neoplastic cells:

FASN inhibitors were evaluated for their effects on alterations in lipid levels in Y79 RB (cancer) cells and 3T3 normal cells. Distribution of triglyceride (TGL), phosphatidyl choline (PC) and total cholesterol (TC) in Y79 RB and 3T3 cells were analysed and compared.

The concentration of different lipids in untreated fibroblasts cells was in the order: phosphatidyl choline > cholesterol > triglycerides. Fibroblasts require phosphatidyl choline for their progression beyond the G1 phase of the cell cycle (Tercé et al., 1994). The lipid distribution obtained here was in line with the lipid profile of fibroblasts reported earlier (Spector et al., 1979; Slotte & Bierman, 1988; Lange et al., 1989) (Figure 8.6a). In Y79 cells, the lipids were distributed in the order of phosphatidyl choline followed by total cholesterol and then triglycerides in terms of their cellular concentration (Figure 8.6a). This corroborated with earlier reports of lipid distribution in Y79 cells (Yorek et al., 1985).

To evaluate the relative distribution of lipids in normal 3T3 cells and Y79 RB cells, the proportion of phospholipids to neutral lipids in each cell type was calculated, wherein phospholipids were represented by phosphatidyl choline, and neutral lipids were represented by the commonly esterified lipids – triglyceride and total

cholesterol. In mammalian cells, phosphatidyl choline constitutes 48% - 50% of total membrane phospholipids (Terce et al., 1994; Spector & Yorek, 1985). Relative proportion of phospholipids to neutral lipids was higher in Y79 RB cells compared to normal fibroblast (3T3) cells (Figure 8.6b). While in the Y79 RB (cancer) cells, about 3.3-fold increased turnover of phosphatidyl choline was found relative to their neutral lipids concentration, in the normal fibroblast cells the phosphatidyl choline versus neutral lipids concentrations were almost comparable (PC/neutral lipid ratio = 1.3). The fate of *de novo* synthesized fatty acids differs between normal and malignant cells. In non-malignant and in hepatic cells, palmitate produced is incorporated in TGL, and used as energy source during β-oxidation (Figure 10.2). In contrast tumour cell palmitate, predominantly form the phospholipids of the cellular membranes (Quinn & Wang, 2008).

In cancer cells, FASN plays the prime role in the synthesis of phospholipids and not triglycerides. These phospholipids are partitioned into detergent resistant membrane microdomains that are involved in key cellular processes such as signal transduction, intracellular trafficking, polarization and migration of cells (Swinnen et al., 2003; Kuhajda, 2006). A comparative study with fibroblasts and neuroblastoma cells showed cellular total sterol mass to be 1.9-fold higher in fibroblasts than the neuroblastoma cells. It is also reported that sphingomyelin levels of the plasma membrane are the major determinants of cholesterol distribution in intact cells (Pörn & Slotte, 1990).

10.6.2.5. Lipid profile on inhibition of lipogenesis:

The impact of FASN inhibitors on the cellular lipid content in both cancer (Y79 RB) and normal (3T3) cells were analysed at the anti-neoplastic IC_{50} dosage (Figure 8.7 a & b). Levels of phosphatidyl choline, triglyceride and total cholesterol reduced when compared with the respective untreated cancer cells (control). The altered levels of lipid profile in the present study were evaluated at their cytotoxic IC_{50}. This indicates

the anti-proliferative effects of FASN inhibitors with concomitant decrease in lipogenesis. Kuhajda et al., 2000 reported that acetate incorporation into phospholipids and triglycerides in human leukemia cells, was inhibited by 87% and 89% respectively (Kuhajda et al., 2000).

Cytotoxic effects of flavonoids such as luteolin, quercetin, and kaempferol correlated with their inhibitory effects on phospholipids and triglycerides in prostate cancer cells, indicating the importance of these lipids for cell proliferation (Brusselmans et al., 2005). The flavonoids also inhibited the ^{14}C acetate incorporation in fibroblasts, indicative of inhibition of *de novo* synthesis of lipids. Fibroblasts are reported to possess 20 times lesser FASN activity compared to the FASN activity in prostate cancer cells (Brusselmans et al., 2005). In fibroblasts, membrane lipid turnover takes place even when the cells are not rapidly growing (Spector et al., 1979).

Ross et al., 2008 reported the inhibitory effects of orlistat over phosphatidyl choline and its precursor phosphocholine content in breast and ovarian cancer cell. The inhibitory effects of cerulenin was analysed in breast cancer MCF-7 cells (Ross et al., 2008). In the present experiments, the lipid levels in FASN inhibitor treated normal fibroblast (3T3) cells decreased, compared to untreated control cells.

Figure 10.2: Schematic representation of FASN regulation in normal and cancer cells

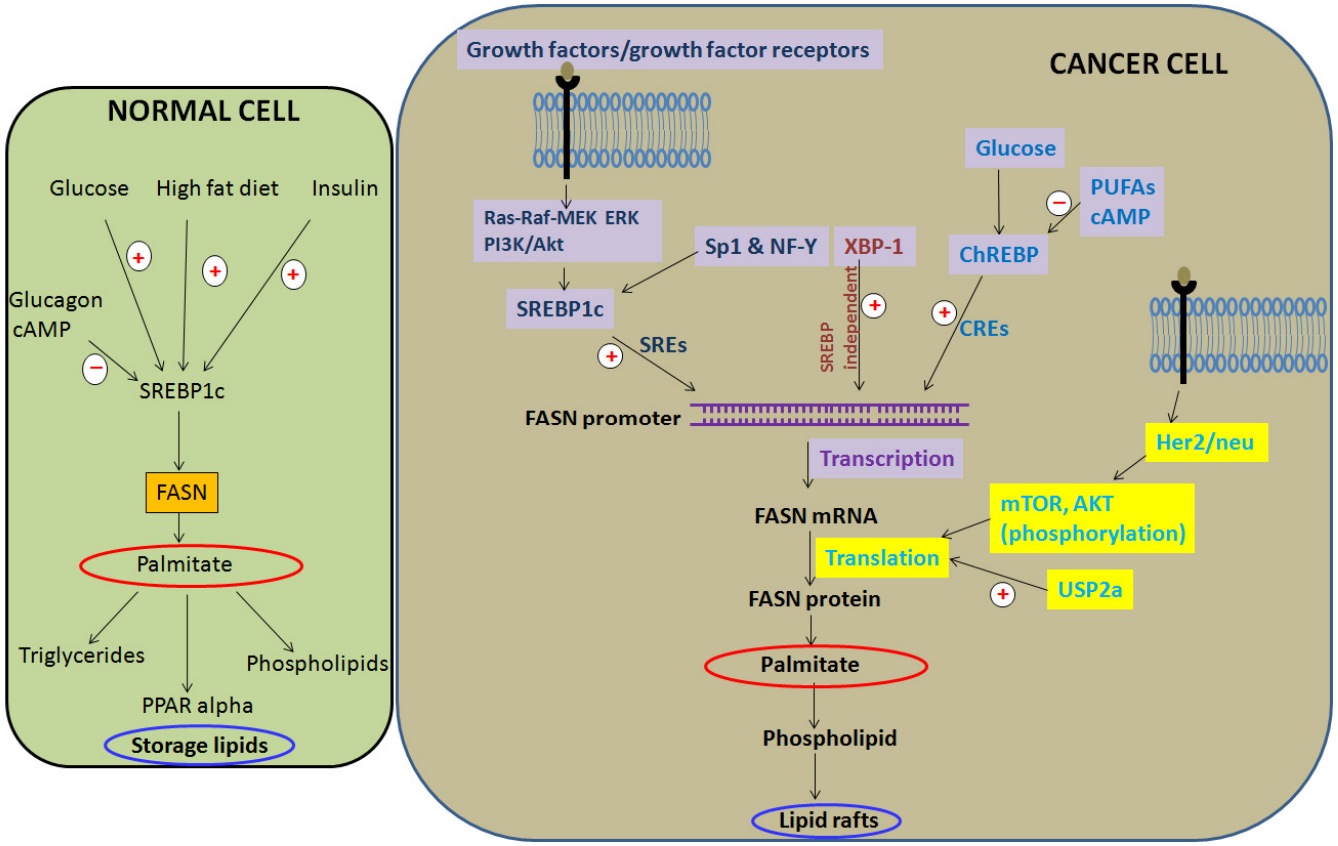

Figure 10.2: Schematic representation of FASN regulation in normal and cancer cells: Regulation of FASN in normal and cancer cells have been depicted. The mechanism that drives the FASN expression in normal and cancer cells and the utilization of its products differs between each other. Palmitate produced in normal cells is stored as triglycerides and in cancer cells the fatty acids synthesized are utilized for membrane production as phospholipids. This picture adapted and modified from Quinn & Wang, 2008

10.6.3. Lipogenic inhibition and Apoptotic effects

10.6.3.1. Apoptotic DNA damage:

The nature of cell damage induced by FASN inhibitors in Y79 RB cancer cells was evaluated by Annexin V staining and agarose gel electrophoretic techniques (Chapter 8). Stronger effects of cerulenin, triclosan and orlistat on DNA were seen with increase in drug concentration, as well as time of incubation, resulting in marked DNA fragmentation (Figure 8.8). Degradation of chromosomal DNA into oligo-nucleosomal sized fragments is very typical of apoptosis, or programmed cell death (Zhang & Xu, 2000). Here, in addition to the DNA fragmentation and smearing, alterations in cell morphology such as cell shrinkage were also observed on drug treatment (Figure 6.13). These results further confirm the anti-proliferative activity of FASN inhibitors. Apoptotic cell death on FASN inhibitor treatment was further substantiated by presence of annexin V positive cells in drug treated samples (Figure 8.9).

Cerulenin-mediated DNA damage was shown in human colonic cancer (LoVo) cells, wherein the characteristic cell morphology changes such as cell shrinkage was reported, along with the nuclear DNA of apoptotic cells appearing as inter-nucleosomal DNA fragments in agarose gel (Huang et al., 2000).

In the present study, cerulenin induced apoptosis was accompanied by lesser amount of necrotic Y79 RB cells at 48 h. Cerulenin, triclosan, and orlistat, all the three FASN inhibitors, showed Annexin V positivity in a dose-dependent manner, in which the percentage of Annexin V positive cells increased dose-dependently and the percentage of live cells decreased when compared with untreated control.

Previous studies with C75 and cerulenin, showed the induction of apoptosis in A-375 melanoma cells. To a lesser extent the inhibitors showed necrotic cell death as evident by PI fluorescence (Ho et al., 2007). Pizer et al., 1996 reported the cerulenin

mediated FASN inhibition and the associated changes such as loss of clonogenic potential, induction of DNA fragmentation and morphologic changes characteristic of apoptotic cell death in breast cancer cells (Pizer et al., 1996).

10.6.3.2. FASN inhibition and oxidative stress:

The nature and the degree of unsaturation of fatty acids determined their sensitivity to lipid peroxidation process. Tumour associated FASN contributes more saturated and monounsaturated fatty acids which are less sensitive to lipid peroxidation, thereby it confers protection to tumour cells from oxidative stress induced apoptotic cell death. During FASN and ACC inhibition with siRNA and soraphen A respectively, the poly unsaturation level increased and mono unsaturation decreased, which led to lipid peroxidation and cell death due to oxidative stress induced apoptosis. FASN inhibition also altered the membrane dynamic properties due to the shift in saturation levels. These findings on the role of *de novo* lipogenesis provided a rationale for exploring FASN inhibitors as anti-neoplastic agents and chemosensitizers (Rysman et al., 2010).

The levels of lipid peroxidation marker, malondialdehyde (MDA), in FASN inhibitor treated Y79 cancer cells were evaluated at 48 h. In the present study, treatment of Y79 RB cells with the three FASN inhibitors increased the MDA levels on an average of 1.66-fold in the supernatant and 3.6-fold in the cell lysates (Figure 8.10).

During FASN inhibition, increased ROS levels is reported to cause oxidative stress which precedes the apoptotic cell death (Zecchin et al., 2011). Previous reports suggested that oxidative stress was induced by depletion of lipids, leading to impaired mitochondrial function (Migita et al., 2009). The above reports substantiate the present findings of apoptotic cell death in Y79 RB cancer cells treated with cerulenin, triclosan and orlistat, concomitant with decrease in lipids and ensuing oxidative stress.

The oxidative stress paradox in cancer progression and cancer control:

ROS contribute to the initiation, promotion and progression of cancer through their effects on the cell cycle, gene expression, DNA damage, apoptosis, angiogenesis and metastasis. This may include modulating the expression of integrins, degradation of extracellular matrix involving matrix metalloproteinases, promoting angiogenesis (by increasing vascular endothelial growth factor, VEGF) resulting in invasiveness and metastasis. Many malignant cells are in a pro-oxidant state producing more reactive species than the body's antioxidant defence and repair activities can cope with. This is evident in the present observations of increased MDA and cellular ROS levels in RB tumours. Enhanced lipogenesis in tumour cells is an adaptive response to redox imbalance during glycolysis. It is also believed that the main role of increased fatty acid biosynthesis is to maintain this redox balance through NADPH oxidation (Chajes et al., 2006). Taken together, the increased oxidative stress and lipogenic FASN over-expression may thus contribute to the aggressiveness of RB (as indicated in the findings in Chapters 4 and 5).

The palmitate alters the mitochondrial membrane and protects prostate cancer cells from diffusion of ROS outside the mitochondria. Relating oxidative stress to cancer control, FASN siRNA caused increase in ROS levels, which resulted in decreased cell proliferation. This effect was counteracted by the addition of palmitate (the product of FASN) to the medium (Migita et al., 2009). Depletion of cellular palmitic acid may be associated with the induction of apoptosis along with concomitant production of ROS and mitochondrial impairment (Chajes et al., 2006). These results indicate that oxidative stress could contribute to carcinogenesis as well as can be used therapeutically. This 'double way sword' nature of oxidative stress (Tandon et al., 2005) is evident in RB pathogenesis, and during the therapeutic lipogenesis-inhibition in RB cells *in vitro*.

Chajes et al. suggested that the effects of dietary intake of lipids such as palmitate and vitamin E may need to be considered for their impact on the efficacy of anti-lipogenic cancer treatment strategies (Chajes et al., 2006). In addition, oxidative stress and oxidative damage could be measured by developing a 'redox signature score' that combines parameters of oxidative damage with those of redox state, DNA repair activity and antioxidant defence. This would be a useful therapeutic tool that would predict the outcome of cancer therapy in patients in a better way (Halliwell, 2007).

10.6.3.3. Differential gene expression on cerulenin treatment:

Differential gene expression profile of Y79 RB cells treated with a FASN inhibitor, cerulenin (7μg/ml – IC_{50}) was studied by microarray analysis. The genes that were differentially regulated were categorised as various pathways/processes (Table A2 & A3; Appendix I) — lipid metabolism, cell cycle, cell proliferation, apoptosis and carbohydrate metabolism (Figure 8.11c). Several genes of importance were validated by real time quantitative PCR (FASN, SKP2, CYCS, PPARA, RXRA, CDK2AP1, ACACB, SSTR2). The real time PCR findings (Figure 8.11b) were consistent with that of the microarray analysis.

An earlier study by Vazquez-Martin et al. the cDNA microarray analysis of cerulenin-treated breast cancer cells had resulted in up-regulation of several genes such as TGF-β2, genes of insulin signaling pathway, caspase 7 in apoptosis and down-regulation of GRB7 (HER2 pathway), FGF5, inhibin and IL-11 (Vazquez-Martin et al., 2004). The following section illustrates the metabolic oncogene nature of FASN, and its potential as an anti-cancer target in retinoblastoma.

10.6.3.3a. Lipid metabolism: Targeting the key lipogenic enzyme, FASN, resulted in aberrant expressions of several genes in the lipid metabolism that in turn explains the anti-proliferative effect of cerulenin observed in the RB cancer cells. The rate-

limiting step in lipogenesis is catalysed by acetyl CoA carboxylase β (ACACB, upstream enzyme of FASN). ACACB which synthesizes malonyl CoA from acetyl CoA, was significantly down-regulated -1.4978 folds in cerulenin-treated Y79 RB cells. To a lesser extent, cerulenin treatment resulted in down-regulation of FASN; microarray analysis revealed down-regulation of FASN expression by -0.1119 folds (statistically non-significant), and by -1.69 fold by real time PCR with respect to untreated control (Figure 8.9b).

Cerulenin treatment also affected certain nuclear receptors that are responsible for lipid homeostasis regulation. Peroxisome proliferator activator receptors (PPARs) are the nuclear receptors that regulate the transcription of genes involved in lipid metabolism and cell differentiation. They are predominantly expressed in metabolically active tissues. Gene expression of PPARA is activated in the presence of fatty acids. PPARA forms a tripartite complex with retinoid X receptor alpha (RXRA), which stimulates the PPARA to bind to its response elements peroxisome proliferator response elements (PPRE), to induce the transcription of PPAR responsive genes and the genes involved in lipid metabolism (Michalik et al., 2006; Issemann et al., 1993). In the present study, PPARA and RXRA were significantly down-regulated by -1.80 and -1.83 folds respectively.

10.6.3.3b. Cell cycle: The present analysis showed down-regulation of SKP2 gene expression by -1.6 fold and up-regulation of CDK2AP1 by 1.2177 folds on cerulenin treatment. These results show that cerulenin mediated anti-proliferative effects involve important genes associated with cell cycle control.

SKP2 (S phase kinase-associated protein 2) is an F box protein of the SCF family ubiquitin ligases. It is a negative regulator of cell cycle that targets several negative cell cycle regulators such as p21, p27, p57, and p130, at the critical cell cycle checkpoints of the retinoblastoma protein (pRb) pathway (Knowles et al., 2004). Orlistat, was reported to down-regulate SKP2 on breast cancer cells, leading to cell

cycle arrest at G1/S phase entry (Knowles et al., 2004). CDK2AP1 is an S phase regulator of cell cycle, by interacting with two components CDK2 and DNA polymerase α/ primase.

10.6.3.3c. Apoptosis: Cytochrome c (CYCS) a mitochondrial redox protein is released from mitochondria to the cytosol during apoptosis. This released protein binds to the adaptor protein Apaf-1 and procaspase-9, thus forming an apoptosome complex which activates the caspase cascade. CYCS was found to be up-regulated by 1.2 folds after cerulenin treatment, indicating the involvement of mitochondria during apoptosis of retinoblastoma cells.

A previous report on cerulenin mediated apoptosis in various cell lines of breast and colon cancers showed the rapid release of CYCS from the mitochondria into the cytosol (Heigligtag et al., 2002).

10.6.3.3d. Cell Proliferation: Cerulenin treatment down-regulated RICTOR by -1.93 folds in RB cells. RICTOR (Rapamycin-insensitive companion of mTOR) is a serine-threonine kinase that belongs to the mTOR (mTORC2 family) pathway of proteins, which are involved in cancer progression (Roulin et al., 2010). Bim L interacts with the DBD domains of the GRB10 in which case, the phosphorylation sites in the DBD domains of GRB10 are important for this interaction and thus regulates the anti-apoptotic activity of Bim L (Hu et al., 2010). In the present microarray analysis, Bim L and GRB10 were found to be down-regulated by -1.1578 fold and -1.065 fold respectively, on cerulenin treatment.

To sum up, the differential gene expression analysis revealed that chemical inhibition of lipogenic fatty acid synthase influenced key molecules in the cell cycle, cell proliferation and apoptotic pathways in RB cancer cells. This in part explains the molecular mechanisms responsible for the anti-cancer effects of targeting lipid metabolism in RB.

10.7. MOLECULAR DOCKING ANALYSIS OF FASN WITH CHEMICAL INHIBITORS

Further to the biological understanding of the FASN inhibitor mediated biochemical and molecular mechanisms in the *in vitro* conditions, the *in silico* docking interactions of these inhibitors with their specific catalytic domains were studied (Chapter 9). Docking results of each inhibitor with the respective catalytic domain revealed significant binding energy, indicating the predictive accuracy of the *in silico* methods adopted. The molecular docking performed here predicted the hydrophobic and hydrogen bonding interactions, and the amino acid residues involved in the active site binding between the three FASN domains and their corresponding inhibitors (Figure 9.5- 9.7).

It is well known that hydrogen bonds and hydrophobic interactions are vital in maintaining the secondary and tertiary structures of biological macromolecules such as DNA and proteins. Hydrogen bonds are also involved in the binding of ligand to active sites of proteins, wherein they contribute to the orientation, recognition, and affinity of the ligand (Kubinyi, 2007). While, hydrophobic interactions between lipophilic surfaces of a ligand and hydrophobic areas of its binding site always contribute positively to binding affinity, the contribution of hydrogen bonds to the overall free binding energy depends on the balance of the desolvation energies and the energies of the newly formed hydrogen bonds, where changing a single functionality of a ligand may have very complex consequences (Kubinyi, 1998).

The theoretical inhibitory constant (Ki or TC_{50}), indicates the molecular affinity between the enzyme active site and the inhibitor, where Ki is inversely related to enzyme affinity. Here, the Ki shown by the FASN inhibitors were in the order, cerulenin < triclosan < Xenical™ (orlistat). Correspondingly, the extent of inhibition of FASN enzyme activity in the ocular cancer cells *in vitro* was found to decrease in the order: cerulenin > triclosan > Xenical™ (orlistat) (Table 9.3). Further, the therapeutic potential of these inhibitors was assessed by the 50% inhibitory

concentration (IC_{50}) in ocular cancer cells. The IC_{50} values were in the order, cerulenin < triclosan < orlistat, implicating the therapeutic potential in the order, cerulenin > triclosan > orlistat (Figure 7.5). The excellent agreement between the molecular docking analysis and the biochemical analysis presented here shows that greater affinity between the FASN enzyme and its inhibitor confers a better biochemical potential to the inhibitor to exert its anti-cancer effect.

Despite the molecular affinity potentials predicted *in silico* and confirmed by *in vitro* assays, the clinical effectiveness of FASN inhibitors in cancer therapy is determined by several factors. For instance, the present analysis indicates cerulenin to be a better cytotoxic agent than triclosan and orlistat. Yet, its reactive epoxide group makes it chemically unstable, limiting its clinical efficacy. This led to synthesis of analogues of cerulenin, such as C75 and C93 that have been tested for their anti-cancer efficacy. C75 causes anorexia and weight loss with parallel stimulation of fatty acid oxidation (Kuhajda et al., 2000), while C93 significantly inhibited FASN without causing anorexia and weight loss in lung cancer cells (Orita et al., 2007). In this context, triclosan's inhibition site, ER domain, may be an attractive target for developing anti-FASN metabolites as its blockade is suggested to increase the levels of the enoyl thiolester intermediate that closely resembles cerulenin and C75 (Menendez & Lupu, 2007). Triclosan's high affinity and slow rate of dissociation contributes to its potency and duration of action (Ward et al., 1999). Orlistat inhibits the TE domain, which catalyses the release of the end-product, palmitate, from FASN. The β-lactone, orlistat has poor solubility and low oral bio-availability (Menendez & Lupu, 2007; Ballinger & Peikin, 2002) hence alternative formulations may alleviate this limitation, and assist in tapping the anti-cancer potential of targeting the TE catalytic domain. Through *in silico* molecular docking analysis, drugs can be designed to improve binding affinity, therapeutic efficacy and bioavailability through optimized hydrophobic interactions and hydrogen bonding that would stabilize the drug ligands at the target active site (Patil et al., 2010).

RB tumours have been managed and treated with conventional treatment procedures of enucleation and chemotherapy. In addition, recent development in the RB treatment highlights the use of intra-arterial chemotherapy which is a novel alternative approach for conventional treatment procedures (Shields et al., 2011; Shields et al., 2012). Apart from the existing strategies of therapy, identification of novel therapeutic targets will be of great use. This is facilitated in the present study, by the molecular understanding of the association of FASN over-expression with the development and progression of RB, particularly with the aggressive biology of the disease. This lipogenic enzyme holds immense scope as a therapeutic target for retinoblastoma.

Figure 10.3: Anti-cancer effects of FASN inhibitors: Summarizing our experimental findings

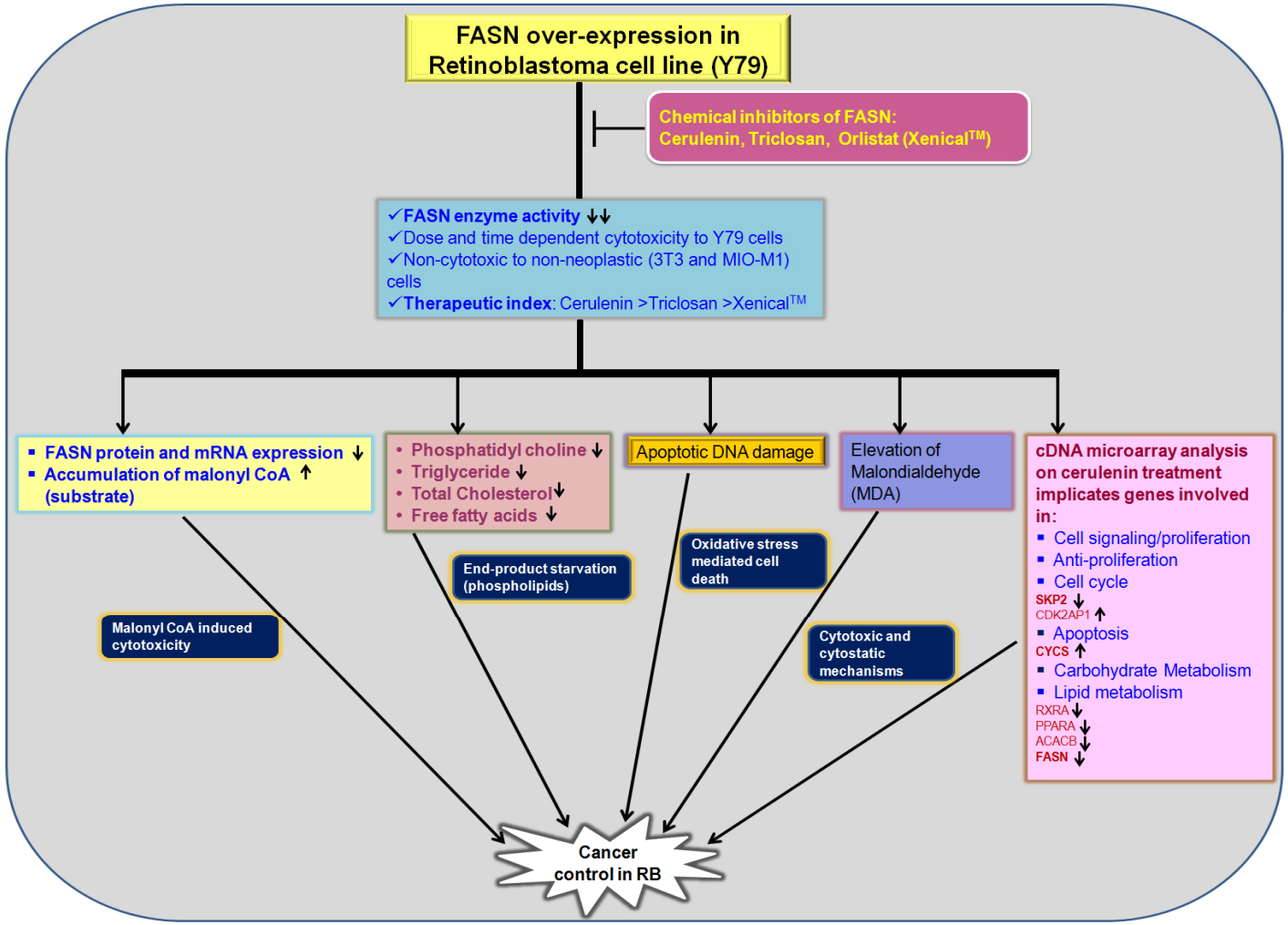

CONCLUSION

- Fatty acid synthase immunoreactivity was negative in non-neoplastic donor retina except for the focal positivity in the ganglion cells. RB tumour tissues revealed cytoplasmic FASN positivity in all the forty four tumour tissues analysed. FASN immunoreactivity was markedly higher in poorly differentiated and in RB tumour tissues invading the choroid and optic nerve and/or orbit. Multi-fold over-expression of FASN mRNA and protein were observed in RB tissues, although at varying levels[*1].

- Oxidative stress was evident in RB tumour tissues by evaluating the presence of malondialdehyde (MDA-biochemical indicator of lipid peroxidation) and its correlation with the RB tumours invading the ocular tissues such as choroid, optic nerve and/or orbit. This was further confirmed by inverse correlation between gene expression of antioxidant enzymes (SOD, GPX, CAT) and the levels of ROS in RB tumors. Microarray analysis of Y79 RB cells (H_2O_2 oxidant-induced model) showed differential expression of several cellular processes such as lipid metabolism, cell proliferation, and angiogenesis and various cell signaling pathways such as JAK-STAT, PI3K and MAPK pathways. Several up-regulated genes such as SOD, GPX, CAT, CDC25A, CREBBP, JUN, MMP2, iNOS, CRYAA, RXRA, ACACB and HMGCR were validated by real time PCR. These results corroborated with the higher gene expression levels in RB tumor tissues compared to the non-neoplastic donor retina[*2, *3].

- The solubilization conditions for testing the anti-proliferative effects of FASN inhibitors (cerulenin, triclosan and orlistat (Xenical™) in cell culture conditions were optimised. FASN inhibitors showed dose- and time-dependent cytotoxic effects in Y79 RB cells. The IC_{50} dosages of each inhibitor were determined at 48, 72 and 96 h. Sensitivity of Y79 RB cells to each

inhibitor in causing cytotoxic effects with respect to time of exposure and concentration were compared[*4, *5, *6].

- FASN inhibitors were also tested for their safety in two non-neoplastic cells (MIO-M1 and 3T3) and were found to be non-toxic to these normal cells at their anti-neoplastic IC_{50} dosage. The therapeutic index defined as the ratio of the drug-concentration which inhibits 50% viability of the normal cells to the concentration which inhibits 50% viability of tumour cells was observed to be in the order cerulenin > triclosan > orlistat (Xenical™) [*5].

- In Y79 RB cells, treatment with FASN inhibitors (cerulenin, triclosan, and orlistat) brought about moderate decrease in expression of FASN protein and mRNA expression. Significant decreases in FASN enzyme activity, along with modulation of free fatty acid levels were observed. FASN inhibition resulted in accumulation of malonyl CoA (substrate). FASN inhibitor treated RB cancer cells and normal fibroblast cells showed decrease in the cellular lipid levels (triglyceride, cholesterol and phosphatidyl choline). Cytotoxicity of FASN inhibitors may be mediated via apoptotic mechanisms (indicated by Annexin V analysis and DNA fragmentation assay) with concomitant increase in lipid peroxidation marker malondialdehyde[*5].

- Microarray analysis of cerulenin treated Y79 RB cells revealed differential expression of genes involved in various cellular processes such as lipid metabolism, cell cycle/apoptosis, cell signaling/proliferation. Cerulenin treatment in Y79 RB cells revealed up-regulation of cytochrome c (CYCS) by 1.2 folds, while S-phase associated protein kinase-2 (SKP2), a negative regulator of cell cycle, and the lipid metabolic genes (PPARA, RXRA and ACACB) were significantly down-regulated by -1.59,-1.8, -1.83, and -1.5 folds respectively, in comparison with untreated Y79 RB cells[*7].

- Molecular docking was carried out with each of the three catalytic domains of FASN (KS, ER, TE) with the FASN inhibitors and the docking characteristics were studied. Human FASN keto acyl synthase (KS) and thioesterase (TE) domain structures were optimized. Human enoyl reductase (ER) domain was modelled and predicted based on porcine FASN I crystal structure and was optimised. *In silico* docking inhibition constant (Ki) correlated well with the biochemical IC_{50} and FASN enzyme activity in Y79 cells treated with FASN inhibitors*6

- These studies suggest FASN to be a potential therapeutic target in the clinical management of retinoblastoma.

---

*1 ***Vandhana S,*** *Deepa PR, Jayanthi U, Biswas J, Krishnakumar S. Clinico-pathological correlations of fatty acid synthase expression in retinoblastoma: an Indian cohort study.* ***Exp Mol Pathol****. 2011 Feb;90(1):29-37.*

*2 *Deepa PR, Nalini V, Mallikarjuna K,* ***Vandhana S,*** *Krishnakumar S. Oxidative stress in retinoblastoma: correlations with clinicopathologic features and tumor invasiveness.* ***Curr Eye Res.*** *2009 Dec;34(12):1011-8.*

*3 ***Vandhana S****, Lakshmi TS, Indra D, Deepa PR, Krishnakumar S. Microarray Analysis and Biochemical Correlations of Oxidative Stress Responsive Genes in Retinoblastoma.* ***Curr Eye Res.*** *2012 Sep; 37(9):830-41.*

*4 ***Vandhana S,*** *Deepa PR, Aparna G, Jayanthi U, Krishnakumar S. Evaluation of suitable solvents for testing the anti-proliferative activity of triclosan – a hydrophobic drug in cell culture.* ***Indian J Biochem Biophys.*** *2010 Jun;47(3):166-71.*

*5 Deepa PR, ***Vandhana S,*** *Jayanthi U, Krishnakumar S. Therapeutic and Toxicological Evaluation of Anti-Lipogenic Agents in Cancer Cells Compared with Non-Neoplastic Cells.* ***Basic Clin Pharmacol Toxicol.*** *2012, 110, 494-503.*

*6 Deepa PR, ***Vandhana S,*** *Muthukumaran S, Umashankar V, Jayanthi U, Krishnakumar S. Chemical inhibition of fatty acid synthase: molecular docking analysis and biochemical validation in ocular cancer cells.* ***J Ocul Biol Dis Inform.*** *2010; 3(4): 117-128*

*7 Deepa PR, ***Vandhana S,*** *Krishnakumar S. Fatty Acid Synthase Inhibition Induces Differential Expression Of Genes Involved In Apoptosis And Cell Proliferation In Ocular Cancer Cells. Short communication.* ***Nutrition and Cancer.*** *2013; 65(2): 1-6*

FUTURE SCOPE

1. Novel small molecule inhibitors targeting FASN could be identified. Chemical modification of existing inhibitors will help in overcoming their limiting properties [For e.g. chemical instability of cerulenin (Kuhajda et al., 2000), low oral bioavailability of orlistat (Ballinger & Peikin, 2002)]. Analogues of cerulenin- C75 & C93 (Kuhajda et al., 2000; Orita et al., 2007) both of which lack the reactive epoxide have also been developed.

2. Crystal structure of some of the human FASN domains [enoyl reductase (target for triclosan inhibition), keto acyl reductase and dehydratase domains], which are not currently available, needs to be elucidated. Using bioinformatics tools, more inhibitors targeting these newly elucidated domains could be identified.

3. In addition to chemical inhibition of FASN, studying the effects of FASN gene silencing by RNAi strategies, in cultured RB cells will provide way to understand the molecular mechanisms involved in FASN mediated apoptosis in cancer cells.

4. FASN inhibitors in combination with conventional cancer chemotherapeutic drugs can be evaluated for their combination index and synergistic effects, which would in turn reduce high dosage chemotherapy and the associated non-specific toxic side-effects (Menendez et al., 2005).

5. Wang et al. (2001) reported a sensitive two-site ELISA for FASN protein which detected the over-expression of FASN protein in serum samples from patients with breast, prostate, colon and ovarian cancers when compared with healthy controls. In another report, Wang et al. (2004) found marked increase in serum FASN protein in breast cancer patients, and suggested that extracellular FASN may serve as a potential prognostic and diagnostic marker

in human breast cancer. Thus serum FASN can be explored as a potential cancer biomarker in RB.

6. The growing importance of the research and development of FASN inhibitors for treating human diseases (such as diabetes, cancer, immune and proliferative diseases) is clearly evident from the patents involving FASN inhibitors. A list of patents in this area was recently published in the journal "Recent Patents on Endocrine, Metabolic & Immune Drug Discovery" by López and Diéguez in the year 2007. A partially modified list from this article is presented here for reference (Table A):

Table A: List of patents involving FASN inhibitors in various human disorders (López and Diéguez, 2007):

Patent number	**Patent Title**	**Country/ Organization**
CN1728994A	Method for inhibiting cancer development by fatty acid inhibitors	China
EP0869784B1	Inhibition of fatty acid synthase as a means reduce adipocyte mass	European Patent Office (EPO)
EP1565180A2	A method for inhibiting cancer development using fatty acid synthase inhibitors	European Patent Office (EPO)
MX5004390A	A method for inhibiting cancer development using fatty acid synthase inhibitors	Mexico
WO05107801A2	Systems and methods for treating human inflammatory and proliferate diseases, with a combination of fatty acid metabolism inhibitors and glycolytic inhibitors and/or UCP and/or FAS antibodies	World Intellectual Property Organization (WIPO)
WO05070126A3	Methods and compositions for treating human diseases and wounds with FAS inhibitors	World Intellectual Property Organization (WIPO)

REFERENCES

BOOKS, CONFERENCE PROCEEDINGS AND WEB RESOURCES

(2001) Schilling, H., H. Yang, et al. "Changes in the retinal pigment epithelium and choroidal invasion in 297 enucleated eyes with retinoblastoma: histologic staging and metastatic rate." Xth International Congress of Ocular Oncology.

(2003) Murray, R.K., D.K. Graner, et al. "Harper's Illustrated Biochemistry." Mc Graw Hill Inc; 26th ed, pp 173-77.

(2004) Vazquez-Martin, A., G. Moreno, et al. "Microarray gene expression analysis of fatty acid synthase (FAS) signaling on breast cancer cell lines." *Journal of Clinical Oncology*, ASCO Annual Meeting Proceedings (Post-Meeting Edition) 22, 9690

(2005) Cukier, D., F. Gingerelli, et al. "Coping with chemotherapy and radiation." Ch 2, pp-23.

(2007) Krishnakumar, S., A. Mohan, et al. "A pilot study on the expression of human papilloma virus genome in Asian Indian retinoblastoma." Invest Ophthalmol Vis Sci 48 EAbstract1591.

(2007) Kubinyi, H. "Hydrogen Bonding: The Last Mystery in Drug Design? in pharmacokinetic Optimization in Drug Research: Biological, physicochemical, and Computational Strategies." Zürich: Verlag Helvetica Chimica Acta.

(2008) Quinn, J.P. and X. Wang, "Lipids in health and disease." Vol 49, Ch 7, pp-169.

(2009) Singh, K.K., and L.C. Costello, "Mitochondria and cancer." Ch.2,pp 39

(2010) Indian Council of Medical Research (ICMR) Publications, National Guidelines in the Management of Retinoblastoma, pp. 1–66.

(2012) American Cancer Society. Cancer Facts & Figures 2012. Atlanta:American Cancer Society; http://www.cancer.gov/cancertopics/cancerlibrary/what-is-cancer

RESEARCH ARTICLES

Adithi, M., V. Nalini, et al. (2005). "The role of nitric oxide synthases and nitrotyrosine in retinoblastoma." Cancer **103**(8): 1701-1711.

Anantharam, V., E. Lehrmann, et al. (2007). "Microarray analysis of oxidative stress regulated genes in mesencephalic dopaminergic neuronal cells: relevance to oxidative damage in Parkinson's disease." Neurochem Int **50**(6): 834-847.

Bakhshi, S., and R. Bakhshi (2007). "Genetics and management of retinoblastoma." J Indian Assoc Pediatr Surg **12**(3): 109-15.

Ballinger, A. and S. R. Peikin (2002). "Orlistat: its current status as an anti-obesity drug." Eur J Pharmacol **440**(2-3): 109-117.

Bandyopadhyay, S., S. K. Pai, et al. (2005). "FAS expression inversely correlates with PTEN level in prostate cancer and a PI 3-kinase inhibitor synergizes with FAS siRNA to induce apoptosis." Oncogene **24**(34): 5389-5395.

Bandyopadhyay, S., R. Zhan, et al. (2006). "Mechanism of apoptosis induced by the inhibition of fatty acid synthase in breast cancer cells." Cancer Res **66**(11): 5934-5940.

Benhar, M., E. David, et al. (2002). "ROS, stress-activated kinases and stress signaling in cancer." EMBO reports **3**: 420-425

Benkert, P., M. Kunzli, et al. (2009). "QMEAN server for protein model quality estimation." Nucleic Acids Res **37**(Web Server issue): W510-514.

Bhargava, H. N. and P. A. Leonard (1996). "Triclosan: applications and safety." Am J Infect Control **24**(3): 209-218.

Biswas, J., D. Das, et al. (2003). "Histopathologic analysis of 232 eyes with retinoblastoma conducted in an Indian tertiary-care ophthalmic center." J Pediatr Ophthalmol Strabismus **40**(5): 265-267.

Browne, C. D., E. J. Hindmarsh, et al. (2006). "Inhibition of endothelial cell proliferation and angiogenesis by orlistat, a fatty acid synthase inhibitor." FASEB J **20**(12): 2027-2035.

Brusselmans, K., R. Vrolix, et al. (2005). "Induction of cancer cell apoptosis by flavonoids is associated with their ability to inhibit fatty acid synthase activity." J Biol Chem **280**(7): 5636-5645.

Bunkoczi, G., S. Misquitta, et al. (2009). "Structural basis for different specificities of acyltransferases associated with the human cytosolic and mitochondrial fatty acid synthases." Chem Biol **16**(6): 667-675.

Bunkoczi, G., S. Pasta, et al. (2007). "Mechanism and substrate recognition of human holo ACP synthase." Chem Biol **14**(11): 1243-1253.

Burr, D.B., S. A. Molina, et al. (2011). "Treatment with connexin 46 siRNA suppresses the growth of human Y79 retinoblastoma cell xenografts in vivo." Exp Eye Res **92**(4): 251-9.

Camassei, F. D., R. Cozza, et al. (2003). "Expression of the lipogenic enzyme fatty acid synthase (FAS) in retinoblastoma and its correlation with tumor aggressiveness." Invest Ophthalmol Vis Sci **44**(6): 2399-2403.

Cha, M. C., A. Lin, et al. (2005b). "Low dose docosahexaenoic acid protects normal colonic epithelial cells from araC toxicity." BMC Pharmacol **5**: 7.

Cha, S. H., Z. Hu, et al. (2005a). "Inhibition of hypothalamic fatty acid synthase triggers rapid activation of fatty acid oxidation in skeletal muscle." Proc Natl Acad Sci U S A **102**(41): 14557-14562.

Chajes,V., M. Cambot, et al. (2006). "Acetyl-CoA carboxylase alpha is essential to breast cancer cell survival." Cancer Res **66**(10): 5287-5294.

Chakravarty, B., Z. Gu, et al. (2004). "Human fatty acid synthase: structure and substrate selectivity of the thioesterase domain." Proc Natl Acad Sci U S A **101**(44): 15567-15572.

Chakraborty, S., S. Khare, et al. (2007). "Identification of genes associated with tumorigenesis of retinoblastoma by microarray analysis." Genomics **90**: 344-53.

Conklin, K. A. (2004). "Chemotherapy-associated oxidative stress: impact on chemotherapeutic effectiveness." Integr Cancer Ther **3**(4): 294-300.

Consolazio, A., P. L. Alo, et al. (2006). "Overexpression of fatty acid synthase in ulcerative colitis." Am J Clin Pathol **126**(1): 113-118.

Corkey, B. E. (1988). "Analysis of acyl-coenzyme A esters in biological samples." Methods Enzymol **166**: 55-70.

Dakubo, G.D. (2010). "The Warburg Phenomenon and Other Metabolic Alterationsof Cancer cells." Ch 2, p39-66

da Silva, S. D., I. W. Cunha, et al. (2009). "Clinicopathological significance of ubiquitin-specific protease 2a (USP2a), fatty acid synthase (FASN), and ErbB2 expression in oral squamous cell carcinomas." Oral Oncol **45**(10): e134-139.

Davies, K.J. (1999). "The broad spectrum of responses to oxidants in proliferating cells: a new paradigm for oxidative stress." IUBMB Life **48**: 41-7.

Devasagayam, T. P. (1986). "Lipid peroxidation in rat uterus." Biochim Biophys Acta **876**(3): 507-514.

Di Vizio, D., F. Sotgia, et al. (2007). "Caveolin-1 is required for the upregulation of fatty acid synthase (FASN), a tumor promoter, during prostate cancer progression." Cancer Biol Ther **6**(8): 1263-1268.

Dils, R. and E. M. Carey (1975). "Fatty acid synthase from rabbit mammary gland." Methods Enzymol **35**: 74-83.

Dimaras, H., V. Khetan, et al. (2009). "Retinoma Underlying Retinoblastoma Revealed After Tumor Response to 1 Cycle of Chemotherapy." Arch Ophthalmol **127**(8): 1066-1068.

Dimaras, H., K. Kimani, et al. (2012). "Retinoblastoma." Lancet **379**(9824): 1436-1446.

Dorn, C., M.O. Riener, et al. (2010). "Expression of fatty acid synthase in non-alcoholic fatty liver disease." Int J Clin Exp Pathol **3**(5): 505-14.

Fernandez-Real, J.M., J.A. Menendez, et al. (2010). "Extracellular fatty acid synthase: a possible surrogate biomarker of insulin resistance." Diabetes **59**(6): 1506-11.

Finger, P. T., J. W. Harbour, et al. (2002). "Risk factors for metastasis in retinoblastoma." Surv Ophthalmol **47**(1): 1-16.

Fiser, A. and A. Sali (2003). "Modeller: generation and refinement of homology-based protein structure models." Methods Enzymol **374**: 461-491.

Gabrielson, E. W., M. L. Pinn, et al. (2001). "Increased fatty acid synthase is a therapeutic target in mesothelioma." Clin Cancer Res **7**(1): 153-157.

Gan, Y., J. Wang, et al. (2008). "Synergistic induction of apoptosis by HMG-CoA reductase inhibitor and histone deacetylases inhibitor in HeLa cells." Biochem Biophys Res Commun **365**(2): 386-392.

Ganguly, A., C. L. Shields. (2010). "Differential gene expression profile of retinoblastoma compared to normal retina." Mol Vis **16**: 1292-303

Gansler, T. S., W. Hardman, 3rd, et al. (1997). "Increased expression of fatty acid synthase (OA-519) in ovarian neoplasms predicts shorter survival." Hum Pathol **28**(6): 686-692.

Gibson, D. M., E. B. Titchener, et al. (1958). "Studies on the mechanism of fatty acid synthesis. V. Bicarbonate requirement for the synthesis of long-chain fatty acids." Biochim Biophys Acta **30**(2): 376-383.

Gipson, P., D. J. Mills, et al. (2010). "Direct structural insight into the substrate-shuttling mechanism of yeast fatty acid synthase by electron cryomicroscopy." Proc Natl Acad Sci U S A **107**(20): 9164-9169.

Gonenc, A., T. Devrim, et al. (2005). "Oxidative stress in relation to lipid profiles in different stages of breast cancer." Indian J Biochem Biophys **42**: 190-194.

Graner, E., D. Tang, et al. (2004). "The isopeptidase USP2a regulates the stability of fatty acid synthase in prostate cancer." Cancer Cell **5**(3): 253-261.

Gulcan, H. G., R. A. Alvarez, et al. (1993). "Lipids of human retina, retinal pigment epithelium, and Bruch's membrane/choroid: comparison of macular and peripheral regions." Invest Ophthalmol Vis Sci **34**(11): 3187-3193.

Haase, D., S. Schmidl, et al. (2010). "Fatty acid synthase as a novel target for meningioma therapy." Neuro Oncol **12**(8): 844-854.

Halliwell, B. (2007). "Oxidative stress and cancer: have we moved forward?" Biochem J **401**(1): 1-11.

Halliwell, B. (2011). "Free radicals and antioxidants - quo vadis?" Trends Pharmacol Sci **32**(3): 125-130.

Hanahan, D. and R. A. Weinberg (2000). "The hallmarks of cancer." Cell **100**(1): 57-70.

Heiligtag, S. J., R. Bredehorst, et al. (2002). "Key role of mitochondria in cerulenin-mediated apoptosis." Cell Death Differ **9**(9): 1017-1025.

Helen, S.L., M.B. Chan, et al. (2005). "Chemotherapy for Retinoblastoma." Ophthalmol Clin N Am **18:** 55-63.

Ho, T. S., Y. P. Ho, et al. (2007). "Fatty acid synthase inhibitors cerulenin and C75 retard growth and induce caspase-dependent apoptosis in human melanoma A-375 cells." Biomed Pharmacother **61**(9): 578-587.

Hogberg, J., R. E. Larson, et al. (1974). "NADPH-dependent reductase solubilized from microsomes by peroxidation and its activity." Biochem Biophys Res Commun **56**(3): 836-842.

Hu, Z.Q., J.Y. Zhang, et al. (2010). "Grb10 interacts with Bim L and inhibits apoptosis." *Mol Biol Rep* ***37****(7):* 3547-52

Huang, P. L., S. N. Zhu, et al. (2000). "Inhibitor of fatty acid synthase induced apoptosis in human colonic cancer cells." World J Gastroenterol **6**(2): 295-297.

Hunt, D.A., H.M. Lane, et al. (2007). "mRNA stability and overexpression of fatty acid synthase in human breast cancer cell lines." Anticancer Res **27**(1A): 7-34.

Innocenzi, D., P. L. Alo, et al. (2003). "Fatty acid synthase expression in melanoma." J Cutan Pathol **30**(1): 23-28.

Issemann, I., R. A. Prince, et al. (1993). "The peroxisome proliferator-activated receptor:retinoid X receptor heterodimer is activated by fatty acids and fibrate hypolipidaemic drugs." J Mol Endocrinol **11**(1): 37-47.

Jain, P. T. and J. T. Pento (1991). "A vehicle for the evaluation of hydrophobic compounds in cell culture." Res Commun Chem Pathol Pharmacol **74**(1): 105-116.

Jensen-Urstad, A.P., and C. F. Semenkovich (2012). "Fatty acid synthase and liver triglyceride metabolism: Housekeeper or messenger?" Biochim biophys Acta **1821**(5): 47-53.

Jenwitheesuk, E. and R. Samudrala (2005). "Prediction of HIV-1 protease inhibitor resistance using a protein-inhibitor flexible docking approach." Antivir Ther **10**(1): 157-166.

Kandalam, M., M. Mitra, et al. (2010). "Molecular pathology of retinoblastoma." Middle East Afr J Ophthalmol **17** (3): 217-23

Kapoor, M., C. C. Reddy, et al. (2004). "Slow-tight-binding inhibition of enoyl-acyl carrier protein reductase from Plasmodium falciparum by triclosan." Biochem J **381**(Pt 3): 719-724.

Kase, S., J. G. Parikh, et al. (2009). "Expression of alpha-crystallin in retinoblastoma." Arch Ophthalmol **127**(2): 187-192.

Knowles, L. M., F. Axelrod, et al. (2004). "A fatty acid synthase blockade induces tumor cell-cycle arrest by down-regulating Skp2." J Biol Chem **279**(29): 30540-30545.

Knowles, L. M. and J. W. Smith (2007). "Genome-wide changes accompanying knockdown of fatty acid synthase in breast cancer." BMC Genomics **8**: 168.

Kohen, R. and A. Nyska (2002). "Oxidation of biological systems: oxidative stress phenomena, antioxidants, redox reactions, and methods for their quantification." Toxicol Pathol **30**(6): 620-650.

Kolesnick, R. (2002). "The therapeutic potential of modulating the ceramide/sphingomyelin pathway." J Clin Invest **110**(1): 3-8.

Kommoss, F., H. O. Wintzer, et al. (1990). "In situ distribution of transforming growth factor alpha in normal human tissues and in malignant tumours of the ovary." J Pathol **162**(3): 223-230.

Kridel, S. J., F. Axelrod, et al. (2004). "Orlistat is a novel inhibitor of fatty acid synthase with antitumor activity." Cancer Res **64**(6): 2070-2075.

Kridel, S. J., W. T. Lowther, et al. (2007). "Fatty acid synthase inhibitors: new directions for oncology." Expert Opin Investig Drugs **16**(11): 1817-1829.

Krishnakumar, S., A. Mohan, et al. (2004). "EpCAM expression in retinoblastoma: a novel molecular target for therapy." Invest Ophthalmol Vis Sci. **45**(12): 4247-50.

Kubinyi, H. (1998). "Structure-based design of enzyme inhibitors and receptor ligands." Curr Opin Drug Discov Devel **1**(1): 4-15.

Kuhajda, F. P., K. Jenner, et al. (1994). "Fatty acid synthesis: a potential selective target for antineoplastic therapy." Proc Natl Acad Sci U S A **91**(14): 6379-6383.

Kuhajda, F. P., S. Piantadosi, et al. (1989). "Haptoglobin-related protein (Hpr) epitopes in breast cancer as a predictor of recurrence of the disease." N Engl J Med **321**(10): 636-641.

Kuhajda, F. P., E. S. Pizer, et al. (2000). "Synthesis and antitumor activity of an inhibitor of fatty acid synthase." Proc Natl Acad Sci U S A **97**(7): 3450-3454.

Kuhajda, F.P. (2006). "Fatty acid synthase and cancer: new application of an old pathway." Cancer Res **66**(12): 5977-80.

Kumar, B., S. Koul, et al. (2008). "Oxidative stress is inherent in prostate cancer cells and is required for aggressive phenotype." Cancer Res **68**(6): 1777-1785.

Kusakabe, T., A. Nashimoto, et al. (2002). "Fatty acid synthase is highly expressed in carcinoma, adenoma and in regenerative epithelium and intestinal metaplasia of the stomach." Histopathology **40**(1): 71-79.

Lange, Y., M. H. Swaisgood, et al. (1989). "Plasma membrane contain half the phospholipid and 90% of the cholesterol and sphingomyelin in cultured human fibroblasts". J Biol Chem **264**(7): 3786-3793

Laskowski, R. A., J. A. Rullmannn, et al. (1996). "AQUA and PROCHECK-NMR: programs for checking the quality of protein structures solved by NMR." J Biomol NMR **8**(4): 477-486.

Lawrence, D. S., J. T. Zilfou, et al. (1999). "Structure-activity studies of cerulenin analogues as protein palmitoylation inhibitors." J Med Chem **42**(24): 4932-4941.

Lee, J.S., M.S. Lee, et al. (2009). "Fatty acid synthase inhibition by amentoflavone induces apoptosis and antiproliferation in human breast cancer cells." Biol Pharm Bull **32**(8): 427.

Li, J. N., M. Gorospe, et al. (2001). "Pharmacological inhibition of fatty acid synthase activity produces both cytostatic and cytotoxic effects modulated by p53." Cancer Res **61**(4): 1493-1499.

Limb, G. A., T. E. Salt, et al. (2002). "In vitro characterization of a spontaneously immortalized human Muller cell line (MIO-M1)." Invest Ophthalmol Vis Sci **43**(3): 864-869.

Liu, B., Y. Wang, et al. (2002). "Triclosan inhibits enoyl-reductase of type I fatty acid synthase in vitro and is cytotoxic to MCF-7 and SKBr-3 breast cancer cells." Cancer Chemother Pharmacol **49**(3): 187-193.

Liu, H., Y. Liu, et al. (2008). "A new mechanism of drug resistance in breast cancer cells: fatty acid synthase overexpression-mediated palmitate overproduction." Mol Cancer Ther **7**(2): 263-270.

Liu, X., Y. Shi, et al. (2006). "Inhibition of the phosphatidylinositol 3-kinase/Akt pathway sensitizes MDA-MB468 human breast cancer cells to cerulenin-induced apoptosis." Mol Cancer Ther **5**(3): 494-501.

Livak, K. J. and T. D. Schmittgen (2001). "Analysis of relative gene expression data using real-time quantitative PCR and the 2(-Delta Delta C(T)) Method." Methods **25**(4): 402-408.

López, M. and C. Diéguez (2007)."C75, a Fatty Acid Synthase (FAS) Inhibitor."Recent Patents on Endocrine, Metabolic & Immune Drug Discovery**1**(1):53-62

Lowry, O. H., N. J. Rosebrough, et al. (1951). "Protein measurement with the Folin phenol reagent." J Biol Chem **193**(1): 265-275.

Lu, S. and M. C. Archer (2005). "Fatty acid synthase is a potential molecular target for the chemoprevention of breast cancer." Carcinogenesis **26**(1): 153-157.

Luscombe, N. M., D. Greenbaum, et al. (2001). "What is bioinformatics? A proposed definition and overview of the field." Methods Inf Med **40**(4): 346-358.

Maier, T., M. Leibundgut, et al. (2008). "The crystal structure of a mammalian fatty acid synthase." Science **321**(5894): 1315-1322.

Mallikarjuna, K., P. Vaijayanthi, et al. (2007). "Cripto-1 expression in uveal melanoma: an immunohistochemical study." Exp Eye Res **84**(6): 1060-1066.

Mallikarjuna, K., C.S. Sundaram, et al. (2010). "Comparative proteomic analysis of differentially expressed proteins in primary retinoblastoma tumors." Proteomics Clin Appl **4**: 449-63

Manju, V., J. Kalaivani Sailaja, et al. (2002). "Circulating lipid peroxidation and antioxidant status in cervical cancer patients: a case-control study." Clin Biochem **35**(8): 621-625.

Martindale, J.L. and N.J. Holbrook (2002). "Cellular response to oxidative stress: signalling for suicide and survival." J Cell Physiol **192**(1): 1-15.

Mashima, T., H. Seimiya, et al. (2009). "De novo fatty-acid synthesis and related pathways as molecular targets for cancer therapy." Br J Cancer **100**(9): 1369-1372.

Mattick, J. S., J. Nickless, et al. (1983b). "The architecture of the animal fatty acid synthetase. II. Separation of the core and thioesterase functions and determination of the N-C orientation of the subunit." J Biol Chem **258**(24): 15300-15304.

Mattick, J. S., Y. Tsukamoto, et al. (1983a). "The architecture of the animal fatty acid synthetase. I. Proteolytic dissection and peptide mapping." J Biol Chem **258**(24): 15291-15299.

McMurry, L. M., M. Oethinger, et al. (1998). "Triclosan targets lipid synthesis." Nature **394**(6693): 531-532.

Menendez, J. A., R. Colomer, et al. (2004a). "Inhibition of tumor-associated fatty acid synthase activity enhances vinorelbine (Navelbine)-induced cytotoxicity and apoptotic cell death in human breast cancer cells." Oncol Rep **12**(2): 411-422.

Menendez, J. A., R. Colomer, et al. (2005). "Why does tumor-associated fatty acid synthase (oncogenic antigen-519) ignore dietary fatty acids?" Med Hypotheses **64**(2): 342-349.

Menendez, J. A. and R. Lupu (2005). "RNA interference-mediated silencing of the p53 tumor-suppressor protein drastically increases apoptosis after inhibition of endogenous fatty acid metabolism in breast cancer cells." Int J Mol Med **15**(1): 33-40.

Menendez, J. A. and R. Lupu (2007). "Fatty acid synthase and the lipogenic phenotype in cancer pathogenesis." Nat Rev Cancer **7**(10): 763-777.

Menendez, J. A., A. Vazquez-Martin, et al. (2007). "Olive oil's bitter principle reverses acquired autoresistance to trastuzumab (Herceptin) in HER2-overexpressing breast cancer cells." BMC Cancer **7**: 80.

Menendez, J. A., A. Vazquez-Martin, et al. (2009). "Fatty acid synthase: association with insulin resistance, type 2 diabetes, and cancer." Clin Chem **55**(3): 425-438.

Menendez, J. A., L. Vellon, et al. (2005a). "Pharmacological and small interference RNA-mediated inhibition of breast cancer-associated fatty acid synthase (oncogenic antigen-519) synergistically enhances Taxol (paclitaxel)-induced cytotoxicity." Int J Cancer **115**(1): 19-35.

Menendez, J. A., L. Vellon, et al. (2005b). "Antitumoral actions of the anti-obesity drug orlistat (Xenical™) in breast cancer cells: blockade of cell cycle progression, promotion of apoptotic cell death and PEA3-mediated transcriptional repression of Her2/neu (erbB-2) oncogene." Ann Oncol **16**(8): 1253-1267.

Menendez, J. A., L. Vellon, et al. (2004b). "Inhibition of fatty acid synthase (FAS) suppresses HER2/neu (erbB-2) oncogene overexpression in cancer cells." Proc Natl Acad Sci U S A **101**(29): 10715-10720.

Meng, X., N. H. Riordan, et al. (2004). "Cell membrane fatty acid composition differs between normal and malignant cell lines." P R Health Sci J **23**(2): 103-106.

Michalik, L., J. Auwerx, et al. (2006). "International Union of Pharmacology. LXI. Peroxisome proliferator-activated receptors." Pharmacol Rev **58**(4): 726-741.

Migita, T., S. Ruiz, et al. (2009). "Fatty acid synthase: a metabolic enzyme and candidate oncogene in prostate cancer." J Natl Cancer Inst **101**(7): 519-532.

Morris, G.M., D.S. Goodsell, et al. (1998). "Automated docking using a Lamarckian genetic algorithm and an empirical binding free energy function." Journal of Computational chemistry **19**(14): 1639-1662.

Mosmann, T. (1983). "Rapid colorimetric assay for cellular growth and survival: application to proliferation and cytotoxicity assays." J Immunol Methods **65**(1-2): 55-63.

Murata, S., K. Yanagisawa, et al. (2010). "Fatty acid synthase inhibitor cerulenin suppresses liver metastasis of colon cancer in mice."Cancer Sci **101**(8): 1861-65

Notarnicola, M., V. Tutino, et al. (2012). "Serum Levels of Fatty Acid Synthase in Colorectal Cancer Patients Are Associated with Tumor Stage." J Gastrointest Cancer **43:** 508-11.

Ogino, S., T. Kawasaki, et al. (2007). "Fatty acid synthase overexpression in colorectal cancer is associated with microsatellite instability, independent of CpG island methylator phenotype." Hum Pathol **38**(6): 842-849.

Omura, S. (1976). "The antibiotic cerulenin, a novel tool for biochemistry as an inhibitor of fatty acid synthesis." Bacteriol Rev **40**(3): 681-697.

Orita, H., J. Coulter, et al. (2007). "Selective inhibition of fatty acid synthase for lung cancer treatment." Clin Cancer Res **13**(23): 7139-7145.

Pace, D. M. and A. Elliott (1962). "Effects of acetone and phenol on established cell lines cultivated in vitro." Cancer Res **22**: 107-112.

Pappenberger, G., J. Benz, et al. (2010). "Structure of the human fatty acid synthase KS-MAT didomain as a framework for inhibitor design." J Mol Biol **397**(2): 508-519.

Pappenberger, G., T. Schulz-Gasch, et al. (2007). "Structure-assisted discovery of an aminothiazole derivative as a lead molecule for inhibition of bacterial fatty-acid synthesis." Acta Crystallogr D Biol Crystallogr **63**(Pt 12): 1208-1216.

Patil, R., S. Das, et al. (2010). "Optimized hydrophobic interactions and hydrogen bonding at the target-ligand interface leads the pathways of drug-designing." PLoS One **5**(8): e12029.

Pemble, C. W. t., L. C. Johnson, et al. (2007). "Crystal structure of the thioesterase domain of human fatty acid synthase inhibited by Orlistat." Nat Struct Mol Biol **14**(8): 704-709.

Piyathilake, C. J., A. R. Frost, et al. (2000). "The expression of fatty acid synthase (FASE) is an early event in the development and progression of squamous cell carcinoma of the lung." Hum Pathol **31**(9): 1068-1073.

Pizer, E. S., F. J. Chrest, et al. (1998). "Pharmacological inhibitors of mammalian fatty acid synthase suppress DNA replication and induce apoptosis in tumor cell lines." Cancer Res **58**(20): 4611-4615.

Pizer, E. S., C. Jackisch, et al. (1996). "Inhibition of fatty acid synthesis induces programmed cell death in human breast cancer cells." Cancer Res **56**(12): 2745-2747.

Pizer, E. S., J. Thupari, et al. (2000). "Malonyl-coenzyme-A is a potential mediator of cytotoxicity induced by fatty-acid synthase inhibition in human breast cancer cells and xenografts." Cancer Res **60**(2): 213-218.

Pizer, E. S., F. D. Wood, et al. (1996a). "Fatty acid synthase (FAS): a target for cytotoxic antimetabolites in HL60 promyelocytic leukemia cells." Cancer Res **56**(4): 745-751.

Porter, J. W., S. J. Wakil, et al. (1957). "Studies on the mechanism of fatty acid synthesis. II. Cofactor requirements of the soluble pigeon liver system." Biochim Biophys Acta **25**(1): 35-41.

Pörn, M.I. and J.P. Slotte. (1990). "Reversible effects of sphingomyelin degradation on cholesterol distribution and metabolism in fibroblasts and transformed neuroblastoma cells." Biochem J. **271**(1): 121-6.

Postic, C., R. Dentin, et al. (2004). "Role of the liver in the control of carbohydrate and lipid homeostasis." Diabetes Metab **30**(5): 398-408

Puig, T., A. Vazquez-Martin, et al. (2008). "Fatty acid metabolism in breast cancer cells: differential inhibitory effects of epigallocatechin gallate (EGCG) and C75." Breast Cancer Res Treat **109**(3): 471-479.

Qiao, S. and P. Tuohimaa (2004). "Vitamin D3 inhibits fatty acid synthase expression by stimulating the expression of long-chain fatty-acid-CoA ligase 3 in prostate cancer cells." FEBS Lett **577**(3): 451-454.

Raman, K., K. Yeturu, et al. (2008). "targetTB: a target identification pipeline for Mycobacterium tuberculosis through an interactome, reactome and genome-scale structural analysis." BMC Syst Biol **19**(2):109.

Rashid, A., E. S. Pizer, et al. (1997). "Elevated expression of fatty acid synthase and fatty acid synthetic activity in colorectal neoplasia." Am J Pathol **150**(1): 201-208.

Ray, G., S. Batra, et al. (2000). "Lipid peroxidation, free radical production and antioxidant status in breast cancer." Breast Cancer Res Treat **59**(2): 163-170.

Ross, J., A.M. Najjar, et al. (2008). "Fatty acid synthase inhibition results in a magnetic resonance-detectable drop in phosphocholine." Mol Cancer Ther **7**(8): 2556-65.

Rossi, S., E. Graner, et al. (2003). "Fatty acid synthase expression defines distinct molecular signatures in prostate cancer." Mol Cancer Res **1**(10): 707-715.

Roulin, D., Y. Cerantola, et al. (2010). "Targeting mTORC2 inhibits colon cancer cell proliferation in vitro and tumor formation in vivo." Mol Cancer **9**: 57.

Rysman, E., K. Brusselmans, et al. (2010). "De novo lipogenesis protects cancer cells from free radicals and chemotherapeutics by promoting membrane lipid saturation." Cancer Res **70**(20): 8117-8126.

Schmidt, L. J., K. V. Ballman, et al. (2007). "Inhibition of fatty acid synthase activity in prostate cancer cells by dutasteride." Prostate **67**(10): 1111-1120.

Schultz, K.R., S. Ranade, et al. (1993). "An increased relative frequency of retinoblastoma at a rural regional referral hospital in Miraj, Maharashtra, India." Cancer **72**(1), 282–286.

Sekiya, M., A. Hiraishi, et al. (2008). "Oxidative stress induced lipid accumulation via SREBP1c activation in HepG2 cells." Biochem Biophys Res Commun **375**(4): 602-607.

Semenkovich, C. F. (1997). "Regulation of fatty acid synthase (FAS)." Prog Lipid Res **36**(1): 43-53.

Shah, U. S., R. Dhir, et al. (2006). "Fatty acid synthase gene overexpression and copy number gain in prostate adenocarcinoma." Hum Pathol **37**(4): 401-409.

Shields, C. L., C. G. Bianciotto, et al. (2011). "Intra-arterial chemotherapy for retinoblastoma: report No. 1, control of retinal tumors, subretinal seeds, and vitreous seeds." Arch Ophthalmol **129**(11): 1399-1406.

Shields, C. L., S. Kaliki, et al. (2012). "Intravenous and intra-arterial chemotherapy for retinoblastoma: what have we learned?" Curr Opin Ophthalmol **23**(3): 202-209.

Shields, C. L. and J. A. Shields (1999). "Recent developments in the management of retinoblastoma." J Pediatr Ophthalmol Strabismus **36**(1): 8-18; quiz 35-16.

Shurbaji, M. S., F. P. Kuhajda, et al. (1992). "Expression of oncogenic antigen 519 (OA-519) in prostate cancer is a potential prognostic indicator." Am J Clin Pathol **97**(5): 686-691.

Skaare, A.B., V. Kjaerheim, et al. (1997). "Does the nature of the solvent affect the anti-inflammatory capacity of triclosan? An experimental study." J Clin Periodontol 24(2): 124-8.

Slade, R. F., D. A. Hunt, et al. (2003). "Characterization and inhibition of fatty acid synthase in pediatric tumor cell lines." Anticancer Res **23**(2B): 1235-1243.

Slotte, J. P. and E. L. Bierman (1988). "Depletion of plasma-membrane sphingomyelin rapidly alters the distribution of cholesterol between plasma membranes and intracellular cholesterol pools in cultured fibroblasts." Biochem J **250**(3): 653-8

Spector, A.A., R.E. Kiser, et al. (1979). "Modification of the fatty acid composition of cultured human fibroblasts." J Lipid Res **20**(4): 536-47

Spector, A.A., and M.A. Yorek (1985). "Membrane lipid composition and cellular function." J Lipid Res **26**(9): 1015-35.

Staubach, S. and F. G. Hanisch (2011). "Lipid rafts: signaling and sorting platforms of cells and their roles in cancer." Expert Rev Proteomics **8**(2): 263-277.

Summa, C. M. and M. Levitt (2007). "Near-native structure refinement using in vacuo energy minimization." Proc Natl Acad Sci U S A **104**(9): 3177-3182.

Surolia, N. and A. Surolia (2001). "Triclosan offers protection against blood stages of malaria by inhibiting enoyl-ACP reductase of Plasmodium falciparum." Nat Med **7**(2): 167-173.

Suryawanshi, P., M. Ramadwar, et al. (2011). "A study of pathologic risk factors in postchemoreduced, enucleated specimens of advanced retinoblastomas in a developing country." Arch Pathol Lab Med **135**(8): 1017-23.

Swinnen, J. V., M. Esquenet, et al. (1997). "Androgens stimulate fatty acid synthase in the human prostate cancer cell line LNCaP." Cancer Res **57**(6): 1086-1090.

Swinnen, J. V., H. Heemers, et al. (2000). "Stimulation of tumor-associated fatty acid synthase expression by growth factor activation of the sterol regulatory element-binding protein pathway." Oncogene **19**(45): 5173-5181.

Swinnen, J. V., P. P. Van Veldhoven, et al. (2003). "Fatty acid synthase drives the synthesis of phospholipids partitioning into detergent-resistant membrane microdomains." Biochem Biophys Res Commun **302**(4): 898-903.

Takahashi, K. A., J. L. Smart, et al. (2004). "The anorexigenic fatty acid synthase inhibitor, C75, is a nonspecific neuronal activator." Endocrinology **145**(1): 184-193.

Tandon, V.R., S. Sharma, et al. (2005). "Oxidative stress: A novel strategy in cancer treatment." New Horizons **7**(1): 1-3

Tercé, F., H. Brun, et al. (1994). "Requirement of phosphatidylcholine for normal progression through the cell cycle in C3H/10T1/2 fibroblasts." J Lipid Res **35**(12): 2130-42.

Thangapazham, R. L., A. K. Singh, et al. (2007). "Green tea polyphenols and its constituent epigallocatechin gallate inhibits proliferation of human breast cancer cells in vitro and in vivo." Cancer Lett **245**(1-2): 232-241.

Thannickal, V.J., B. L. Fanburg. (2000). "Reactive oxygen species in cell signaling." Am J Physiol Lung Cell Mol Physiol **279**: L1005-28

Thupari, J. N., M. L. Pinn, et al. (2001). "Fatty acid synthase inhibition in human breast cancer cells leads to malonyl-CoA-induced inhibition of fatty acid oxidation and cytotoxicity." Biochem Biophys Res Commun **285**(2): 217-223.

Tietz, A. (1957). "Studies on the mechanism of fatty acid synthesis. IV. Biosynthesis of long-chain fatty acids in a reconstructed system of soluble enzymes from chicken liver." Biochim Biophys Acta **25**(2): 303-310.

Tsuji, T., M. Yoshinaga, et al. (2004). "Fatty acid synthase expression and clinicopathological findings in endometrial cancer." Acta Obstet Gynecol Scand **83**(6): 586-590.

Tsui, J.Y., C. Dalgard, et al. (2008). "Subconjunctival topotecan in fibrin sealant in the treatment of transgenic murine retinoblastoma." Invest Ophthalmol Vis Sci **49**(2): 490-6.

Tsukamoto, Y., H. Wong, et al. (1983). "The architecture of the animal fatty acid synthetase complex. IV. Mapping of active centers and model for the mechanism of action." J Biol Chem **258**(24): 15312-15322.

Uddin, S., A.K. Siraj, et al. (2008). "Fatty acid synthase and AKT pathway signaling in a subset of papillary thyroid cancers." J Clin Endocrinol Metab **93**(10): 4088-97.

Uddin, S., A. R. Hussain, et al. (2010). "Inhibition of fatty acid synthase suppresses c-Met receptor kinase and induces apoptosis in diffuse large B-cell lymphoma." Mol Cancer Ther **9**(5): 1244-1255.

Uddin, S., Z. Jehan, et al. (2011). "Overexpression of fatty acid synthase in Middle Eastern epithelial ovarian carcinoma activates AKT and Its inhibition potentiates cisplatin-induced apoptosis." Mol Med **17**(7-8): 635-645.

Valko, M., D. Leibfritz, et al. (2007). "Free radicals and antioxidants in normal physiological functions and human disease." Int J Biochem Cell Biol **39**(1): 44-84.

Valko, M., C. J. Rhodes, et al. (2006). "Free radicals, metals and antioxidants in oxidative stress-induced cancer." Chem Biol Interact **160**(1): 1-40.

Van de Sande, T., E. De Schrijver, et al. (2002). "Role of the phosphatidylinositol 3'-kinase/PTEN/Akt kinase pathway in the overexpression of fatty acid synthase in LNCaP prostate cancer cells." Cancer Res **62**(3): 642-646.

Vazquez, M. J., W. Leavens, et al. (2008). "Discovery of GSK837149A, an inhibitor of human fatty acid synthase targeting the beta-ketoacyl reductase reaction." FEBS J **275**(7): 1556-1567.

Vischer, W. A. and J. Regos (1974). "Antimicrobial spectrum of Triclosan, a broad-spectrum antimicrobial agent for topical application." Zentralbl Bakteriol Orig A **226**(3): 376-389.

Wakil, S. J. (1989). "Fatty acid synthase, a proficient multifunctional enzyme." Biochemistry **28**(11): 4523-4530.

Wakil, S. J., J. W. Porter, et al. (1957). "Studies on the mechanism of fatty acid synthesis. I. Preparation and purification of an enzymes system for reconstruction of fatty acid synthesis." Biochim Biophys Acta **24**(3): 453-461.

Wakil, S. J., E. B. Titchener, et al. (1958). "Evidence for the participation of biotin in the enzymic synthesis of fatty acids." Biochim Biophys Acta **29**(1): 225-226.

Wang, C., C. Xu, et al. (2009). "Acetyl-CoA carboxylase-alpha inhibitor TOFA induces human cancer cell apoptosis." Biochem Biophys Res Commun **385**(3): 302-306.

Wang, Y. Y., F. P. Kuhajda, et al. (2004). "Fatty acid synthase as a tumor marker: its extracellular expression in human breast cancer." J Exp Ther Oncol **4**(2): 101-110.

Wang, Y., F.P. Kuhajda, et al. (2001). "Two-site ELISA for the quantitative determination of fatty acid synthase." Clin Chim Acta **304**(1-2): 107-15.

Ward, W. H., G. A. Holdgate, et al. (1999). "Kinetic and structural characteristics of the inhibition of enoyl (acyl carrier protein) reductase by triclosan." Biochemistry **38**(38): 12514-12525.

Wei, X., J. G. Schneider, et al. (2011). "De novo lipogenesis maintains vascular homeostasis through endothelial nitric-oxide synthase (eNOS) palmitoylation." J Biol Chem **286**(4): 2933-2945.

Wong, H., J. S. Mattick, et al. (1983). "The architecture of the animal fatty acid synthetase. III. Isolation and characterization of beta-ketoacyl reductase." J Biol Chem **258**(24): 15305-15311.

Yorek, M.A., P.H. Figard, et al. (1985). "A comparison of lipid metabolism in two human retinoblastoma cell lines." Invest Ophthalmol Vis Sci **26**(8):1148-54.

Zareparsi, S., A. Hero, et al. (2004). "Seeing the unseen: Microarray-based gene expression profiling in vision." Invest Ophthalmol Vis Sci **45**(8): 2457-2462.

Zecchin, K. G., F. A. Rossato, et al. (2011). "Inhibition of fatty acid synthase in melanoma cells activates the intrinsic pathway of apoptosis." Lab Invest **91**(2): 232-240.

Zeng, X. F., W. W. Li, et al. (2011). "Discovery of novel fatty acid synthase (FAS) inhibitors based on the structure of ketoaceyl synthase (KS) domain." Bioorg Med Chem Lett **21**(16): 4742-4744.

Zhang, J. H. and M. Xu (2000). "DNA fragmentation in apoptosis." Cell Res **10**(3): 205-211.

Zhang, X. and F. L. Kiechle (2006). "Fatty acid synthase and its mRNA concentrations are decreased at different times following Hoechst 33342-induced apoptosis in BC3H-1 myocytes." Ann Clin Lab Sci **36**(2): 185-193.

Zhang, J., C. A. Benavente, et al. (2012). "A novel retinoblastoma therapy from genomic and epigenetic analyses." Nature **481**(7381): 329-34.

Zhou, W., P. J. Simpson, et al. (2003). "Fatty acid synthase inhibition triggers apoptosis during S phase in human cancer cells." Cancer Res **63**(21): 7330-7337.

Zhou, W., Y. Tu, et al. (2009). "Malonyl-CoA decarboxylase inhibition is selectively cytotoxic to human breast cancer cells." Oncogene **28**(33): 2979-2987.

APPENDIX I

TABLE A1: DIFFERENTIALLY EXPRESSED GENES (UP-REGULATED AND DOWN-REGULATED) IN Y79 RB CELLS (H_2O_2 OXIDANT-INDUCED MODEL) COMPARED TO CONTROL CELLS

Gene classification/Description	Gene Symbol	Fold change	Genbank accession	Chromosome location
Oxidative stress				
Selectin E	SELE	1.23	NM_000450	1q24.2
Vascular cell adhesion molecule 1	VCAM1	1.19	NM_001078	1p21.1
Calpain 9	CAPN9	1.19	NM_016452	1q42.2
C-Reactive protein	CRP	1.19	NM_000567	1q23.2
5,10-methylenetetrahydrofolatereductase (NADPH)	MTHFR	1.25	ENST00000376585	1p36.22
S100 calcium binding protein A12	S100A12	1.25	NM_005621	1q21.3
SHC (Src homology2 domain containing) transforming protein 1	SHC1	-1.53	NM_183001	1q21.3
24-dehydrocholesterol reductase	DHCR24	1.09	NM_014762	1p32.3
Phospholipase A2, group IIA	PLA2G2A	1.22	NM_000300	1p36.13
Prostaglandin-endoperoxide synthase 2	PTGS2	1.25	NM_000963	1q31.1
Platelet-activating factor acetylhydrolase 2, cytoplasmic	PAFAH2	-1.16	NM_000437	1p36.11
Mitochondrial thioredoxin reductase	TXNRD2	-2.28	AF201385	22q11.21
PRO1748	PRDX3	-1.06	AF118073	10q26.11
Oncogenes				
Ephrin-A1 (EFNA1), transcript variant 1, mRNA	EFNA1	2.37	NM_004428	1q22
Cadherin 5, type 2, VE-cadherin mRNA	CDH5	1.25	NM_001795	16q21
Tumor-associated calcium signal transducer 2 mRNA	TACSTD2	1.18	NM_002353	1p32.1
Vav 3 oncogene, transcript variant 1, mRNA	VAV3	1.25	NM_006113	1p13.3
Lymphocyte-specific protein tyrosine kinase, transcript variant 2, mRNA	LCK	3.62	NM_005356	1p35.1
Inhibitor of kappa light polypeptide gene enhancer in B-cells, kinase epsilon,	IKBKE	1.19	NM_014002	1q32.1
Jun oncogene, mRNA	JUN	2.72	NM_002228	1p32.1
PDZK1 interacting protein 1 (PDZK1IP1), mRNA	PDZK1IP1	1.19	NM_005764	1p33
Angiogenesis				
cDNA FLJ13544 fis, clone	ADAMTSL4	2.8	AK023606	1q21.2

Adenosine A3 receptor, transcript variant 2, mRNA	ADORA3	1.24	NM_000677	1p13.2
Ephrin-A1 (EFNA1), transcript variant 1, mRNA	EFNA1	2.37	NM_004428	1q22
Fas ligand (TNF superfamily, member 6) (FASLG), mRNA	FASLG	1.24	NM_000639	1q24.3
Guanylate binding protein 1, interferon-inducible, mRNA	GBP1	1.23	NM_002053	1p22.2
Duffy blood group, chemokine receptor (DARC), mRNA	DARC	-2.54	NM_002036	1q23.2
Tyrosine kinase with immunoglobulin-like and EGF-like domains 1	TIE1	1.25	NM_005424	1p34.2
S100 calcium binding protein A4, transcript variant 1, mRNA	S100A4	-1.12	NM_002961	1q21.3
Angiopoietin-like 3, mRNA	ANGPTL3	1.25	NM_014495	1p31.3
Inhibitor of DNA binding 3, dominant negative helix-loop-helix protein	ID3	-1.54	NM_002167	1p36.12
Tumour suppressor genes				
CD58 molecule, mRNA	CD58	-1.71	NM_001779	1p13.1
Chloride channel, calcium activated, family member 2, mRNA	CLCA2	1.23	NM_006536	1p22.3
Coagulation factor III (thromboplastin, tissue factor), mRNA	F3	1.19	NM_001993	1p21.3
Alkaline phosphatase, liver/bone/kidney, mRNA	ALPL	1.24	NM_000478	1p36.12
S100 calcium binding protein A11, mRNA	S100A11	1.15	NM_005620	1q21.3
Interleukin 24, transcript variant 1, mRNA	IL24	1.52	NM_006850	1q32.1
S100 calcium dbinding protein A4, transcript variant 1, mRNA	S100A4	-1.12	NM_002961	1q21.3
Solute carrier family 39 (zinc transporter), member 1, mRNA	SLC39A1	-1.14	NM_014437	1q21.3
Ribonuclease L (2',5'-oligoisoadenylate synthetase-dependent)	RNASEL	-2.28	NM_021133	1q25.3
Kinesin-like protein (Klp).	KIF1B	2.44	ENST00000377093	1p36.22
Calmodulin binding transcription activator 1 (CAMTA1)	CAMTA1	1.42	NM_015215	1p36.23
Prospero-related homeobox 1, mRNA	PROX1	1.25	NM_002763	1q41
Cell adhesion molecules				
Brevican, mRNA	BCAN	1.21	BC005081	1q23.1
Nidogen 1, mRNA	NID1	1.52	NM_002508	1q42.3
von Willebrand factor A domain-related protein isoform 1	VWA1	-1.55	ENST00000338660	1p36.33
Tenascin N, mRNA	TNN	2.49	NM_022093	1q25.1
Poliovirus receptor-related 4, mRNA	PVRL4	-1.73	NM_030916	1q23.3
Serpin peptidase inhibitor, clade C (antithrombin), member 1, mRNA	SERPINC1	2.22	NM_000488	1q25.1
5-hydroxytryptamine (serotonin) receptor 1D, mRNA	HTR1D	1.24	NM_000864	1p36.12
Fc fragment of IgG, low affinity IIIa, receptor (CD16a), mRNA	FCGR3A	1.25	NM_000569	1q23.3
Chloride channel, calcium activated, family member 2, mRNA	CLCA2	1.23	NM_006536	1p22.3

Regulator of G-protein signalling 1, mRNA	RGS1	1.23	NM_002922	1q31.2
Netrin G1, mRNA	NTNG1	1.17	NM_014917	1p13.3
Neuronal growth regulator 1, mRNA	NEGR1	1.35	NM_173808	1p31.1
Neurofascin homolog (chicken)	NFASC	-1.28	NM_015090	1q32.1
Podoplanin, transcript variant 2, mRNA	PDPN	1.12	NM_198389	1p36.21
Spectrin, alpha, erythrocytic 1 (elliptocytosis 2), mRNA	SPTA1	1.16	NM_003126	1q23.1
C-reactive protein, pentraxin-related, mRNA	CRP	1.19	NM_000567	1q23.2
Actin, alpha 1, skeletal muscle, mRNA	ACTA1	2.42	NM_001100	1q42.13
Thrombospondin 3, mRNA	THBS3	-1.25	NM_007112	1q22
Actinin, alpha 2, mRNA	ACTN2	2.43	NM_001103	1q43
CD244 molecule, natural killer cell receptor 2B4, mRNA	CD244	1.22	NM_016382	1q23.3
Tektin 2 (testicular), mRNA	TEKT2	3.95	NM_014466	1p34.3
Lymphocyte-specific protein tyrosine kinase, transcript variant 2	LCK	3.62	NM_005356	1p35.1
S100 calcium binding protein A8, mRNA	S100A8	1.15	NM_002964	1q21.3
Myocilin, trabecular meshwork inducible glucocorticoid response	MYOC	1.24	NM_000261	1q24.3
Interleukin 24, transcript variant 1, mRNA	IL24	1.52	NM_006850	1q32.1
Angiopoietin-like 3, mRNA	ANGPTL3	1.25	NM_014495	1p31.3
Plexin A2, mRNA	PLXNA2	-2.42	NM_025179	1q32.2
Astrotactin 1, transcript variant 1, mRNA	ASTN1	1.25	NM_004319	1q25.2
v-akt murine thymoma viral oncogene homolog 3 (protein kinase B, gamma)	AKT3	1.54	NM_005465	1q44
Collagen, type XI, alpha 1, transcript variant B, mRNA	COL11A1	1.23	NM_080629	1p21.1
Cornulin, mRNA	CRNN	1.23	NM_016190	1q21.3
Brevican, mRNA	BCAN	1.21	BC005081	1q23.1
Nidogen 1, mRNA	NID1	1.52	NM_002508	1q42.3
von Willebrand factor A domain-related protein isoform 1	VWA1	-1.55	ENST00000338660	1p36.33
Tenascin N, mRNA	TNN	2.49	NM_022093	1q25.1
Poliovirus receptor-related 4, mRNA	PVRL4	-1.73	NM_030916	1q23.3
PRAME family				
Preferential antigen in melanoma family member 3	PRAMEF3	3.42	NM_001013692	1p36.21
Preferential antigen in melanoma family member 12	PRAMEF12	2.52	NM_001080830	1p36.21
Preferential antigen in melanoma family member 18	PRAMEF18	1.62	NM_001099850	1p36.21

LIPID METABOLISM/FATTY ACID BIOSYNTHESIS				
Malonyl CoA:ACP acyltransferase (mitochondrial)	MCAT	3.42	NM_014507	22q13.2
Acetyl-Coenzyme A carboxylase beta, mRNA	ACACB	3.04	NM_001093	12q24.11
Acyl-CoA synthetase long-chain family member 3, transcript variant 1	ACSL3	1.73	NM_004457	2q36.1
Fatty acid binding protein 1, liver, mRNA	FABP1	1.61	NM_001443	2p11.2
Acetyl-Coenzyme A carboxylase alpha, transcript variant 2, mRNA	ACACA	1.28	NM_198839	17q12
Acyl-CoA thioesterase 2, mRNA	ACOT2	1.25	NM_006821	14q24.3
Fatty acid binding protein 2, intestinal, mRNA	FABP2	1.24	NM_000134	4q26
Acyl-CoA thioesterase 4, mRNA	ACOT4	1.18	NM_152331	14q24.3
Acyl-CoA synthetase long-chain family member 5, transcript variant 3	ACSL5	1.16	NM_203380	10q25.2
Cell cycle / Cell Proliferation				
Cell division cycle 25 homolog A (S. pombe), transcript variant 1, mRNA	CDC25A	1.34	NM_001789	3p21.31
Heat shock proteins				
Heat shock 70kDa protein 6, mRNA	HSPA6	5.56	NM_002155	1q23.3
Heat shock 70kDa protein 2, mRNA	HSPA2	3.45	NM_021979	14q23.3
Heat shock 70kDa protein 1A, mRNA	HSPA1A	2.70	NM_005345	6p21.33
JAK-STAT PATHWAY				
Suppressor of cytokine signaling 3, mRNA	SOCS3	1.71	NM_003955	17q25.3
Janus kinase 3 (a protein tyrosine kinase, leukocyte	JAK3	3.74	BC028068	19p13.11
Signal transducer and activator of transcription 4, mRNA	STAT4	1.21	NM_003151	2q32.3
N-myc interactor, mRNA	NMI	1.24	NM_004688	2q23.3
CREB binding protein, transcript variant 1, mRNA	CREBBP	2.83	NM_004380	16p13.3
MAPK PATHWAY				
Mitogen-activated protein kinase kinase kinase 5, mRNA	MAP3K5	-1.15	NM_005923	6q23.3
Mitogen-activated protein kinase kinase 3 mRNA	MAP2K3	1.48	NM_145109	17p11.2
Mitogen-activated protein kinase kinase 2, mRNA	MAP2K2	1.43	NM_030662	19p13.3
Mitogen-activated protein kinase 10, transcript variant 3, mRNA	MAPK10	1.22	NM_138980	4q21.3
Mitogen-activated protein kinase 15, mRNA	MAPK15	1.25	NM_139021	8q24.3
PI3K PATHWAY				
Phosphatidylinositol-4-phosphate 5-kinase, type I, alpha, mRNA	PIP5K1A	1.21	NM_003557	1q21.2
Phosphoinositide-3-kinase, catalytic, gamma polypeptide, mRNA	PIK3CG	1.25	NM_002649	7q22.3

Drug resistance genes					
ATP-binding cassette, sub-family C (CFTR/MRP), member 2, mRNA	ABCC2	1.95	NM_000392	10q24.2	

TABLE A2: LIST OF UP-REGULATED GENES IN Y79 RETINOBLASTOMA CELLS TREATED WITH CERULENIN

S.No	Gene classification/description	Gene symbol	Fold change	Genbank accession	Chromosome location
1	Transferrin receptor	TFRC	2.0708	NM_003234	3q29
2	Chondroitin sulphate glucuronyl transferase	CSGlcA-T	2.0094	NM_019015	7q36.1
3	Adenomatous polyposis 2	APC2	1.0871	NM_005883	19p13.3
4	Platelet endothelial cell adhesion molecule 1	PECAM1	1.673	NM_000442	17q23.3
5	Phosphatidylinositol glycan anchor biosynthesis, class G	PIGG	1.513	NM_017733	4p16.3
6	Laminin beta 4	LAMB	1.4335	NM_007356	7q31.1
7	Histone deacetylase 4	HDAC4	1.3664	NM_006037	2q37.3
8	Phosphatidylinositol glycan anchor biosynthesis, class M	PIGM	1.3541	NM_145167	1q23.2
9	Uridine phosphorylase 1	UPP1	1.3092	NM_181597	7p12.3
10	ADP-ribosyl hydrolase 1	ADPRHL1	1.3015	NM_199162	13q34
11	Phosphodiesterase 11A	PDE11A	1.2721	NM_016953	2q31.2
12	Asparagine-linked glycosylation 13	ALG13	1.2623	NM_018466	Xq23
13	CDC42 effector protein	CDC42EP2	1.2403	NM_006779	11q13.1
14	CDK2-associated protein 1	CDK2AP1	1.2177	NM_004642	12q24.31
15	Somatostatin receptor 2	SSTR2	1.2157	NM_001050	17q25.1
16	Cytochrome c oxidase	THC2685096	1.2005	THC2685096	11q21
17	Activator of basal transcription 1	ABT1	1.1917	NM_013375	6p22.1
18	Hyaluronoglucosaminidase 3	HYAL3	1.1394	NM_003549	3p21.31
19	RhoGTPase activating proetin 17	ARHGAP17	1.1112	NM_001006634	16p12.1
20	Mitogen-activated protein kinase kinase kinase kinase 4	MAP4K4	1.0781	NM_145686	2q11.2
21	Cytochrome c	CYCS	1.2089	NM_018947	7p15.2

TABLE A3: LIST OF DOWN-REGULATED GENES IN Y79 RETINOBLASTOMA CANCER CELLS TREATED WITH CERULENIN

S.No	Gene classification/description	Gene symbol	Fold change	Genbank accession	Chromosome location
1	Upstream transcription factor 1	USF1	-2.2112	NM_007122	1q23.3
2	Arrestin domain containing 3	ARRDC3	-1.9915	NM_020801	5q14.3
3	Rapamycin-insensitive companion of Mtor	RICTOR	-1.9256	NM_152756	5p13.1
4	Retinoid X receptor, alpha	RXRA	-1.831	NM_002957	9q34.2
5	Peroxisome proliferator activated receptor	PPARA	-1.8007	L02932	22q13.31
6	ADAM metallopeptidase domain 9 (meltrin gamma)	ADAM9	-1.7593	NM_001005845	8p11.23
7	Inositol polyphosphate-4-phosphatase, type I	INPP4A	-1.6219	NM_004027	2q11.2
8	S-phase kinase-associated protein 2	SKP2	-1.5964	NM_032637	5p13.2
9	Acetyl CoA carboxylase beta	ACACB	-1.4978	NM_001093	12q24.11
11	ADAM metallopeptidase type I motif 2	ADAMTS2	-1.2369	NM_021599	5q35.3
12	6-phosphofructo-2-kinase/fructose-2,6-biphosphatase 4	PFKFB4	-1.1944	NM_004567	3p21.31
13	Heat shock protein 27kDa 3	HSB3	-1.1678	NM_006308	5q11.2
14	Bim-alpha1	BCL2L11	-1.1578	AB071195	2q13
16	Ras responsive element binding protein 1	RREB1	-1.1066	NM_002955	6p24.3
17	Growth factor receptor bound protein 10	GRB10	-1.065	NM_001001555	7p12.2
18	Neural cell adhesion molecule 1	NCAM1	-1.0581	NM_000615	11q23.1
19	Kinesin family member 17	KIF17	-1.0574	NM_020816	1p36.12

APPENDIX II

LIST OF CONSUMABLES

S.No.	CONSUMABLES	COMPANY
1	Acetyl CoA	Sigma Aldrich
2	Acetone	Merck
3	Acetonitrile	Merck
4	Annexin V apoptosis kit	BD Biosciences
5	Antibiotic antimycotic solution	HiMedia
6	Anti-FASN antibody	BD Biosciences
7	Anti-MDA antibody	Chemicon
8	Anti-β actin antibody	Sigma Aldrich
9	C18 Gemini HPLC column	Phenomenex
10	Cerulenin	Sigma Aldrich
11	Chloroform	Merck
12	Cholesterol assay kit	BioVision
13	Dicholorodihydrofluorescein fluorescence assay kit	CellBiolabs
14	Diethyl ether	Merck
15	Diethyl pyrocarbonate	Sigma Aldrich
16	Dimethyl sulfoxide	Sigma Aldrich
17	DMEM with L-glutamine	GIBCO
18	DNTP mix	Sanmar speciality centre
19	DTT	SRL
20	Enhanced chemiluminescence kit	Pierce
21	FAS ELISA KIT	FASgen
22	Fetal bovine serum	Gibco
23	Free CoA	Sigma Aldrich
24	Free fatty acid assay kit	BioVision
25	HMG CoA	Sigma Aldrich
26	Hydrogen peroxide	Jeyam scientific
27	Isopropanol	Merck
28	LSAB kit	Dako
29	Malonyl CoA	Sigma Aldrich
30	MTT	Sigma Aldrich
31	NADPH	SRL
32	Orlistat (Xenical™)	Roche Pharmaceuticals
33	PEG 400	HiMedia
34	Phosphatidyl choline assay kit	BioVision
35	Ponceau S	Sigma Aldrich
36	Rabbit anti-mouse antibody	Santa-Cruz
37	RNAse out	Biocorporals
38	Sensiscript reverse transcriptase kit	Qiagen
39	Succinyl CoA	Sigma Aldrich
40	SYBR green real time RT-PCR master mix	SABiosciences

41	Taqman real time RT-PCR probes	Labindia
42	Thiobarbituric acid	Sigma Aldrich
43	Triclosan	Sigma Aldrich
44	Triglyceride assay kit	BioVision
45	Triton X 100	HiMedia
46	Trizol	Sigma Aldrich
47	Trypsin	HiMedia

LIST OF PUBLICATIONS

1. Deepa PR, Nalini V, Mallikarjuna K, **Vandhana S,** Krishnakumar S. Oxidative stress in retinoblastoma: correlations with clinicopathologic features and tumor invasiveness. ***Curr Eye Res.*** 2009 Dec;34(12):1011-8. Impact factor – 1.28

2. **Vandhana S,** Deepa PR, Aparna G, Jayanthi U, Krishnakumar S. Evaluation of suitable solvents for testing the anti-proliferative activity of triclosan – a hydrophobic drug in cell culture. ***Indian J Biochem Biophys.*** 2010 Jun;47(3):166-71. Impact factor – 1.142

3. **Vandhana S,** Deepa PR, Jayanthi U, Biswas J, Krishnakumar S. Clinico-pathological correlations of fatty acid synthase expression in retinoblastoma: an Indian cohort study. ***Exp Mol Pathol***. 2011 Feb;90(1):29-37. Impact factor – 2.47

4. Deepa PR, **Vandhana S,** Jayanthi U, Krishnakumar S. Therapeutic and Toxicological Evaluation of Anti-Lipogenic Agents in Cancer Cells Compared with Non-Neoplastic Cells. ***Basic Clin Pharmacol Toxicol.*** 2012, 110, 494-503. Impact factor – 2.179

5. Deepa PR, **Vandhana S,** Muthukumaran S, Umashankar V, Jayanthi U, Krishnakumar S. Chemical inhibition of fatty acid synthase: molecular docking analysis and biochemical validation in ocular cancer cells. ***J Ocul Biol Dis Inform.*** 2010; 3(4): 117-128

6. **Vandhana S**, Lakshmi TS, Indra D, Deepa PR, Krishnakumar S. Microarray Analysis and Biochemical Correlations of Oxidative Stress Responsive Genes in Retinoblastoma. ***Curr Eye Res.*** 2012 Sep; 37(9):830-41. Impact factor – 1.28

7. Deepa PR, **Vandhana S,** Krishnakumar S. Fatty Acid Synthase Inhibition Induces Differential Expression Of Genes Involved In Apoptosis And Cell Proliferation In Ocular Cancer Cells. Short communication. ***Nutr Cancer.*** 2013; 65(2): 1-6 Impact factor – 2.55

Manuscript under review in the journal: BBA – Molecular and Cell Biology of Lipids

Biochemical changes accompanying apoptotic cell death in retinoblastoma cancer cells treated with lipogenic enzyme inhibitors.

CONFERENCE PRESENTATIONS

1. Attended International Conference on the Interface of Chemistry-Biology in Biomedical Research conducted by ISCB at BITS, Pilani and presented poster titled *"Experimental Evaluation of Suitable Solvents for Studying Triclosan, A Hydrophobic Drug, In Cell Culture"* ***on February 2008.***
2. Attended the "International Conference on Nano-medicine & Recent Advances in Ophthalmic Research" organized by the 'Kamalnayan Bajaj Institute for Research in Vision and Ophthalmology', Vision Research Foundation, Chennai and presented a poster titled *"Oxidative Stress in Retinoblastoma: Clinicopathologic Correlations of Malondialdehyde Levels"* ***on*** **September 2008.**
3. Attended the International Conference on Vision and ophthalmology "Asia ARVO" held at LVPEI Hyderabad and presented a poster *titled "Expression of Fatty Acid Synthase in Retinoblastoma"* **on January 2009.**
4. Attended the 18th annual meeting of the Indian eye research group (IERG) at LVPEI, Hyderabad and presented a paper titled *"Lipogenic enzyme-inhibitor cerulenin shows Pro-apoptotic and anti-proliferative activity in retinoblastoma y79 cells"* on **August 2010.**

LIST OF AWARDS

1. Awarded **consolation best poster award** in the International Conference on the Interface of Chemistry-Biology in Biomedical Research conducted by ISCB at **BITS, Pilani** for the work titled *"Experimental Evaluation of Suitable Solvents for Studying Triclosan, A Hydrophobic Drug, In Cell Culture"* **on February 2008**
2. Granted with a **travel fellowship** for attending the 18th annual meeting of the **Indian eye research group (IERG) at LVPEI, Hyderabad** and for presenting the paper titled *"Lipogenic enzyme-inhibitor cerulenin shows Pro-apoptotic and anti-proliferative activity in retinoblastoma y79 cells"* **on August 2010**

BRIEF BIOGRAPHY OF THE CANDIDATE

Ms. S. Vandhana obtained her B.Sc Biochemistry degree from The Ethiraj College, University of Madras, Chennai in the year 2003. She obtained her M.S. (Medical Laboratory Technology) degree of Birla Institute of Technology and Science, Pilani in 2006 with course work at Medical Research Foundation, Chennai. She did her 1 year internship project in the Department of Biochemistry, Sankara Nethralaya and studied the role of lysyl oxidase and matrix metalloproteinase enzymes in retinal pigment epithelium under hyperosmotic conditions. Then she joined the Clinical laboratory, Sankara Nethralaya as Junior Scientist in the Haematology lab and worked for a year and was recruited into project in 2007 which was funded by Indian council of medical research (ICMR). She registered for Ph. D in January 2008 in Birla Institute of technology & Science, Pilani. She has made presentations in 1 national and 3 international conference, comprising 4 poster presentations and 1 oral presentation. She has 6 publications. 1 paper is under review, and 1 more paper is under preparation which is related to thesis. She has received "Consolation Best Poster Award" for poster titled "Experimental Evaluation of Suitable Solvents for Studying Triclosan, A Hydrophobic Drug, In Cell Culture" in the International Conference on the Interface of Chemistry-Biology in Biomedical Research conducted by ISCB at BITS, Pilani in February 2008. Apart from scientific research, she has profound interest in carnatic music vocal and has performed in several small concerts in local temples in Chennai. Currently she is working as SRF in a DBT funded Nanotechnology based grant in the Ocular Pathology Lab, Sankara Nethralaya.

BRIEF BIOGRAPHY OF THE SUPERVISOR

DR. S. KRISHNAKUMAR

Dr. S. Krishnakumar, is a MD Pathology, from Madras University. He is currently working as the Faculty at Vision Research Foundation, Sankara Nethralaya, Chennai, and Ocular Pathologist and Professor in Ophthalmology in the Larsen and Toubro Department of Ocular Pathology. He has undergone six months research fellowship in ophthalmic pathology at Doheny Eye Institute, University of Southern California, USA. He has been selected as DBT Associate and awarded short-term Overseas Fellowship Award in nanotechnology at University of Missouri-Columbia and ICMR Fellowship for training in nanotechnology and drug delivery at University of Nebraska Medical Center, Omaha. He was selected for "Sir Sriram Travel Fellowship Award" for training in proteomics for the year 2006-2007 by National Academy of Medical Sciences. His total publications are 70 in number in the international journals. His research interests are: tumor biology of retinoblastoma, corneal and retinal stem cell culture and characterization, and nanomedicine. His current research grants involve proteomics, siRNA, nanotechnology, RNA aptamer, novel recombinant molecules, nanofiber scaffolds. He collaborates with IIT Madras, ILS Orissa, CCMB, Deakin University Melbourne, University of Missouri, Columbia, and NASA. Currently there are 15 students pursuing their Ph D his guidance, and there are 23 SRFs and 2 JRFs working in his lab under his supervision.

BRIEF BIOGRAPHY OF THE CO – SUPERVISOR

Dr. P. R. DEEPA

Dr. P. R. Deepa (Assistant Professor, Dept. of Biological Sciences, BITS Pilani) has been involved (since 2005) in teaching and co-ordination of the off-campus collaborative bio-medical programmes of BITS Pilani at Chennai Centre. She also mentors students from BITS, Pilani during their final year internship (Practice School – II) at various industrial and research organizations in Chennai. Dr. Deepa has been collaborating with the Department of Ocular Pathology, Sankara Nethralaya (Chennai) for her ongoing research in the evaluation of molecular targets for diagnosis and therapy of retinoblastoma. Her other ongoing collaborative research efforts are in the areas of bio-mathematical modelling, bioinformatics, and bio-chemical engineering. She earned her doctoral degree in 2005 for her research titled *"Biochemical Evaluation of a Low-Molecular Weight Heparin (certoparin sodium) in Experimental Atherogenic and Cytotoxic Conditions"* (Dept. of Medical Biochemistry, University of Madras, 2005).